NONLINEAR FINITE ELEMENT ANALYSIS OF

PLATES AND SLABS

by

TAHER H. GANABA, B.sc.(Hons.), M.sc.

A Thesis submitted for the Degree of

Doctor of Philosophy

Department of Engineering Science,

The University of Warwick

August 1985

SYNOPSIS

The behaviour of steel plates and reinforced concrete slabs which undergo large deflections has been investigated using the finite element method. Geometric and material nonlinearities are both considered in the study.

Two computer programs have been developed for the analysis of plates and slabs. The first program is for the elastic stability of plates. The elastic buckling loads obtained for plates with and without openings and under different edge loading conditions have been compared with the analytical and numerical results obtained by other investigators using different techniques of analyses. Good correlation between the results obtained and those given by others has been achieved. Improvements in the accuracy of the results and the efficiency of the analysis for plates with openings have been achieved.

The second program is for the full range analysis of steel plates and reinforced concrete slabs up to collapse. The analysis can trace the load-deflection response up to collapse including snap-through behaviours. The program allows for the yielding of steel and the cracking and crushing of concrete. The modified Newton-Raphson with load control and displacement control methods is used to trace the structural response up to collapse. The line search technique has been included to improve the rate of convergence in the analysis of reinforced concrete slabs. The program has been tested against experimental and numerical results obatined by other investigators and has been shown to give good agreement.

The accuracy of a number of integration rules usually adopted in nonlinear finite element analyses to evaluate the stress resultants from the stress distribution throughout concrete sections has been investigated. A new integration rule has been proposed for the integration of stress distributions through cracked concrete sections or cracked and crushed concrete sections.

LIST OF TABLES

LIST OF FIGURES

CHAPTER 6

REINFORCED CONCRETE SLABS

REINFORCED CONCRETE SLABS

ACKNOWLEDGEMENT

I am grateful to my supervisor, Dr. I. M. May, for his guidance and encouragement throughout the period of my study.

I am also grateful to my wife, Namia, for her support and encouragement during the last two years.

My gratitude extends to Mr. A. J. Hulme, the Engineering Computer Manger, for his help.

My friends at Warwick are also thanked for the pleasant time we had during my stay.

DECLARATION

It is declared that this thesis contains the original work of the author. This work has not been submitted for a degree to any other university.

NOTATION

General symbols

$\{\ \}$, $\{\ \}^T$ vector,

$[\ ]$, $[\ ]^T$, $[\ ]^{-1}$ rectangular matrix,

T denotes transpose of the vectors and matrices,

-1 denotes inverse of the matrix

$\|\ \|$ Euclidean norm of a vector

Scalars

A area

D diameter of a circular hole

d length of square hole

E modulus of elasticity

E_c initial modulus of elasticity of concrete

E_s secant modulus

E_{sh} modulus of strain hardening

E_{st} initial modulus of elasticity of steel

F	yield function
f'_c	compressive strength of concrete
f'_t	tensile strength of concrete
K	biaxial principal stress ratio
k	strain hardening parameter
L	plate length
N	isoparametric shape functions
P	Lagrange shape functions
S	ratio of the uniaxail ultimate compressive strength of concrete to its uniaxail ultimate tensile strength
S_o, S	measure of potential energy in previous and present iterations respectively
t	plate thickness
u,v	in-plane displacements at the plate middle surface

u',v' in-plane displacements at an aribtrary point located at a distance from the plate middle surface

V volume

w,w' lateral displacements

W_c lateral displacement of the plate centre

W_i weight function

x,y,z cartesian co-ordinates

z_1,z_2 co-ordinates of the top and bottom of the plate

α_D,α_E displacement and energy convergence tolerances

β tension stiffening parameter

ε_{cu} strain corresponding to the uniaxial ultimate compressive strength of concrete

ε_{su} ultimate compressive strain of concrete

σ_i,ε_i ultimate strain of steel

stress and strain in principal direction i

$\sigma_{pi}, \varepsilon_{pi}$ peak compressive stress and corresponding strain in principal direction i

σ_{ti} tensile strength of concrete in principal direction i

$\sigma^*_{1,2}$ pseudo principal stresses

$\sigma_{1,2}, \varepsilon_{1,2}$ principal stresses and strains

σ_{cr} critical shear stress

σ_o uniaxial yield stress

σ_{xo}, σ_{yo} uniaxial compressive stresses

η, ξ local co-ordinates

ν Poisson's ratio

ν_c Poisson's ratio of concrete

Σ summation

λ stress factor, load factor

θ_x, θ_y rotations of the normals to the undeformed middle surface in the xz and yz planes respectively

ϕ_x, ϕ_y average transverse shear deformations

$\Delta\delta_i$ specified incremental displacement component

η_i acceleration scalar

ψ tolerance for η_i

Φ potential energy

Vectors

{F} internal forces

{f} internal forces for an element

$\{\bar{f}\}$ body forces

{P} applied loads

{p} surface tractions

$\{\sigma\},\{\varepsilon\}$ stress and strain vectors

$\{\bar{\sigma}\},\{\bar{\varepsilon}\}$ stress resultants and associated strain vector

$\{\varepsilon^L\}$ linear strains

$\{\varepsilon^{NL}\}$ nonlinear strains

$\{\delta\}$ nodal displacements

$\{\psi\}$ residual forces

Matrices

[B] strain-displacements

$[B_L]$ linear strain-displacements

$[B_{NL}]$ nonlinear strain-displacmenets

$[K_T]$ tangent stiffness matrix

$[K_o]$ small displacements stiffness matrix

$[K_{\ }]$ small displacements stiffness matrix with the length of the midsurface assumed to remain constant

$[K_\sigma]$ geometric stiffness matrix

$[K_L]$ large displacement stiffness matrix

$[K_p]$ in-plane stiffness matrix

$[\hat{\sigma}]$ stress matrix

$[D]$ material matrix

$[\bar{D}]$ material matrix associated with the stress resultants

$[D^*]$ elasto-plastic material matrix

$[J]$ Jacobian matrix

Subscripts

b flexural

p in-plane

s transverse shear

e element

i iteration number

n increment number

DEDICATION

To my family

CHAPTER 1

INTRODUCTION

1.1 GENERAL REMARKS

Steel and reinforced concrete are being used for the construction of increasingly more sophisticated and complex structures such as nuclear reactor containment vessels, offshore platforms, longspan bridges and highrise buildings. Attempts at the analysis of such structures has been made possible by the development of more powerful analytical techniques which rely on the increasing power of modern electronic computers. However, even with such techniques an understanding of the behaviour of such structures is far from complete.

In the design of plates and slabs, design methods based on the assumption of linear elastic behaviour or using empirically derived formulas can give very conservative estimates of the load carrying capacity of such structures. Methods of analysis based on plasticity theory, for example yield line analysis of slabs, have been developed to provide more realistic design tools. In the yield line method a knowledge of either or both the actual collapse mechanism or the equilibrium distribution of forces near failure is required. The collapse mechanism is then used to predict an upper-bound load which is either the correct collapse load or too high a collapse load. The equilibrium distribution of forces is required to predict a lower-bound load which is either the correct collapse load or too low a collapse load. Unfortunately this informattion cannot be determined in a straightforward manner. Moreover the membrane forces are usually ignored in the methods of design mentioned above.

Experimental tests carried out on plates and slabs indicated higher collapse loads than those predicted by the various analytical methods. The finite element method provides an alternative approach to investigate the behaviour of structures throughout the different stages of loadings. The nonlinear material effects such as the elasto-plastic behaviour of steel stuctures, the nonlinear stress-strain relationships for concrete, concrete cracking and yielding of the reinforcing steel can be included in the analysis. The effect of change of geometry can be also considered using the finite element method.

Tests carried out [1-5] on reinforced concrete slabs have shown that two-way slabs which are restrained against movement at their edges have ultimate loads which are far higher than the ultimate loads for unrestrained slabs. A typical load-deflection curve for a restrained slab is shown in Fig.1.1. For small deflections as the load increases membrane forces develop. At load B, the compressive membrane forces are at their maximum values. As the deflections of the slab are further increased, the load carried decreases, and the compressive membrane forces also reduce. At load C, the membrane forces in the central region of the slab change from compression to tension. As the deflections are further increased the tensile membrane forces increase in size and spread toward the boundaries. These forces are predominantly carried by the reinforcing steel and continue to increase until the steel ruptures and collapse occurs.

A review of the finite element literature indicated that a number of attempts have been made to analyse the various aspects of the

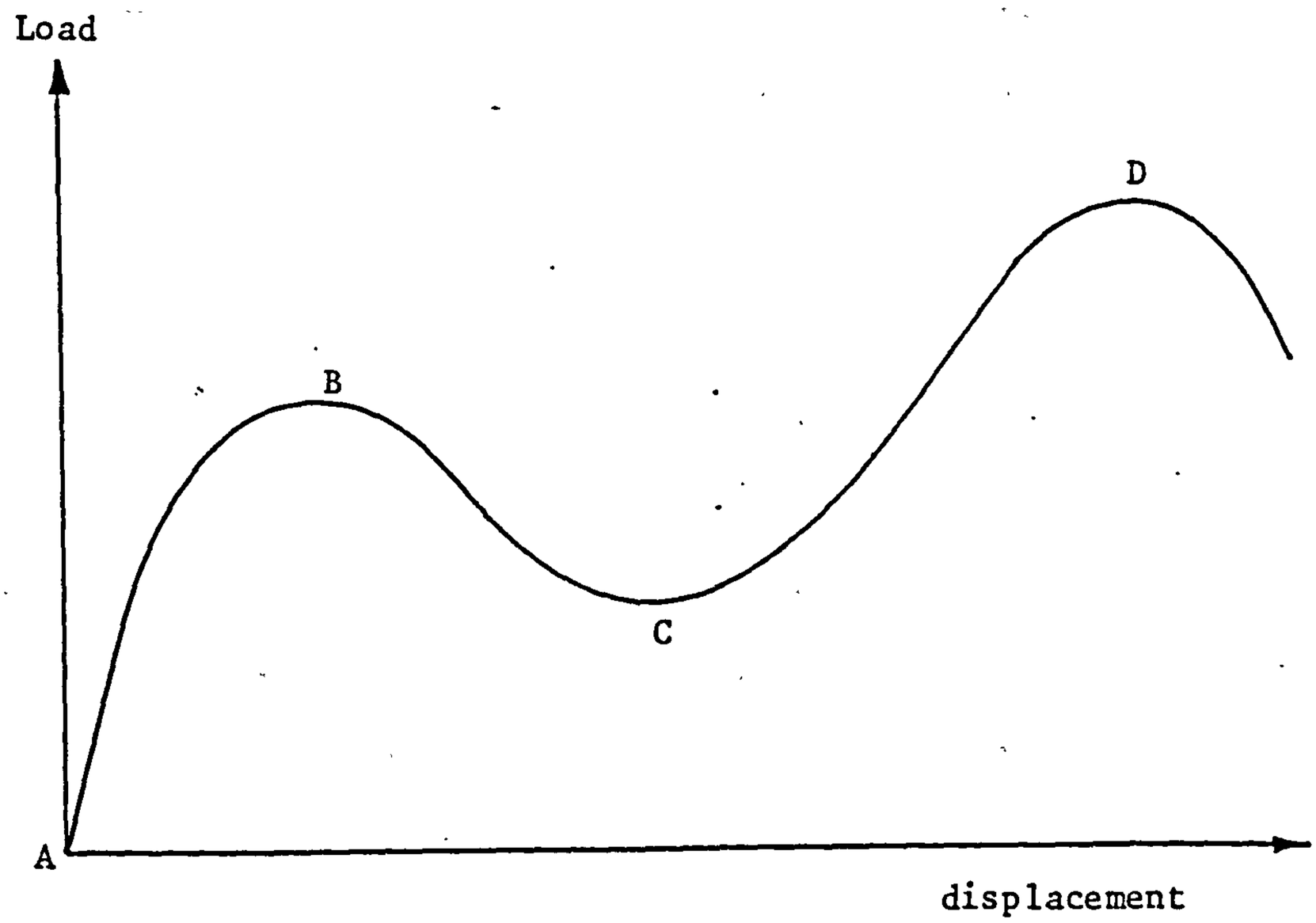

Figure 1.1. Load-deflection curve for fully restrained reinforced concrete slab

behaviour of restrained slabs described above. Van Greunen [6] has included both geometric and material nonlinearities in the analysis but load control was used throughout the analysis and therefore the analysis failed to predict the true response. Crisfield [7] and others have taken the analyses beyond the load B, Fig.1.1, using displacement control or the arc length method. However, because only material nonlinearity was considered the analyses failed to obtain the curve beyond load C. Further discussions are given in Chapters 6 and 7.

1.2 OBJECTIVE AND SCOPE

Ultimate loads may be of interest in the design of structures which may be subjected to extreme loadings. The analysis procedures developed in this study may not be used in a day to day analysis of structures in a design office, however they could be used to assess the performance of existing plates and slabs under particular overloads and when damaged. The study may provide a more detailed understanding of the behaviour of plates and slabs which may be useful in the development of the design codes for such structures.

The objective of the present study is to develop a computer program for the nonlinear analysis of steel plates and reinforced concrete slabs which undergo large deflections.

The aim of the analysis is to predict the response of plates and slabs through both the elastic and inelastic ranges and up to collapse.

Both in-plane and flexural effects are considered in the analysis. Collapse will occur due to plastic yielding in steel plates and cracking and crushing of concrete and yielding of the reinforcing steel in reinforced concrete slabs. Failure due to transverse shear forces is ignored. The effect of the membrane forces on the behaviour of plates and slabs has been investigated.

The various types of analyses which have been carried out are as follows:

1- Linear and elastic stability analyses in which the displacements and strains are assumed to remain small, Chapters 2, 3 and 4.

2- Geometric nonlinear analysis in which large deflections occur but strains are assumed to remain small, Chapters 2, 3, 6 and 7.

3- Material nonlinear analysis in which nonlinear material properties are assumed. Displacements and strains are assumed to remain small, Chapters 2, 3, 5, 6 and 7.

4- Geometric and material nonlinear analysis in which both nonlinearities described above are assumed to occur, Chapters 2, 3, 5, 6 and 7.

1.3 LAYOUT OF THE THESIS

The basic theoretical background required for the derivation of the governing equilibrium equations using the virtual work equation is presented in Chapter 2 together with the formulation of the Mindlin plate theory using a total Lagrangian approach.

In Chapter 3, Mindlin plate bending elements are discussed with special reference to the Heterosis element which has been used in the analysis. The 8-node isoparametric membrane element which has been employed in the investigation of the elastic stability of plates is also presented. Evaluation of the element stiffness matrices is also considered.

In Chapter 4, linear elastic analysis of plates, and an investigation of the elastic stability of plates are discussed. Several plates with and without openings and under different edge loading conditions have been analysed. The elastic buckling loads obtained for the various cases investigated have been compared with the available analytical and numerical results obtained by other investigators.

In Chapter 5, the constitutive relationships for the elasto-plastic behaviour of metals is established. Discussion of the material models used for concrete under biaxial states of stress is given. The modelling of cracking and tension stiffening effect are also discussed and a model for reinforcing steel is introduced.

In Chapter 6, the solution techniques employed in the study are presented. Details of the load and displacement control methods are given. The line search technique is presented. An investigation into the accuracies of the different numerical integration schemes most commonly used to evaluate the stress resultants from the stress distribution throughout a concrete cross-section is presented. A new integration rule is established and recommendations on the use of the numerical integration rules are given.

In Chapter 7 details of several numerical examples to demonstrate the validity and applicability of the analysis are given. Different combinations of the nonlinearities have been considered. The numerical results obtained from the analysis are compared to the experimental, analytical and numerical results available.

Finally a summary of the procedure developed in the study is given in Chapter 8. Recommendations and suggestions for future work are also given.

CHAPTER 2

BASIC RELATIONSHIPS AND FINITE ELEMENT FORMULATION

2.1 INTRODUCTION

In the elastic analysis of plates, the membrane forces developed through geometrically nonlinear behaviour may cause a considerable decrease of displacements as compared with the linear solution. Geometric nonlinearity should be considered in the analysis of plates if the membrane forces are to be included or large deflections occur. In this chapter the finite element formulation for the analysis of elastic geometrically nonlinear structures will be presented.

The assumptions that are generally made to derive the equations of plate theory and which are used in the finite element formulation will be discussed in section 2.2.

In section 2.3 the various Lagrangian approaches that could be used in the finite element formulation are discussed and the three basic sets of elasticity equations, namely those of strain-displacement, stress-strain and equilibrium are presented in section 2.4.

In section 2.5 the use of the virtual work equation, to establish the incremental equilibrium equation for use in the finite element formulation is discussed and the finite element formulation is presented in section 2.6.

In section 2.7 the basic assumptions discussed in this chapter and on which the present solution procedure is based, will be summarized.

2.2 BASIC ASSUMPTIONS

The classical plate theory based on Kirchhoff assumptions, in which normals to the plate middle surface are assumed to remain straight and normals during deformation, excludes transverse shear deformations.

Attempts to correct the theory and develop equations which allow for transverse shear deformations have been numerous [8]. Mindlin plate theory [9], in which the lateral displacements and the rotations are allowed to vary independently, has become the most commonly adopted theory for the analysis of plates using the finite element method. The independent variation of the lateral displacements and the rotations permits transverse shear deformations to be included in the formulation. These shear deformations are assumed to vary linearly throughout the thickness of the plate, Fig.2.1. Mindlin plate theory provides a more powerful alternative to the classical plate theory based on Kirchhoff assumptions. Finite element formulation based on Mindlin plate theory only require the continuity of the displacements across the element boundaries which makes the formulation of Mindlin elements simple and straightforward.

The main assumptions of Mindlin plate theory are:

a) Normal stresses in the direction normal to the plate middle surface are neglected.

b) Normal lines to the plate middle surface before deformation remain straight but not necessarily normal after deformation.

In order to determine the displacements u', v' and w' of an arbitrary point P' located at z from the middle surface, Fig.2.1, the displacements can be expressed in terms of the displacements at the middle surface such that

$$\begin{aligned} u' &= u - z\vartheta_x \\ v' &= v - z\vartheta_y \\ w' &= w \end{aligned} \tag{2.1}$$

where u,v and w are the displacements at the plate middle surface and θ_x and θ_y are the rotations of the normals to the undeformed middle surface in the xz and yz planes respectively. These rotations are given by

$$\begin{aligned} \theta_x &= \frac{\partial w}{\partial x} + \phi_x \\ \theta_x &= \frac{\partial w}{\partial y} + \phi_y \end{aligned} \tag{2.2}$$

where ϕ_x and ϕ_y are the average transverse shear deformations

2.3 LAGRANGIAN FORMULATION

In the geometric nonlinear finite element analysis of structures a total Lagrangian or an updated Lagrangian approach can be employed. In the total Lagrangian approach the initial configuration is used as reference configuration and any differentiation or integration is carried out over the undeformed original configuration. In the

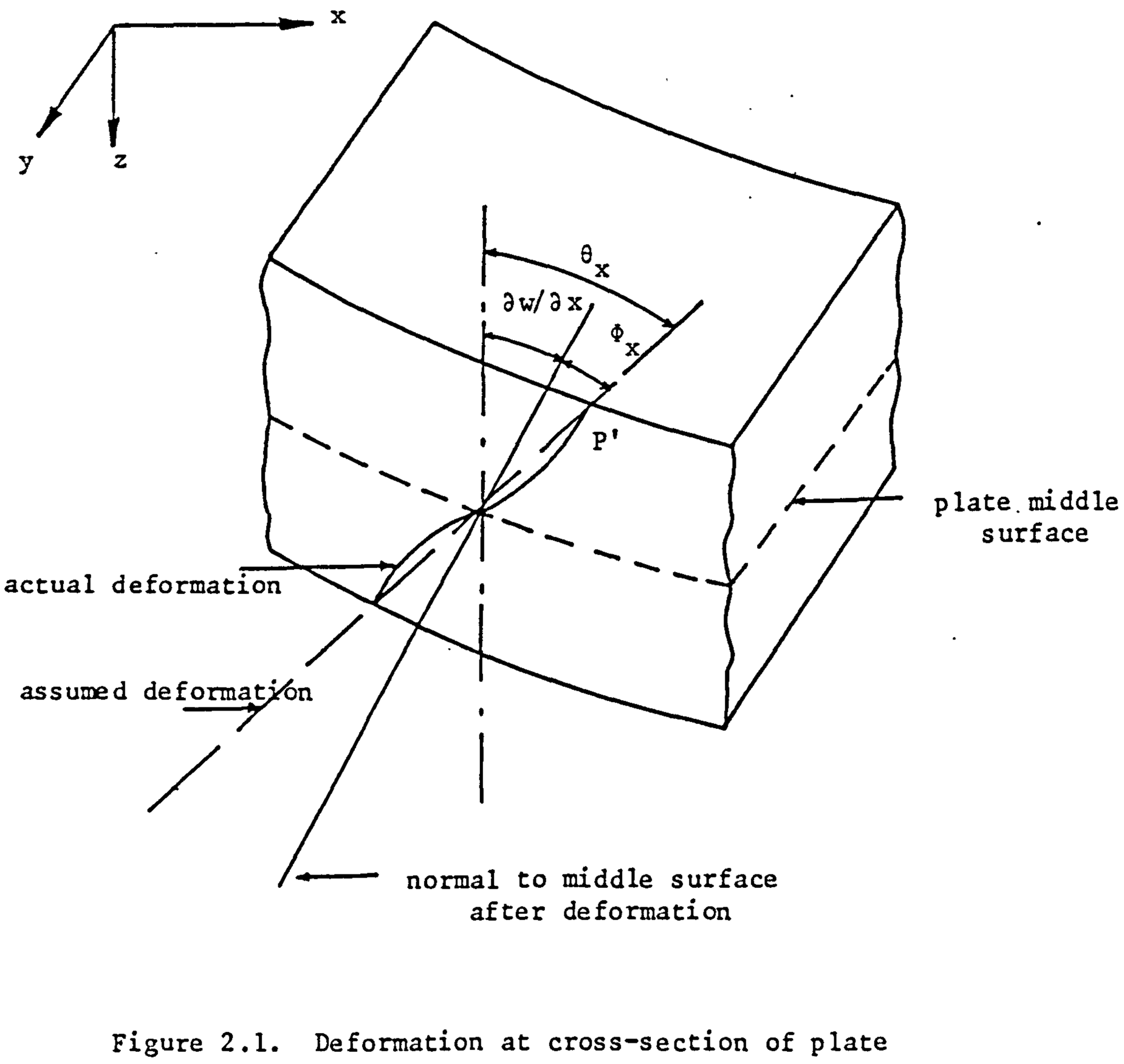

Figure 2.1. Deformation at cross-section of plate

updated Lagrangian approach the reference configuration corresponds to the last updated deformed configuration and any differentiation or integration is carried out over the deformed configuration.

Both the total Lagrangian and the updated Lagrangian approaches can be formulated to include geometric and material nonlinearties and lead to identical results [10-11]. The only reason for using one approach rather than the other is computational efficiency. An advantage of the total Lagrangian approach is that derivatives of the displacements are with respect to the initial configuration, and therefore need only be formed once. In this study the total Lagrangian approach is used.

2.4 BASIC RELATIONSHIPS

The behaviour of a solid body subjected to external forces is governed by three fundamental equations, namely strain-displacement, stress-strain and equilibrium equations. These relationships will be presented in this section with reference to a Mindlin plate formulation.

2.4.1 STRAIN-DISPLACEMENT RELATIONSHIP

The basic measure of strains at an arbitrary point located at z from the middle surface of a plate is represented by Green's strain vector ε' and is given by [12]

$$\{\varepsilon'\} = \begin{bmatrix} \varepsilon'_x \\ \varepsilon'_y \\ \gamma'_{xy} \\ \gamma'_{xz} \\ \gamma'_{yz} \end{bmatrix} = \begin{bmatrix} \frac{\partial u'}{\partial x} + \frac{1}{2}\left(\frac{\partial u'}{\partial x}\right)^2 + \frac{1}{2}\left(\frac{\partial v'}{\partial x}\right)^2 + \frac{1}{2}\left(\frac{\partial w'}{\partial x}\right)^2 \\ \frac{\partial v'}{\partial y} + \frac{1}{2}\left(\frac{\partial u'}{\partial y}\right)^2 + \frac{1}{2}\left(\frac{\partial v'}{\partial y}\right)^2 + \frac{1}{2}\left(\frac{\partial w'}{\partial y}\right)^2 \\ \frac{\partial u'}{\partial y} + \frac{\partial v'}{\partial x} + \frac{\partial u'}{\partial x}\cdot\frac{\partial u'}{\partial y} + \frac{\partial v'}{\partial x}\cdot\frac{\partial v'}{\partial y} + \frac{\partial w'}{\partial x}\cdot\frac{\partial w'}{\partial y} \\ \frac{\partial u'}{\partial z} + \frac{\partial w'}{\partial x} + \frac{\partial u'}{\partial x}\cdot\frac{\partial u'}{\partial z} + \frac{\partial v'}{\partial x}\cdot\frac{\partial v'}{\partial z} + \frac{\partial w'}{\partial x}\cdot\frac{\partial w'}{\partial z} \\ \frac{\partial v'}{\partial z} + \frac{\partial w'}{\partial y} + \frac{\partial u'}{\partial y}\cdot\frac{\partial u'}{\partial z} + \frac{\partial v'}{\partial y}\cdot\frac{\partial v'}{\partial z} + \frac{\partial w'}{\partial y}\cdot\frac{\partial w'}{\partial z} \end{bmatrix} \tag{2.3}$$

Equation (2.3) is valid for whether displacements or strains are large or small. If the strains are assumed to remain small, using the Von Karman assumptions [13], implies that derivatives of u' and v' are small, and therefore multiples of such derivatives can be neglected. The strain-displacement equation, equation (2.3), can be expressed in terms of the deformations of the plate middle surface, equation (2.1), such that

$$\{\varepsilon\} = \begin{bmatrix} \varepsilon_p^L \\ 0 \end{bmatrix} + \begin{bmatrix} z\varepsilon_b^L \\ \varepsilon_s^L \end{bmatrix} + \begin{bmatrix} \varepsilon_p^{NL} \\ 0 \end{bmatrix} \tag{2.4}$$

where the linear in-plane strains are given by

$$\varepsilon_p^L = \begin{bmatrix} \frac{\partial u}{\partial x} \\ \frac{\partial u}{\partial y} \\ \frac{\partial u}{\partial y} + \frac{\partial v}{\partial x} \end{bmatrix} \tag{2.5a}$$

the linear flexural strains are given by

$$\varepsilon_b^L = \begin{bmatrix} -\frac{\partial \theta x}{\partial x} \\ -\frac{\partial \theta v}{\partial y} \\ -\frac{\partial \theta x}{\partial y} - \frac{\partial \theta v}{\partial x} \end{bmatrix} \tag{2.5b}$$

the linear transverse shear strains are given by

$$\varepsilon_s^L = \begin{bmatrix} \frac{\partial w}{\partial x} - \theta_x \\ \frac{\partial w}{\partial y} - \theta_y \end{bmatrix} \tag{2.5c}$$

and the nonlinear in-plane strains are given by

$$\varepsilon_p^{NL} = \begin{bmatrix} \frac{1}{2} \left(\frac{\partial w}{\partial x}\right)^2 \\ \frac{1}{2} \left(\frac{\partial w}{\partial y}\right)^2 \\ \frac{\partial w}{\partial x} \cdot \frac{\partial w}{\partial y} \end{bmatrix} \tag{2.5d}$$

2.4.2 STRESS-STRAIN RELATIONSHIP

For a linear elastic isotropic material, Green's strain vector ε is related to the Piola-Kirchhoff stress vector σ by the following constitutive relationship:

$$\{\sigma\} = [D] \{\varepsilon\} \tag{2.6}$$

where the Piola-Kirchhoff stress vector is given by

$$\{\sigma\} = \{\sigma_x \ \sigma_y \ \tau_{xy} \ \tau_{xz} \ \tau_{yz}\}^T \tag{2.7a}$$

the elastic material matrix [D] is given by

$$[D] = \frac{E}{(1-\nu^2)} \begin{bmatrix} 1 & \nu & 0 & 0 & 0 \\ \nu & 1 & 0 & 0 & 0 \\ 0 & 0 & \frac{1-\nu}{2} & 0 & 0 \\ 0 & 0 & 0 & \frac{1-\nu}{2} & 0 \\ 0 & 0 & 0 & 0 & \frac{1-\nu}{2} \end{bmatrix} \qquad (2.7b)$$

where E and ν are Young's modulus and Poisson's ratio respectively.

The plate formulation can be reduced to a two-dimensional form by virtue of the Mindlin assumptions that normals to the plate middle surface remain straight during deformations. The strains can be expressed in terms of the deformations at the plate middle surface and the stresses in terms of their resultants. The stress resultants, $\bar{\sigma}$, can be obtained by integrating the stress distribution throughout the plate thickness. For an elastic material the integration can be carried out explicitly such that

$$\{\bar{\sigma}\} = \int_{z_2}^{z_1} \begin{bmatrix} \sigma_x \\ \sigma_y \\ \tau_{xy} \\ \hline z\sigma_x \\ z\sigma_y \\ z\tau_{xy} \\ \hline \tau_{xz} \\ \tau_{yz} \end{bmatrix} \cdot dz = \begin{bmatrix} \bar{\sigma}_p \\ \hline \bar{\sigma}_b \\ \hline \bar{\sigma}_s \end{bmatrix} \qquad (2.8)$$

where z_1 and z_2 are the co-ordinates of the top and bottom of the plate respectively, with the z-direction being the normal to the plate surface. The stress resultant components acting per unit width of the plate, $\bar{\sigma}_p$, $\bar{\sigma}_b$ and $\bar{\sigma}_s$ are the in-plane forces, moments and transverse shear forces respectively.

The strain vector associated with the stress resultants given in equation (2.8) may be expressed in terms of a linear and a nonlinear strain parts such that

$$\{\bar{\varepsilon}\} = \{\bar{\varepsilon}^L\} + \{\bar{\varepsilon}^{NL}\} = \begin{bmatrix} \varepsilon_p^L \\ \varepsilon_b^L \\ \varepsilon_s^L \end{bmatrix} + \begin{bmatrix} \varepsilon_p^{NL} \\ 0 \\ 0 \end{bmatrix} \qquad (2.9)$$

The constitutive relationship, equation (2.6), can be written in terms of the stress resultant vector, equation (2.8), and the associated total strain vector, equation (2.9), such that

$$\{\bar{\sigma}\} = [\bar{D}]\ \{\bar{\varepsilon}\} \qquad (2.10)$$

Rewriting equation (2.10) in terms of the stress resultant components the constitutive relationship is given by

$$\begin{bmatrix} \bar{\sigma}_p \\ \hline \bar{\sigma}_b \\ \hline \bar{\sigma}_s \end{bmatrix} = \left[\begin{array}{c|c|c} \bar{D}_p & 0 & 0 \\ \hline 0 & \bar{D}_b & 0 \\ \hline 0 & 0 & \bar{D}_s \end{array}\right] \left(\begin{bmatrix} \varepsilon_p^L \\ \hline \varepsilon_b^L \\ \hline \varepsilon_s^L \end{bmatrix} + \begin{bmatrix} \varepsilon_p^{NL} \\ \hline 0 \\ \hline 0 \end{bmatrix} \right) \qquad (2.11a)$$

where the in-plane material matrix $\bar{D}_p$ is given by

$$[\bar{D}_p] = \frac{Et}{(1-\nu^2)} \begin{bmatrix} 1 & \nu & 0 \\ \nu & 1 & 0 \\ 0 & 0 & \frac{1-\nu}{2} \end{bmatrix} \qquad (2.11b)$$

the flexural material matrix $\bar{D}_b$ is given by

$$[\bar{D}_b] = \frac{Et^3}{12(1-\nu^2)} \begin{bmatrix} 1 & \nu & 0 \\ \nu & 1 & 0 \\ 0 & 0 & \frac{1-\nu}{2} \end{bmatrix} \qquad (2.11c)$$

and the transverse shear material matrix $\bar{D}_s$ is given by

$$[\bar{D}_s] = \frac{Et\kappa}{(1-\nu^2)} \begin{bmatrix} \frac{1-\nu}{2} & 0 \\ 0 & \frac{1-\nu}{2} \end{bmatrix} \qquad (2.11d)$$

where t is the plate thickness, κ is a transverse shear correction factor which is necessary to account for the assumption of constant transverse shear strains and is equal to 5/6 for a homogeneous rectangular cross-section [14].

2.4.3 EQUILIBRIUM EQUATIONS

The equilibrium equations for a three-dimensional solid body can be written as [15]

$$\frac{\partial \sigma_x}{\partial x} + \frac{\partial \tau_{xv}}{\partial y} + \frac{\partial \tau_{xz}}{\partial z} = f_x$$

$$\frac{\partial \sigma_y}{\partial y} + \frac{\partial \tau_{xv}}{\partial x} + \frac{\partial \tau_{vz}}{\partial z} = f_y \qquad (2.12)$$

$$\frac{\partial \sigma_z}{\partial z} + \frac{\partial \tau_{xz}}{\partial x} + \frac{\partial \tau_{yz}}{\partial y} = f_z$$

where f_x, f_y and f_z are body forces acting per unit volume.

The principle of virtual work has been used to determine the governing equilibrium equations for use in the finite element formulation. Consider a body with volume V and surface S which consists of two parts. On one part, S_1, the surface tractions P are prescribed, while the boundary conditions are prescribed on the other part, S_2. Then using equation (2.12), the prescribed conditions on the surface and Green's theorem the virtual work equation can be written as [16]

$$\int_v d\varepsilon^T \sigma dv - \int_v du^T f dv - \int_{S_1} du^T p ds = 0 \qquad (2.13)$$

where $d\varepsilon$ is the virtual Green's strain vector due to the virtual displacement field du and σ and f are the stresses and body forces respectively. Equation (2.13) satisfies the equilibrium and

compatability conditions but no assumptions have been made about the material properties and the size of the deformations. Therefore it can be used for solution of problems involving geometric and material nonlinearities.

2.5 VIRTUAL WORK EQUATION

In the application of the finite element method to the solution of nonlinear structrual problems using a total Lagrangian or an updated Lagrangian approaches, an incremental equilibrium equation can be established using the virtual work equation. Such an equation makes the solution of a series of linear problems possible, leading to a stable equilibrium position of the structure in the deformed position.

The virtual work equation, equation (2.13), can be expressed in terms of the stress resultants and the associated strains such that

where $d\bar{\varepsilon}$ is the virtual strain vector due to the virtual displacement at the plate middle surface du. $\bar{f}$ is the body forces per unit area.

In the next section it will be shown how equation (2.14) is used to obtain an incremental finite element formulation.

2.6 FINITE ELEMENT FORMULATION

In the last decade the finite element method has become one of the most powerful approximate methods in engineering analysis. Several texts [16-17] have been written containing details about the method, therefore only a brief description of the method, will be presented here.

The basic concept of the method, when applied to problems of structural analysis, is that the structure can be modelled analytically by subdividing it into regions or finite elements joined at and interacting with each other only at selected nodal points. The elements are assumed to be able to represent the general behaviour of the structure between the nodal points. To accomplish this a function representing displacement, strain or stress fields within an element is approximated by a set of interpolation functions. In the displacement formulation the displacement field u is expressed in terms of the nodal values δ and a set of interpolation functions N such that

$$u = N.\delta \tag{2.15}$$

Strains are related to the nodal values by the following relations

$$\varepsilon = L.u \tag{2.16a}$$

$$\varepsilon = B.\delta \tag{2.16b}$$

where L is a differential matrix operator and B is a strain-displacement matrix.

The virtual work equation, equation (2.14), contains the variation of the strain vector $d\bar{\varepsilon}$ due to the virtual displacement du. The variation of the displacement field, equation (2.15), is given by

$$du = N.d\delta \tag{2.17}$$

The variation of the strain vector, equation (2.9), can be expressed in terms of the linear and nonlinear components such that

$$d\bar{\varepsilon} = d\bar{\varepsilon}^{L} + d\bar{\varepsilon}^{NL} \tag{2.18}$$

The variation of the strain vector, equation (2.18), may be written in terms of the variation of the nodal displacements δ such that

$$d\bar{\varepsilon} = [B_L + B_{NL}].d\delta \tag{2.19}$$

where B_L and B_{NL} are a linear and a nonlinear strain-displacement matrices.

In the application of the finite element method the equilibrium is established by calculating the internal resistance forces in the structure due to the deformations and comparing these forces with the externally applied loads. When the difference, which can be considered as unbalanced forces, is within an acceptable tolerance, equilibrium is assumed to have occurred. The equilibrium equation for internal and external forces can be obtained by substituting equations (2.17) and (2.19) into the virtual work equation, equation (2.14) such that

$$\psi(\delta) = F - P \tag{2.20}$$

where the internal force vector F is given by

$$F = \sum_{ele} \int_{A_e} [B_L + B_{NL}]^T \{\bar{\sigma}\} dA_e \tag{2.21a}$$

the applied load vector P is given by

$$P = \sum_{ele} \int_{A_e} N^T \bar{f} dA_e + \int_{S_1} N^T p ds \tag{2.21b}$$

$\psi(\delta)$ is the unbalanced forces and $\sum_{ele}$ and A_e denote the summations over all elements and the area of an element respectively.

Taking variations of equation (2.20) with respect to the nodal displacements δ. The tangent stiffness matrix can be obtained such that

$$\frac{d\psi}{d\delta} = K_T \tag{2.22}$$

where K_T is the tangent stiffness matrix and is given by [16].

$$K_T = K_o + K_\sigma + K_L \tag{2.23}$$

where K_o represents the usual, small displacement stiffness matrix and is given by

$$[K_o] = \sum_{ele} \int_{A_e} [B_L]^T [\bar{D}] \ [B_L] dA_e \tag{2.24a}$$

K_σ is the geometric stiffness matrix which depends on the stress level and is given by

$$[K_\sigma]\,d\delta = \sum_{ele} \int_{A_e} d[B_{NL}]^T\{\bar{\sigma}\}dA_e \qquad (2.24b)$$

K_L is the large displacement matrix which depends on the current displacements and is given by

$$[K_L] = \sum_{ele}\left[\int_{A_e}[B_L]^T[\bar{D}][B_{NL}]dA_e + \int_{Ae}[B_{NL}]^T[\bar{D}][B_L]dA_e + \int_{A_e}[B_{NL}]^T[\bar{D}][B_{NL}]dA_e\right] \qquad (2.24c)$$

2.7 SUMMARY

The basic assumptions which are used for the development of the solution procedure employed in this study have been summarized. The total Lagrangian approach is used, which means that the initial undeformed configuration is used as the reference. It should be noted that although deflections can be large the resulted strains are assumed to remain small.

The constitutive models for the materials to be considered, namely steel, concrete and reinforcing steel, are dealt with in detail in Chapter 5. The finite elements used and the evaluation of the stiffness matrices are presented in Chapter 3.

CHAPTER 3

FINITE ELEMENTS AND EVALUATION OF THE STIFFNESS MATRICES

3.1. INTRODUCTION

In the finite element displacement formulation based on the classical plate theory, the shape functions require C^1 continuity of the lateral displacement and its derivatives across the element boundaries. Shape functions which satisfy the C^1 continuity condition are complex and difficult to specify. Non-conforming shape functions, in which the continuity of the derivatives of the lateral displacements across the element boundaries is ignored, have led to the development of several successful non-conforming plate bending elements [18-21]. However the convergence of all such elements is not guaranteed and in order to ensure the convergence of a particular element it is necessary that it should pass the patch test [21]. In the patch test a set of nodal displacements corresponding to various states of constant strain are imposed on an arbitrary patch of elements. If nodal equilibrium is simultaneously achieved, without the imposition of external nodal forces, and a state of constant stress is obtained, then such an element is likely to converge and thus lead to correct solutions [16].

In the finite element formulation using Mindlin theory, because the lateral displacements and the normal rotations are allowed to vary independently, the shape functions only require C^o continuity. This requirement makes Mindlin elements easier to formulate and such formulation can be applied to thick and thin plates, curved boundaries and composite materials.

In Section 3.2 the various Mindlin plate bending elements are discussed. The elements used in the study are presented in Section 3.3 and the finite element representation is given in Section 3.4. The stiffness matrices and the numerical evaluation of such matrices are presented in Sections 3.5 and 3.6.

3.2 MINDLIN PLATE BENDING ELEMENTS

Several Lagrangian and serendipity elements based on Mindlin formulation have been developed and used in the finite element analysis of plates and shells. However, when exact numerical integration is used with such elements, unstable convergence characteristics have been observed in the analysis of thin plates. This phenomena is usually referred to in the literature as "locking" and is caused by the constraints imposed by shear strain energy terms existing in the total energy formulation, which require the derivatives of the lateral displacements to be equal to the normal rotations. These constraints will lead to overstiff results in the analysis of thin plates.

The performance of Mindlin elements has been improved dramatically using reduced and selective integration schemes [22-26]. The reduced and selective integration have been employed for numerical efficiency and to avoid locking in the analysis of thin plates. Lagrangian elements are generally the most accurate Mindlin elements, yet they contain spurious zero-energy modes. On the other hand the serendipity elements exhibit bizzare convergence characteristic and divergence for

thin plates [27]. This problem has been resolved with the emergence of the Heterosis element [28], which employs a combination of Lagrangian and serendipity shape functions. The Heterosis element has an advantage over Lagrangian and serendipity elements in that it contains no zero-energy modes and it does not lock [28]. A comparison of the performance of these elements in an elastic linear analysis conducted by Hughes et al [28] and also shown in Fig.3.1 indicates that both Lagrangian and the Heterosis elements exhibit stable convergence characteristics for very thin plates, while the serendipity element diverges rapidly for plates with small aspect ratios. Pica et al [12] and Yang et al [29] have investigated the performance of several Mindlin elements for geometrically nonlinear analyses of thin plates and concluded that the Heterosis element has given the best overall performance when compared with Lagrangian and serendipity elements.

More recently Hughes et al [30] have developed a new 4-node quadrilateral element employing bilinear isoparametric shape functions. The element does not lock in the analysis of thin plates and contains no zero-energy modes, however its aspect ratio behaviour on some problems is disappointing.

3.3 ELEMENTS USED IN THE STUDY

Two elements have been employed in the study. The first is the Heterosis plate bending element which has been used for the analysis

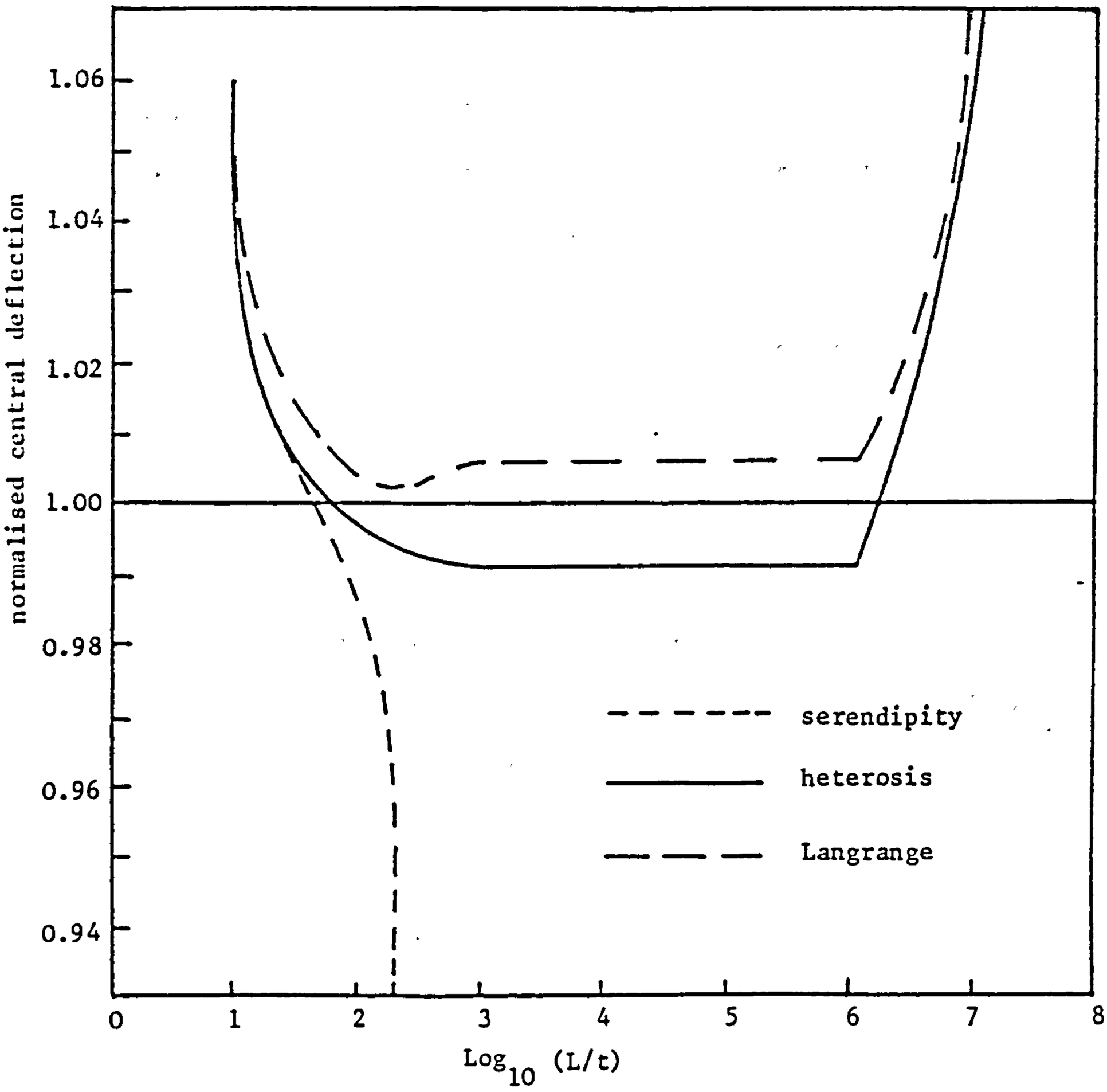

Figure 3.1. Aspect ratio study for clamped square plate [28]

of plates and slabs which undergo either small or large deflections. The second is the 8-node membrane element which has been used for the analysis of elastic stability of plates.

3.3.1 THE HETEROSIS PLATE BENDING ELEMENT

The Heterosis element is a 9-node quadrilateral with 8 nodes lying on the element boundary, Fig.3.2, which have W, θ_x and θ_y degrees of freedom and a node at the mid point which has θ_x and θ_y only. The element employs serendipity shape functions for the lateral displacements and Lagrangian shape functions for the rotations. The serendipity shape functions have been also employed to model the in-plane displacements u and v, for the nodes lying on the element boundaries, for the analysis of plates which undergo large deflections. The Heterosis element, the local numbering system and the local co-ordinates of the element are shown in Fig.3.2. The serendipity shape functions $N_i(\xi,\eta)$ for node i in terms of the local co-ordinates ξ,η are:

for the corner nodes i=1,3,5,7

$$N_i(\xi,\eta) = \tfrac{1}{4}(1 + \xi\xi_i)(1 + \eta\eta_i)(\xi\xi_i + \eta\eta_i - 1) \qquad (3.1)$$

for the midside nodes i=4,8

$$N_i(\xi,\eta) = \tfrac{1}{2}(1 - \xi^2)(1 + \eta\eta_i) \qquad (3.2)$$

and the midside nodes i=2,6

$$N_i(\xi,\eta) = \tfrac{1}{2}(1 - \eta^2)(1 + \xi\xi_i) \qquad (3.3)$$

The Lagrangian shape functions $P_i(\xi,\eta)$ for node i in terms of the local co-ordinates ξ,η are:

for nodes i=1,2,3

$$P_i(\xi,\eta) = N_1(\xi).N_j(\eta) \qquad j = 1,2,3 \qquad (3.4)$$

for nodes i=4,8,9

$$P_i(\xi,\eta) = \bar{N}_2(\xi).\ \bar{N}_j(\eta) \qquad j = 3,1,2 \qquad (3.5)$$

and nodes i=5,6,7

$$P_i(\xi,\eta) = \bar{N}_3(\xi).\ \bar{N}_j(\eta) \qquad j = 3,2,1 \qquad (3.6)$$

where

$$\bar{N}_1(\xi) = \xi(\xi - 1)/2$$

$$\bar{N}_2(\xi) = (1 + \xi)(1 - \xi) \qquad (3.7)$$

$$\bar{N}_3(\xi) = \xi(\xi + 1)/2$$

3.3.2 ISOPARAMETRIC MEMBRANE ELEMENT

The 8-node element employs the serendipity shape functions given in equations (3.1), (3.2) and (3.3) to represent the in-plane displacement fields u and v. The element, the local numbering system and the local co-ordinates are shown in Fig.3.3.

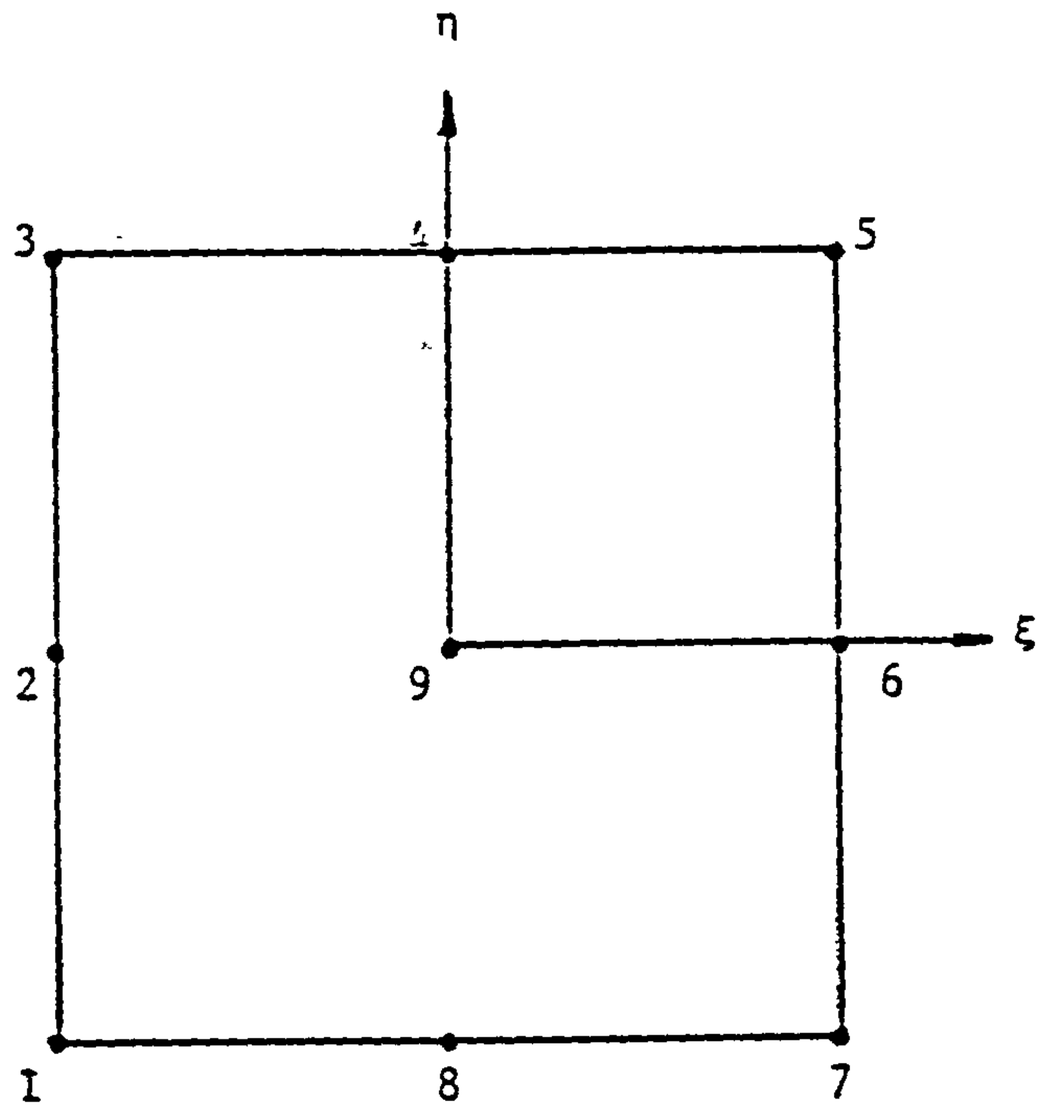

Figure 3.2. Heterosis plate bending element

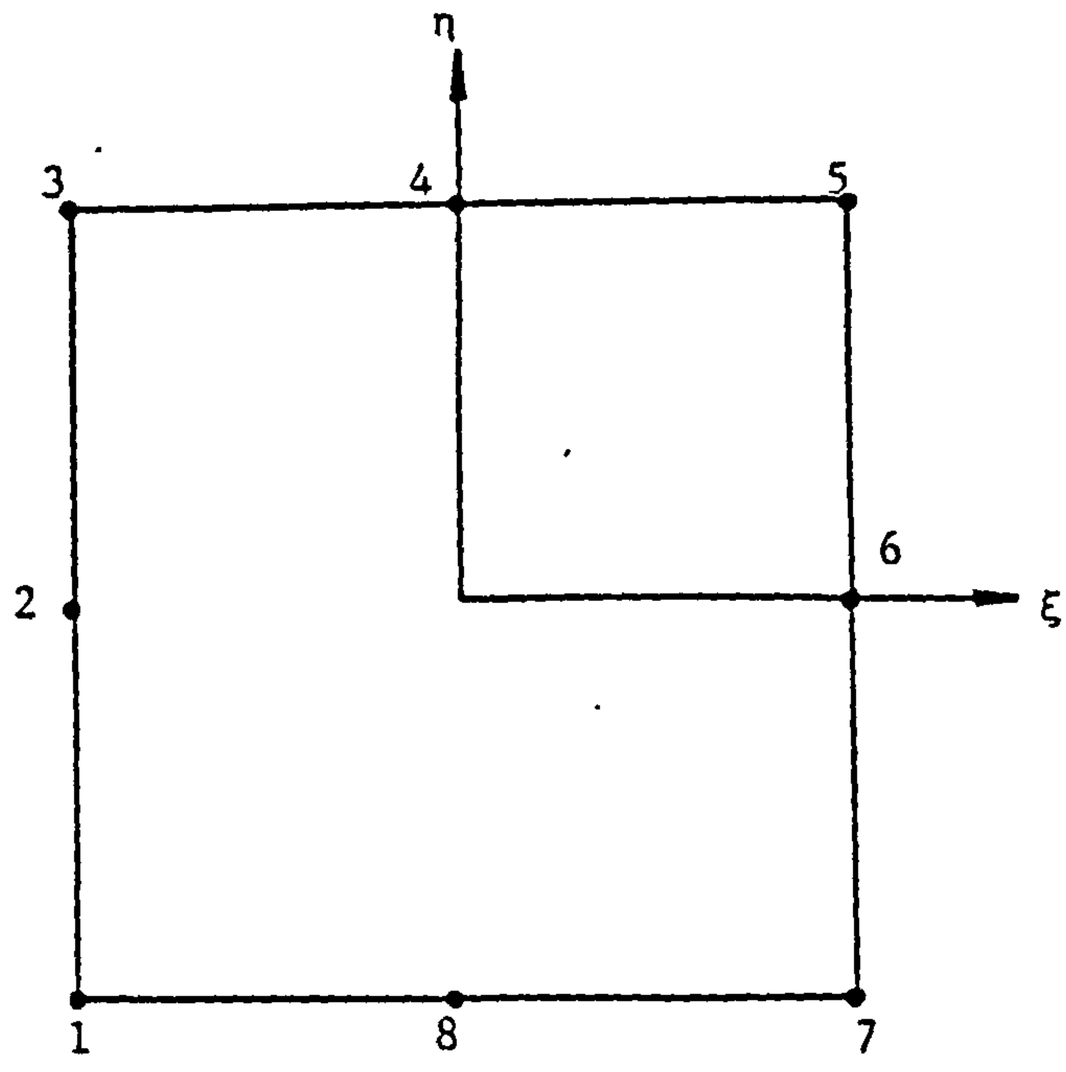

Figure 3.3. Serendipity membrane element

3.4 FINITE ELEMENT REPRESENTATION

The displacement fields within an element are assumed to be functions of a discrete nodal values and the shape functions.The in-plane displacement components u and v are approximated by

$$\begin{bmatrix} u \\ v \end{bmatrix} = \sum_{i=1}^{8} N_i \begin{bmatrix} U_i \\ V_i \end{bmatrix} \tag{3.8}$$

where N_i are the serendipity shape functions.

The lateral displacement w and the rotations θ_x and θ_y are approximated by

$$w = \sum_{i=1}^{8} N_i W_i \tag{3.9a}$$

$$\begin{bmatrix} \theta_x \\ \theta_y \end{bmatrix} = \sum_{i=1}^{9} P_i \begin{bmatrix} \theta_{xi} \\ \theta_{yi} \end{bmatrix} \tag{3.9b}$$

where P_i are Lagrangian shape functions

3.5 STIFFNESS MATRICES

The stiffness matrices used in the various analyses to be carried out will be formulated in this section using the finite element approximation given in equations (3.8) and (3.9). The small

displacement stiffness matrix K_o, equation (2.24a), is given by

$$K_o = \sum_{ele} \left[\int_{A_e} \left[\begin{array}{c|c} \begin{matrix} B_P^T \bar{D}_P B_P \end{matrix} & \begin{matrix} 0 \end{matrix} \\ \hline \begin{matrix} 0 \end{matrix} & \begin{matrix} B_b^T \bar{D}_b B_b \end{matrix} \end{array}\right] dA_e + \int_{A_e} \left[\begin{array}{c|c} \begin{matrix} 0 \end{matrix} & \begin{matrix} 0 \end{matrix} \\ \hline \begin{matrix} 0 \end{matrix} & \begin{matrix} B_s^T \bar{D}_s B_s \end{matrix} \end{array}\right] dA_e \right] \tag{3.10}$$

where the first term of equation (3.10) is the in-plane and flexural parts and the second term is the transverse shear part. The in-plane strain-displacement matrix B_p is given by

$$[B_p] = \begin{bmatrix} \frac{\partial N_i}{\partial x} & 0 \\ 0 & \frac{\partial N_i}{\partial y} \\ \frac{\partial N_i}{\partial y} & \frac{\partial N_i}{\partial x} \end{bmatrix} \tag{3.11a}$$

the flexural strain-displacement matrix B_b is given by

$$[B_b] = \begin{bmatrix} 0 & -\frac{\partial P_i}{\partial x} & 0 \\ 0 & 0 & -\frac{\partial P_i}{\partial y} \\ 0 & -\frac{\partial P_i}{\partial y} & -\frac{\partial P_i}{\partial x} \end{bmatrix} \tag{3.11b}$$

and the transverse shear strain-displacement matrix B_s is given by

$$[B_s] = \begin{bmatrix} \frac{\partial N_i}{\partial x} & -P_i & 0 \\ \frac{\partial N_i}{\partial y} & 0 & -P_i \end{bmatrix} \tag{3.11c}$$

If the length of the midsurface of the plate is assumed to remain constant, equation (3.10) can be expressed by

$$[K_b] = \sum_{ele} \left[\int_{A_e} B_b^T \bar{D}_b B_b \, dA_e + \int_{A_e} B_s^T \bar{D}_s B_s \, dA_e \right] \tag{3.12}$$

The geomtric stiffness matrix k_σ , equation (2.24b), can be expressed in terms of a flexural and a transverse shear parts such that [31-32]

$$[K_G] = \sum_{ele} \left[\int_{A_e} G_b^T \hat{\sigma} G_b . t \, dA_e + \int_{A_e} G_s^T \hat{\sigma} G_s . \frac{t^3}{12} . dA_e \right] \tag{3.13}$$

in which

$$[G_b] = \begin{bmatrix} 0 & 0 & \frac{\partial N_i}{\partial x} & 0 & 0 \\ 0 & 0 & \frac{\partial N_i}{\partial y} & 0 & 0 \end{bmatrix} \tag{3.14a}$$

$$[G_s] = \begin{bmatrix} 0 & 0 & 0 & \frac{\partial N_i}{\partial x} & \frac{\partial N_i}{\partial x} \\ 0 & 0 & 0 & \frac{\partial N_i}{\partial y} & \frac{\partial N_i}{\partial y} \end{bmatrix} \tag{3.14b}$$

$$[\hat{\sigma}] = \begin{bmatrix} \sigma_x & \tau_{xy} \\ \tau_{xy} & \sigma_y \end{bmatrix} \tag{3.14c}$$

where t is the plate thickness

The large displacement stiffness matrix K_L , equation (2.24c), is given by

$$[K_L] = \sum_{ele} \int_{A_e} \left[\begin{array}{c|cc} 0 & B_p^T \bar{D}_p & B_{NL} \\ \hline B_{NL}^T \bar{D}_p B_p & B_{NL}^T \bar{D}_p & B_{NL} \end{array}\right] dA_e \qquad (3.15)$$

where the nonlinear strain-displacement matrix B_{NL} is a function of the lateral displacement w and is given by

$$[B_{NL}] = \begin{bmatrix} \frac{\partial w}{\partial x} & 0 \\ 0 & \frac{\partial w}{\partial y} \\ \frac{\partial w}{\partial y} & \frac{\partial w}{\partial x} \end{bmatrix} \begin{bmatrix} \frac{\partial N_i}{\partial x} & 0 & 0 \\ \frac{\partial N_i}{\partial y} & 0 & 0 \end{bmatrix} \qquad (3.16)$$

The total stiffness matrix for in-plane behaviour of a plate loaded in its plane is given by

$$[K_p] = \sum_{ele} \int_{A_e} B_p^T \bar{D}_p B_p \, dA_e \qquad (3.17)$$

3.6 EVALUATION OF THE STIFFNESS MATRICES

The various stiffness matrices have been evaluated numerically using a selective integration scheme based on Gauss quadrature. A 3x3 rule for in-plane and flexural components and a 2x2 rule for the transverse shear component have been used. The derivatives of the shape functions are determined at the Gauss quadrature points in the local

co-ordinate system (ξ,η). The inverse of the Jacobian matrix is used to convert the derivatives from the local co-ordinate system to the global co-ordinate system (x,y), such that

$$\begin{bmatrix} \frac{\partial N}{\partial x} \\ \\ \frac{\partial N}{\partial y} \end{bmatrix} = [J]^{-1} \begin{bmatrix} \frac{\partial N}{\partial \xi} \\ \\ \frac{\partial N}{\partial \eta} \end{bmatrix} \qquad (3.18)$$

The integrations are carried out in the local co-ordinate system using the following transformation

$$\int\int f(x,y)\ dx\ dy = \sum_{i=1}^{n} f(\xi_i, \eta_i)\ \det\ [J].W_i \qquad (3.19)$$

where n is the number of Gauss points and W_i is the weight at the ith Gauss point.

CHAPTER 4

LINEAR ELASTIC ANALYSIS AND ELASTIC STABILITY OF PLATES

4.1 INTRODUCTION

In this chapter the results obtained for linear elastic analyses carried out to check the program and the finite element formulation are discussed in Section 4.2.

The geometric stiffness matrix required for the elastic stability of plates, depends on the in-plane stress distribution throughout the plate, for the load under consideration. Therefore the elastic stability analysis of plates can be carried out in two stages. In the first stage the internal distribution of stresses due to the applied loads is determined in an independent linear analysis. In the second stage of the analysis the geometric stiffness matrix is formed and the elastic buckling load can then be determined.

Several plates with and without openings and under different edge loading conditions were analysed. The buckling loads obtained for the various cases investigated were compared with the available analytical and numerical results obtained by other investigators. The elastic stability of plates is discussed in Section 4.3.

4.2 LINEAR ELASTIC ANALYSIS

Linear elastic analyses have been carried out to investigate the convergence characteristics of the elements used , to test the program and the finite element formulation.

The results obtained for the analysis of several plates with various boundary conditions under different loadings gave identical results to those obtained by others [28].

4.3 ELASTIC STABILITY OF PLATES

The finite element method was first applied to the elastic stability of plates by Kapur et al [33], who used non-conforming rectangular bending elements to obtain the buckling loads for plates with no holes. Pifko et al [34] used conforming rectangular bending elements, the result of this was that the convergence characteristics of the solution were improved. The buckling loads given in Refs. [33-34] have been obtained where the in-plane stress distribution throughout the plate is constant. Obviously this approach cannot be applied to plates with holes because the stresses change rapidly in the vicinity of holes.

The first attempt to determine the buckling loads for square plates with circular holes under pure shear using the finite element method was made by Rockey et al [35], who used three noded triangular elements to determine the in-plane stresses and buckling loads. Shanmugan et al [36] used four noded rectangular elements to determine the in-plane stresses and buckling loads for square plates with square holes under pure shear. The solutions given in Refs. [35-36] failed

to converge onto the analytical solutions for plates with no holes as the size of the holes become small. Sabir et al [37] used a combination of triangular and rectangular strain based elements to determine the buckling loads for plates with holes. The use of triangular elements around circular holes resulted in inaccurate modelling for small circular holes.

4.3.1 GOVERNING EQUATIONS

The governing equation for the elastic stability of a plate loaded in its plane can be shown to take the following form

$$\left[[K] + \lambda[K_\sigma]\right]\{\delta\} = \{0\} \tag{4.1}$$

where K is the elastic flexural stiffness matrix, equation (3.12), K_σ is the geometric stiffness matrix which depends on the in-plane stress distribution through the plate, equation (3.13), λ is a stress factor necessary to achieve neutral equilibrium and δ is a displacement vector which consists of the lateral displacements and the rotations about the plane of the plate.

The in-plane stresses due to the various edge loadings are determined prior to the solution of equation (4.1), which can be shown to be related to the applied loads by the following relationship:

$$\{\sigma_p\} = [D_p][B_p][K_p]^{-1}\{P\} \tag{4.2}$$

where σ_p is the in-plane stresses due to the applied load P and B_p and K_p are the in-plane strain-displacement and the stiffness matrices given by equations (3.11a) and (3.17) respectively and the material matrix D_p is given by

$$[D_p] = \frac{E}{(1-\nu^2)} \begin{bmatrix} 1 & \nu & 0 \\ \nu & 1 & 0 \\ 0 & 0 & \frac{1-\nu}{2} \end{bmatrix} \qquad (4.3)$$

where E and ν are Young's modulus and Poisson's ratio respectively.

Equation (4.1) can be written in a generalized eigenvalue problem form, such that

$$\bar{\lambda} K \delta = \bar{K}_\sigma \delta \qquad (4.4)$$

where

$$\bar{\lambda} = \frac{1}{\lambda} \qquad (4.5a)$$

$$\bar{K}_\sigma = -K_\sigma \qquad (4.5b)$$

The elastic flexural stiffness matrix given in equation (4.4) is positive definite and the geometric stiffness matrix $\bar{K}_\sigma$ is in general indefinite. In solving equation (4.4) the highest eigenvalue is determined in order that the reciprocal of $\bar{\lambda}$ gives the lowest eigenvalue. The governing equation for the elastic stability was solved numerically using the NAG [38] library routines.

4.3.2 SOLUTION PROCEDURE

The procedures adopted to determine the elastic buckling loads are summarized as follows:

1- The in-plane stiffness matrix was formed, equation (3.17), using the 8-node isoparametric membrane element.

2- The in-plane stresses σ_p due to the edge loadings were determined by solving equation (4.2).

3- The flexural and geometric stiffness matrices were formed, equations (3.12) and (3.13), using the Heterosis element.

4- The elastic buckling loads were determined by solving equation (4.4), details of which are given in Appendix I.

4.3.3 NUMERICAL RESULTS

For a square plate under in-plane uniaxial, biaxial or shear loadings, the critical buckling stress, σ_{cr}, can be related to the buckling cofficient k by

$$\sigma_{cr} = \frac{k\,\pi^2 E}{12(1-\nu^2)} \cdot \left(\frac{t}{L}\right)^2 \qquad (4.6)$$

where t and L are the thickness and the length of the plate respectively.

The values of k for a square plate simply supported and subjected to a uniaxial, biaxial or shear loading are 4.0, 2.0 and 9.34. These values become 10.0, 5.3 and 14.7 when the edges are clamped.

4.3.3.1 SOLUTION CONVERGENCE

Convergence of the solution has been investigated for square plates under various edge loading conditions. To test the formulation the

buckling cofficients, for square plates with no holes under uniaxial and biaxial compression with both clamped and simply supported edges, were determined. A 4x4 mesh per quadrant of the plate gave good results compared with the analytical values. The percentage errors in the buckling cofficients were 0.5% and 0.12% for clamped and simply supported edges respectively for both loading conditions. Details of the rate of convergence with increasing the number of degrees of freedom for the cases mentioned are shown in Fig.4.1.

For clamped and simply supported square plates with and without openings under pure shear no use of symmetry was made because this requires a pre-knowledge of the lowest buckling modes. The convergence investigation, Fig.4.2, showed that for a square plate with a central circular hole 52 elements for clamped edges and 40 elements for simply supported edges gave sufficiently accurate results. Similarly for a square plate with a central square hole 60 elements were required for clamped edges and 48 elements for simply supported edges to produce sufficiently accurate results. A plate without a hole under pure shear using 49 and 36 elements gave a percentage error in the buckling cofficients of less than 1.5% for both clamped and simply supported edges compared with the analytical values.

4.3.3.2 SQUARE PLATES WITH CENTRAL CIRCULAR HOLES UNDER PURE SHEAR

The variations of the buckling coefficients with the ratio of the hole diameter to the plate length for both clamped and simply supported edges are shown in Fig.4.3, together with the results given in Refs.

[35] and [37]. The results obtained by Rockey et al [35] failed to converge onto the analytical solution for a plate without a hole. The results obtained in the study and those given in Ref. [37], which have been obtained using 85 elements to model a quarter of the plate, showed good agreement for plates with large circular holes and both results converge onto the analytical solutions for plates with no holes, however the buckling coefficients obtained in the present analyses are larger than those given in Ref. [37] for plates with small circular holes. This discrepancy is most likely due to the better modelling obtained by the use of the serendipity elements around the holes when compared with that obtained by using triangular elements in the vicinity of the hole as used by Sabir et al [37]. The finite element idealization for a square plate with a central circular hole is shown in Fig.4.4.

4.3.3.3 SQUARE PLATES WITH CENTRAL SQUARE HOLES UNDER PURE SHEAR

The finite element idealization for a square plate with a central square hole is shown in Fig.4.5. The variations of the buckling coefficients with the ratio of the hole length to the plate length for both clamped and simply supported plates are shown in Fig.4.6, together with the results given in Refs. [36] and [37]. The results obtained by Shanmugam et al [36] indicated that the buckling coefficients failed to converge onto the corresponding analytical values for a plate without a hole and that the buckling coefficients would reach a zero value before the plate is entirely covered by the hole. The results obtained gave good agreement with those obtained by Sabir et al [37] using 75 elements to model a quarter of the plate.

4.3.3.4 CIRCULAR PLATES UNDER RADIAL COMPRESSIVE PRESSURE

The buckling cofficients for a circular plate under radial compressive pressure with both clamped and simply supported edges, were determined using 12 elements to model a quarter of the plate for both cases. The buckling cofficients obtained were 4.21 and 14.77 for simply supported and clamped plates respectively compared with the corresponding analytical values of 4.20 and 14.68. The finite element idealization used to model a quarter of the circular plate is shown in Fig.4.7.

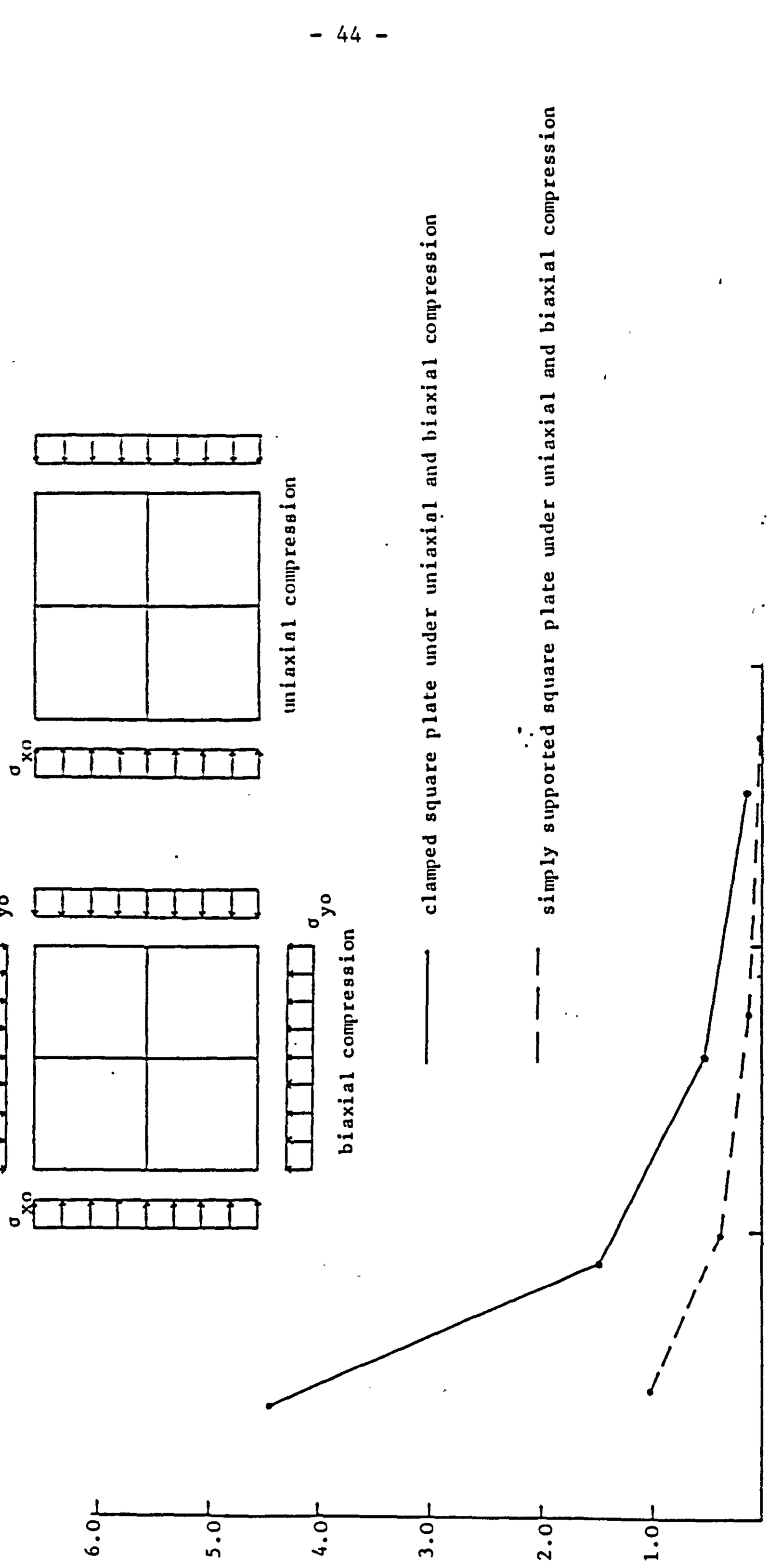

Figure 4.1. Convergence study for square plates under uniaxial and biaxial compression

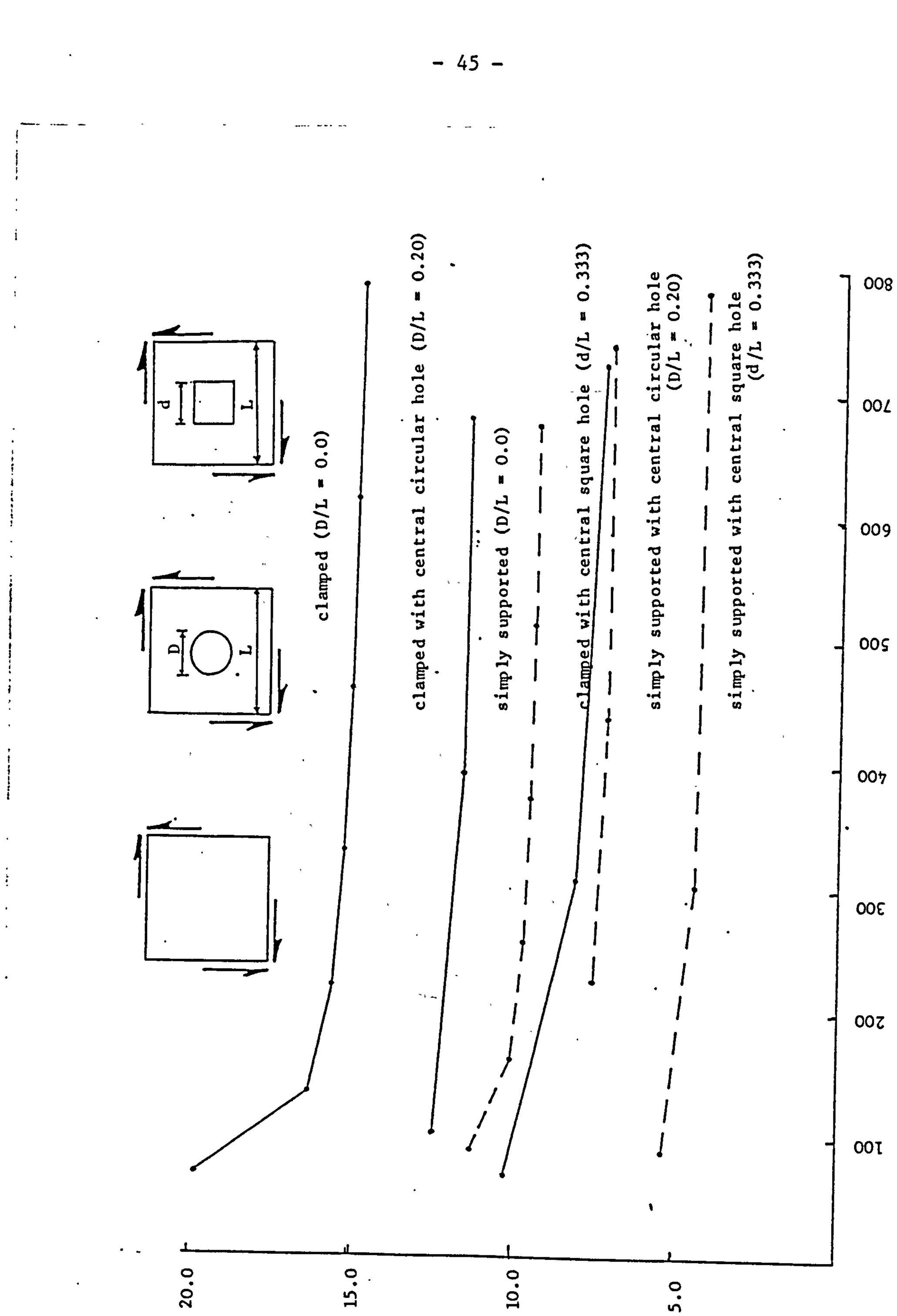

Figure 4.2. Convergence study for square plates with and without openings under pure shear

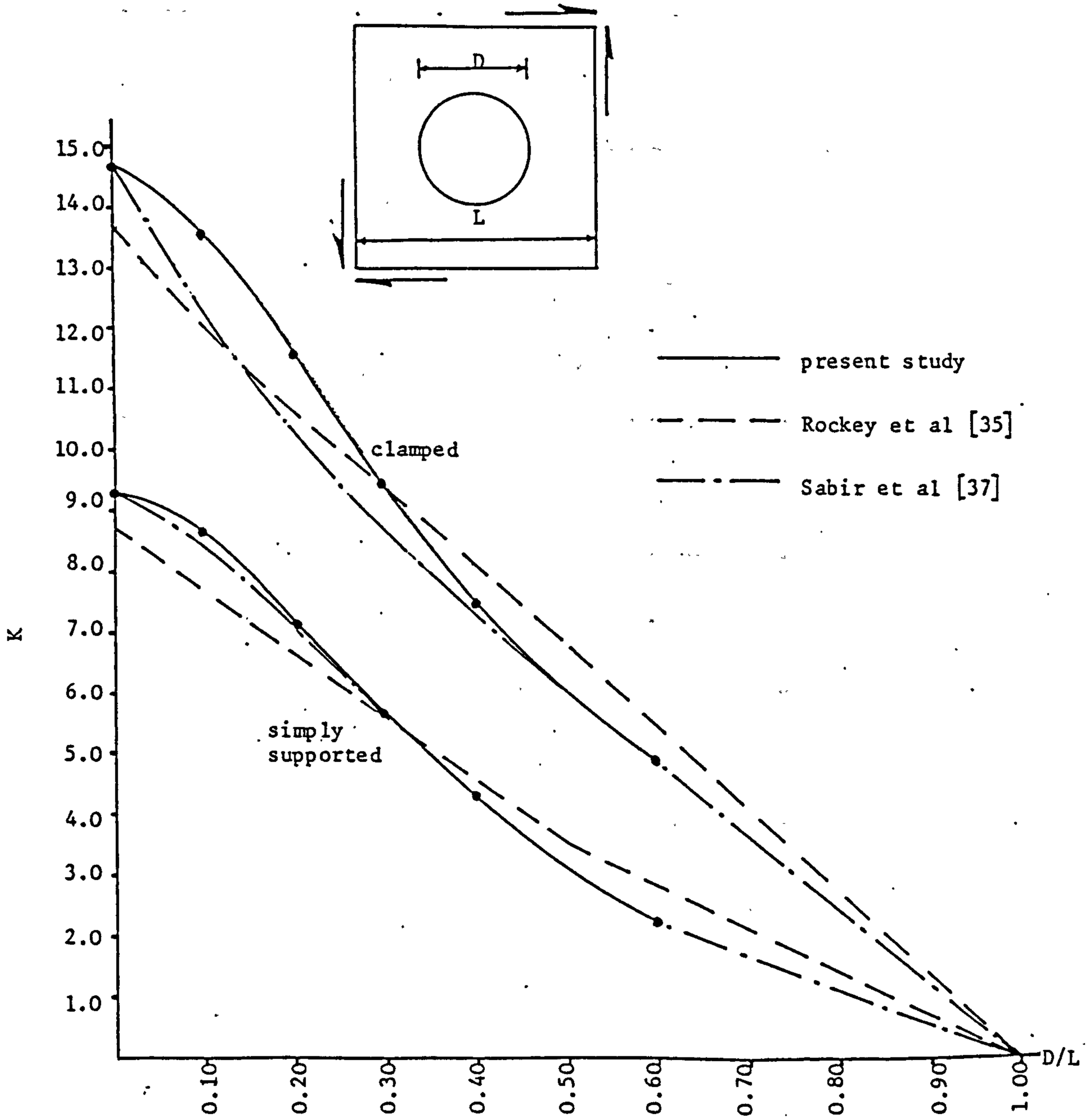

Figure 4.3. Variation of the buckling coefficient with the ratio of hole diameter to plate length for square plates under pure shear

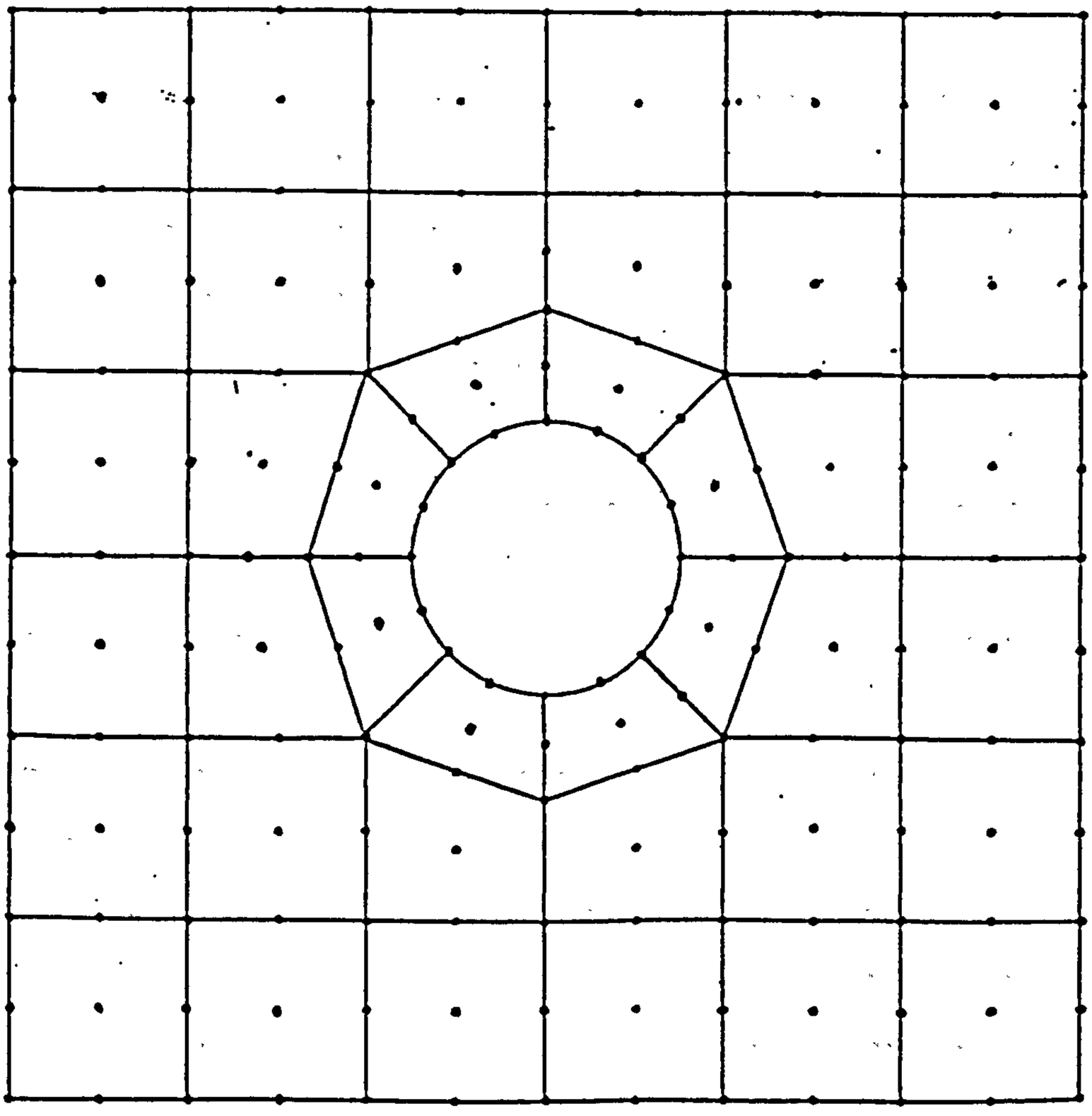

Figure 4.4. Finite element idealization for square plate with central circular hole

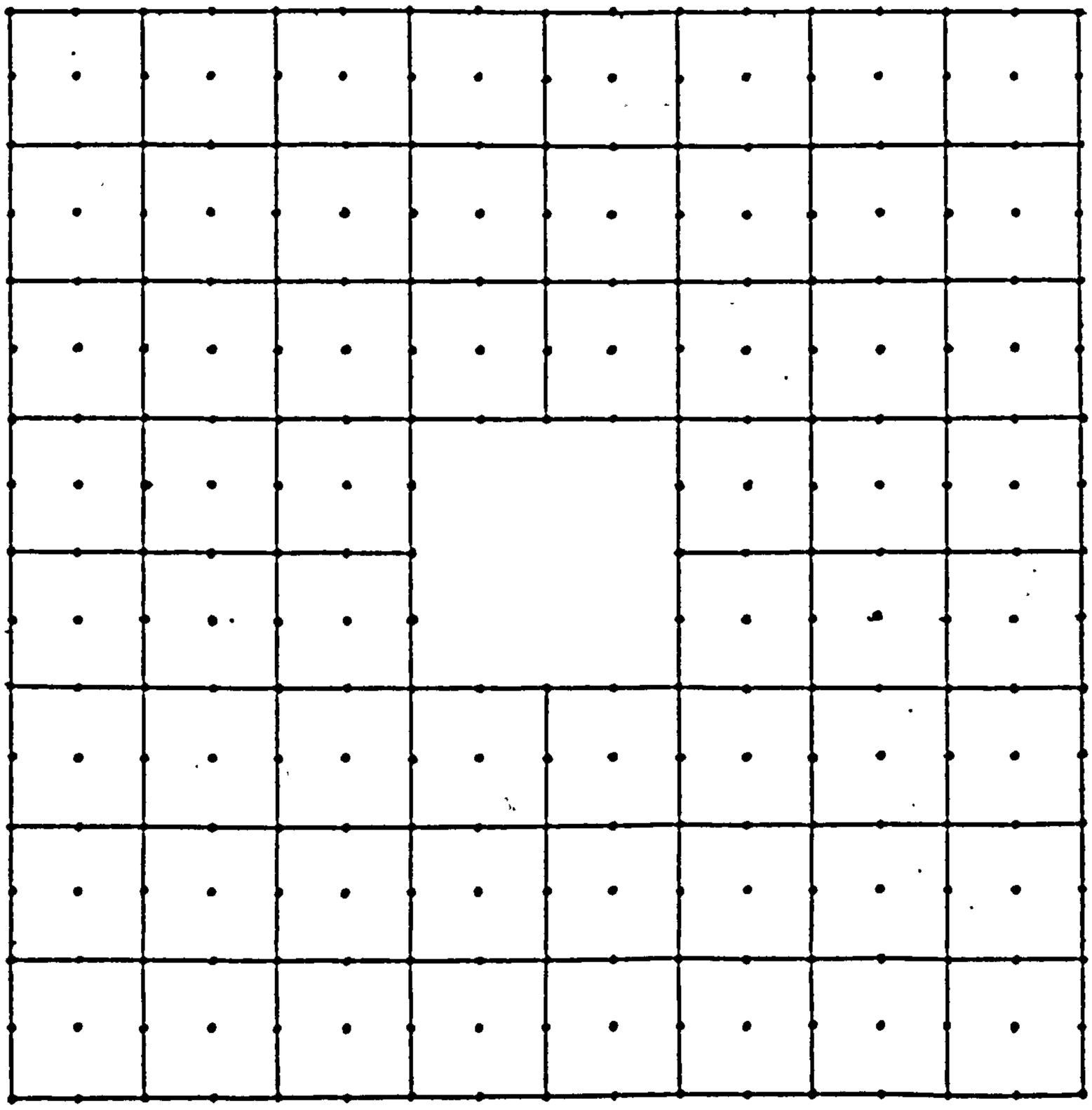

Figure 4.5. Finite element idealization for square plate with central square hole

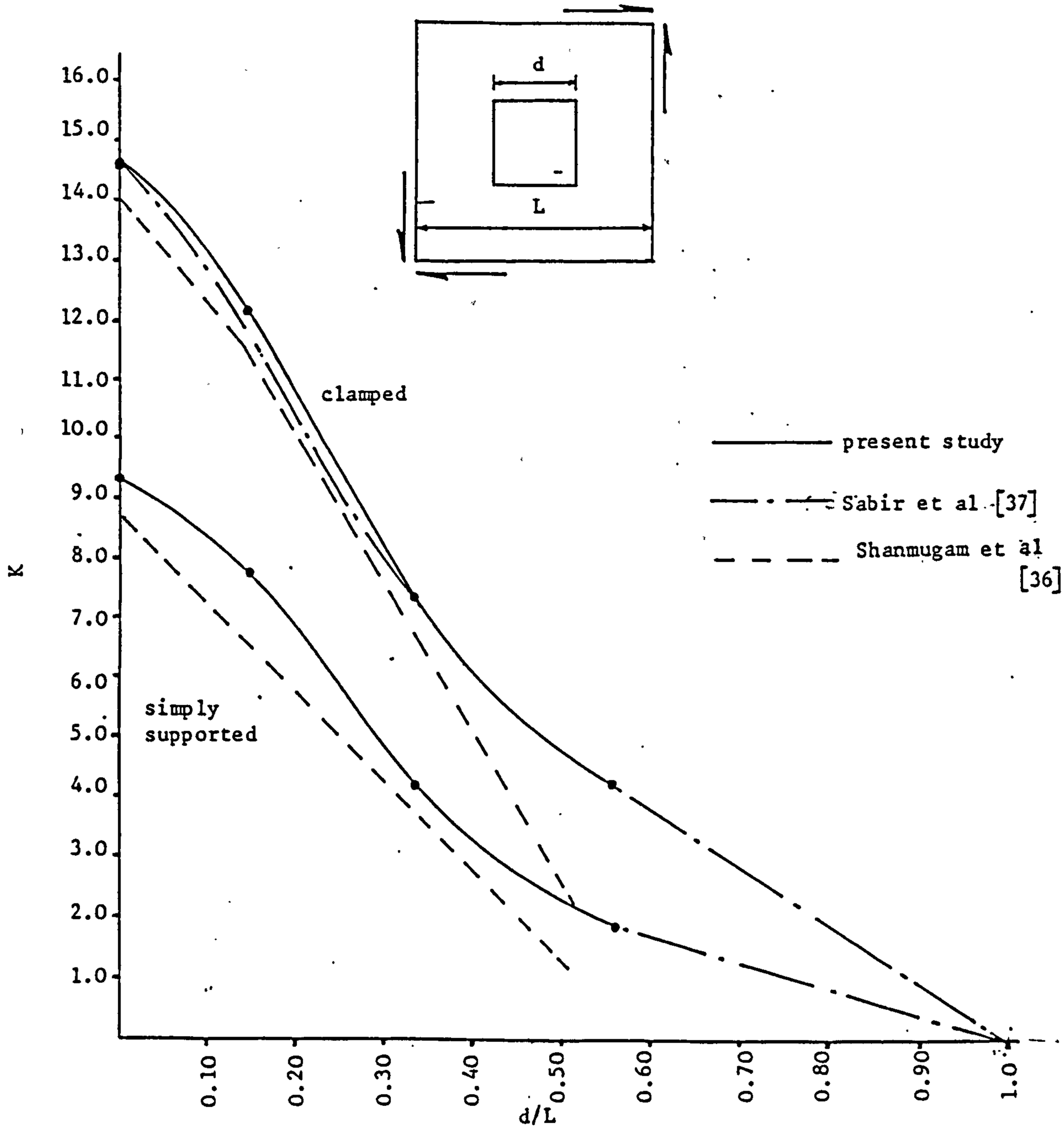

Figure 4.6. Variation of the buckling coefficients with the ratio of hole length to plate length for square plates under pure shear

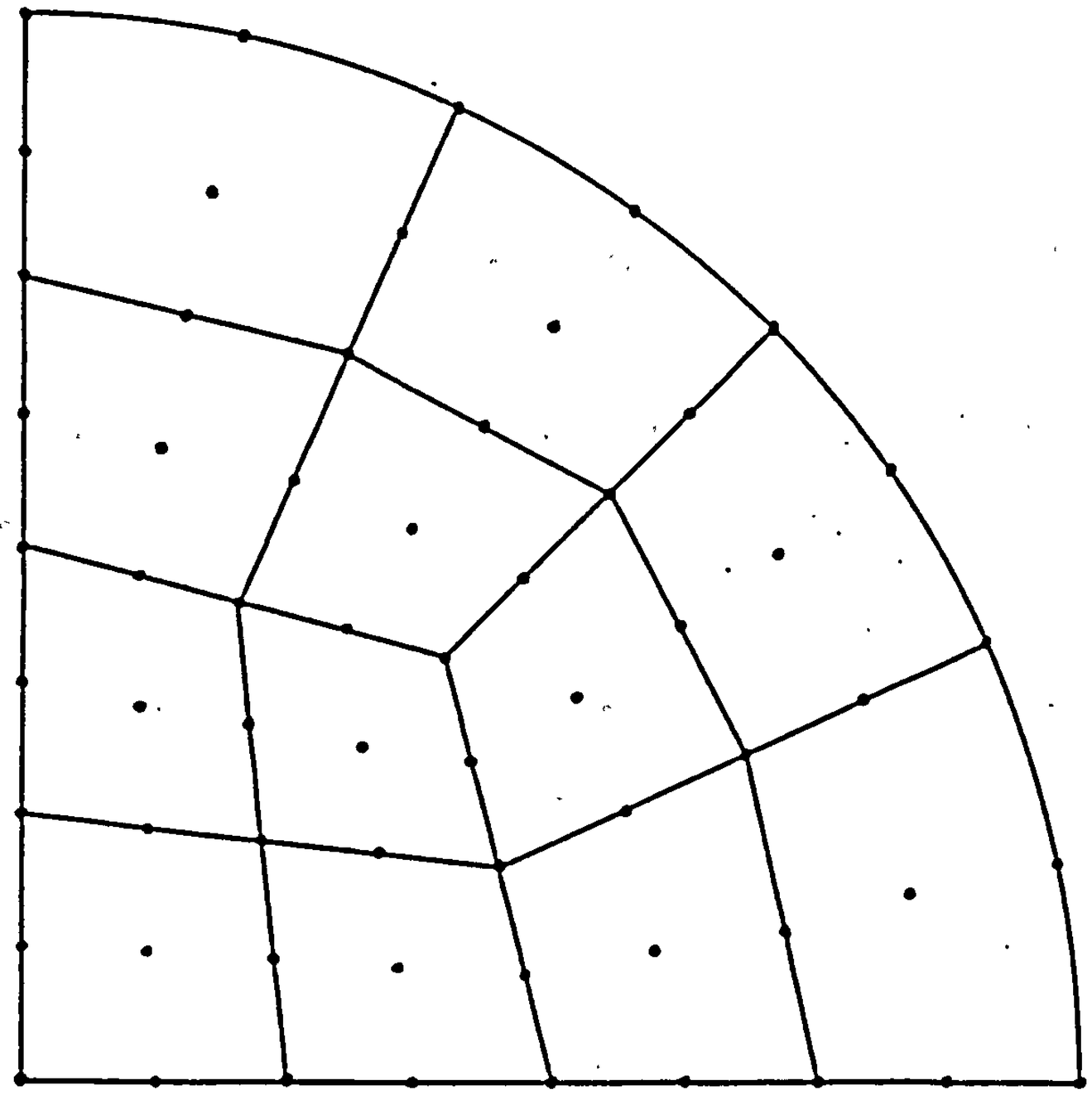

Figure 4.7. Finite element idealization for circular plate.

CHAPTER 5

NUMERICAL MODELLING OF THE MATERIAL PROPERTIES

5.1 INTRODUCTION

The numerical modelling of the material properties for use in a nonlinear finite element analysis is one of the most difficult and important aspects of any realistic analysis. The modelling of all of the aspects of the behaviour of a particular material would be extremely difficult. It is therefore more usual to use models which represent those aspects of behaviour which will effect most the response of the structure under the particular loading to be considered.

The analyses carried out involved both steel plates and reinforced concrete slabs and the relevant modelling of the material properties will be discussed for each type of analysis.

In the analysis of the steel plates the steel was considered as a homogeneous material with similar behaviour in tension and compression. The major source of material nonlinearity considered was flow due to plastic yielding.

Discussion of the model used for steel is presented in Section 5.2.

Reinforced concrete is a heterogeneous material consisting of concrete and steel reinforcing bars, the two materials having very different properties. In order to simulate the behaviour of the composite the two constituents were modelled independently. The interaction between

the two materials can be modelled by assuming some bond characteristic at the interface. Partial interaction can be modelled by assuming a bond-slip relationship. Full interaction, which was used throughout the study, assumes no slip and thus compatibility of deformations, at the interface between the two materials, was assumed to exist.

The major sources of nonlinearity in reinforced concrete structures are the inelastic response of concrete in compression, cracking of concrete in tension and the yielding of the reinforcing steel.

The behaviour of the concrete depends on the level and nature of stress to which it is subjected. Under uniaxial compression the concrete behaviour is approximately linear elastic, Fig.5.1, up to approximately 30% of its uniaxial ultimate compressive strength, f'_c. Beyond that concrete exhibits a nonlinear response. After the concrete reaches its ultimate compressive strength, the stress carried by the concrete decreases with increasing strain, until it reaches its ultimate strain, ε_{cu}, when it crushes and carry zero stress. Under uniaxial tensile stress, concrete is generally considered to behave as a linear elastic-brittle material. Cracks will form when the stress reaches the concrete tensile strength, f'_t.

Under biaxial compression, concrete exhibits an increased initial stiffness, compared with the uniaxial behaviour, that may be attributed to the Poisson's ratio effect. Under biaxial tension-compression, concrete exhibits a reduced strength in both tension and compression compared to the strengths achieved under uniaxial loading. Under biaxial tension, the behaviour about each

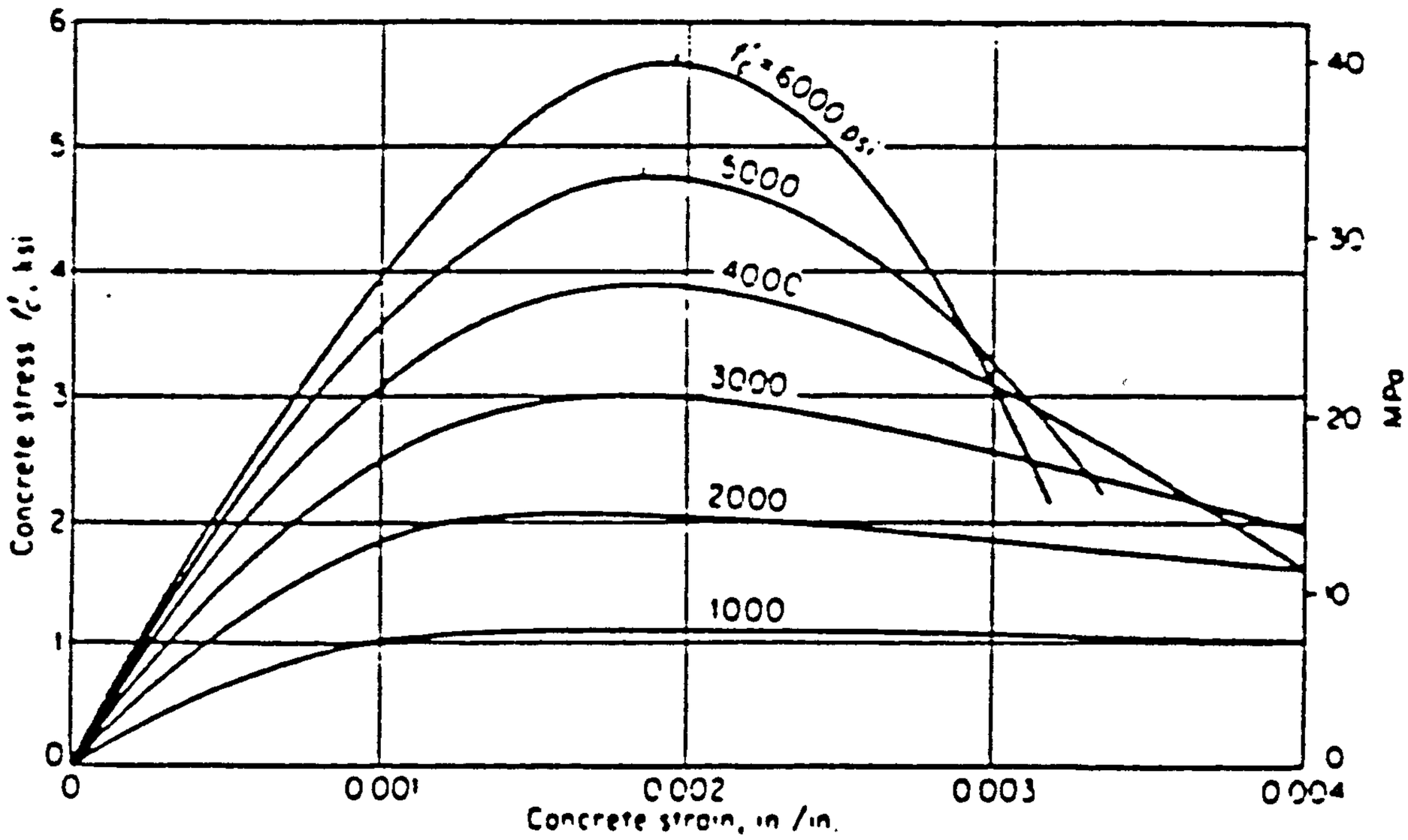

Figure 5 .1. Typical stress-strain curve in compression for concrete under uniaxial monotonic loading [39]

principal axis is similar to that under uniaxial tension [40].

The properties of concrete also depend on other time-dependent factors such as creep and shrinkage, however since the present analysis is limited to short term loading these factors have been ignored.

A review of the different numerical models that can be employed for concrete for use in a finite element analysis is presented in Section 5.3, and the models adopted in the analysis are discussed in Section 5.4. Cracking and the representation of the tension stiffening effect are discussed in Section 5.5.

The model used for the reinforcing steel is presented in Section 5.6.

5.2. STEEL

It is a well known fact that the nonlinear material behaviour of most metals is due to plastic flow. In a nonlinear analysis of a metal structure a yield criterion indicating the stress level at which plastic flow commences must be established, beyond this stress level the behaviour becomes nonlinear.

Several yield criteria can be used in the modelling of elasto-plastic behaviour of metals, however the most commonly used criteria are Tresca and Von Mises. Both criteria give good correlation with the experimental data, however Von Mises fits the experimental data more closely than Tresca's [41].

The analytical model adopted in the analysis is an incremental model with the constitutive relationship being a function of the stress level. Derivation of the constitutive relationship is similar to that given by Zienkiewicz [16] and is presented here. Before yielding the material was assumed to be linear elastic and the constitutive relationship is given by

$$\{\Delta\sigma\} = [D_b]\ \{\Delta\varepsilon\} \tag{5.1a}$$

where $\Delta\sigma$ and $\Delta\varepsilon$ are the incremental elastic stress and strain vectors respectively. The elastic matrix D_b is given by

$$[D_b] = \frac{E}{(1-\nu^2)}\begin{bmatrix} 1 & \nu & 0 \\ \nu & 1 & 0 \\ 0 & 0 & \frac{1-\nu}{2} \end{bmatrix} \tag{5.1b}$$

Yielding was assumed to occur when the stresses satisfy the general yield criterion

$$F(\sigma,k) \geq 0 \tag{5.2}$$

where k is a strain hardening parameter.

During plastic flow the total incremental strains, $\Delta\varepsilon$, were assumed to be divisable into elastic and plastic parts such that

$$\{\Delta\varepsilon\} = \{\Delta\varepsilon_e\} + \{\Delta\varepsilon_p\} \tag{5.3}$$

where the subscripts e and p denote elastic and plastic components respectively.

If the normality condition is assumed, which requires that the increment of plastic strain is in a direction normal to the yield surface, this condition can be expressed as

$$\{\Delta\varepsilon_p\} = \lambda \left\{\frac{\partial F}{\partial \sigma}\right\} \qquad (5.4)$$

where λ is a scalar.

The total incremental strains, equation (5.3), can be written in terms of its elastic and plastic incremental parts, equations (5.1a) and (5.4), such that

$$\{\Delta\varepsilon\} = [D_b]^{-1} \{\Delta\sigma\} + \lambda \left\{\frac{\partial F}{\partial \sigma}\right\} \qquad (5.5)$$

Following Nayak et al [42], the scalar λ can be shown to be expressed by

$$\lambda = \left\{\frac{\partial F}{\partial \sigma}\right\} [D_b] \left[A + \left\{\frac{\partial F}{\partial \sigma}\right\}^T [D_b] \left\{\frac{\partial F}{\partial \sigma}\right\}\right]^{-1} \qquad (5.6)$$

where A is a scalar representing the slope of the uniaxial plastic part of the stress-strain curve.

The elasto-plastic incremental stress-strain relationship can be obtained from equations (5.5) and (5.6), such that

$$\{\Delta\sigma\} = [D^*] \{\Delta\varepsilon\} \qquad (5.7a)$$

where the elasto-plastic material matrix D^* is given by

$$[D^*] = [D_b] - [D_b]\left\{\frac{\partial F}{\partial \sigma}\right\}\left\{\frac{\partial F}{\partial \sigma}\right\}^T [D_b] \left[A + \left\{\frac{\partial F}{\partial \sigma}\right\}^T [D_b] \left\{\frac{\partial F}{\partial \sigma}\right\}\right]^{-1} \qquad (5.7b)$$

Equation (5.7b) is a nonlinear constitutive relationship and is a function of the stress level. For a stress-strain relationship with no strain hardening, which was assumed in the analysis, the scalar A is set to zero.

The Von Mises yield criterion was used in the analysis. This criterion can be expressed for a two-dimensional stress state and for a material with no strain hardening as

$$F(\sigma) = \sigma_x^2 - \sigma_x\sigma_y + \sigma_y^2 + 3\tau_{xy}^2 - \sigma_o^2 \geq 0 \qquad (5.8)$$

where σ_o is the uniaxial yield stress for the material.

Three material properties are required to develop the constitutive relationship. These properties are the uniaxial elastic modulus, E, Poisson's ratio, ν, and the uniaxial yield stress, σ_o. All these properties can be determined experimentally.

5.3 CONCRETE

5.3.1 REVIEW OF NUMERICAL MODELS

In a nonlinear finite element analysis of a reinforced concrete structure, the numerical modelling of the material properties requires the following: (1) a constitutive relationship, (2) a yield or maximum stress criterion,(3) a failure criterion, generally in terms of strains, (4) a cracking criterion, and(5) a model for tension stiffening.

Although several numerical models have been developed and used in nonlinear finite element analyses during the last decade, no agreement on a single constitutive relationship under one or multi-dimensional states of stress for short term loading has been reached at the present time. An extensive review of the various models developed for use in the finite element method is given in Ref.[43].

In most numerical models the constitutive relationship for one or multi-dimensional stress states are usually expressed in terms of one or more of the measured properties of concrete, such as the uniaxial ultimate compressive strength, the uniaxial ultimate tensile strength, the initial elastic modulus of elasticity, and Poisson's ratio.

The most widely used approaches for defining the constitutive models can be divided into three groups [43]: (1) nonlinear elasticity, (2) plasticity and (3) endochronic.

5.3.2 NONLINEAR ELASTICITY MODELS

Elasticity based models can be utilized with either a total or an incremental stress-strain formulation. In the total stress-strain formulation, the current state of stress is assumed to be uniquely determined as a function of the current state of strain. This type of formulation is path-independent and is suitable for concrete structures under short term monotonic loading.

Incremental stress-strain formulations are used when unloading is likely to be significant or in analyses when time-dependent factors are included. This type of formulation is path-dependent and provides a good representation for concrete under non-monotonic loading.

The following investigators have developed numerical elasticity based models for concrete under biaxial states of stress.

Ngo et al [44] proposed a model in which concrete is represented as a linear isotropic material. Nonlinear behaviour in the concrete is limited to the effects of cracking.

Kupfer et al [45] proposed a more sophisticated isotropic model based on a total stress-strain formulation. In this model the constitutive relationship is expressed in terms of secant shear and bulk moduli, which were represented by a series of expressions. These expressions were derived by fitting curves to the experimental data obtained for concrete under various biaxial states of stress. This model employed a maximum stress envelope which was expressed in terms of the test data obtained for concrete under biaxial states of stress.

Gerstle [46] proposed an incremental isotropic model in which the constitutive relationship was expressed in terms of tangential bulk and shear moduli. These moduli were assumed to vary linearly with the octahedral normal and shear stresses.

In all the models described above, concrete was modelled as an isotropic material, whereas experimental data [40] showed that concrete exhibits stress-induced orthotropic behaviour when in a state of biaxial stress.

Liu et al [47] proposed an orthotropic model for concrete based on a total stress-strain formulation. A stress-strain equation for the representation of the behaviour of concrete was developed, based on their test data [48]. This equation is valid for compression only.

Darwin et al [49-50] proposed an incremental model in which concrete was modelled as an orthotropic material. The model was based on the concept of an equivalent uniaxial strain. For biaxial compression a family of curves, known as equivalent uniaxial stress-strain curves, and which were functions of the stress ratio in the two orthotropic directions, was proposed. The equivalent uniaxial stress-strain curves were expressed in terms of the values of the peak stresses, the strains corresponding to the peak stresses and the total equivalent uniaxial strains. The peak stresses were expressed in terms of a maximum stress criterion similar to that proposed by Kupfer et al [45]. The strains corresponding to the peak stresses were expressed using analytical expressions based on experimental data obtained for

concrete under biaxial states of stress. The total equivalent uniaxial strains were obtained by scalar summation for all the strain increments along the loading path. In tension, concrete was modelled as a linear elastic-brittle material. Evaluation of the modului of elasticity is based on the equivalent uniaxial stress-strain curves. In this model the total equivalent uniaxial strains have been treated as scalar quantities despite the fact that strains are vectors. These strains were called fictitious strains rather than true strains.

Tasuji et al [51] extended the model proposed by Liu et al [47] for biaxial compression to a general stress-strain relationship that described the behaviour of concrete in biaxial tension-compression and biaxial tension in addition to biaxial compression.

Details of this model will be presented in Section 5.4.

5.3.3 PLASTICITY BASED MODELS

Plasticity models are based on the assumption that concrete behaves as a plastic material although generally with only limited ductility. The constitutive relationships for these models are defined by [43]:(1) the shape of an initial yield surface, (2) the evalution of subsequent loading surface, (3) the formulation of the appropriate flow rule and (4) a crushing surface expressed in terms of strains.

The following investigators have utilized models for concrete based on the concept of plasticity.

Lin et al [52] idealized the concrete as perfectly elasto-plastic

material and used the Von Mises criterion to approximate the yield surface in biaxial compression. Crushing of concrete was represented by a crushing surface, defined in terms of the principal strains, beyond which the concrete was assumed to crush and carry zero stress. The stress-strain curve for concrete in tension was considered to have uncracked elastic portion and a cracked unloading nonlinear portion.

Chen et al [53] proposed a plasticity model assuming concrete to be an isotropic, linear elastic-plastic, strain hardening and fracturing material. The initial yield surface and failure surface were developed by describing a loading function in terms of the stress invariants.

Buyukozturk [54] proposed a model in which the loading surface was based on the experimental test data obtained by Kupfer et al [40] and Liu et al [48].

5.3.4 ENDOCHRONIC THEORY

The endochronic theory was originally proposed by Valanis [55] for metals. Bazant et al [56] have extended the application of this theory to concrete.

The endochronic theory represents a special type of viscoplasticity with a strain rate dependent viscosity. The concept of the theory is that of the intrinsic time, which depends on the strain increments and is assumed to govern the magnitude of the inelastic strain increments.

The major difference of the endochronic formulation from the elasticity and plasticity is that it is incrementally nonlinear. However, because of the large number of material parameters required to model the behaviour of the concrete using the endochronic theory, further research is required to simplify and reduce the material parameters used in the existing versions of the theory.

Most of the types of models described have been used successfully in the analysis of reinforced concrete structures. However, elasticity based models provide good overall representation of the concrete behaviour. For reinforced concrete structures in which the nonlinear behaviour is mainly due to the cracking of concrete and yielding of the reinforcing steel, the use of elasticity based models seems to be justified [43].

Two biaxial nonlinear elasticity based models for concrete have been used in the analysis. Details of these models are presented in the next Section.

5.4 CONCRETE MODELS ADOPTED IN THE ANALYSIS

Two nonlinear elasticity based models based on the total stress-strain formulation have been utilized for the representation of the concrete behaviour. From the experimental results, Fig.5.2, obtained by Kupfer et al [40] it can be seen that concrete behaves as an orthotropic material in the two principal directions, and the behaviour in each

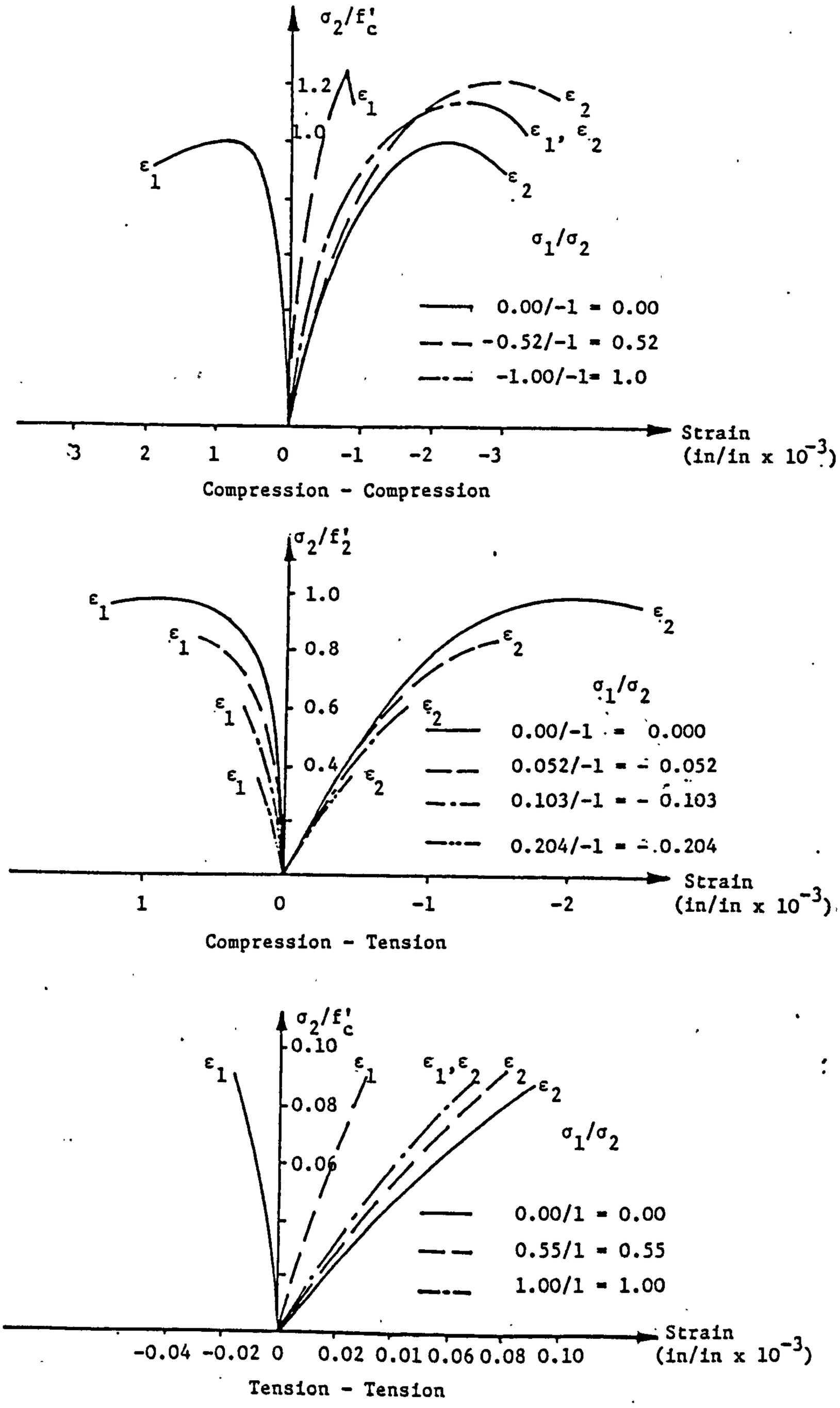

Figure 5.2. Experimental stress-strain curves for concrete under biaxial stresses [40]

direction depends on the stress in the other direction. This assumption was made in the formulation of the two models.

5.4.1 MODEL I

This model is similar to that proposed by Cope et al [57] and used in their investigation of the behaviour of reinforced concrete slabs. It was assumed for the model that pseudo stresses in the principal directions could be calculated independently of each other, based on uniaxial stress-strain relationships. The biaxial effect was assumed to be due to the interaction of the two principal directions through the Poisson's ratio effect.

Two uniaxial stress-strain curves for concrete in compression were used in the analysis, Fig.5.3 and 5.4. The first curve was bi-linear and is similar to that used by Hand et al [58] in the analysis of concrete plates and shells. The second was a nonlinear curve proposed by Saenz [59].

In both stress-strain curves, concrete was assumed to carry compressive stress beyond the strain corresponding to the concrete ultimate compressive strength , ε_c, up to an ultimate compressive strain ε_{cu}. When concrete reaches its ultimate compressive strain it was assumed to crush and carry zero stress.

In tension, the stress-strain relationship was assumed to be linear prior to cracking, which was assumed to occur when the tensile stress reaches the ultimate tensile strength of concrete. The post cracking

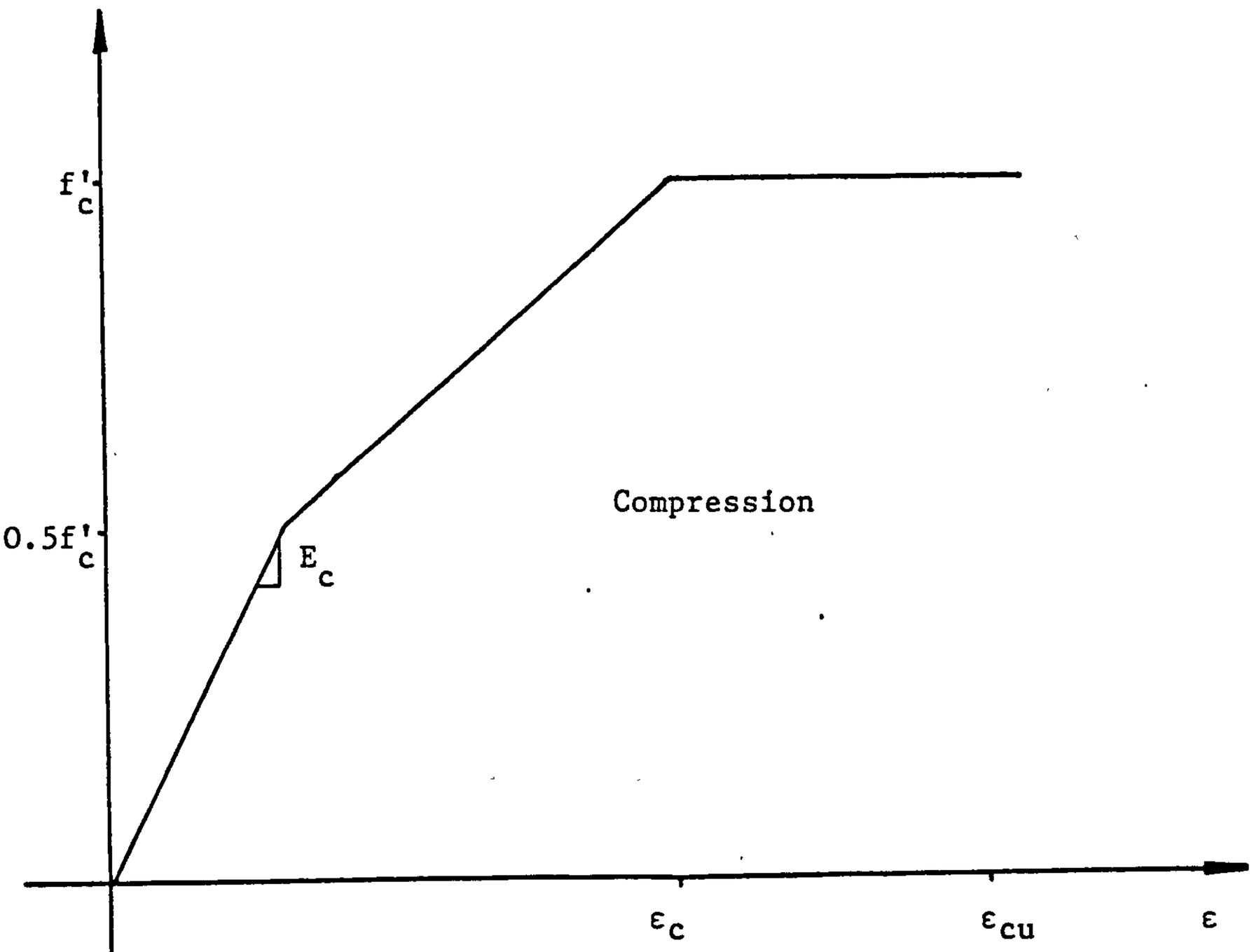

Figure 5.3. Multi-linear stress-strain curve for concrete in compression

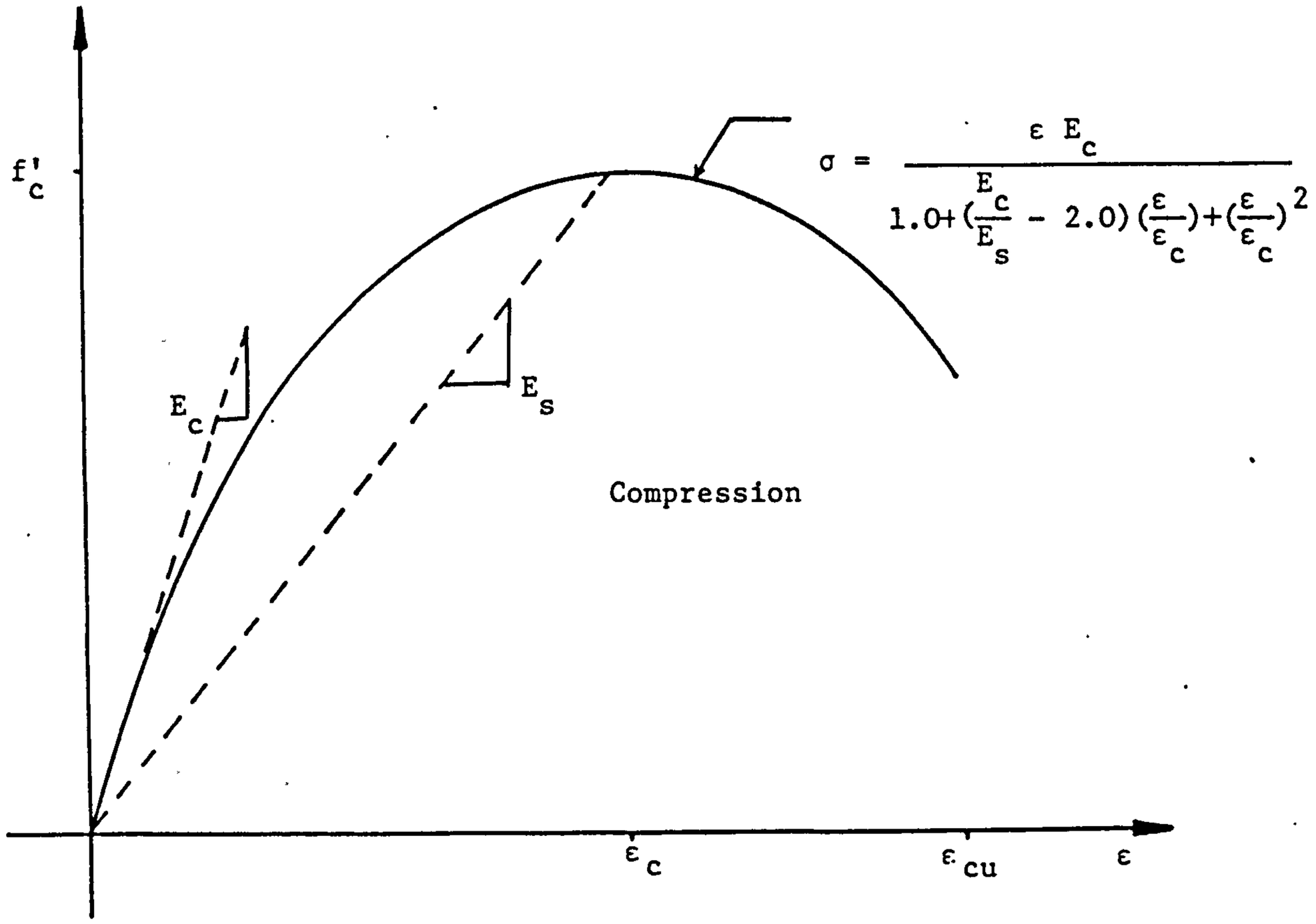

Figure 5.4. Nonlinear stress-strain curve for concrete in compression [59]

behaviour of concrete will be discussed in detail in Section 5.5.

The procedure adopted for the evaluation of the stress level is summarized as follows:

1- Principal strains, $\varepsilon_{1,2}$, and the angle between the cartesian and the principal directions were determined from the given strains in the cartesian directions, ε_x, ε_y, γ_{xy}, using

$$\varepsilon_{1,2} = \frac{\varepsilon_x + \varepsilon_y}{2} \pm \sqrt{\left(\frac{\varepsilon_x - \varepsilon_y}{2}\right)^2 + \gamma_{xy}^2} \qquad (5.9)$$

$$\theta = \tfrac{1}{2} \tan^{-1} \frac{\gamma_{xy}}{\varepsilon_x - \varepsilon_y} \qquad (5.10)$$

2- From the uniaxial stress-strain relationship, the pseudo principal stresses, $\sigma^*_{1,2}$, were determined using the principal strains.

3- Effective or true principal stresses, which include the biaxial effect due to Poisson's ratio effect, were determined using the following relationship:

$$\begin{bmatrix} \sigma_1 \\ \sigma_2 \end{bmatrix} = \frac{1}{(1-\nu_c^2)} \begin{bmatrix} 1 & \nu_c \\ \nu_c & 1 \end{bmatrix} \begin{bmatrix} \sigma^*_1 \\ \sigma^*_2 \end{bmatrix} \qquad (5.11)$$

4- Poisson's ratio, ν_c, was kept constant unless the concrete had cracked or crushed, after which it was assumed no interaction between the two principal stresses occurs and thus ν_c was set to zero.

5- The effective principal stresses were then resolved to obtain stresses in the cartesian directions using the following transformation.

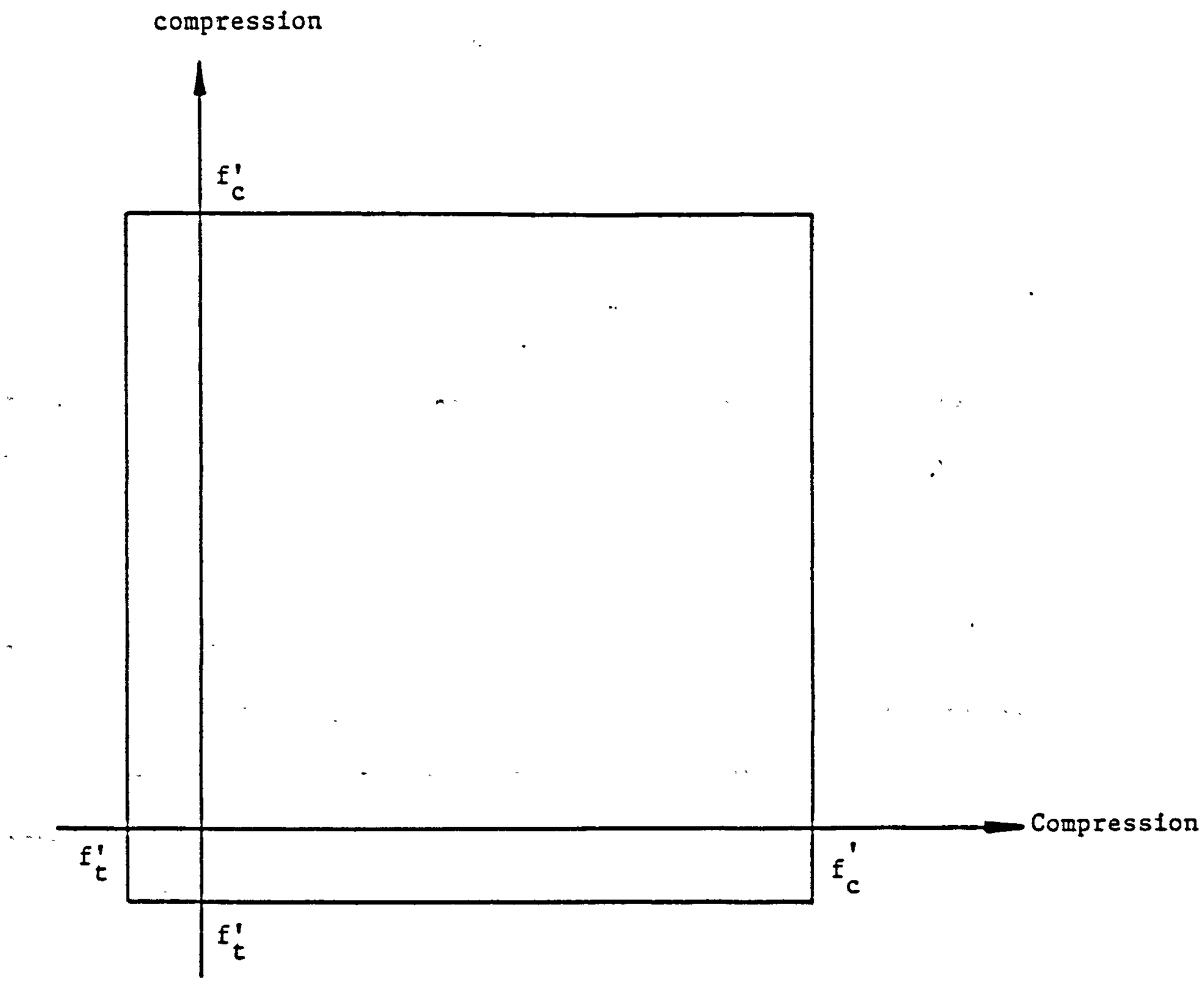

Figure 5.5. Square maximum stress criterion

$$\begin{bmatrix} \sigma_x \\ \sigma_y \\ \tau_{xy} \end{bmatrix} = \begin{bmatrix} \frac{1}{2} - \frac{1}{2}\cos 2\theta & \frac{1}{2} + \frac{1}{2}\cos 2\theta \\ \frac{1}{2} + \frac{1}{2}\cos 2\theta & \frac{1}{2} - \frac{1}{2}\cos 2\theta \\ -\frac{1}{2}\sin 2\theta & \frac{1}{2}\sin 2\theta \end{bmatrix} \begin{bmatrix} \sigma_1 \\ \sigma_2 \end{bmatrix} \qquad (5.12)$$

In order to check for yielding the square maximum stress criterion, Fig. 5.5, was used.

5.4.2 MODEL II

Tasuji et al [51] have proposed a model for concrete which represents the behaviour of concrete under biaxial states of stress and assumes concrete to be an orthotropic material. This model was used by Edwards [60] for the analysis of concrete bridge decks.

The stress-strain equation developed by Liu et al [47] was extended to represent the behaviour of concrete under different biaxial states of stress. The equation developed is

$$\sigma_i = \frac{\varepsilon_i E_c}{(1-\nu_c K)\left[1 + \left(\frac{1}{1-\nu_c K} \cdot \frac{E_c}{E_s} - 2\right)\left(\frac{\varepsilon_i}{\varepsilon_{pi}}\right) + \left(\frac{\varepsilon_i}{\varepsilon_{pi}}\right)^2\right]} \qquad (5.13)$$

where :

σ_i = stress in principal direction i

ε_i = strain in principal direction i

E_c = initial modulus of elasticity

$E_s = \frac{\sigma_{pi}}{\varepsilon_{pi}}$ = secant modulus

σ_{pi}, ε_{pi} = peak compressive stress and corresponding strain in principal direction i.

K = biaxial principal stress ratio defined by

$$K = \frac{\sigma_2}{\sigma_1} \qquad (5.14)$$

where $\sigma_2 \geq \sigma_1$ algebraically

For uniaxial stresses, equation (5.13), reduces to Saenz's equation, Fig.5.4, [59].

A simplified biaxial strength envelope, similar to that proposed by Kupfer et al [45], was proposed. The strength envelope is shown in Fig.5.6, together with those proposed by Liu et al [47] and Kupfer et al [45].

The peak stresses, σ_{pi}, and the corresponding strains, ε_{pi}, in the principal directions are functions of the biaxial principal stress ratio, k. Tasuji et al [51] gave expression for the peak stresses in terms of k. For the corresponding strains, ε_{pi}, expressions were obtained from the test data reported by Tasuji [61] for the behaviour of concrete under biaxial states of stress, Fig.5.7, by using a least square fit.

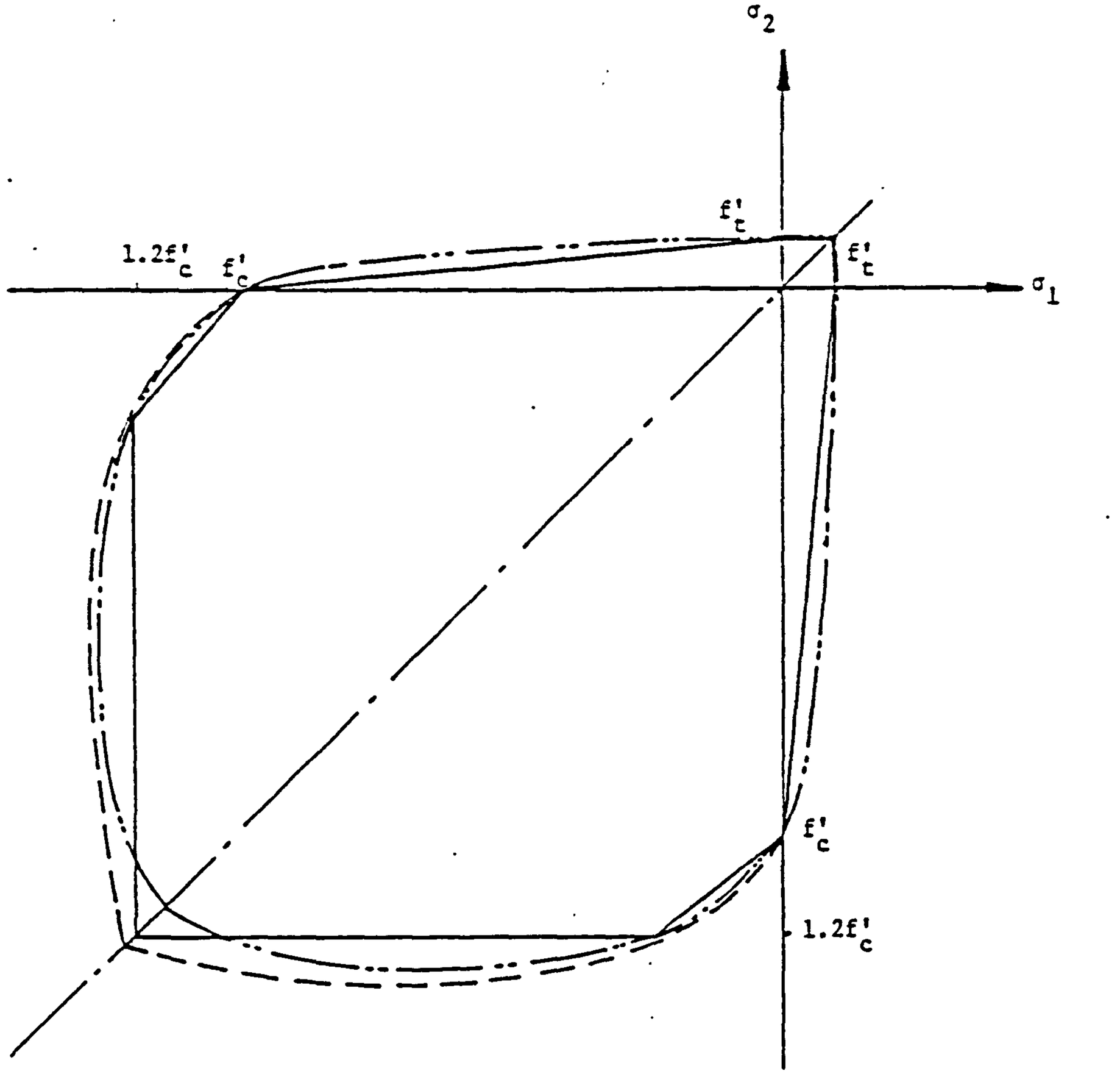

— — — Liu et al [47]

—·—·— Kupfer et al [45]

——— Tasuji et al [51]

Figure 5.6. Strength envelopes

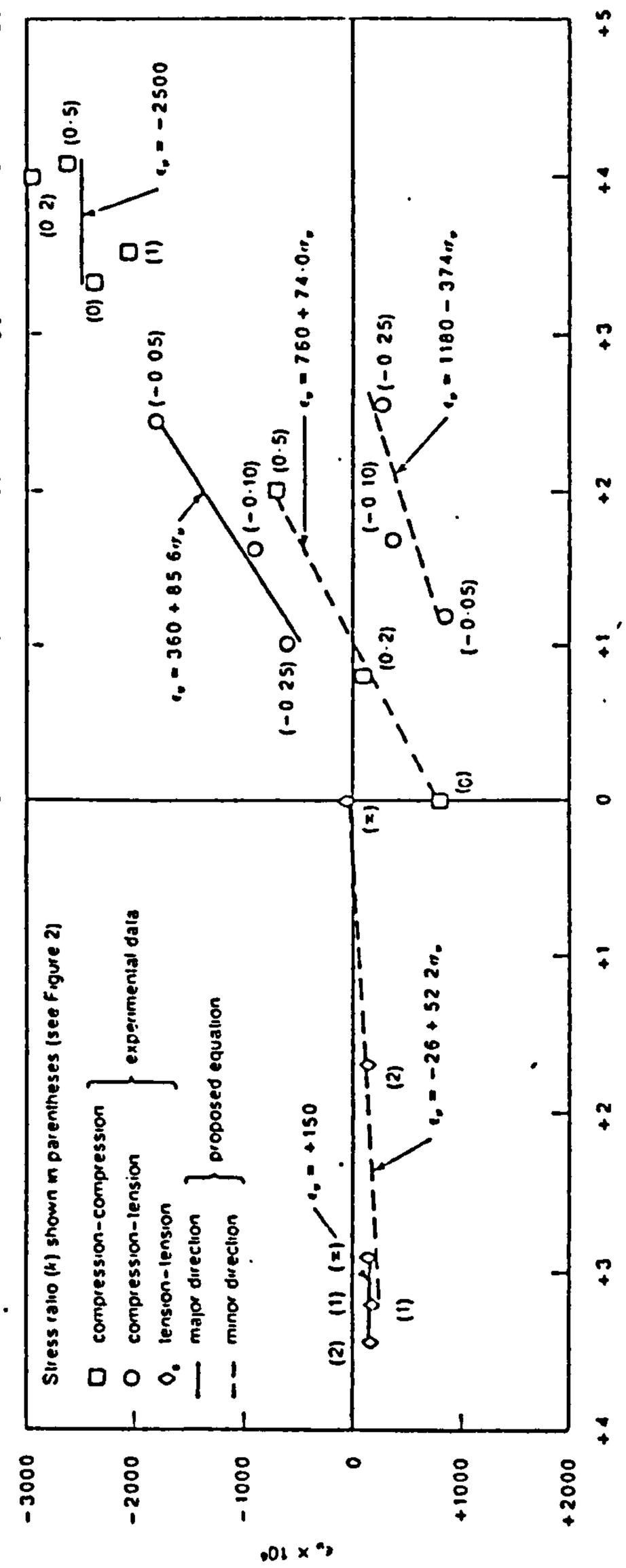

Figure 5.7. Peak-load stress-strain relationship for concrete under biaxial state of stress [61]

The biaxial strength envelope is divided into three regions, Fig.5.8, which depend on the state of stresses, as represented by the biaxial principal stress ratio, k. The three regions of the strength envelope with the expressions for the peak stresses and the corresponding strains as proposed by Tasuji et al [51] are summarized as follows:

Compression-Compression region $0.0 \leq K \leq 1.0$

σ_1 = compression σ_2 = compression

for $0.0 \leq K \leq 0.20$

$$\frac{\sigma_{p1}}{f'_c} = 1.0 + \frac{K}{1.2-K} \tag{5.15a}$$

for $0.2 \leq K \leq 1.0$

$$\frac{\sigma_{p1}}{f'_c} = 1.20 \tag{5.15b}$$

for $0.0 \leq K \leq 1.0$

$$\sigma_{p2} = K.\sigma_{p1} \tag{5.15c}$$

$$\varepsilon_{p1} = -2500 \times 10^{-6} \tag{5.15d}$$

$$\varepsilon_{p2} = 760 + 74.0\ \sigma_{p2} \tag{5.15e}$$

Tension-Compression region $-\infty \leq K \leq 0.0$

σ_1 = compression σ_2 = tension

$$\frac{\sigma_{p1}}{f'_c} = \frac{1.0}{1.0+ks} \tag{5.16a}$$

where $S = \frac{f'_c}{f'_t}$ = ratio of the uniaxial ultimate compressive strength of concrete to its uniaxial tensile strength.

$$\sigma_{p2} = K\ \sigma_{p1} \tag{5.16b}$$

$$\varepsilon_{p1} = 360.0 + 85.6\ \sigma_{p1} \tag{5.16c}$$

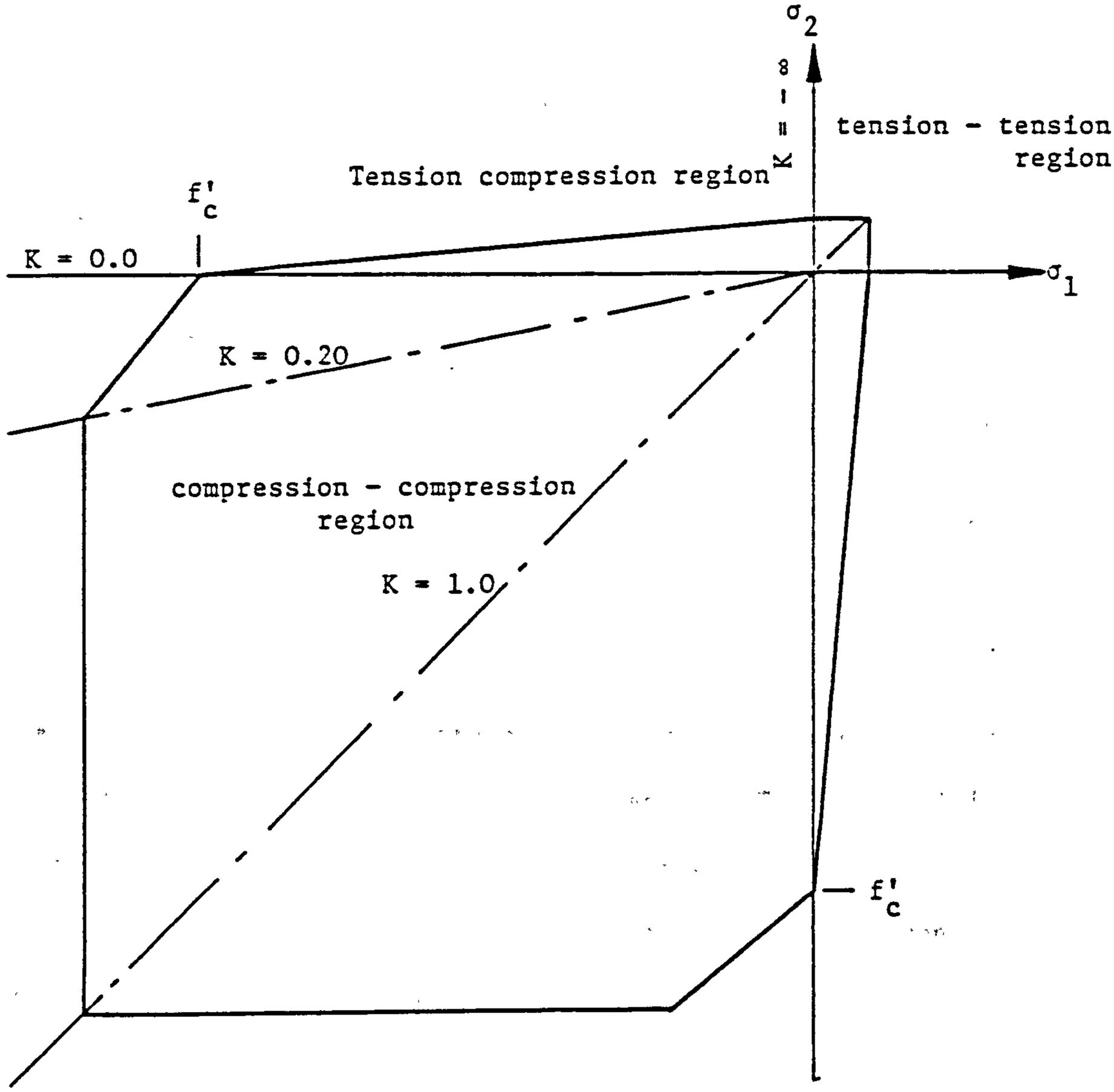

Figure 5.8. Biaxial strength envelope used in the present study

Tension-Tension region $\qquad 1.0 \leq K \leq \infty$

σ_1 = tension $\qquad \sigma_2$ = tension

$$\frac{\sigma_{p2}}{f'_c} = \frac{1}{S} \tag{5.17a}$$

$$\sigma_{p1} = K\,\sigma_{p2} \tag{5.17b}$$

$$\varepsilon_{p2} = 150 \times 10^{-6} \tag{5.17c}$$

$$\varepsilon_{p1} = -26.0 + 52.2\,\sigma_{p1} \tag{5.17d}$$

The values of the peak strains corresponding to the peak stresses, ε_{pi}, obtained using the expressions proposed by Tasuji et al [51] showed inconsistencies at the boundaries of the different biaxial stress regions, Fig.5.9. For example consider the case of a concrete with a uniaxial ultimate compressive strength of 24.0 N/mm^2, under equal biaxial compression stresses (k=1.0). Values for ε_{pi} of -2500.0×10^{-6} and -1371.2×10^{-6} were obtained using equations (5.15d) and (5.15e) respectively.

For the same concrete under uniaxial compression (k=0.0). The values for ε_{pi} were, -2500.0×10^{-6} from equation (5.15d), which is valid for the compression region, and a value of -1694.4×10^{-6} was obtained using equation (5.16c), which is valid for the tension-compression region.

These inconsistencies in the values of the strains corresponding to the peak stresses have been rectified by proposing expressions for the strains which satisfy the boundary conditions at the intersections of the different biaxial stress regions.

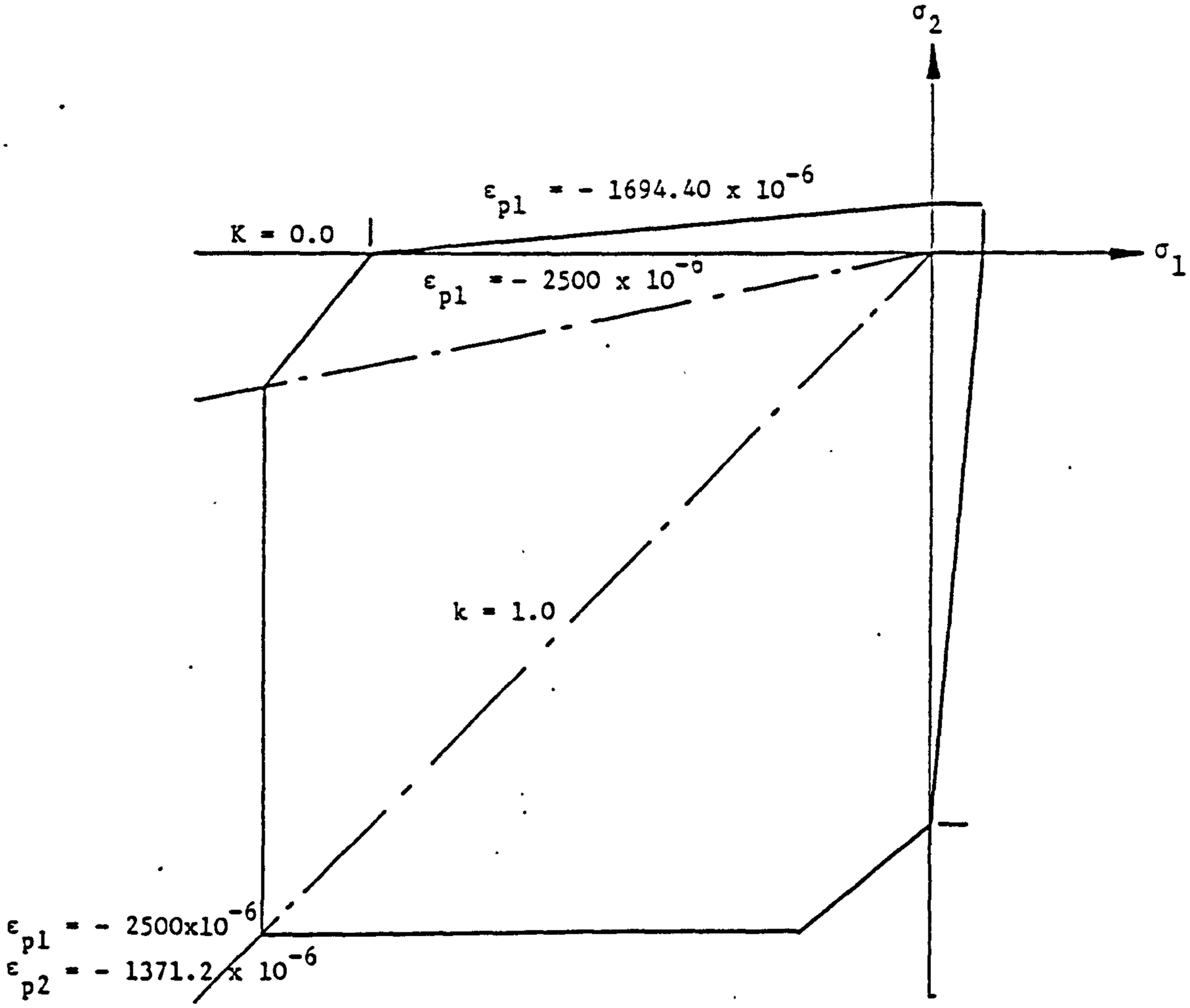

Figure 5.9. Strains corresponding to the peak stresses evaluated at the boundaries of the different stress regions.

Fig.5.10 indicates the proposed expressions for the strains corresponding to the peak stresses obtained using the data reported by Tasuji [61]. Additionally the stresses were non-dimensionalized in order to make use of all the available data. The proposed expressions avoid the inconsistencies in the values of the strains corresponding to the peak stresses at the boundaries of the stress regions inherent in the expression proposed by Tasuji et al [51].

In the proposed model the behaviour of concrete under compression, for biaxial compression and biaxial tension-compression, is assumed to be represented by equation (5.13).

The analytical expressions for the peak stresses and the corresponding strains used in this model for the different stress regions, are summarized as follows:

Compression-Compression region $0.0 \leq K \leq 1.0$

σ_1 = compression σ_2 = compression

for $0.0 \leq K \leq 0.20$

$$\frac{\sigma_{p1}}{f'_c} = 1.0 + \frac{K}{1.20-K} \qquad (5.18a)$$

for $0.20 \leq K \leq 1.0$

$$\frac{\sigma_{p1}}{f'_c} = 1.20 \qquad (5.18b)$$

for $0.0 \leq K \leq 1.0$

$$\sigma_{p2} = K\,\sigma_{p1} \qquad (5.18c)$$

$$\varepsilon_{p1} = \varepsilon_c \qquad (5.18d)$$

ε_c = strain corresponding to the uniaxial ultimate compressive strength of concrete.

for $0.0 \lesssim K \lesssim 0.50$

$$\varepsilon_{p2} = \varepsilon_c \left[- 0.3040 + 0.9768 \frac{\sigma_{p2}}{f'_c} \right] \qquad (5.18e)$$

for $0.5 \lesssim K \lesssim 1.0$

$$\varepsilon_{p2} = \varepsilon_c \left[- 0.4385 + 1.1985 \frac{\sigma_{p2}}{f'_c} \right] \qquad (5.18f)$$

Tension-Compression region $-\infty \lesssim K \lesssim 0.0$

σ_1 = compression σ_2 = tension

for $-\infty \lesssim K \lesssim 0.0$

$$\frac{\sigma_{p1}}{f'_c} = \frac{1.0}{1.0+KS} \qquad (5.19a)$$

$$\sigma_{t2} = K \sigma_{p1} \qquad (5.19b)$$

for $-0.05 \lesssim K \lesssim 0.0$

$$\varepsilon_{p1} = \varepsilon_c \left[- 0.1685 + 1.1685 \frac{\sigma_{p1}}{f'_c} \right] \qquad (5.19c)$$

for $-\infty \lesssim k \lesssim - 0.05$

$$\varepsilon_{p1} = \varepsilon_c \left[-0.1440 + 1.1290 \frac{\sigma_{p1}}{f'_c} \right] \qquad (5.19d)$$

for $-\infty \lesssim K \lesssim 0.0$

$$\varepsilon_t = \sigma_{t2}/E_c \qquad (5.19e)$$

Under biaxial tension, experimental observations [40] showed that the behaviour of concrete about each axis is approximately similar to that under uniaxial tension. Thus for tension the stress-strain relationship is given by

$$\sigma_i = \varepsilon_i E_c \text{ for } \sigma_i \lesssim \sigma_{ti} \qquad (5.20)$$

where

σ_{ti} = tensile strength of concrete in principal direction i.

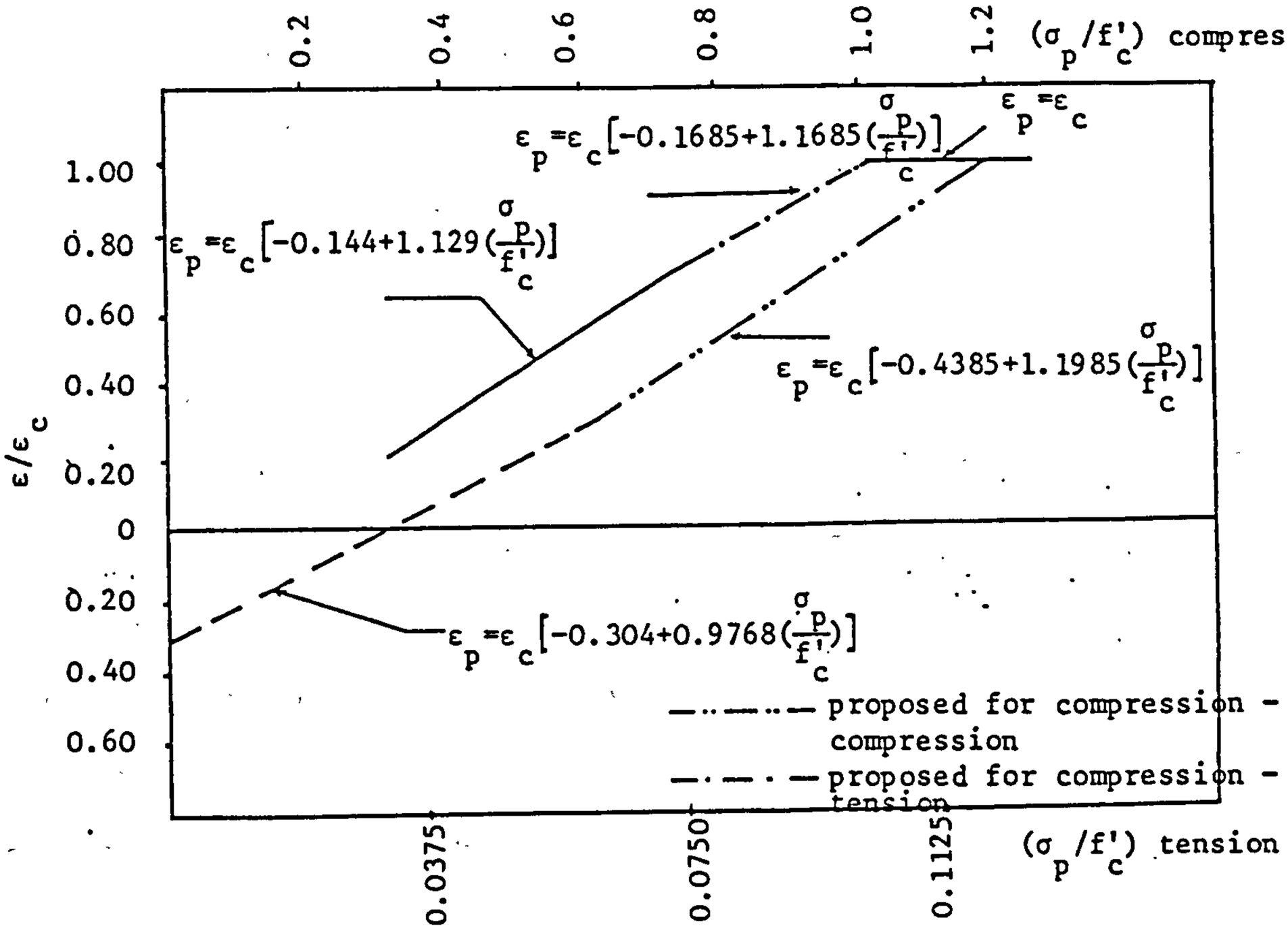

Figure 5.10. Peak-load strain-stress relationships for concrete under biaxial loading

The expression for the ultimate tensile strength for concrete and the corresponding strains in the tension-tension region is summarized as follows:

Tension-Tension region $1.0 \leq K \leq \infty$

σ_1 = tension $\qquad$ σ_2 = tension

$$\sigma_{t1} = \sigma_{t2} = f'_t \tag{5.21a}$$

$$\varepsilon_t = \frac{f'_t}{E_c} \tag{5.21b}$$

The stress-strain curves for concrete under biaxial compression predicted using the proposed equations are identical to those reported by Tasuji et al [51]. For biaxial tension-compression, a comparison of the stress-strain curves obtained using the proposed equations together with those obtained by Tasuji et al [51] and the experimental curves obtained by Kupfer et al [40], is shown in Fig.5.11. The concrete stress-strain curves predicted by the proposed equations are closer to the experimental results.

The existence of the falling branch of the stress-strain curve beyond the peak compressive stress has long been established. Tasuji et al [51] suggested that inclusion of such a branch might complicate the stress-strain relationship, equation (5.13). A simple approach to the inclusion of the falling branch was adopted in the present work. Beyond the peak compressive stress, the stress-strain relationship is assumed linear, Fig.5.12. Concrete is assumed to crush and carry zero stress when the strain reaches its ultimate value, ε_{cu}.

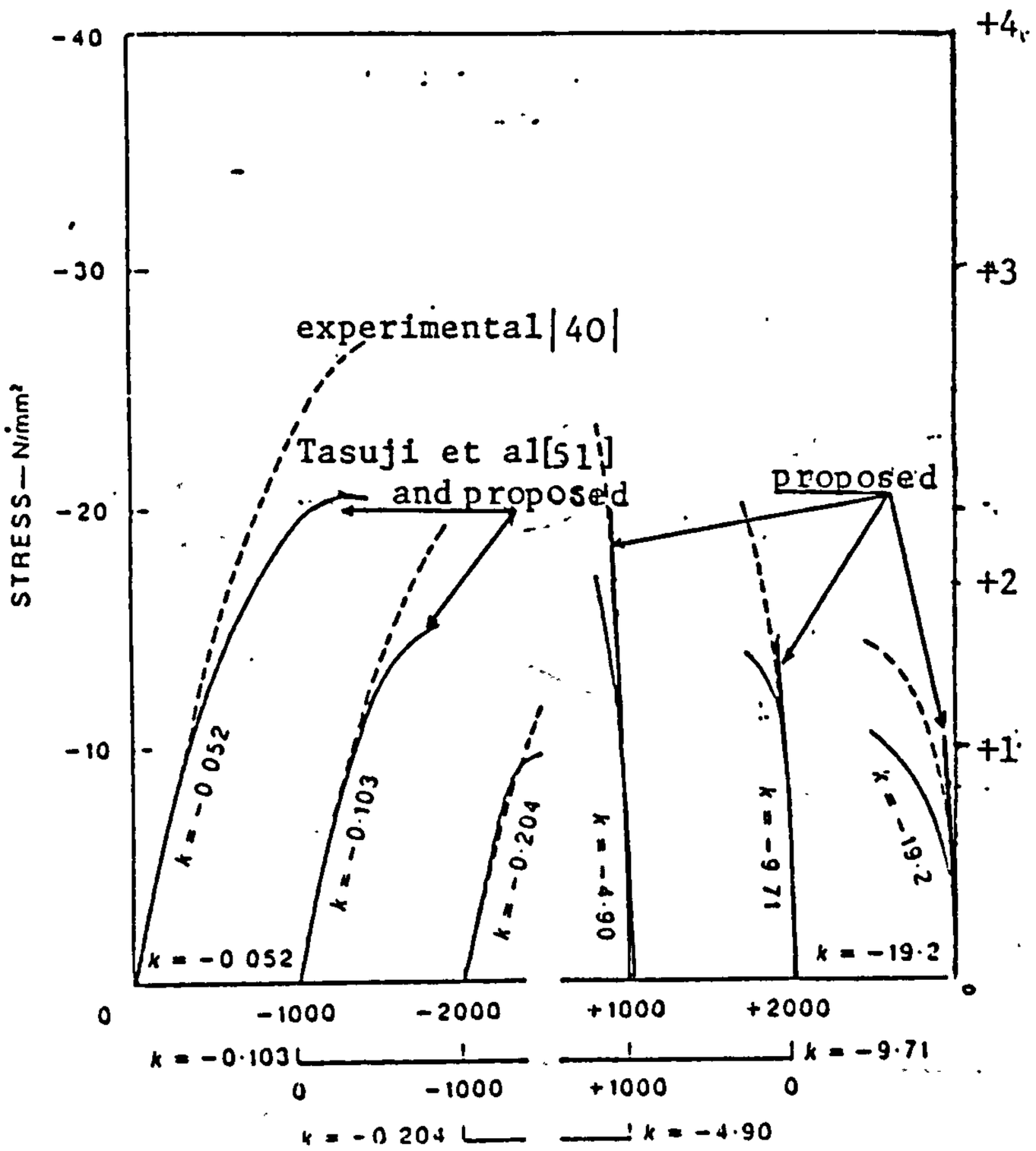

Figure 5.11. Stress-strain curves for concrete under biaxial tension-compression

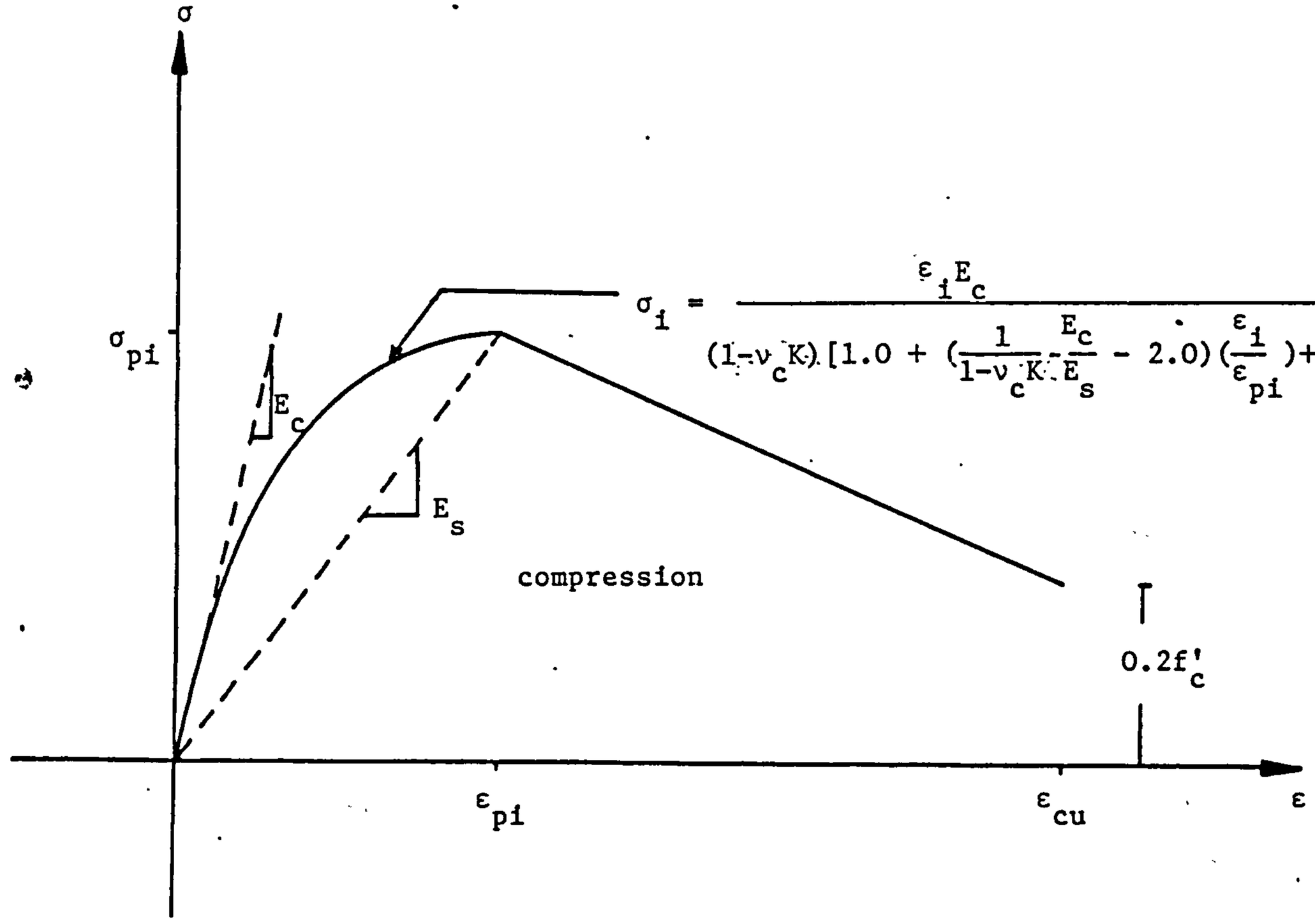

Figure 5.12. Assumed stress-strain curve for concrete in compression under biaxial stresses

The procedure adopted for the evaluation of the stresses at any particular location is summarized as follows:

1- The principal strains, ε_i, and the angle between the cartesian and the principal directions are determined from the strains in the cartesian directions using equations (5.9) and (5.10).

2- Using the biaxial principal stress ratio, k, evaluated at the end of the previous iteration, the peak stress and hence the corresponding strains are determined using the expressions given for the different stress regions, equations (5.18), (5.19) and (5.21).

3- The principal stresses, σ_i, are determined from the stress-strain relationships, equations (5.13) and (5.20).

4- The biaxial principal ratio, k, is determined again using equation (5.14), with the principal stresses, σ_i.

5- Steps 3 and 4 are repeated until the biaxial principal stress ratio converges to an acceptable level (1% difference between two sucessive iterations). Investigation of the convergence of the biaxial principal stress ratio indicated that convergence occurred within three iterations.

6- The principal stresses are then resolved, using equation (5.12), to obtain stresses in the cartesian directions.

Six material properties for concrete are required in order to construct the stress-strain relationship. These properties are the uniaxial initial elastic modulus, E_c, Poisson's ratio, ν_c, the uniaxial ultimate tensile strength, f'_t, the uniaxial ultimate compressive strength, f'_c, and its corresponding strain, ε_c, and the uniaxial ultimate strain, ε_{cu}. All six properties can be determined

experimentally.

5.5 CRACKING AND TENSION STIFFENING

5.5.1 GENERAL REMARKS

The low tensile strength of concrete and the cracking that results, is a major source of the nonlinear behaviour in reinforced concrete structures under short term loading.

In tension, concrete is assumed to behave as a linear elastic material up to cracking, which is assumed to occur when a principal tensile stress reaches the ultimate tensile strength. The direction of the crack is assumed normal to the direction of the corresponding principal stress.

The post cracking behaviour of reinforced concrete is complicated by the presence of the aggregate interlock, dowel action and tension stiffening effect. The phenomena of aggregate interlock and the dowel action allow the concrete to transfer some in-plane shear force. Under direct loads, the presence of the reinforcing steel and the influence of the concrete between adjacent cracks allows the concrete to carry direct stress beyond that required to initiate cracks. The basic cracking mechanism for a reinforced concrete element under uniaxial tension is illustrated in Fig.5.13. When the concrete reaches its ultimate tensile strength, primary cracks will form. At these primary cracks the stress carried by the concrete drops to zero and the steel carries all the load, however the concrete between the

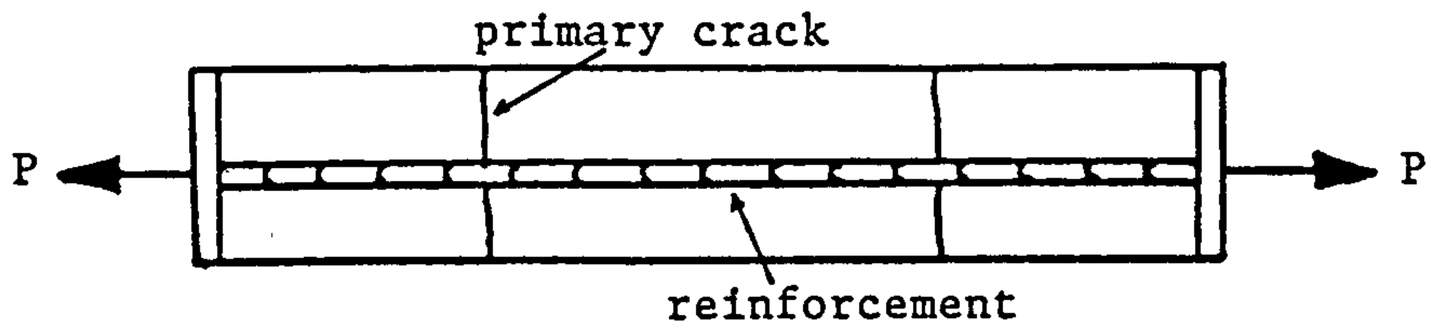

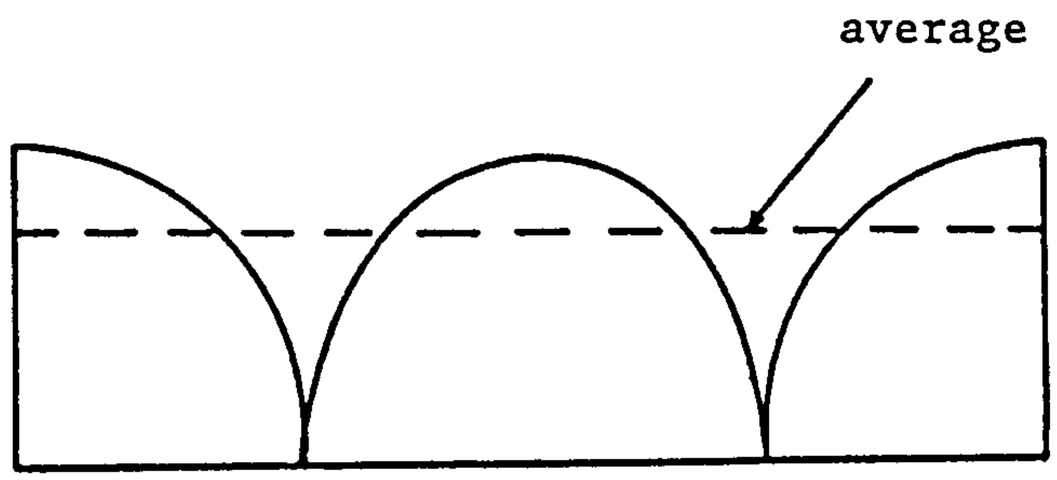

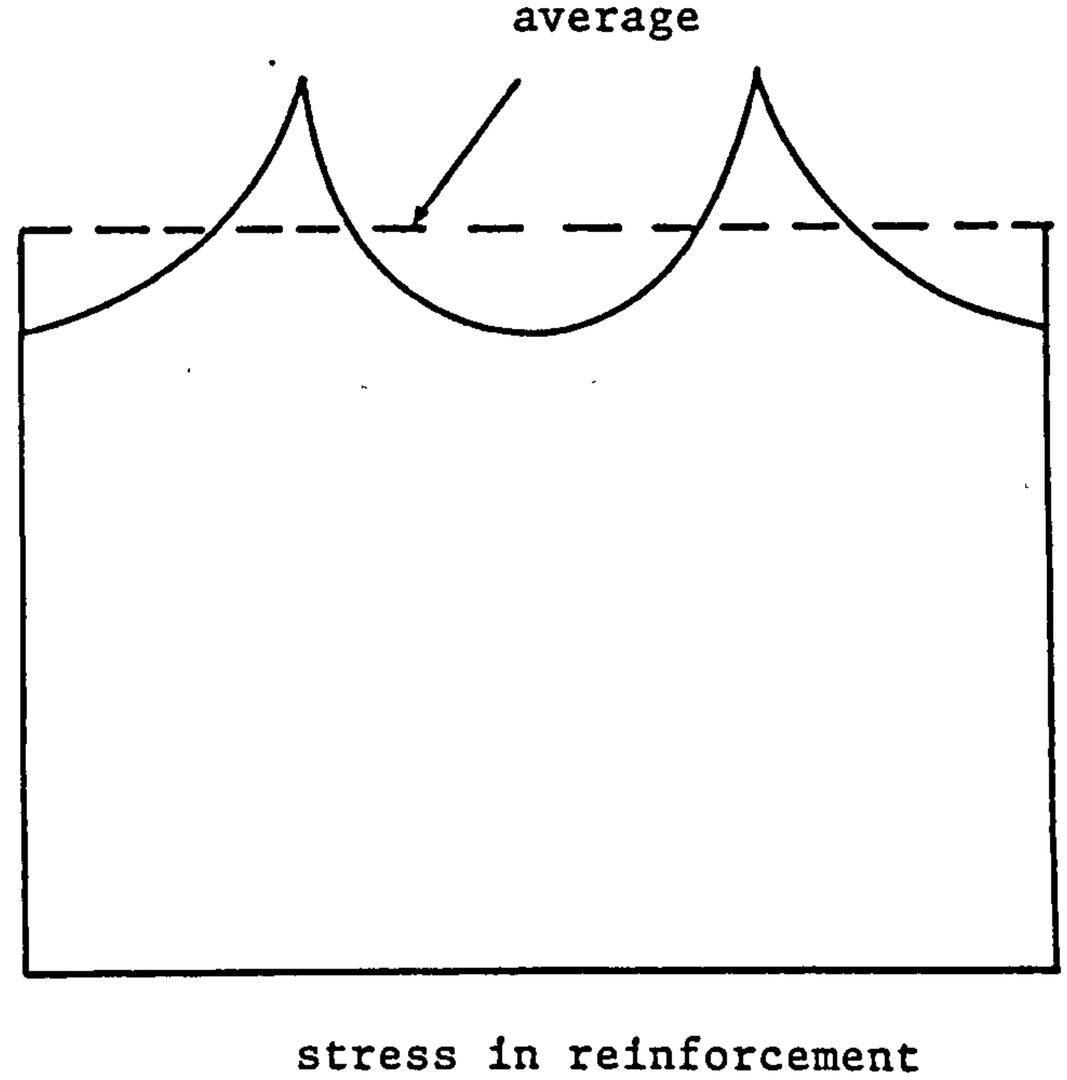

Figure 5.13. Stress distribution in a cracked reinforced concrete element

cracks is still capable of carrying some tensile stress. The average effect is that the concrete carries some load. This is often referred to as the tension stiffening effect. As the load increases secondary cracks will form resulting in a decrease in the average stress carried by the concrete. Eventually a secondary system of internal cracks develop around the reinforcing steel resulting in a breakdown of the bond between the concrete and the reinforcing steel. At this stage the concrete carries no load.

The modelling of cracks and the representation of the tension stiffening effect in a finite element analysis are discussed in the next two sections.

5.5.2 CRACKING MODELS

Several models for cracking have been developed for use in a finite element analysis. Most models relay on a strength criterion for crack initiation.

Cracking in concrete may be represented using discrete or smeared models, Fig.5.14. In the discrete model, cracks are allowed to develop along the element boundaries. The nodal points are separated when cracks occur. This approach has the disadvantage that it involves changes in the topology of the finite element mesh following the formation of a crack and the lack of generality in possible crack direction.

In the smeared crack modelling, local discontinuities due to cracking

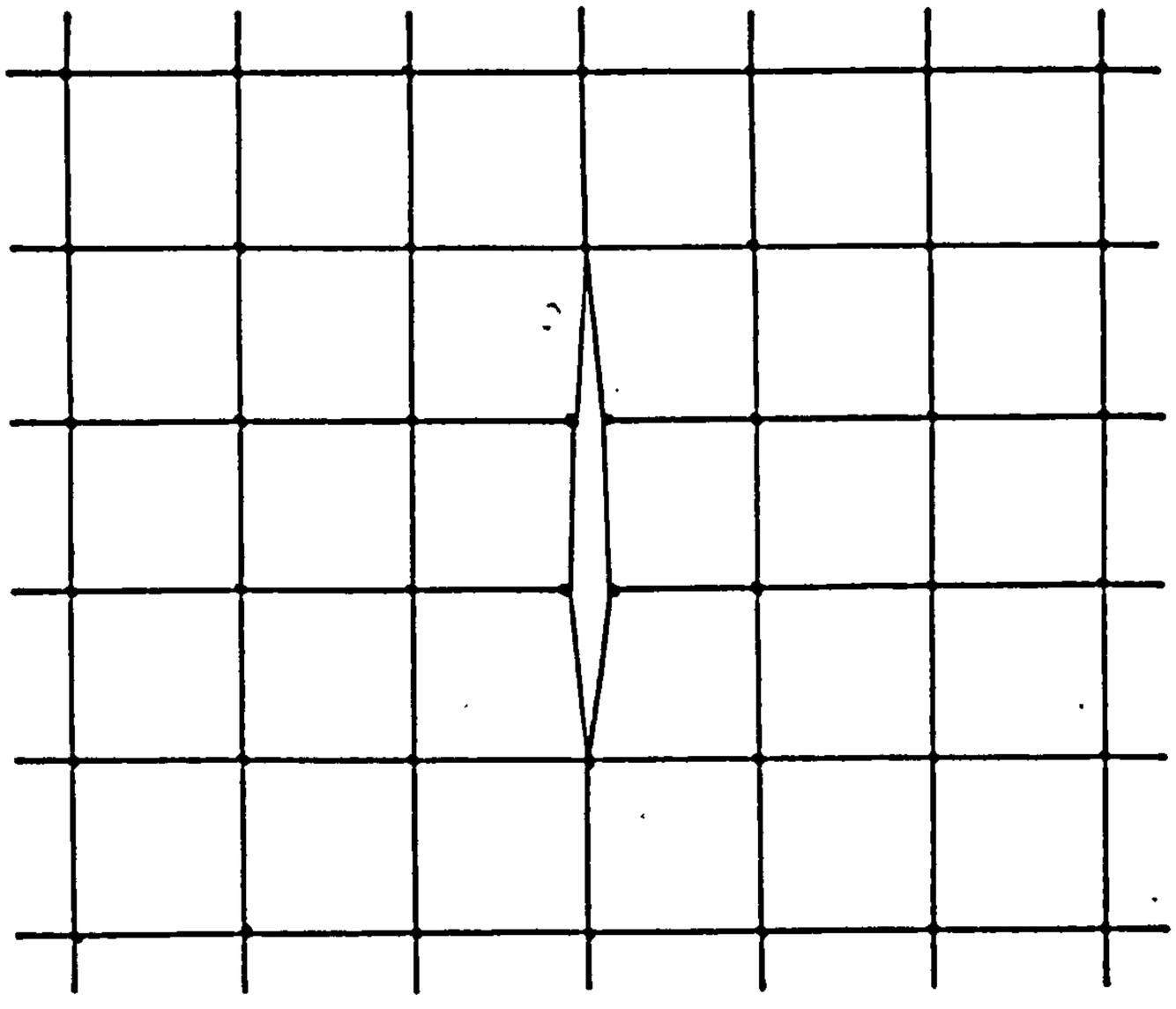

Discrete representation

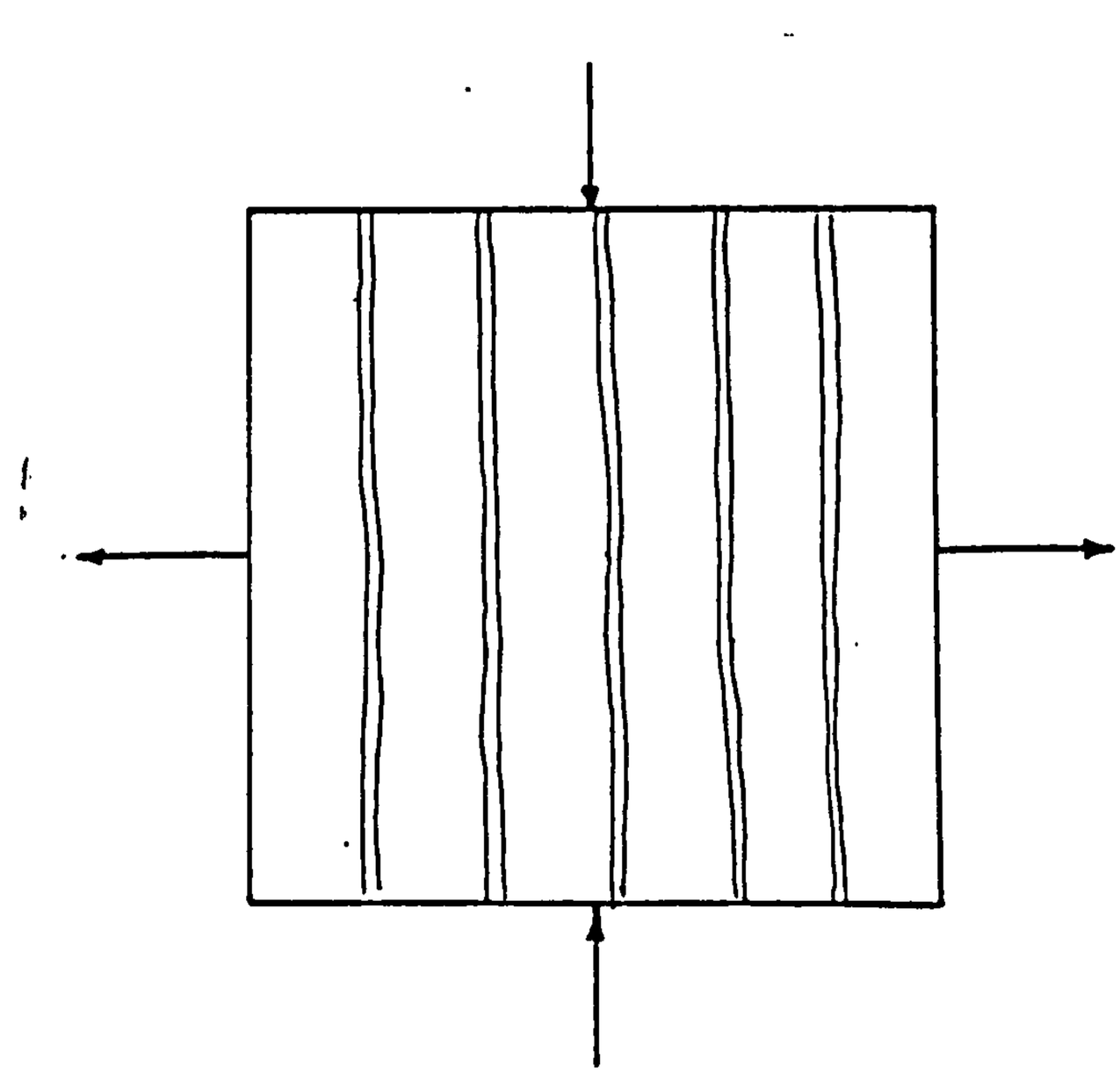

smeared representation

Figure 5.14. Discrete and smeared representation of a single crack

are represented in a distributed manner. This type of crack model, which has been adopted in the analysis, fits the finite element displacement method, since the continuity of the displacement field remains intact. It is also suitable for the layered approach.

The main criticism of the smeared crack model has been that it cannot model a discrete crack so that it would be incapable of predicting local fracture. However, a study using a smeared crack model of a problem which involved local fracture showed that the model can lead to realistic results [62].

After a crack has formed its direction can be taken as fixed or can be rree to rotate. In the fixed crack approach the crack direction is defined by the orientation of the initial crack and is then held fixed regardless of the change in the principal directions as the load is changed.

The rotating crack approach, which has been adopted in the analysis, was originaly proposed by Cope et al [63]. This model is based on the assumption that the crack direction is always normal to the direction of the maximum tensile principal stress.

Comparison of the performance of the fixed and the rotating crack models have been carried out by Milford et al [64] and Cerrera et al [65] using a finite element analyses with a layered elements.

Milford et al [64] investigated the behaviour of reinforced concrete panels tested by Vecchio et al [66] and reinforced concrete slabs

tested by Cardenas et al [67], while Cervera et al [65] analysed a corner supported reinforced concrete slab tested by Duddeck et al [68]. Both studies concluded that the results obtained using the rotating crack model correlated better with the experimental data than the results obtained using the fixed crack model, which gave stiffer responses.

Milford and his co-workers stated that the cracks defined by the rotating crack model are not cracks in the strict sense, but rather notational cracks defining the average crack rotation.

5.5.3 REPRESENTATION OF TENSION STIFFENING

The inclusion of the tension stiffening effect in analyses of reinforced concrete structures, should improve the results for the post cracking behaviour.

Two approaches can be employed to incorporate the tension stiffening effect, Fig.5.15. The first is to assume a descending branch for the concrete stress-strain curve in tension. This form of tension stiffening representation has been developed as a step reduction [69] and a gradual unloading [52].

The second approach is to ignore the concrete after cracking and increase the reinforcing steel stiffness fictitiously [70]. This approach implies that the tension stiffening effect is concentrated at the reinforcing steel level, whereas experimental observations showed

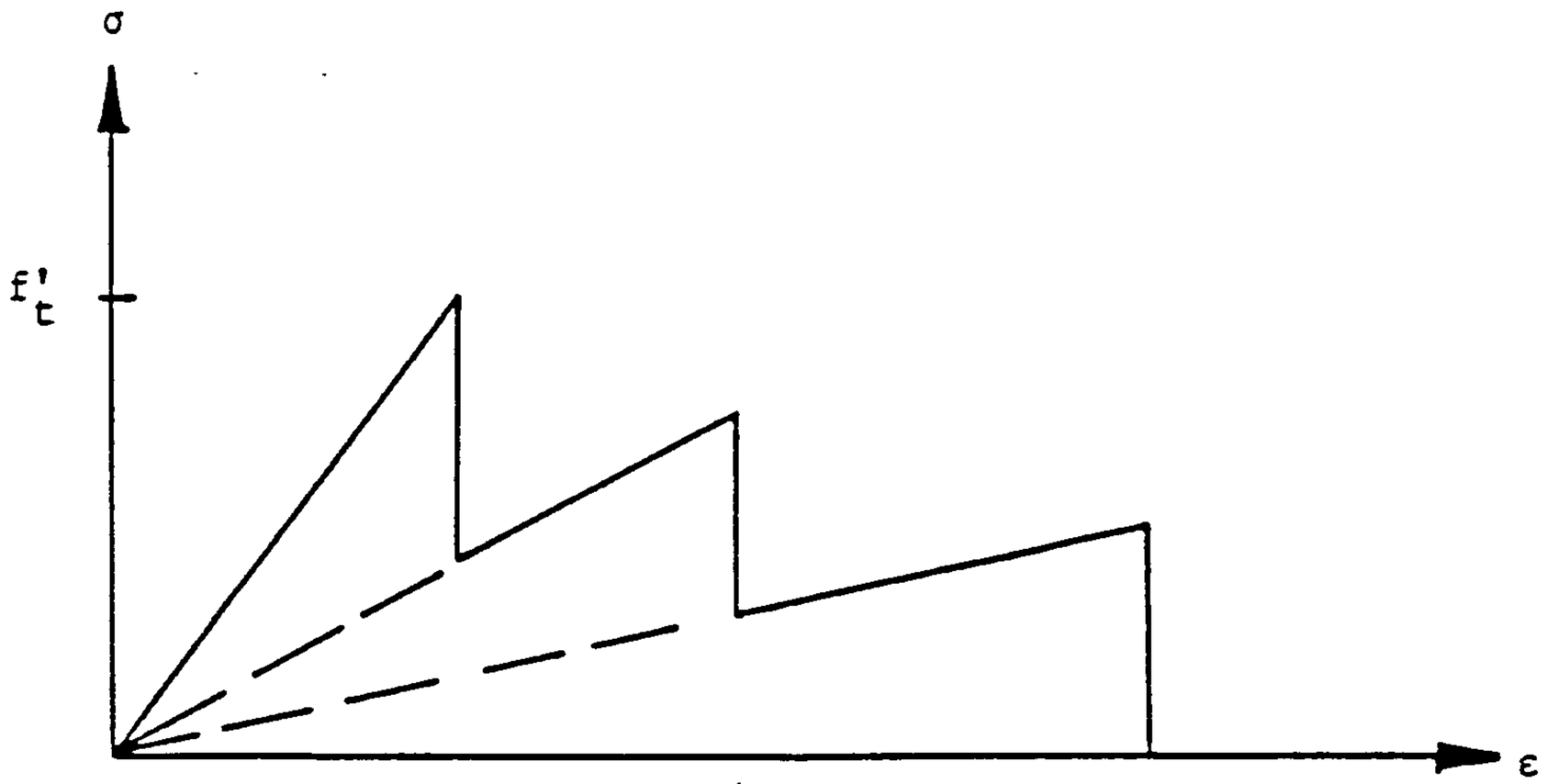

Scanlon's stepped unloading [69]

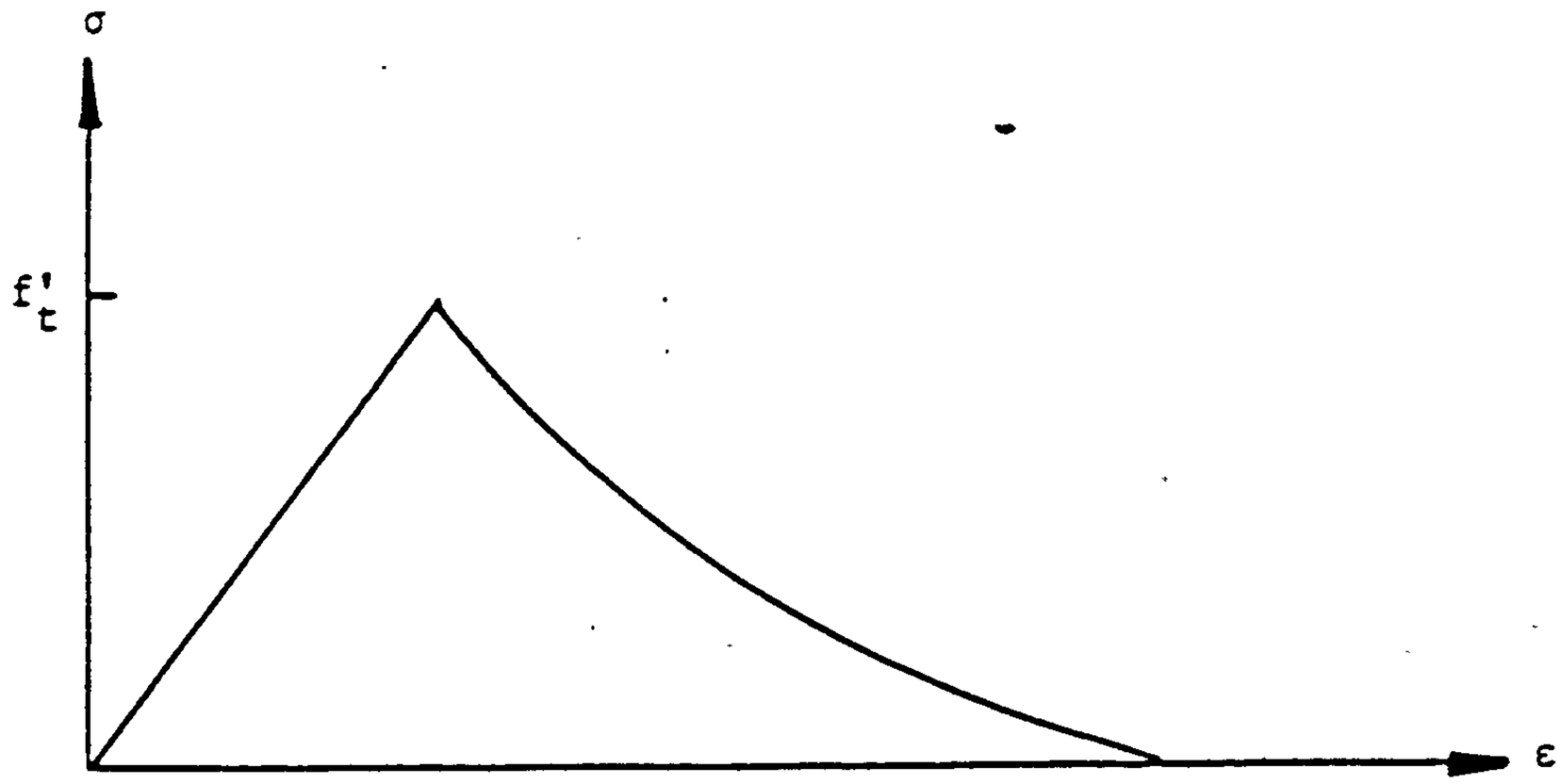

Lin's gradual unloading [52]

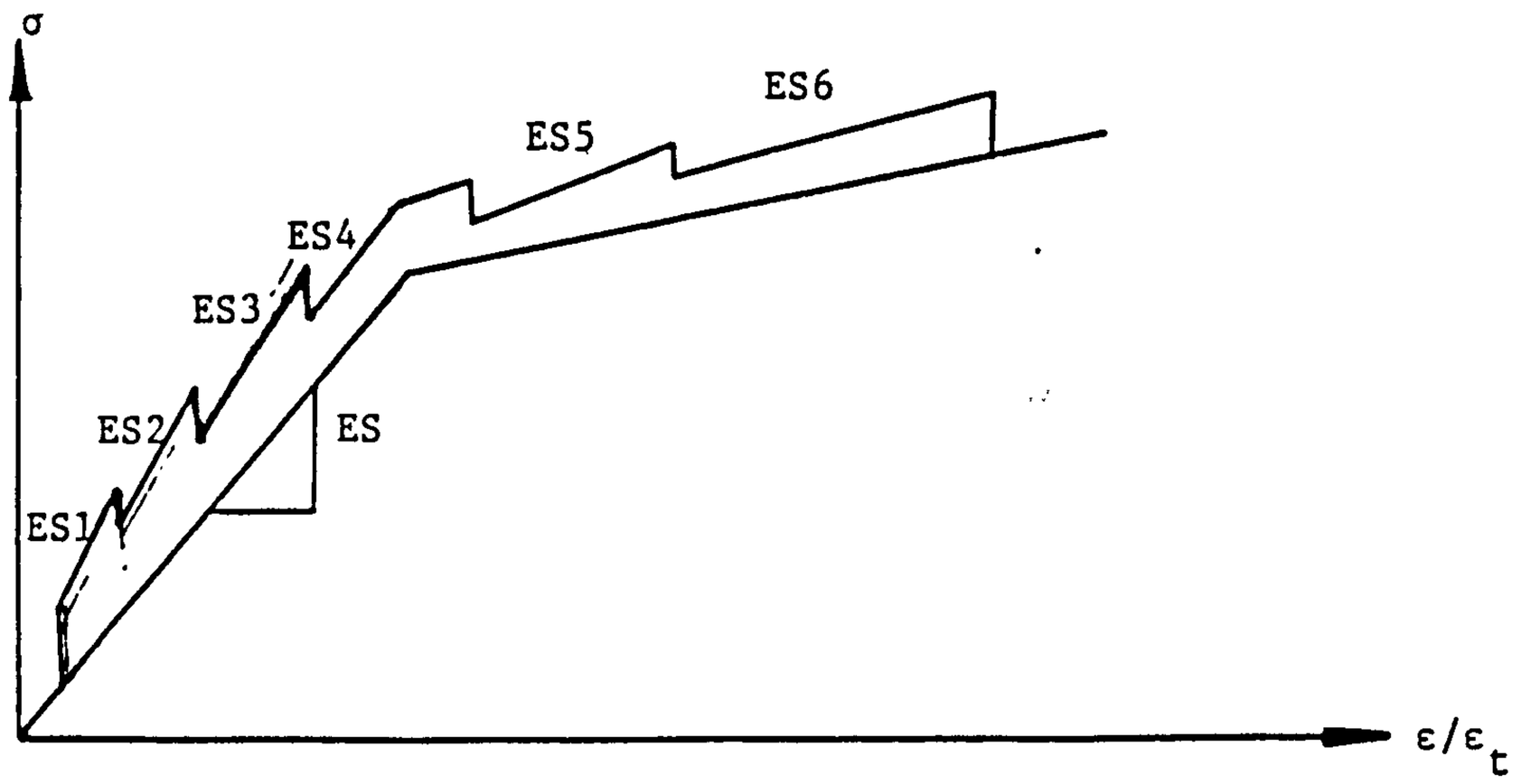

Modified stress-strain diagram for reinforcing steel [70]

Figure 5.15. Representation of tension stiffening

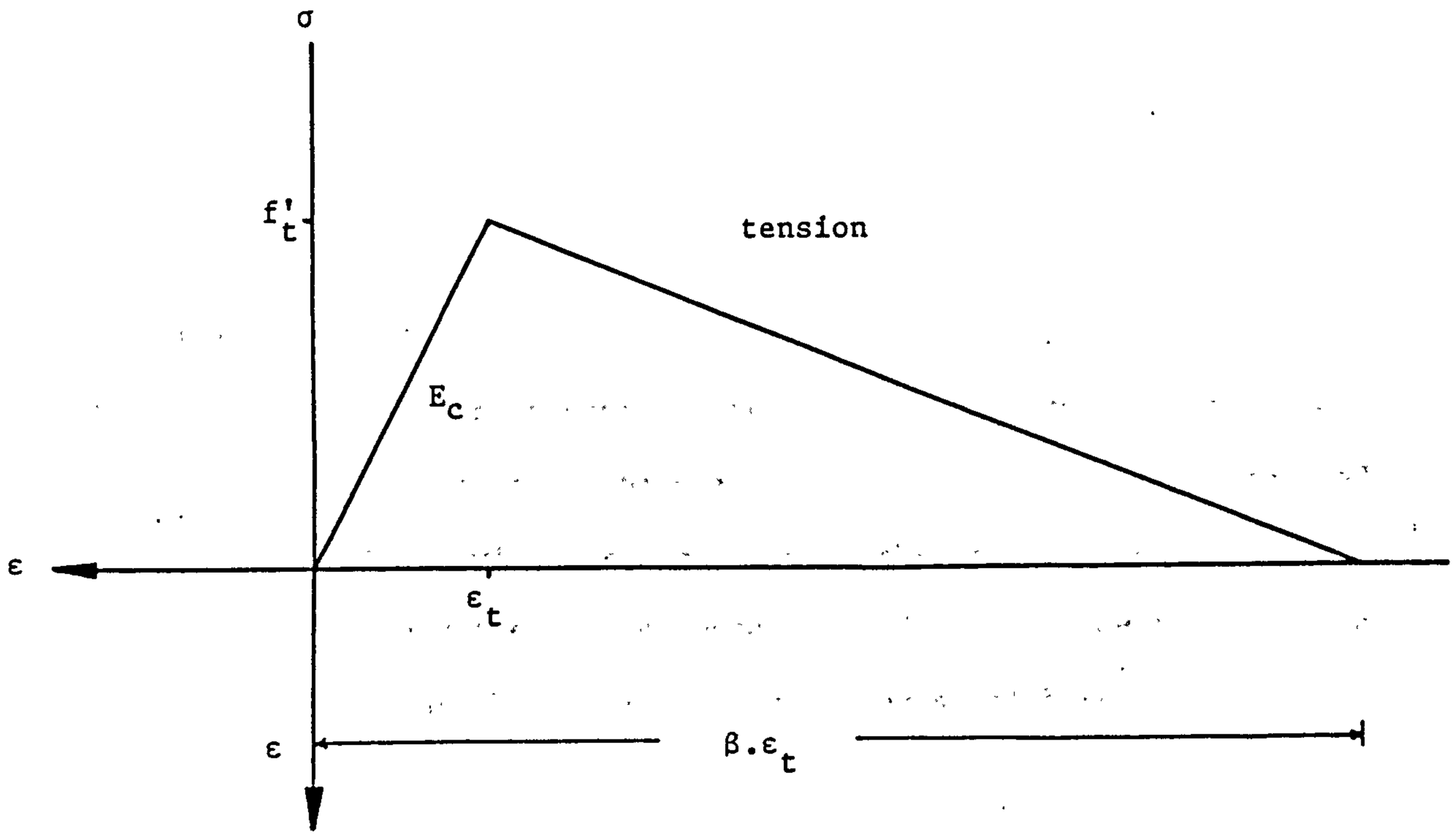

Figure 5.16. Concrete tension model with tension stiffening

that this effect is distributed throughout the depth of the tension zone.

The first approach using a descending branch similar to that adopted by Lin [52] but employing a linear curve was incorporated in the analysis. The stress-strain relationship for concrete in tension is shown in Fig.5.16.

5.6 REINFORCING STEEL

Reinforcing steel was assumed to be capable of carrying axial forces only. The reinforcing steel bars at a specific depth were smeared into a steel layer with the same area as the original reinforcement. Each steel layer had the same orientation and had its centre at the same position as the the original reinforcing steel bars.

To model the stress-strain relationship of the reinforcing steel layer a bi-linear model was used in the analysis. As shown in Fig.5.17, the following properties were required to construct the stress-strain curve

E_{st} = initial modulus of elasticity

E_{sh} = modulus of strain hardening

σ_o = yield stress

ε_{su} = ultimate strain

The strain hardening effect could be included in the representation of

the reinforcing steel, however if the modulus of the strain hardening, E_{sh}, was set equal zero the stress-strain relation became an elasto-plastic one. Loading in tension and compression was assumed to be elastic until the stress reaches the yield stress, σ_o, beyond that yielding was assumed to have occurred. Failure was assumed to occur when the strain reached the ultimate strain, ε_{su}. The reinforcing steel was then assumed to rupture and carry zero stress.

The elastic constitutive relationship for a reinforced steel layer orientated in the x-direction is given by

$$\begin{bmatrix} \sigma_x \\ \sigma_y \\ \tau_{xy} \end{bmatrix} = \begin{bmatrix} E_{st} & 0 & 0 \\ 0 & 0 & 0 \\ 0 & 0 & 0 \end{bmatrix} \begin{bmatrix} \varepsilon_x \\ \varepsilon_y \\ \varepsilon_{xy} \end{bmatrix} \qquad (5.22)$$

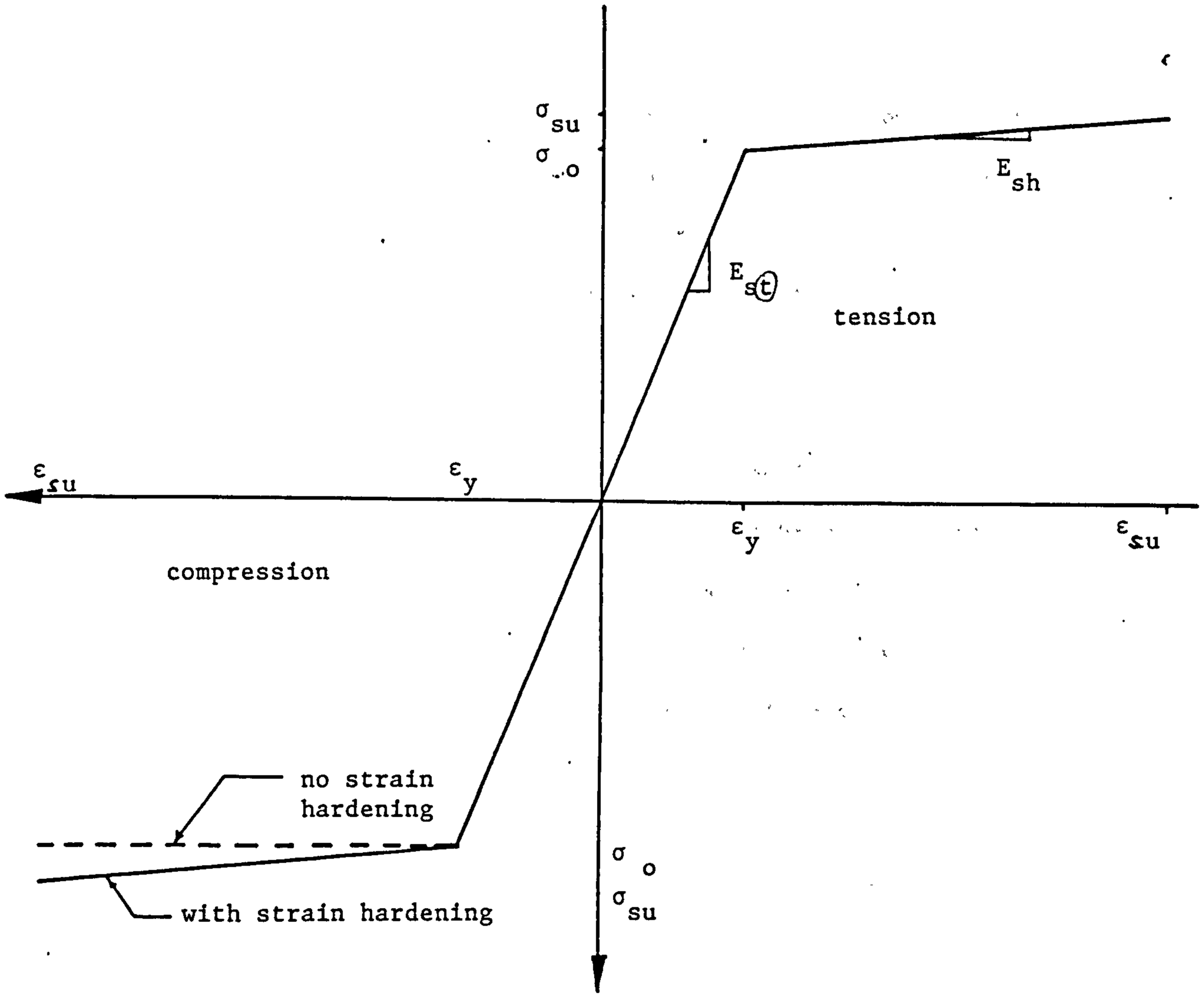

Figure 5.17. Stress-strain curve for reinforcing steel

CHAPTER 6

METHODS OF ANALYSIS AND NUMERICAL INTEGRATION

6.1 INTRODUCTION

In the analysis of a linear problem using the finite element method, the solution of the governing equations can be achieved in a direct manner. For nonlinear analysis, a more sophisticated solution strategy has to be employed because it is not possible to solve the nonlinear governing equations directly.

This Chapter describes the method of analysis used in the present work to solve the nonlinear governing equations. A brief description of the incremental and iterative methods which are usually adopted in nonlinear analyses is given in Section 6.2 and a full description of the solution techniques employed in the analysis is given in Section 6.3.

Convergence of the solution for nonlinear problems is presented in Section 6.4.

In the analysis of reinforced concrete structures the cracking and crushing of the concrete and yielding of the reinforcing steel are likely to slow the convergence process because large number of iterations are required. Improvement of the rate of convergence for such situations is discussed in Section 6.5.

The strategy for the solution used in the analysis is presented in Section 6.6.

In order to check the equilibrium of a structure, the internal forces mobilised by the structure must be determined. These forces are determined from the stress resultants around the structure which are evaluated from the stress distributions throughout the thickness.

The accuracy of a number of the most commonly used integration rules was investigated. Modifications to the numerical integration rules to improve their accuracy have been proposed and also recommendations for the use of numerical integration rules have been made. Detailed discussion is given in Section 6.7.

6.2 SOLUTION OF THE NONLINEAR EQUATIONS

Most nonlinear solution methods are based on the assumption that the nonlinear response can be approximated by a series of linear solutions. An incremental formulation of the governing equations, which is based on equilibrium between the external applied loads and the internal forces, is usually adopted. Derivations of the governing equations was given in Chapter 2, equation (2.20), which is given by

$$\{\psi(\delta)\}^n = \{F\}^n - \{P\}^n \qquad (6.1)$$

where

ψ = residual force vector

F = internal force vector

P = applied load vector

Solution of the governing equations, equation (6.1), can be carried out using either an incremental or iterative methods of solution.

6.2.1 INCREMENTAL METHODS

In these methods the solution of equation (6.1) is usually carried out by applying the external loads as a sequence of sufficiently small increments so that the structure can be assumed to respond linearly within each increment. This method can lead to deviation from the true response, Fig.6.1.

More efficient incremental schemes can be obtained by combining the pure incremental method with a single equilibrium correction. Better approximation of the true response can be obtained using this technique, Fig.6.2.

The accuracy of the solution using either the pure incremental or the corrected incremental methods depends on the size of the load increment. The increments need to be small enough in order to obtain a good approximation of the true response since the accumulating errors are carried from one increment to the next throughout the solution process.

6.2.2 ITERATIVE METHODS

In these methods the load is applied incrementaly and a series of iterations are carried out within each increment to eliminate the cumulative errors inherent in the previous methods.

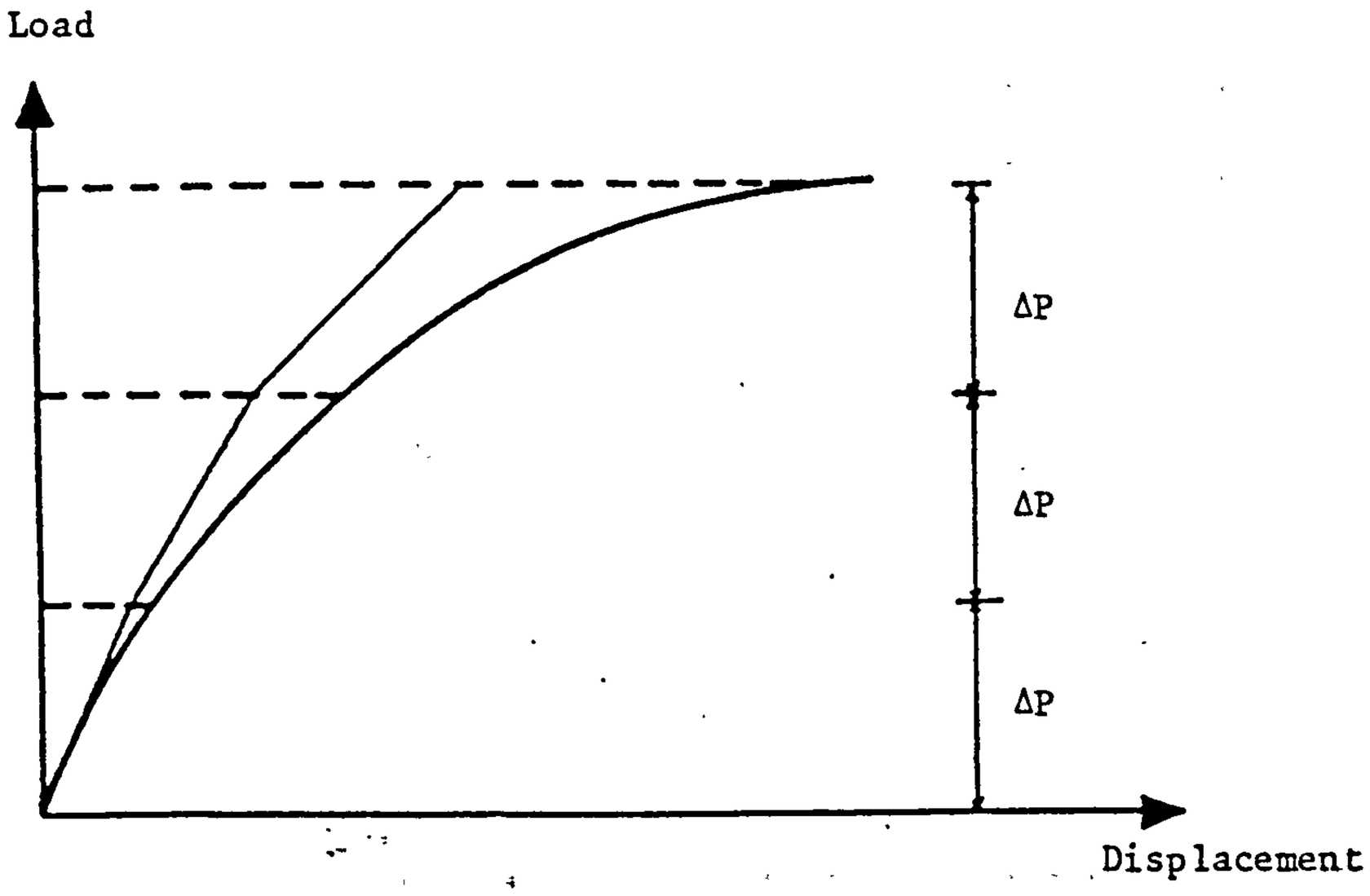

Figure 6.1. Incremental load method without corrections

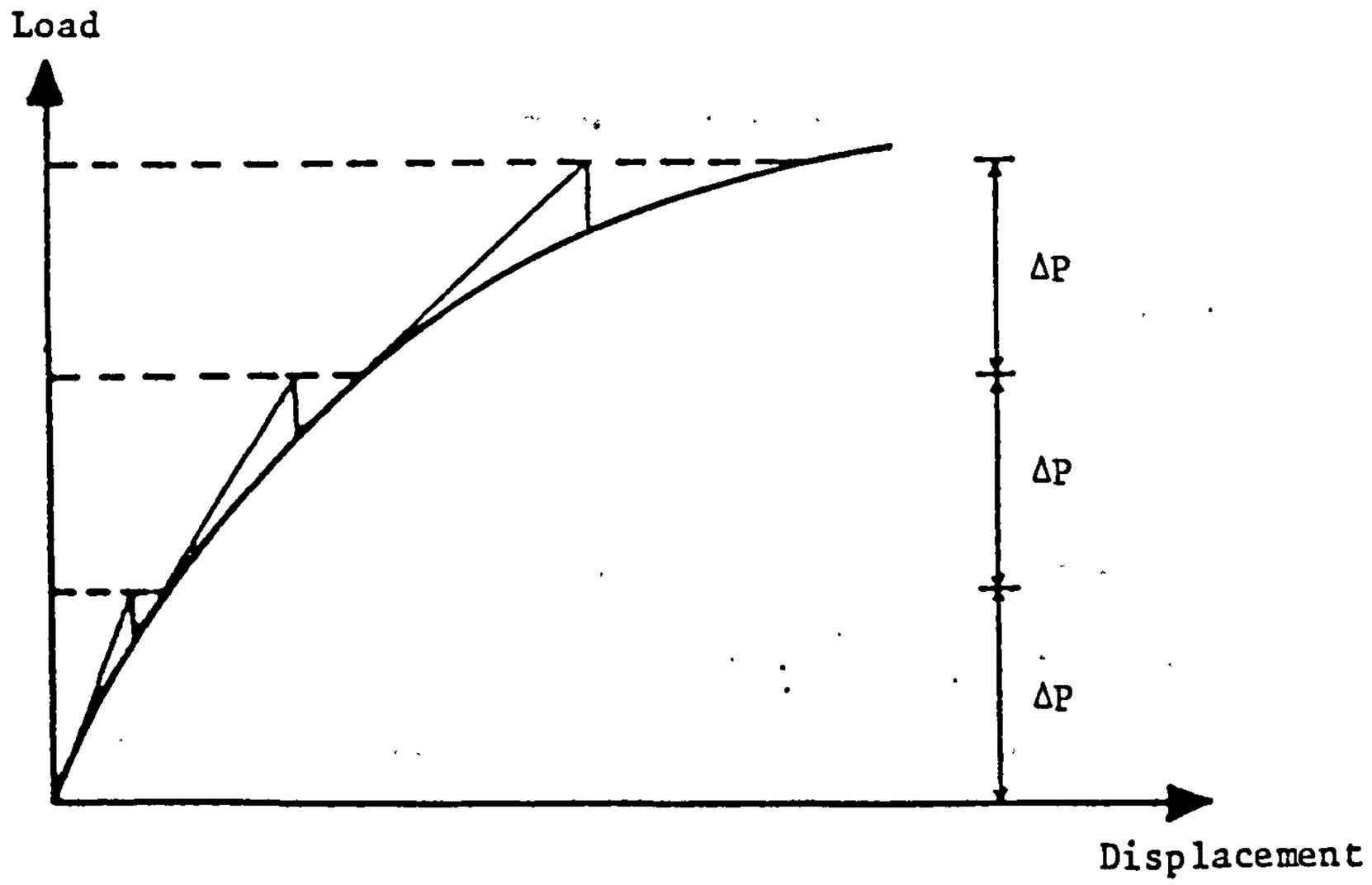

Figure 6.2. Incremental load method with equilibrium corrections

If an approximate solution $\{\delta\}^n$ to equation (6.1) is reached, an improved solution can be obtained using a truncated Taylor series expression.

$$\{\psi(\delta)\}^n_{i+1} = \{\psi(\delta)\}^n_i + \left.\frac{d\psi}{d\delta}\right|_{\delta^n_i} \{\Delta\delta\}^n_i \tag{6.2}$$

where

$$\left.\frac{d\psi}{d\delta}\right|_{\delta^n_i} = [K_T]^n_i \tag{6.3}$$

Equation (6.3) represents the tangential stiffness matrix for increment n at iteration i.

An improved value of the displacement $\{\delta\}^n_{i+1}$ can be obtained by computing

$$\{\delta\}^n_{i+1} = \{\delta\}^n_i + \{\Delta\delta\}^n_i \tag{6.4}$$

The incremental displacements $\{\Delta\delta\}^n_i$ can be determined from equations (6.2) and (6.3) such that

$$\{\Delta\delta\}^n_i = - [K_T]^{n\,-1}_i \{\psi\}^n_i \tag{6.5}$$

The solution is carried out by solving a new set of linearized equations, equation (6.5). Displacements are then updated using equation (6.4) and the residual forces are calculated from equation (6.1). The process is repeated until the solution converges.

Various methods can be classified based on the manner in which the stiffness matrix is formed.

6.2.2.1 NEWTON-RAPHSON METHOD

In this method the tangential stiffness matrix is formed and decomposed at the beginnig of every iteration. The solution process is illustrated diagrammatically in Fig.6.3, for a one degree of freedom. The major drawback of this method is the high cost of it. The repeated formations and decompositions of the stiffness matrices requires much more time than that required for the solution of the system of equations.

6.2.2.2 MODIFIED NEWTON-RAPHSON METHOD

In this method the tangential stiffness matrix is updated and held constant for a number of iterations, after which it is again updated. The solution process is illustrated diagrammatically in Fig.6.4, for a one degree of freedom. This method is more economical than the Newton-Raphson method since it involves fewer expensive reformations and decompositions of the stiffness matrix, however it may require more iterations than those required using the standard Newton-Raphson method.

6.2.2.3 INITIAL STRESS METHOD

In this method the initial elastic stiffness matrix is formed and decomposed at the beginning and held constant throughout the analysis. This method was introduced by Zienkiewicz et al [71] for the solution of elastic-plastic problems. The solution process is illustrated

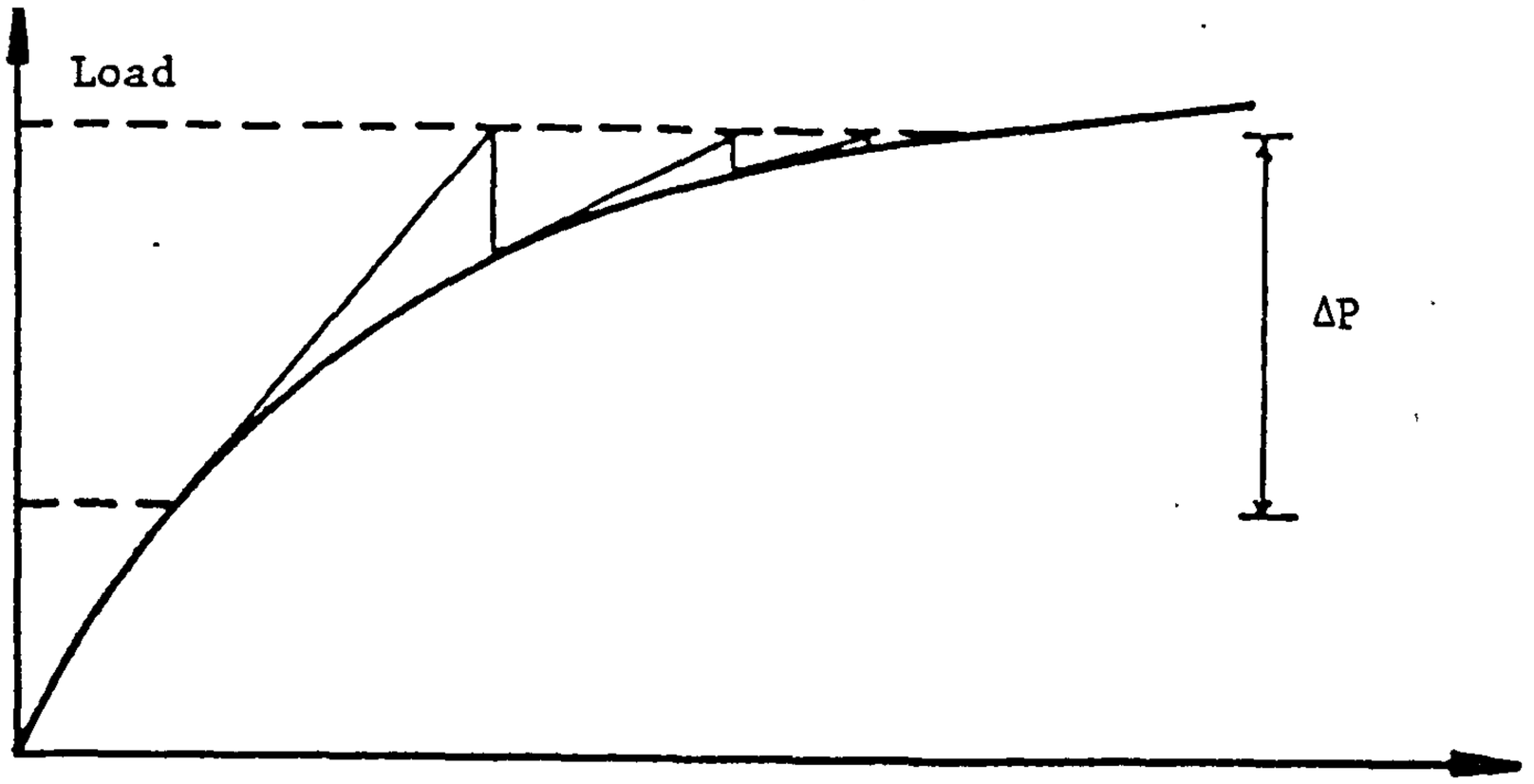

Figure 6.3. Newton-Raphson method

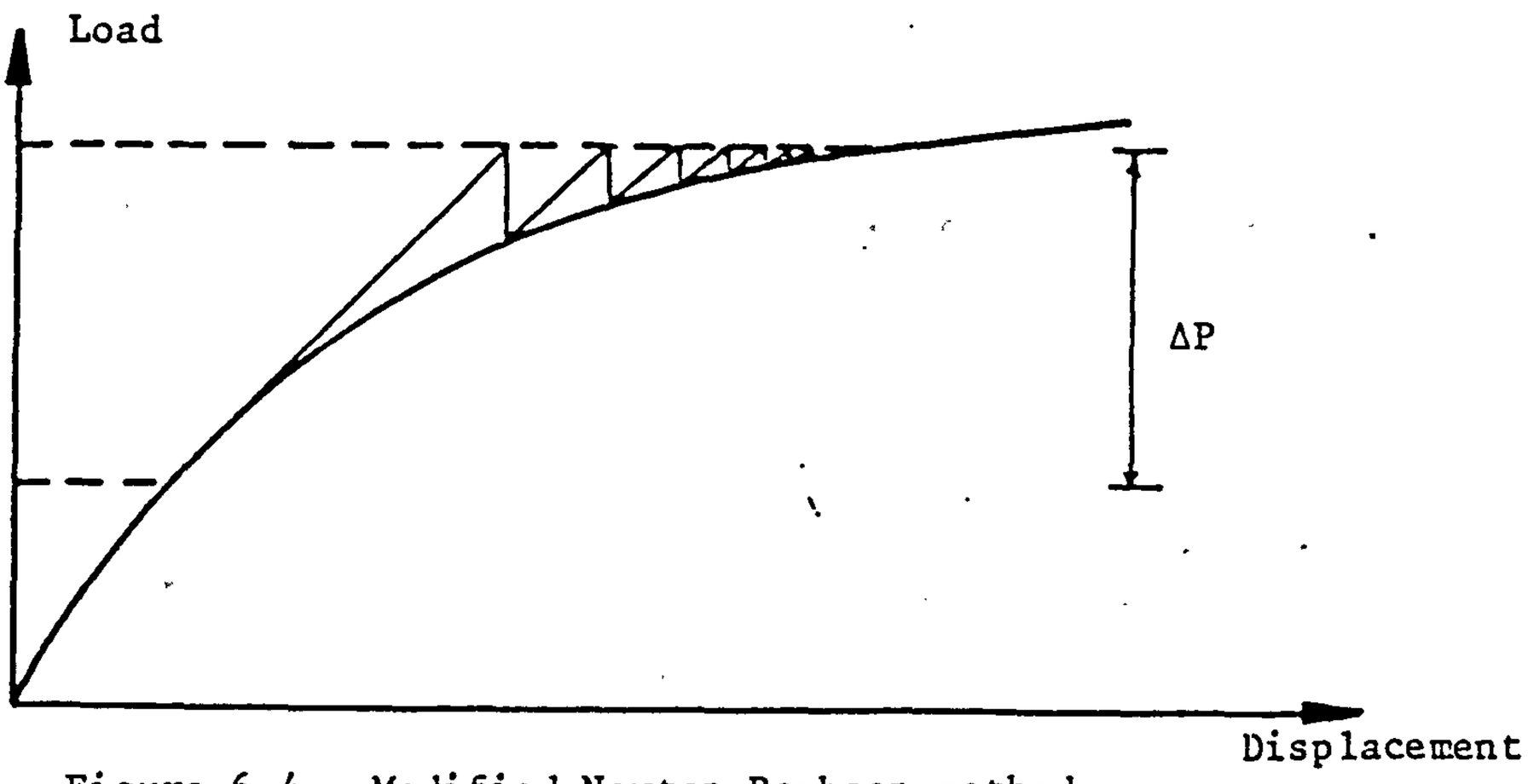

Figure 6.4. Modified Newton-Raphson method

Figure 6.5. Initial stress method

diagrammatically in Fig.6.5, for a one degree of freedom. This method is less efficient than the previous Newton-Raphson methods because the convergence of the solution requires more iterations than those required by the previous iterative methods.

6.3 DESCRIPTION OF THE TECHNIQUES USED IN THE SOLUTION OF THE GOVERNING EQUATIONS

The technique used in the analysis to solve the governing equations was based on the modified Newton-Raphson method. The nonlinear behaviour of the structures considered was assumed to be due to both geometric and material nonlinearities.

To avoid any numerical instabilities that might be encountered due to either unloading, which may take place during an iteration due to redistribution of the residual forces, or due to ill-conditioned stiffness matrices at or near the ultimate load, the linear elastic constitutive relationships were used in the formulation of the stiffness matrices throughout the analysis. At no stage modifications of the stiffness matrices attempted to take account of the material nonlinearities because such modifications are also very expensive in a finite element layered approach. The reformation of the stiffness matrices involves updating the nonlinear part of the stiffness matrix which is dependent on both the current displacements and stress level.

Two techniques were adopted to control the solution of the governing equations. In the first the independent variable was the applied load

and the nodal displacements were the unknowns in the solution of the governing equations.

Consider the structural response shown in Fig.6.6, the load control technique can be used to trace the ascending part of the response, indicated by points 0 and 1.

The load control technique obviously fails to trace the falling part of the response, indicated by points 1 and 3, it can only trace point 3 after tracing point 1.

The arc length method [72] and the displacement control [73] techniques can be used to trace the nonlinear response in the analysis of such problems. Although the arc length method has been recognised as a very powerful technique for tracing the stable and unstable equilibrium paths, it has been found to fail for some problems involving the nonlinear analysis of reinforced concrete structures. Abdel Rahmman [74] used the arc length method in a finite element analysis of reinforced concrete slabs and concluded that the method yields unusual results. This is likely due to the fact that the arc length method may pick up unstable positions along the falling part of the response.

A displacement control technique similar to that proposed by Stricklen et al [73] was adopted in the analysis. In this technique an incremental displacement component is specified and the corresponding load becomes one of the unknowns.

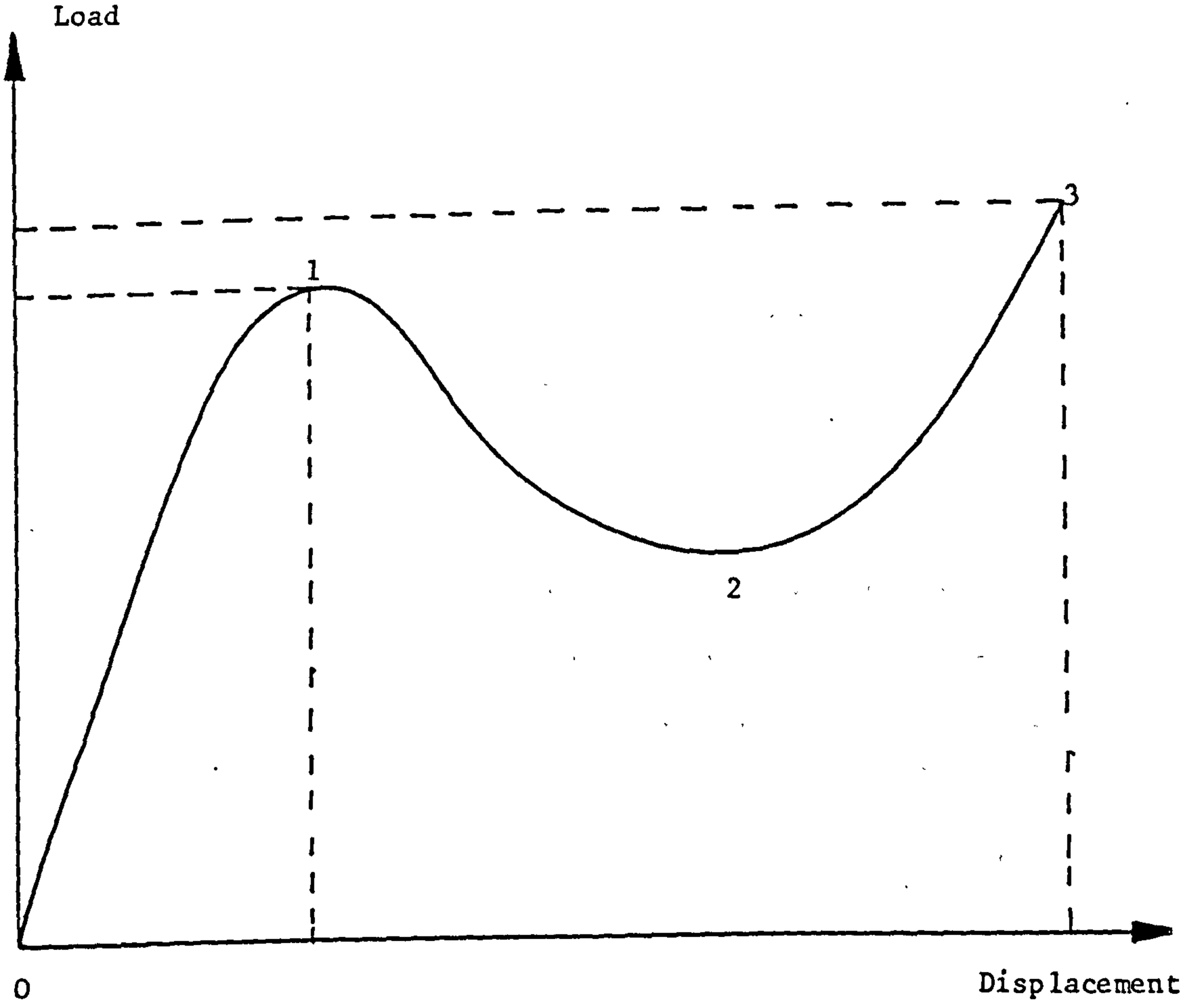

Figure 6.6. Load-deflection curve

6.3.1 LOAD CONTROL

The main operations performed in the load control technique are shown in Fig.6.7. At the beginning of a load increment, the approximate solution of the governing equations is obtained by solving for the incremental nodal displacements such that

$$\{\Delta\delta\}_i^n = [K_T]^{-1} \{P_1\} \tag{6.6}$$

where the vector $\{P_1\}$ is made equal to the vector of the applied incremental load $\{P\}^n$, $[K_T]$ is the overall tangential stiffness matrix and $\{\Delta\delta\}$ is the vector of the incremental nodal displacements.

At the end of every iteration the vector $\{P_1\}$ is made equal to the residual force vector $\{\psi\}$. Improved values of the incremental displacements are obtained by computing the iterative nodal displacements, equation (6.6), and hence updating the total nodal displacements using equation (6.4). The process is repeated until convergence occurs.

6.3.2 DISPLACEMENT CONTROL

The concept of this technique is based on the interchange of the dependent and independent variables of the governing equations. A single incremental nodal displacement component is selected and specified as a controlling parameter while the corresponding load value is considered one of the unknowns. The nonlinear governing equations, equation (6.1), can be rewritten as

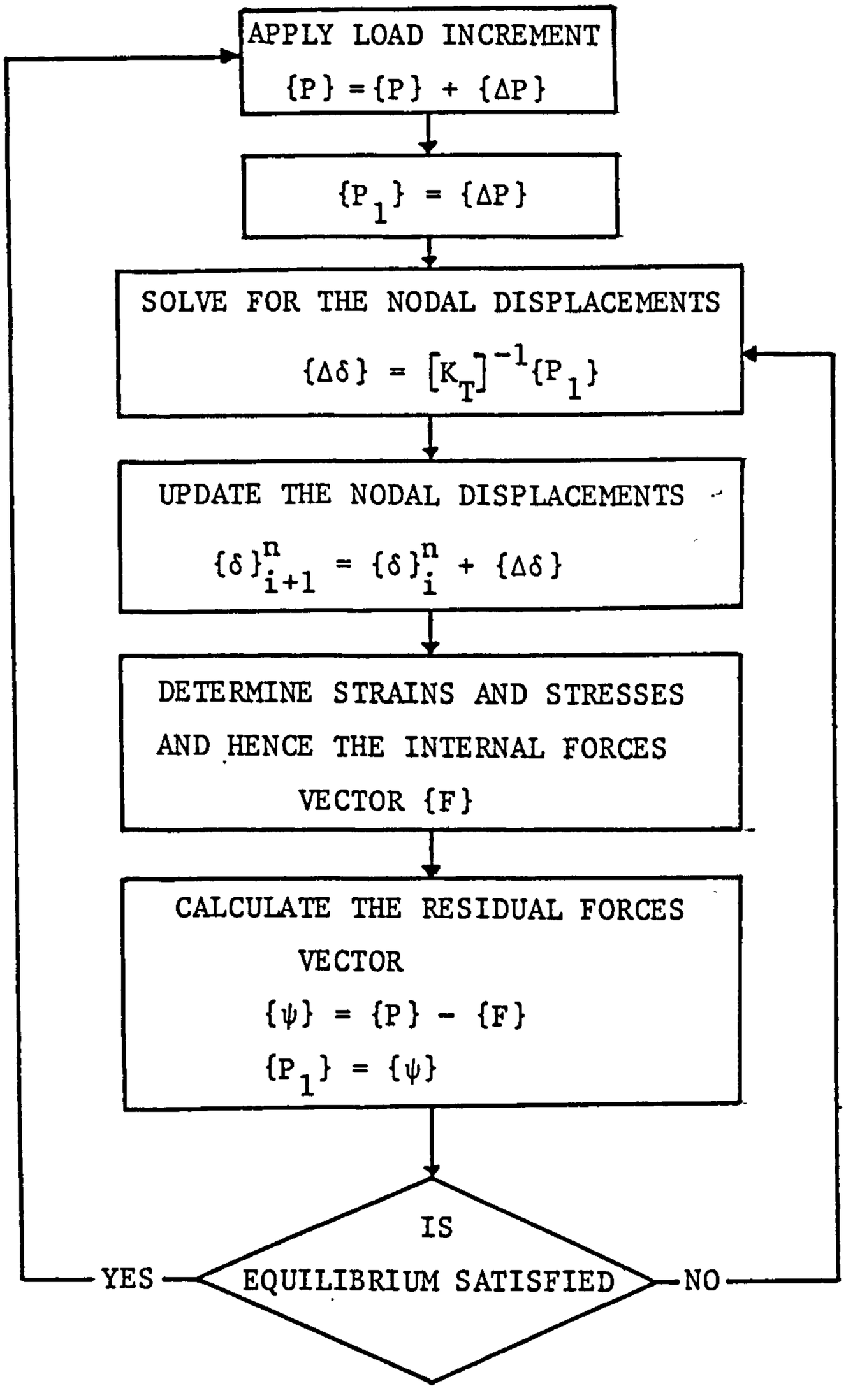

Figure 6.7. Main operations used in the load control

$$[K]\ \{\Delta\delta\} - \{P\} = \{\psi\} \tag{6.7}$$

where the incremental generalized force vector $\{P\}$ can be expressed in terms of an incremental load factor $\Delta\lambda$ and a generalized force vector $\{P^*\}$ due to a unit load, such that

$$\{P\} = \Delta\lambda\{P^*\} \tag{6.8}$$

Using equation (6.8), equation (6.7) can be rewritten as

$$[K]\{\Delta\delta\} - \Delta\lambda\{P*\} = \{\psi\} \tag{6.9}$$

Assume that the ith incremental displacement component $\Delta\delta_i$ is specified and for simplicity, assume that equation (6.9) is reordered such that the specified displacemet component is the final term in the vector $\Delta\delta$. The later assumption enables the theoretical derivation to be simplified. In practice it is not necessary that the specified displacement component should be the final term, further details are given in Appendix II. Equation (6.9) can be rewritten as

$$\left[\begin{array}{c:c} [K_{11}] & -\{P_1^*\} \\ \hdashline \{K_{21}\} & -P_i^* \end{array}\right]\left[\begin{array}{c} \{\Delta\delta_1\} \\ \hdashline \Delta\lambda \end{array}\right] = \left[\begin{array}{c} \{\psi_1\} \\ \hdashline \psi_i \end{array}\right] - \Delta\delta_i \left[\begin{array}{c} \{K_{12}\} \\ \hdashline K_{22} \end{array}\right] \tag{6.10}$$

where K_{22}, $\Delta\delta_i$, P_i^* and ψ_i are scalars K_{12} is a column vector and K_{21} is a row vector.

The matrix on the left hand side of equation (6.10) is a nonsymmetric

matrix, however the submatrix $[K_{11}]$ is symmetric if the original stiffness matrix [K] is symmetric. To avoid solving a nonsymmetric system of equations the unknown incremental displacement components and the incremental load factor can be obtained by expanding equation (6.10), such that

$$[K_{11}]\{\Delta\delta_1\} = \Delta\lambda\,\{P_1^*\} + \{\psi_1\} - \Delta\delta_i\{K_{12}\} \tag{6.11}$$

$$\{K_{21}\}\{\Delta\delta_1\} = \Delta\lambda.P_i^* + \psi_i - \Delta\delta_i\, K_{22} \tag{6.12}$$

where $\Delta\delta_1$ can be obtained from equation (6.11), such that

$$\{\Delta\delta_1\} = [K_{11}]^{-1}[\Delta\lambda.\{P_1^*\} + \{\psi_1\} - \Delta\delta_i\{K_{12}\}] \tag{6.13}$$

and the incremental load factor can be obtained from equations (6.12) and (6.13), such that

$$\Delta\lambda = \frac{\psi_i - \{K_{21}\}[K_{11}]^{-1}\{\psi_1\} + [\{K_{21}\}[K_{11}]^{-1}\{K_{12}\} - K_{22}]\Delta\delta_i}{\{K_{21}\}[K_{11}]^{-1}\{P_1^*\} - P_i^*} \tag{6.14}$$

The solution of the nonlinear system of equations, equation (6.10), is found by solving equation (6.14) followed by equation (6.13). The main operations performed in the displacement control method are shown in Fig.6.8. At the beginning of each increment a load factor λ is set equal to zero and the incremental displacement component is assigned a preset value. The incremental load factor was obtained

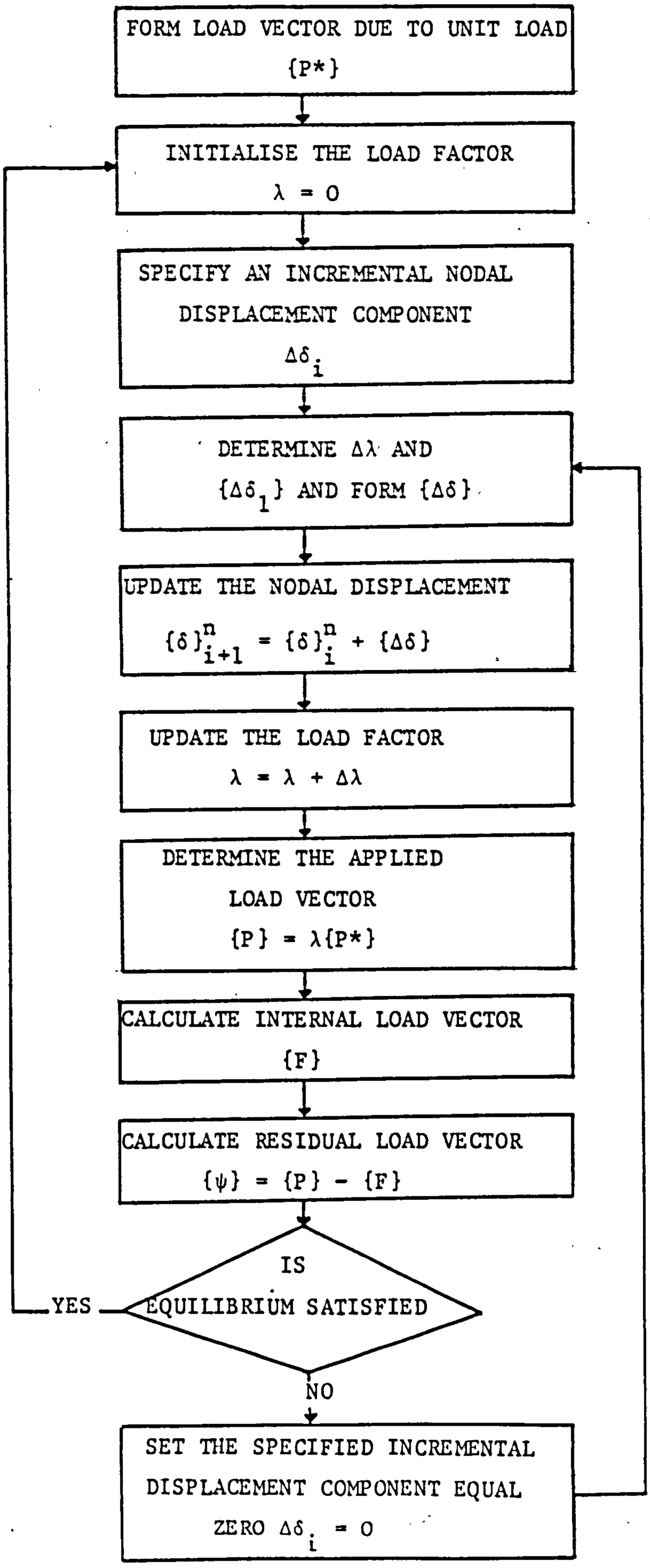

Figure 6.8. Main operations used in the displacement control

from equation (6.14) and hence the incremental displacements $\{\Delta\delta_1\}$ were determined form equation (6.13). Details of the formation of the different matrices required to solve equations (6.13) and (6.14) are given in Appendix II.

Since the specified incremental displacement component was specified at the beginning of the increment, it must be held constant during the iterative process, therefore it was set equal to zero after the first iteration.

At the end of each iteration the load factor λ was updated such that

$$\lambda = \lambda + \Delta\lambda \tag{6.15}$$

The nodal displacements were then updated using equation (6.4) and the process was repeated until convergence occurred.

6.4 CONVERGENCE CRITERIA

In a nonlinear analysis convergence is assumed to occur when the difference between the applied loads and the internal forces has reached an acceptably small value. The criteria used are set so that the iterative process is terminated when it is considered that additional iterations would not improve the accuracy of the solution significantly.

Several convergence criteria can be used to monitor equilibrium. These criteria are usually based on forces, displacements or energy.

In the Mindlin plate formulation in which the transverse shear deformations are included, the transverse shear stresses are determined independently of the in-plane and flexural stresses. These stresses are adjusted according to the current material state, whilst the transverse shear stresses are held constant. The transverse internal forces are determined from the transverse shear stresses, therefore equilibrium between the lateral applied loads and the lateral internal forces is always achieved and cannot be used to monitor the convergence of the solution.

Two convergence criteria, based on displacements and energy respectively, were used in the analysis to check for convergence. The displacement criterion is that

$$\frac{||\Delta\delta||_i}{||\delta||_{i+1}} \leq \alpha_D \qquad (6.16)$$

where

$||\quad||_i$ is the euclidean norm at iteration i

and $||\Delta\delta||_i = \sqrt{\sum_{i=1}^{n} \{\Delta\delta\}_i^2}$

α_D is the displacement convergence tolerance.

The energy criterion used in the analysis is similar to that used by Cope et al [57] in which the energy released during an iteration by the residual forces and the iterative displacements are compared to the maximum energy released in a previous iteration of that particular increment. Thus convergence is assumed when

$$\frac{\{\psi\}^T\{\Delta\delta\}_i}{\{\psi\}_1^T\{\Delta\delta\}_1} \leq \alpha_E \qquad (6.17)$$

where

α_E is the energy convergence tolerance

The use of the energy norms, which involves monitoring both displacements and forces, has been recommended by Bathe et al [75].

6.5 ACCELERATORS

6.5.1 INTRODUCTORY REMARKS

The increasing interest in nonlinear structural analysis has led to attempts to improve the convergence characteristics of the iterative methods.

Several acceleration schemes have been developed and introduced in nonlinear finite element analyses.

Phillips et al [76] used the 'Alpha' constant stiffness method [77] in the analysis of reinforced concrete structures, however it was found that the procedure was unstable.

Cope et al [78] used the modified Aitken method [79] procedure in the analysis of reinforced concrete slabs and concluded that the procedure did not significantly speed up convergence.

Recently, line search techniques have been introduced to accelerate the rate of convergence of the solution for nonlinear structural analyses. The importance of the line search in speeding up the convergence of the analysis of reinforced concrete structures has been recognized [80-81]. The line search technique was incorporated in the analysis to improve the rate of convergence of the modified Newton-Raphson method in the analysis of reinforced concrete slabs. Formulation of the line search technique which is similar to that given by Crisfield [82] is presented in the next section.

6.5.2 LINE SEARCH

In the iterative procedure represented by equation (6.4), The iterative displacements $\Delta\delta$ can be multplied by an acceleration scalar such that

$$\{\delta\}_{i+1} = \{\delta\}_i + \eta_i \{\Delta\delta\}_i \qquad (6.18)$$

The concept of the line search is to find the optimum or near optimum value of the scalar η_i. Effectively the line search process tries to find a stable equilibrium state by choosing a value of η_i such that the residual forces in the next iteration are zero. Hence

$$S = \{\Delta\delta\}_i^T \{\psi\}_{i+1} = 0 \qquad (6.19)$$

In energy terms, this coincides with searching to find an optimum scalar by seeking a stationary value of the total potential energy Φ with respect to the displacements δ_i, since

$$\{\psi\}_{i+1} = \frac{\partial \Phi}{\partial \{\delta\}_{i+1}} \qquad (6.20)$$

Equation (6.19) can be satisfied by trial and error. Achieving this requires recalculation of the residual forces. Instead of obtaining the exact solution of equation (6.19), it is more efficient to satisfy

$$|S| < \Psi |S_o| \tag{6.21}$$

where

Ψ is a tolerance given by

$$0.0 \leq \Psi \leq 1.0$$

The concept is illustrated in Fig.6.9. It was shown that a slack tolerance of 0.8 gave similar results to those obtained using a tighter tolerance of 0.4 and required less computation time [82]. Therfore a tolerance of 0.8 was adopted in equation (6.21).

The following approach was employed to obtain suitable estimate of the acceleration scalar. The main operations performed in the line search technique are shown in Fig.6.10. The first trial of η_i was 1.0. If equation (6.21) is not satisfied, linear interpolation or extrapolation was used to find a better estimate of the optimum accelerator scalar, η_{i+1}.

$$\frac{\eta_{i+1}}{\eta_i} = \frac{- S_o}{S - S_o} \tag{6.22}$$

If η_{i+1} is greater than η_i the process involves extrapolation which may lead to overestimation of the displacements. Consequently a maximum limit of the ratio η_{i+1}/η_i was set equal to 10.0. If η_{i+1} was very small the change in the displacements would be small, hence the

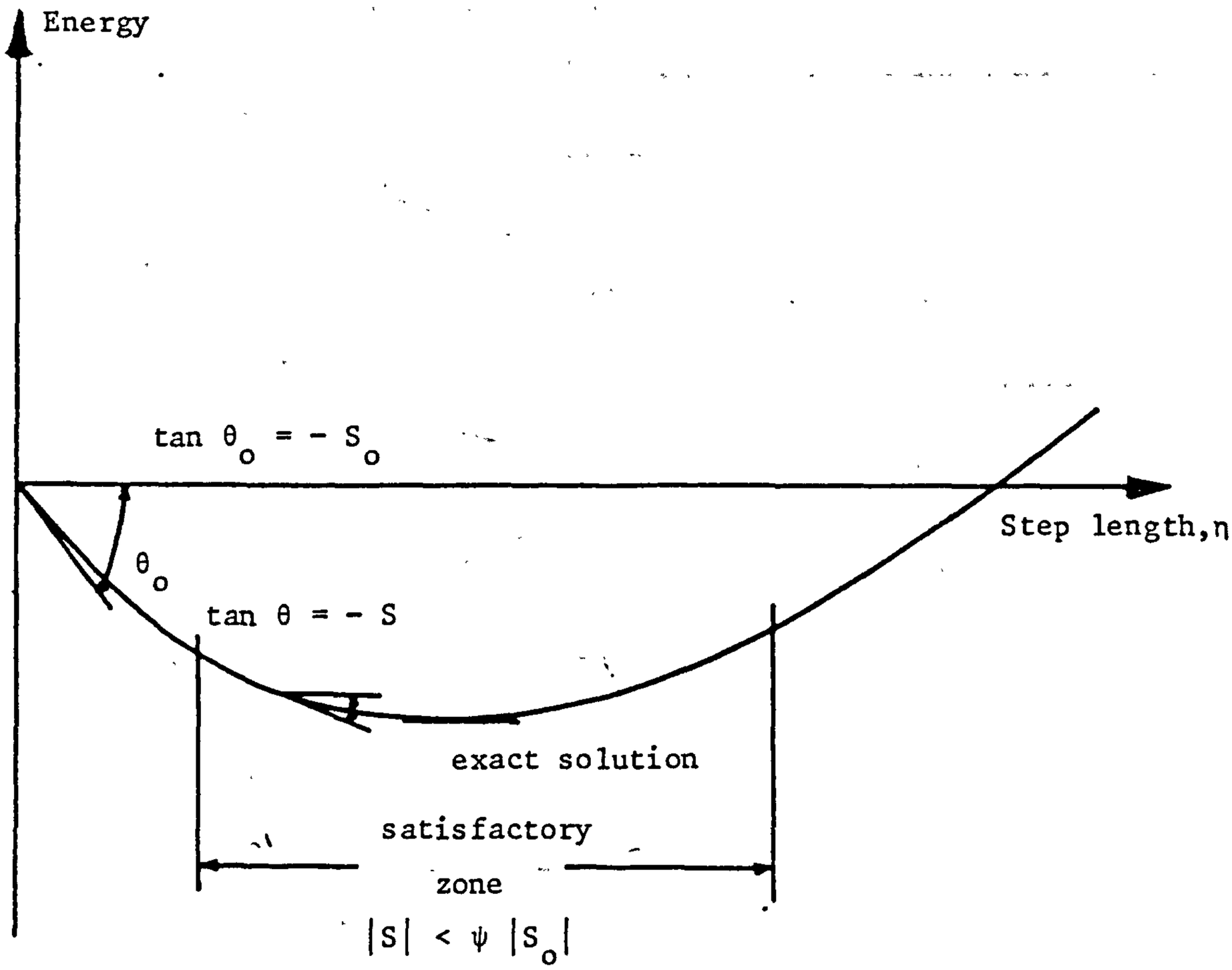

Figure 6.9. Line search concept

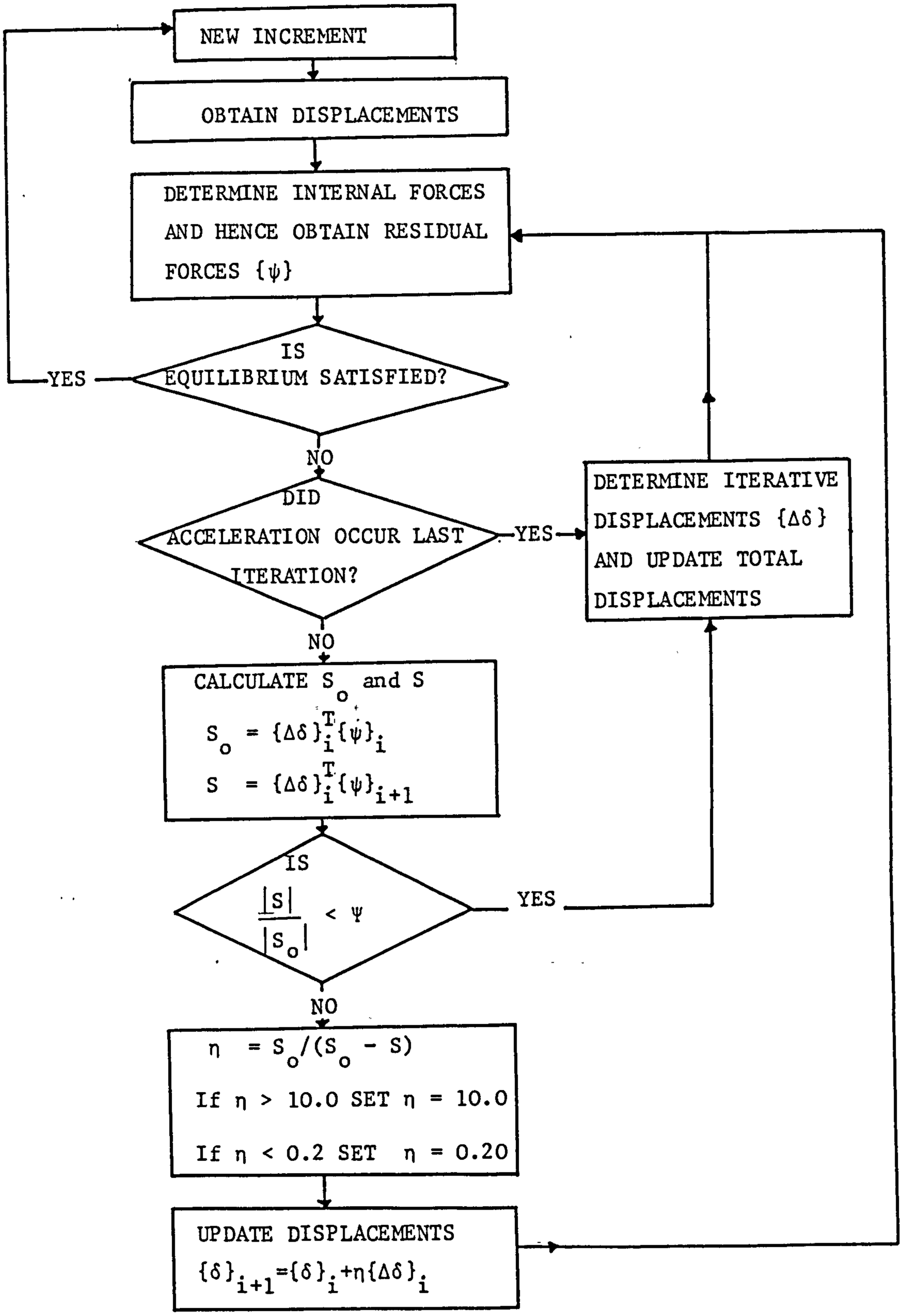

Figure 6.10. Main operations performed in the line search

procedure may fail to converge, therefore the ratio was set equal to 0.20.

Tellett [83] used the line search technique in a nonlinear finite element analysis of pocket-type reinforced brickwork retaining walls using the initial stress method and reported that the inclusion of the line search reduced the number of iterations considerably.

The use of more sophisticated line search techniques such as the 'Second Derivative Method' were reported by Crisfield [82]. It was found that these sophisticated techniques have not shown any improvement on the simple line search technique described above.

6.6 SOLUTION STRATEGY

The modified Newton-Raphson method was used to trace the nonlinear response. Solution of the governing equations was carried out by incrementing the applied load or a specified displacement component as described in Section 6.3. The main operations performed in the analysis are shown in Fig.6.11. At the beginning of each increment the iterative nodal displacements were calculated by solving the governing equations, equation (6.6) when load control was used, and equations (6.13) and (6.14) when displacement control was used. The nodal displacements were then updated to obtain the total nodal displacements using equation (6.4). Using the nodal displacements, the strains at the Gauss quadrature points of each element were then determined. Fig.6.12 indicates the various Gauss quadrature schemes

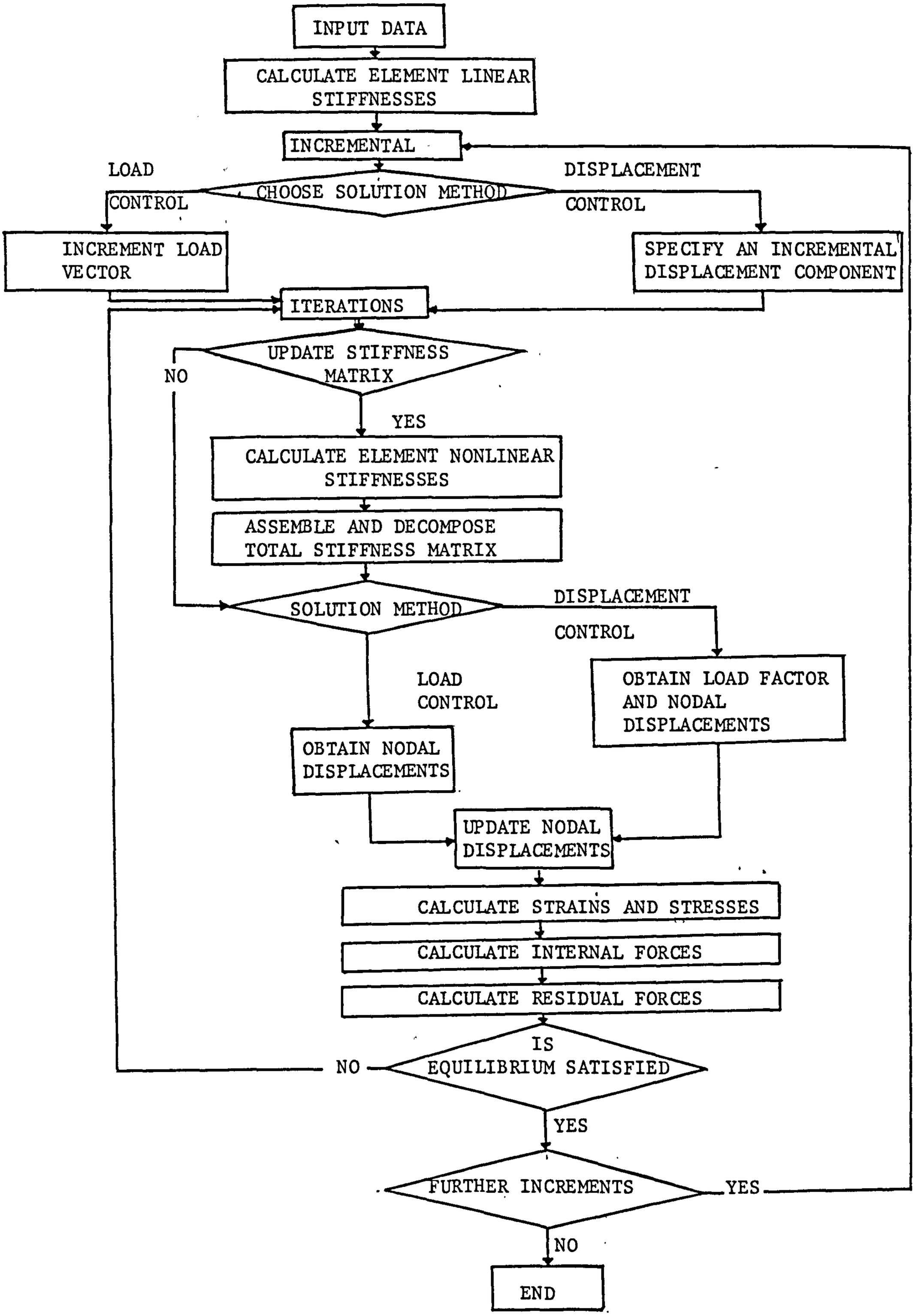

Figure 6.11. Main operations performed in the analysis

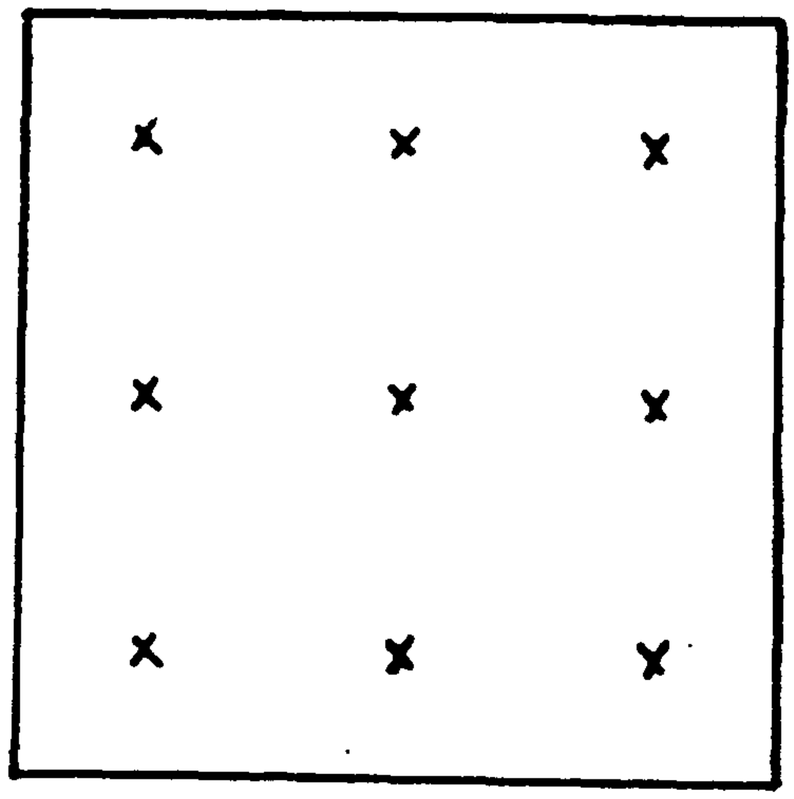

3 x 3 Gauss quadrature rule for in-plane and flexual stress components

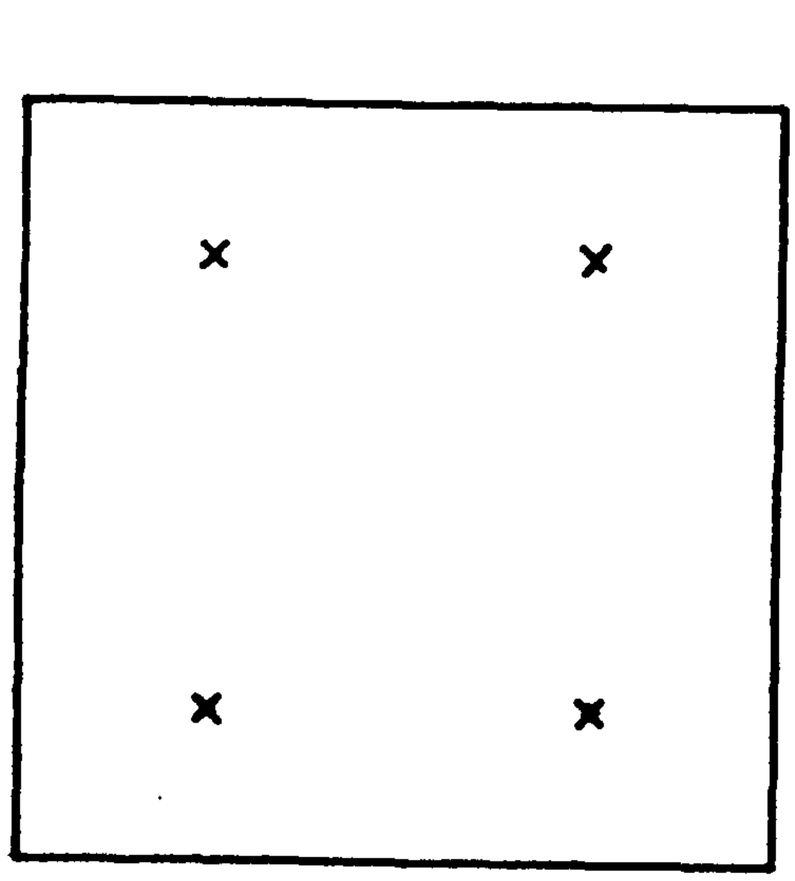

2 x 2 Gauss quadrature rule for transverse shear stress component

Figure 6.12. Integration rules used in the analysis

used for the evaluation of the different stress components. The transverse shear resultants were determined in a direct manner since the transverse shear stress was assumed to vary linearly throughout the thickness as described in chapter 2.

The in-plane and flexural stresses were determined from the strains at the sampling points through the cross-section using the material models described in Chapter 5. The in-plane and the flexural stress resultants were determined numerically by integrating the corresponding stresses through the thickness.

The internal forces were then determined for each element using

$$\begin{bmatrix} f_p \\ \hline f_b \end{bmatrix} = \int_{A_e} \left[\begin{array}{c|c} B_p & \frac{1}{2} B_{NL} \\ \hline 0 & B_b \end{array}\right]^T \begin{bmatrix} \bar{\sigma}_p \\ \hline \bar{\sigma}_b \end{bmatrix} dA_e \qquad (6.23a)$$

$$\{f_s\} = \int_{A_e} [B_s]^T \{\bar{\sigma}_s\} \; dA_e \qquad (6.23b)$$

where the subscripts p, b and s refer to the in-plane, flexural and transverse shear components respectively.

{f} of all elements were added together to obtain an internal force vetor {F}, for all the structure.

The internal force vector {F} was then subtracted from the applied load vector {P} to obtain a vector of residual forces {ψ}. If the applied load vector and the internal force vector were in equilibrium

$\{\psi\}=0$. Generally this is not true, so $\{\psi\}$ has to be reapplied around the structure. This can be achieved by solving the governing equations again and updating the nodal displacements.

As the analysis is repeated, the terms in $\{\psi\}$ become smaller if the analysis converges. When an iteration has converged, the incremental process is repeated until the analysis is terminated.

6.7 NUMERICAL INTEGRATION

6.7.1 INTRODUCTORY REMARKS

In the layered approach, the stress resultants such as in-plane forces and moments are determined by integrating the stresses at the various layers or sampling points through the thickness. Analytical integration in the nonlinear analysis is impossible since the stress function is unknown, therefore, numerical integration must be resorted to.

Two integration schemes were used in the analysis. The first scheme is based on a modified trapezoidal rule in which the trapezoid was divided into a rectangle and a triangle in order to improve the accuracy of the calculated moments. This rule was used with the multi-linear stress-strain curves, Fig.5.3.

The second scheme is based on the Lobbato rule, which was selected from various numerical integration rules because of its expected accuracy for estimating the stress resultants for a concrete section

with various stress distribution conditions. This rule was used with the nonlinear stress-strain curves, Fig.5.4.

Discussion of the accuracy of the different numerical integration rules which were investigated and a proposed modification are presented in the next sections.

6.7.2 NUMERICAL INTEGRATION RULES

In numerical integration the function to be integrated is replaced by the sum of a series such that

$$\int_a^b f(x)\,dx = \sum_{i=1}^{n} W_i f_i \qquad (6.24)$$

where W_i are the weights and f_i is $f(x)$ evaluated at the ith sampling points.

The selection of the positions at which $f(x)$ is evaluated determines the type of the rule. In "closed" rules the function is evaluated at the extreme points as well as at points between the extremes. In "open" rules the function is not evaluated at the extremes. Generally an open rule is more accurate than a closed one when the same number of integration points are used. However the behaviour at the extreme points is important in the modelling of concrete structures in which cracking and crushing occur or at the onset of yield in steel or other metal structures.

Four numerical integration rules were investigated. Three of these

rules were of the closed type, these were compound Simpson's, Lobbato and Newton-Cotes. The fourth rule investigated was the Gauss rule which is an open type rule. The 3 point Simpson's rule integrates a cubic function exactly. Lobbato rule with n points integrates a polynomial of order 2n-3 exactly. Newton-Cotes rule with n points, where n is odd, integrates a polynomial of order n exactly. Gauss rule with n points integrates a polynomial of order 2n-1 exactly. The abscissas and weights for the various integration rules are given in Refs.[16] and [84].

6.7.3 ACCURACY OF THE RULES

To investigate the accuracy of the various integration rules for a cracked or cracked and crushed concrete section,a stress-strain relationship for concrete in compression proposed by Saenz [59] was used. In tension the following modes of behaviour for concrete were investigated.

(a) no tensile strength

(b) brittle failure in tension

(c) linear tension stiffening or strain softening

The various stress-strain relationships for concrete used are shown in Fig.6.13.

Aldstedt et al [85] suggested better accuracy could be achieved by using a special rule for Gaussian integration of moments, however, this rule has the drawback that different integration points and weights are used for integration of in-plane forces and moments. Bergan [86] suggested that modifying the weight of the last

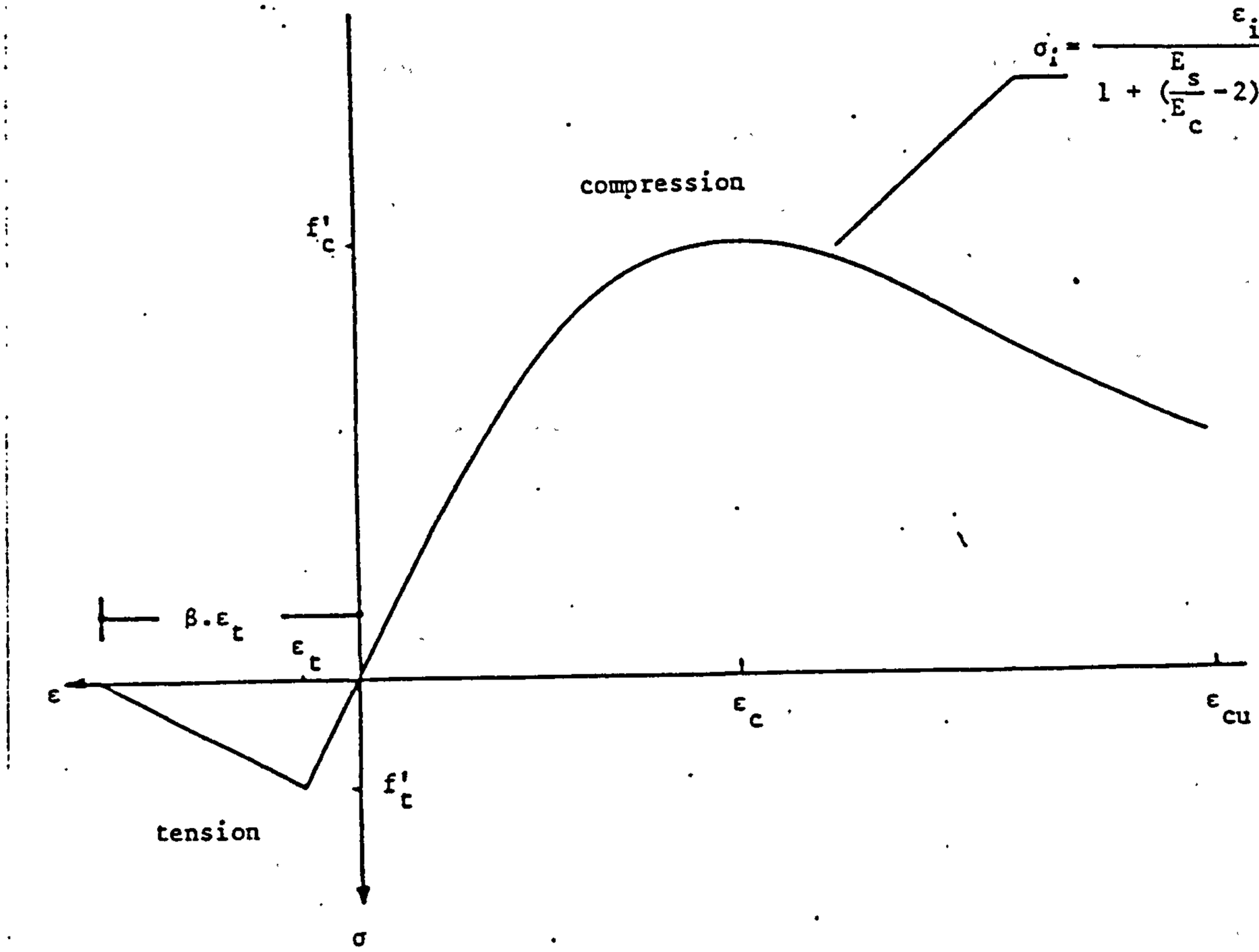

$f'_t = 0$ no tension

$\beta = 1.0$ brittle failure

$\beta > 1.0$ tension stiffening or strain softening

Figure 6.13. Stress-strain relationships for concrete

integration point before the crack front would improve the accuracy of the stress resultants, however, this rule has not been derived analytically.

Numerical examples investigated in this study using the rule suggested by Bergan showed no improvement in the accuracy of the stress resultants and in some cases produced worse results. The various integration rules investigated in this study were used with 5, 7 and 9 integration points. The accuracy of the various rules for a cracked or cracked and crushed plain concrete cross-sections are discussed in the next sections. The results have been compared to the values of in-plane forces and moments obtained using compound Simpson's rule with a large number of sampling points (999 points).

6.7.3.1 CRACKED CONCRETE SECTION

A concrete cross-section with cracks extending through approximately 65% of the depth was investigated using the various numerical integration rules. The percentage errors in the in-plane force and moment about the middle of the cross-section when the concrete was assumed to carry no tensile stresses are given in Fig.6.14. Simpson's rule with 9 integration points gave good results when compared with the other integration rules, with percentage errors of -0.58 and +1.10 in the in-plane force and moment respectively. Fig.6.15, shows the corresponding percentage errors for a cracked concrete cross-section when brittle failure was assumed to occur. Simpson's rule with 9 integration points again gave good results with percentage errors of -0.24 and +1.25 in the in-plane force and moment respectively. For a

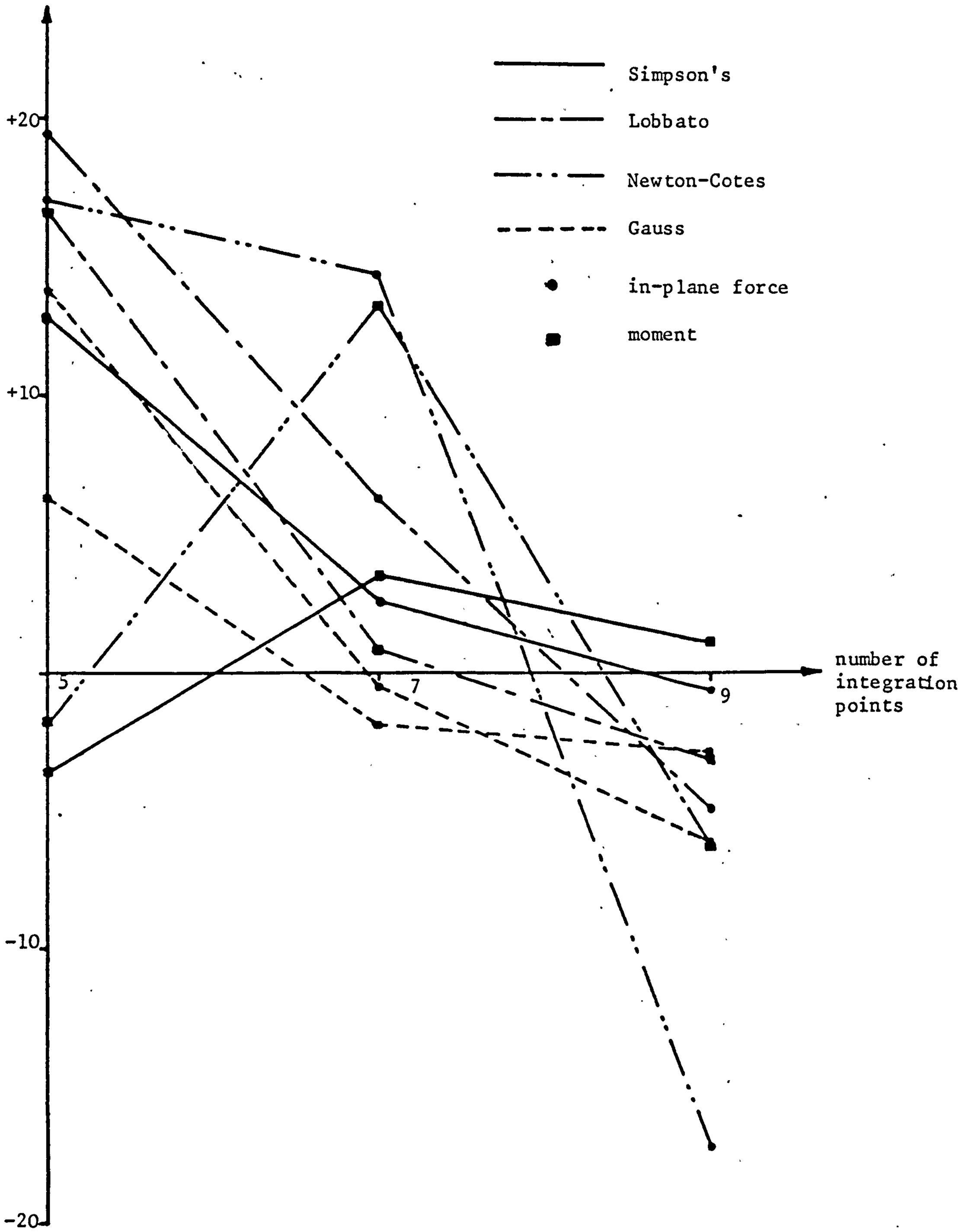

Figure 6.14. Percentage errors for a cracked concrete section with concrete assumed to carry no tensile stresses

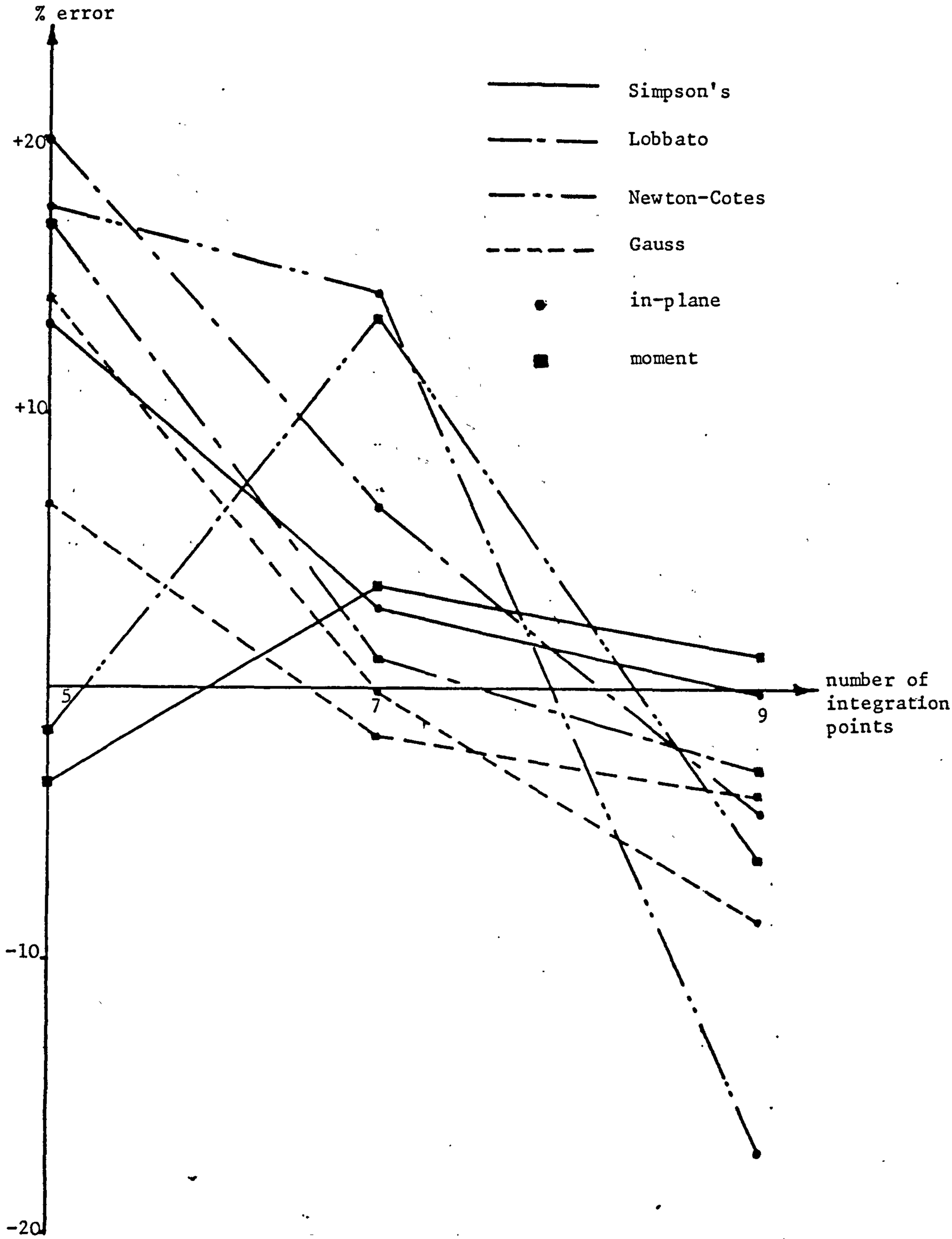

Figure 6.15. Percentage errors for a cracked concrete section with concrete assumed to have brittle failure in tension

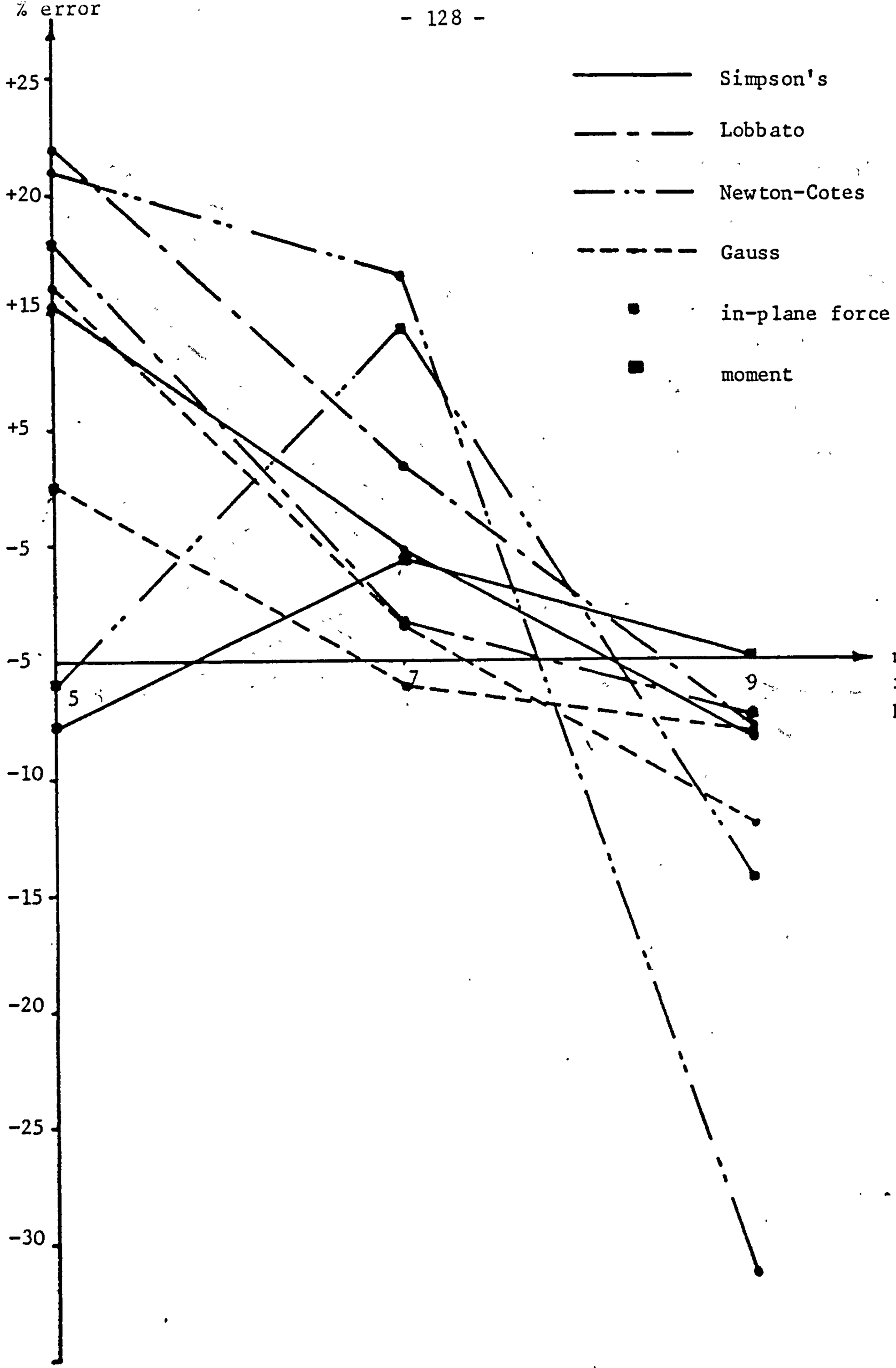

Figure 6.16. Percentage errors for a cracked concrete section with the concrete assumed to have linear tension stiffening with $\beta = 6.0$

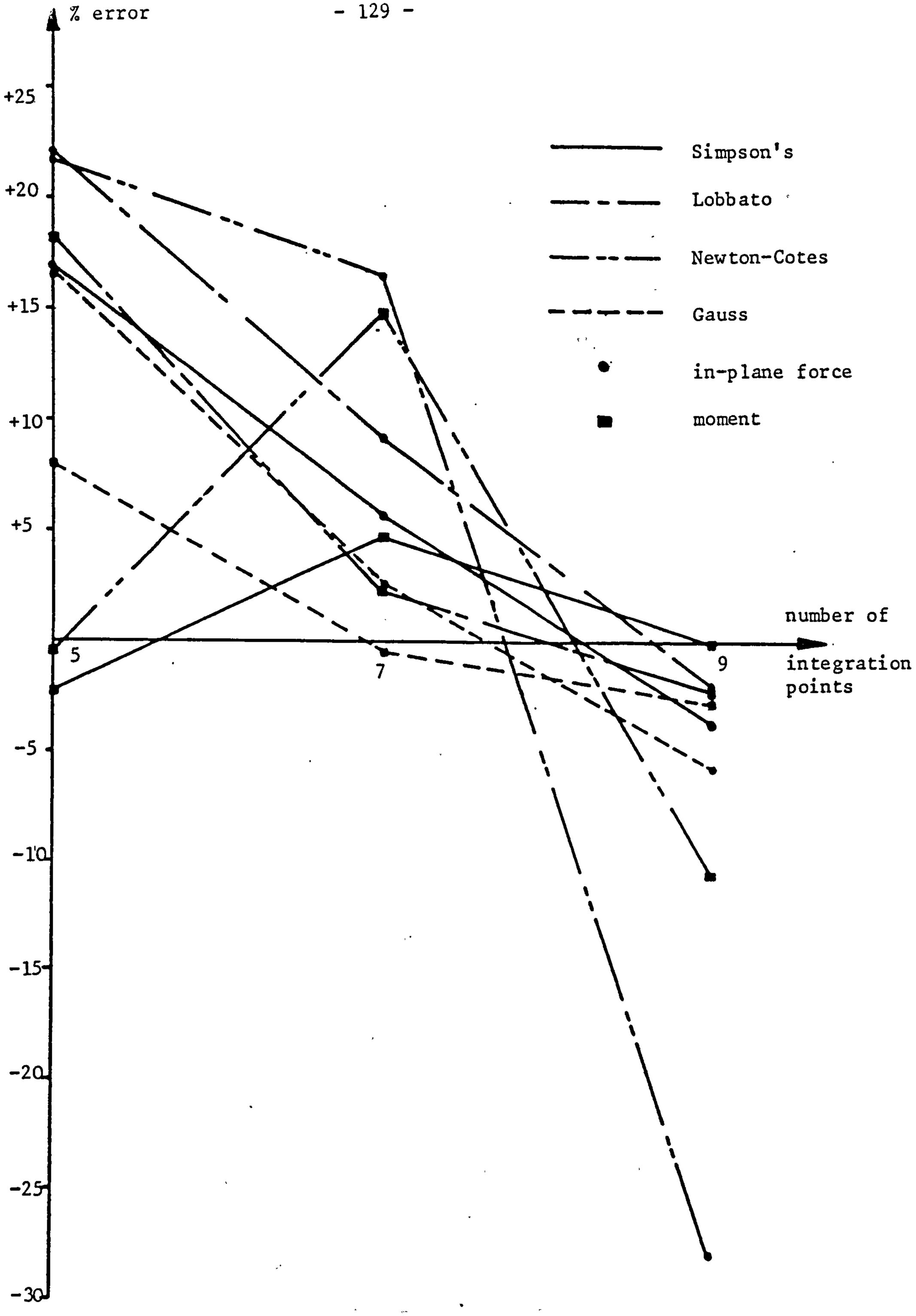

Figure 6.17. Percentage errors for a cracked concrete section with the concrete assumed to have linear tension stiffening with $\beta = 15.0$.

cracked concrete cross-section with a linear tension stiffening with different β , Fig.6.13, the percentage errors are shown in Figs.6.16 and 6.17. In these cases the percentage errors obtained were higher than those obtained for the previous cases, however for concrete with β =6.0, Gauss's rule with 7 points gave the best accuracy with percentage errors of +1.51 and -1.18 in the in-plane force and moment respectively. For concrete with β =15.0 Gauss's rule with 7 points again gave the best results with percentage errors of +2.59 and -0.62 in the in-plane force and moment respectively. The errors for the cases investigated are also given in Tables 6.1-6.4.

A comparsion between results obtained from both the Lobbato and the modified Lobbato rule proposed by Bergan [86] are given in Table 6.5 which shows that Bergan's rule generally results in higher errors.

6.7.3.2 CRACKED AND CRUSHED CONCRETE SECTION

A concrete section with approximately 67% of the concrete cracked and crushed was investigated using the various numerical integration rules. The extent of cracking and crushing of the cross-section are shown in Fig.6.18. The percentage errors for a concrete section with the concrete assumed to carry no tensile stresses are given in Fig.6.19. Gauss's rule with 5 points gave the most accurate stress resultants when compared with the other rules, with percentage errors of -5.10 and +12.51 in the in-plane force and moment respectively. The percentage errors for a concrete section with the concrete assumed to have a linear tension stiffening are given in Figs.6.20 and 6.21. The most accurate stress resultants for concrete with β=6.0 were

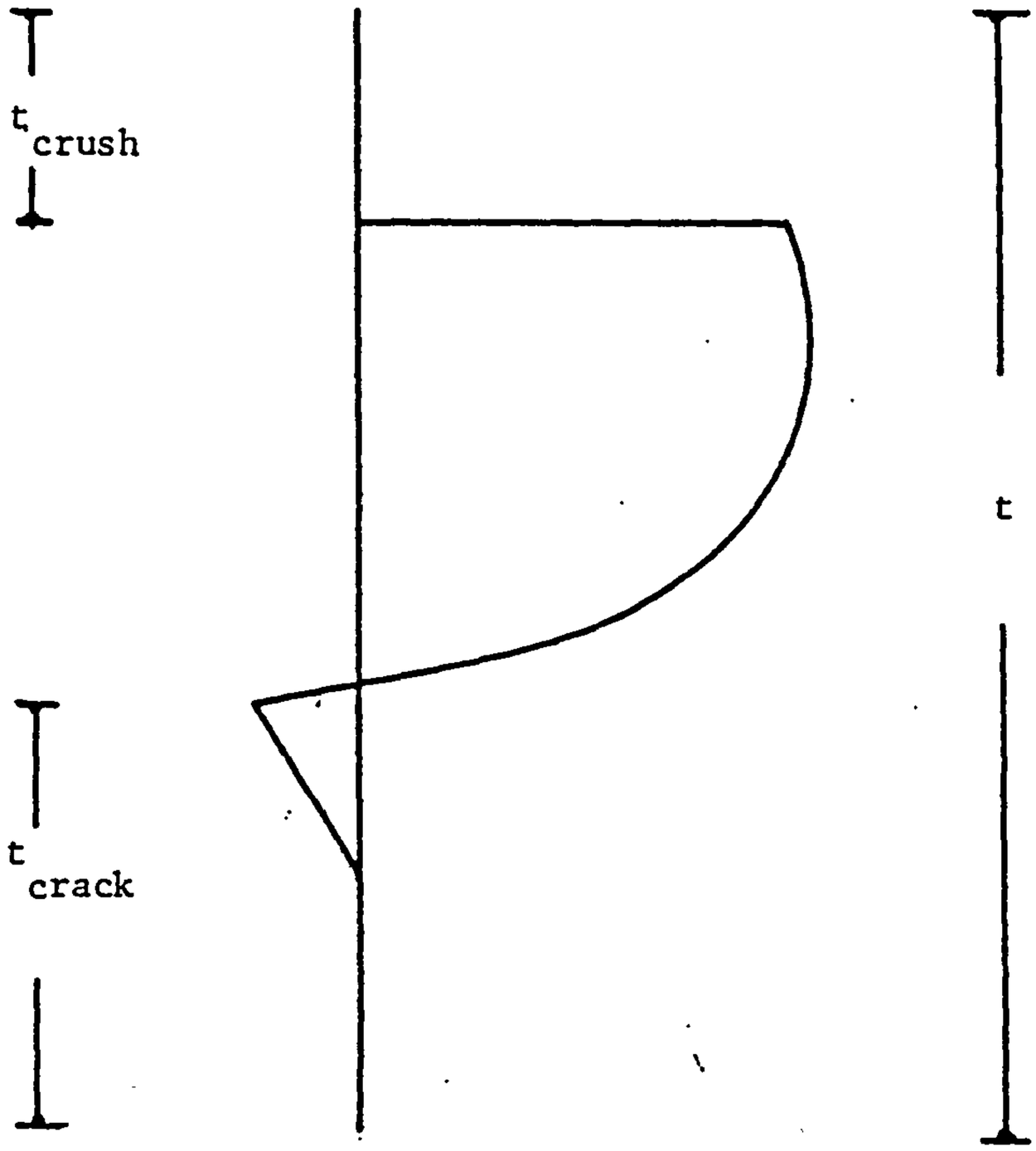

$$\frac{t_{crush}}{t} = 0.14$$

$$\frac{t_{crack}}{t} = 0.53$$

Figure 6.18. Extent of cracking and crushing in a cracked and crushed concrete section

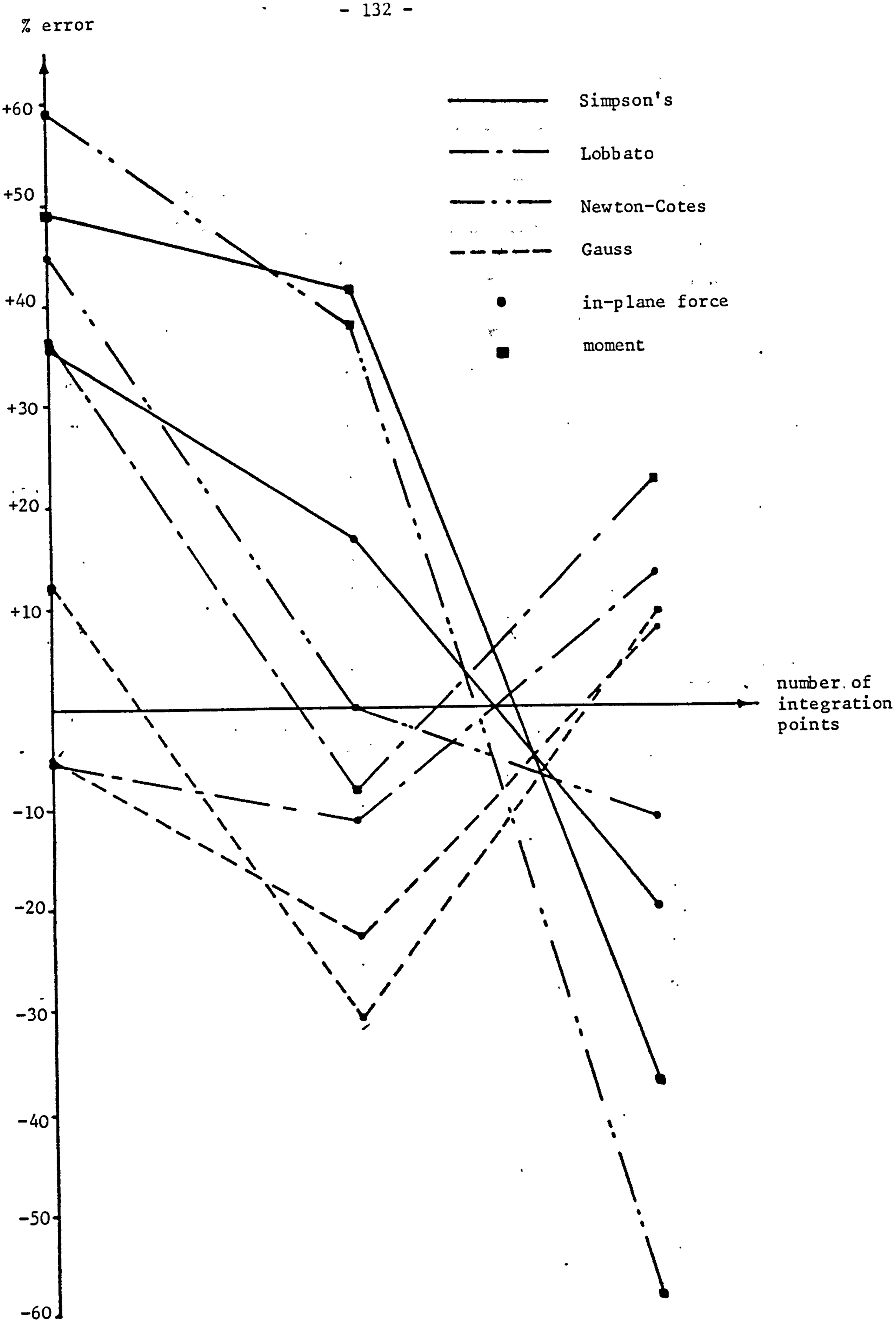

Figure 6.19. Percentage errors for a cracked and crushed concrete section with concrete assumed to carry no tensile stresses.

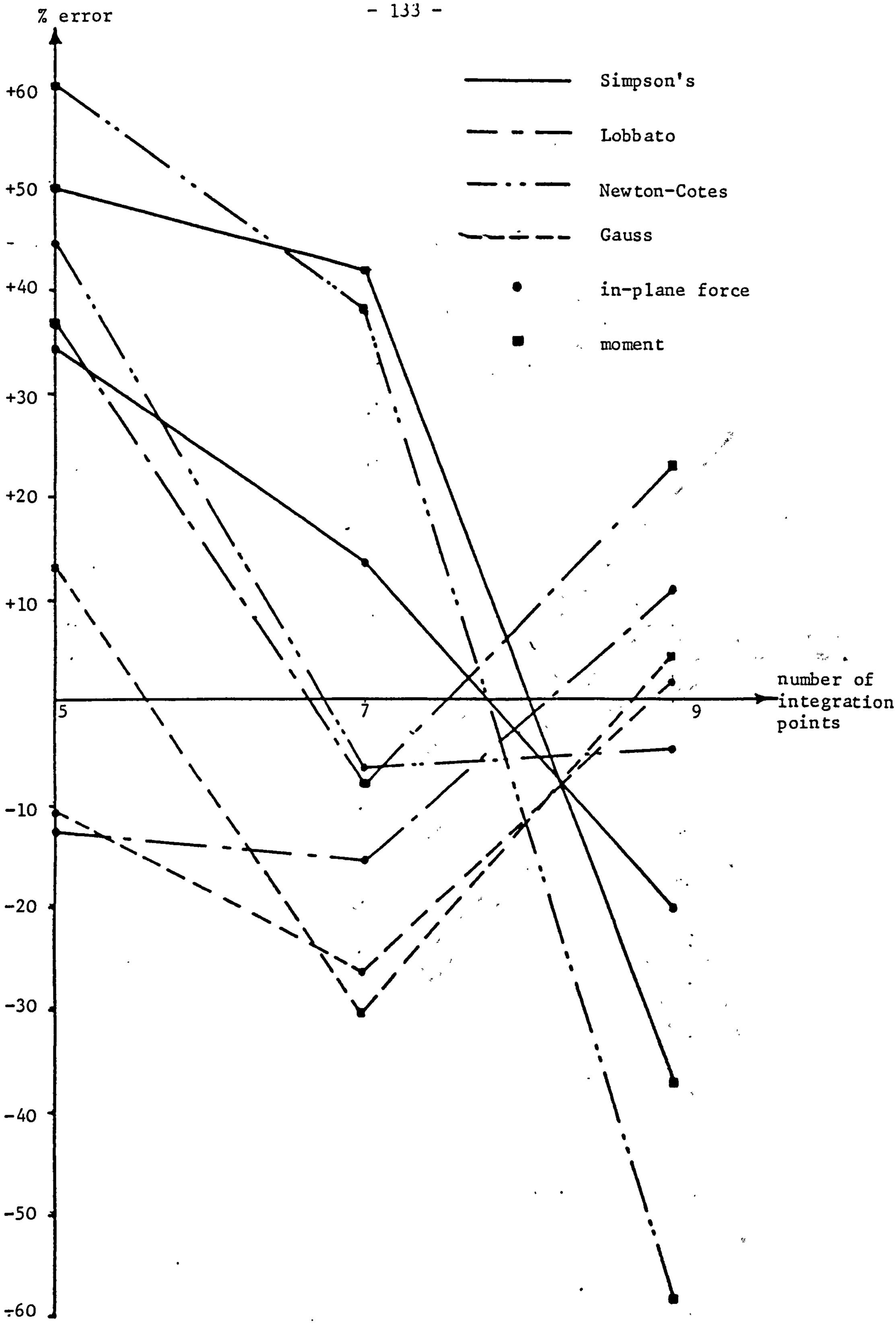

Figure 6.20. Percentage errors for a cracked and crushed concrete section with concrete assumed to have linear tension stiffening with $\beta = 6.0$

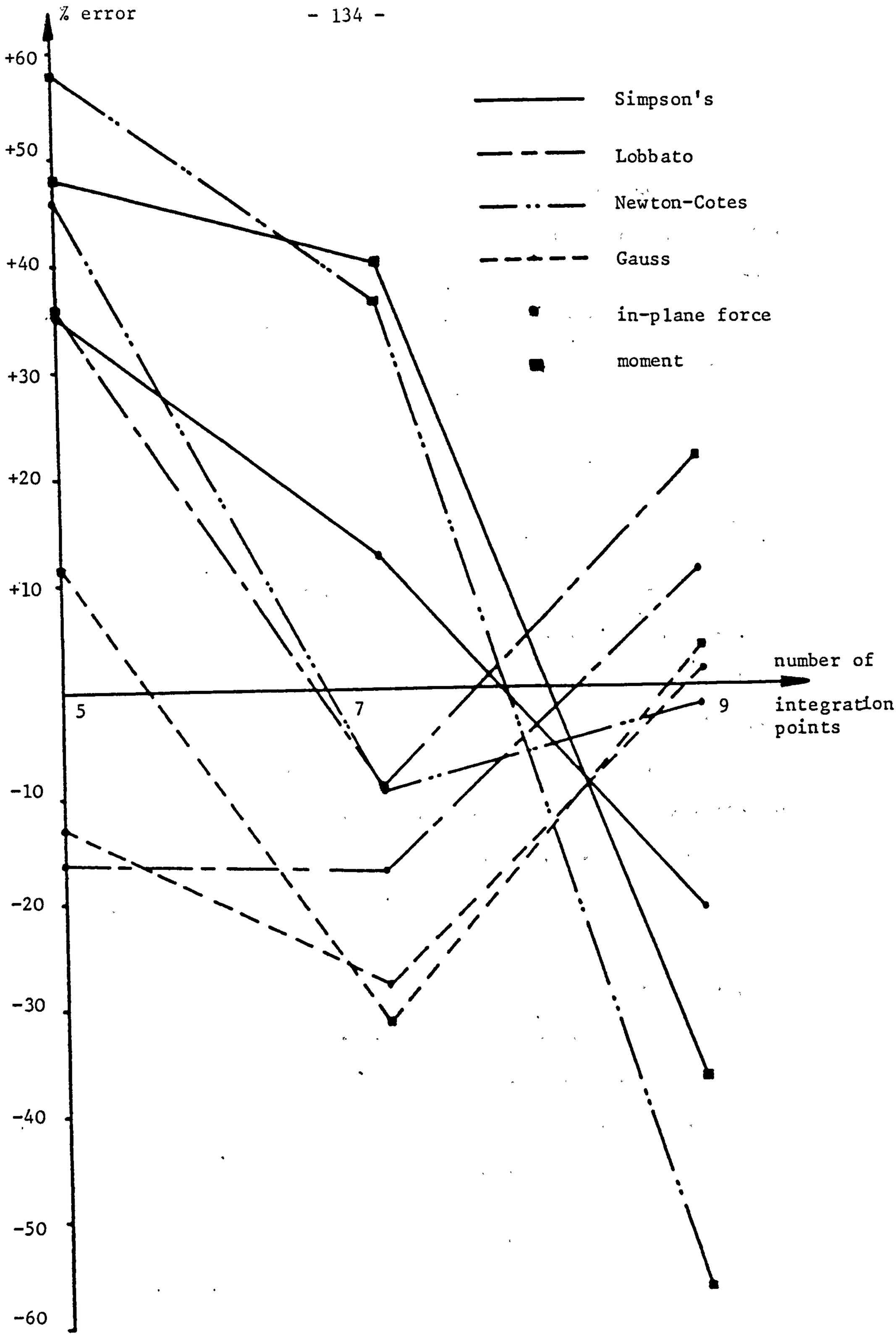

Figure 6.21. Percentage errors for a cracked and crushed concrete section with concrete assumed to have linear tension stiffening with $\beta = 15.0$

obtained using Gauss rule with 9 points with percentage errors of +1.73 and +4.79 in the in-plane forces and moments respectively. For χ concrete with β =15.0 Gauss rule with 9 points again gave the best results with percentage errors of +1.91 and +3.84 in the in-plane force and moment respectively. The calculated percentage errors are also given in Tables 6.6-6.8.

6.7.4 MODIFIED INTEGRATION RULE

The various numerical rules are based on the integrand being a continuous function, however, the stress distribution for a cracked or crushed concrete section is discontinuous. For this reason, large errors may result when the integration points are spatially fixed through the cross-section. From the above results, it can be seen that the accuracy obtained from the integration rules is generally not particularly good and, since a large number of points is needed, their use is relatively expensive.

For this reason a new rule is proposed for the integration of discontinuous stress distribution through cross-sections sujected to uniaxial stresses and cross-sections composed of isotropic materials subjected to biaxial stresses. Observations on the use of integration rules for cross-sections composed of orthotropic materials subjected to biaxial stresses are also made.

6.7.4.1 UNIAXIAL BEHAVIOUR

For a total stress-strain material model, the accuracy of the stress

resultants, for a cross-section under uniaxial stresses, can be retained with a reduction in cost if the following procedure is adopted. The extent of cracking and crushing is determined from the calcualted principal strains. The compression region of the stress distribution through the cross-section can be integrated using a numerical integration rule. However, for a stress-strain relationship which includes a linear tension stiffening or strain softening the tension region may be integrated exactly using exact linear integration based on the trapezoidal rule. The main points of the proposed modified integration rule are illustrated diagrammatically in Fig.6.22. This modified rule has the advantge that stress resultants in the compression zone are found using the same number of integration points regardless of the depth of the zone. The position of the integration points obviously changes with the progression of cracking and crushing of concrete. This is important for situations when most of the cross-section has cracked or crushed. Open type rules can be used successfully with the proposed rule since the extent of cracking and crushing has been determined and the numerical integration is carried out in the effective compression zone.

To investigate the accuracy of the proposed modified rule, the cases previouly analysed had been reanalysed using the proposed rule with 5 and 3 integration points. The calculated percentage errors in the in-plane forces and moments are given in Tables 6.9-6.12. Simpson's, Lobbato, Newton-Cotes and Gauss gave good results using 5 integration points. The Gauss rule with 3 points gave good results while the other rules gave relatively large errors when used with 3 points.

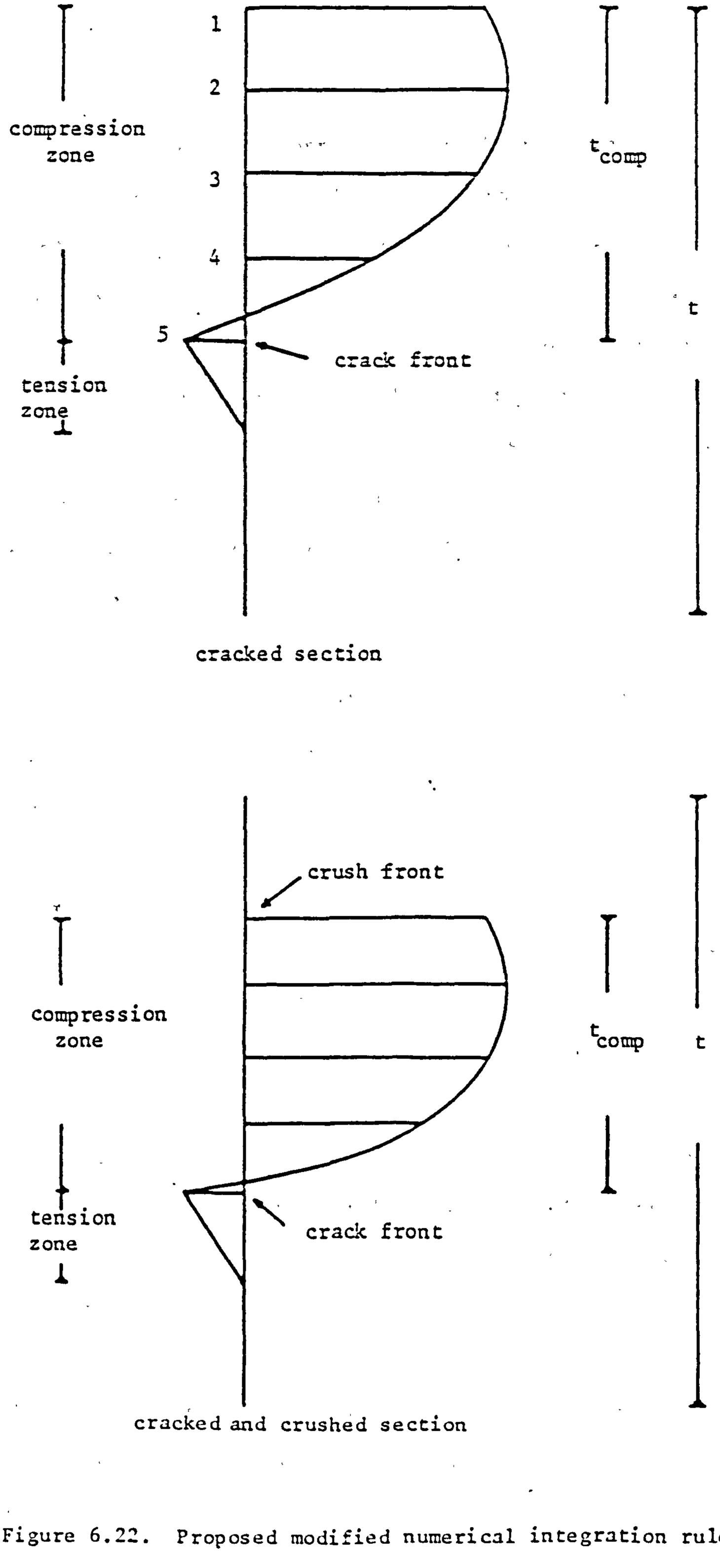

Figure 6.22. Proposed modified numerical integration rule.

6.7.4.2 BIAXIAL BEHAVIOUR

The rule can also be used for isotropic material in biaxial stress when a total stress-strain model is used. The integration is carried out for each axis separately. Of course it is possible that the positions of the intergration points will be different for each axis. In biaxial analysis in which orthotropic material behaviour is assumed the orientation of the principal axes through the depth of the cross-section at any particular load level is likely to vary. The use of the proposed rule for such material is not practical. In this case a large number of fixed integration points must be used to retain the accuracy of the stress resultants.

The accuracy of the various numerical integration rules had been investigated for a cracked section and a cracked and crushed section under biaxial stresses. The assumed strain distributions for the various concrete sections are shown in Figs.6.23 and 6.24. The concrete was assumed to crack when the strain in the principal direction reaches a cracking strain vaule of 0.00015 and crushing was assumed to occur when the principal strain reaches a crushing strain value of -0.0035.

The average percentage errors in the in-plane forces and moments for a cracked section and a cracked and crushed section with concrete assumed to have a linear tenison stiffening with β =6.0 are given in Tables 6.13 and 6.14.

Simpsons's rule with 9 points gave the most accurate results for a cracked concrete section with average percentage errors of -0.39 and

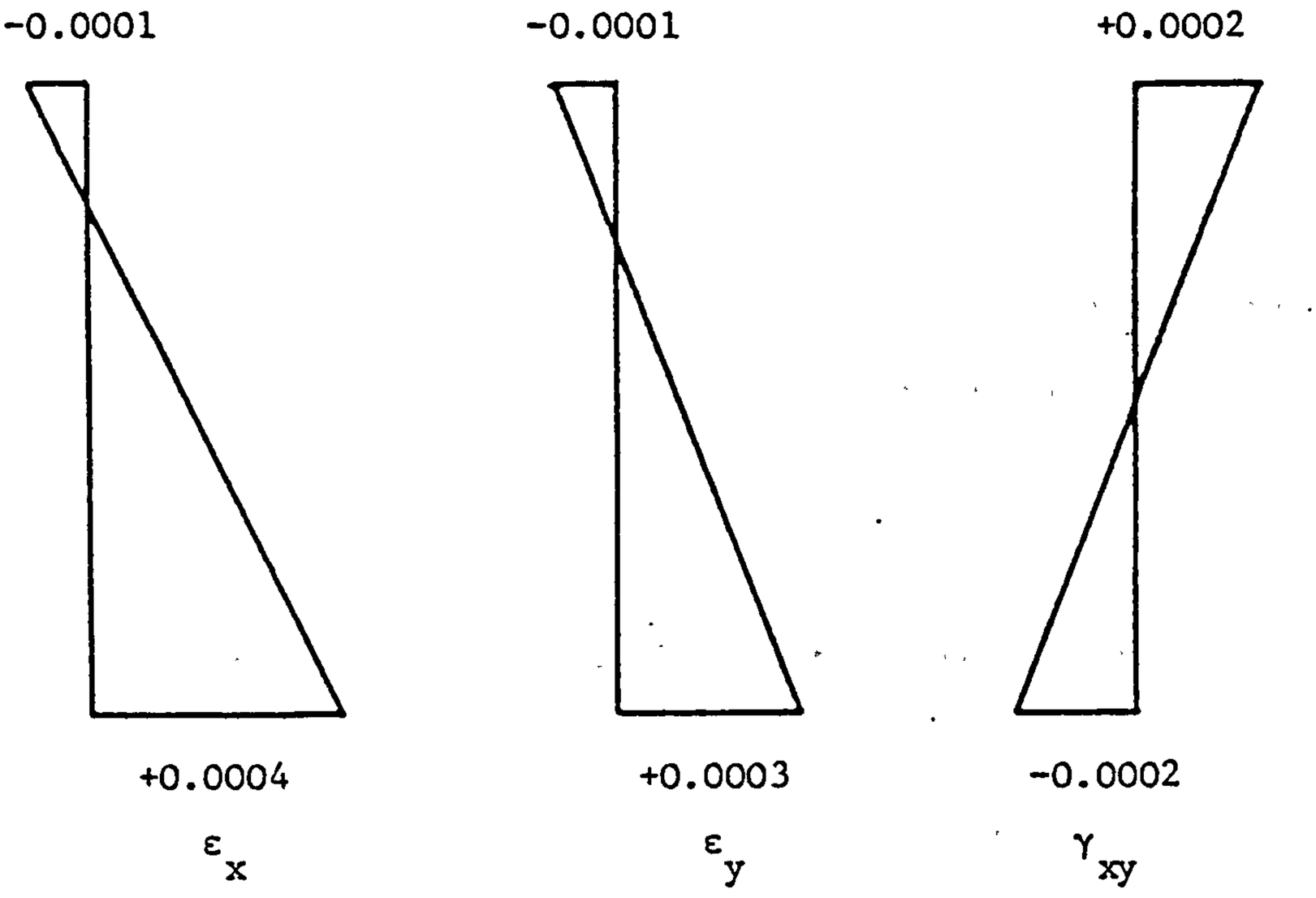

Figure 6.23. Assumed strain distribution for a cracked concrete section under biaxial loading

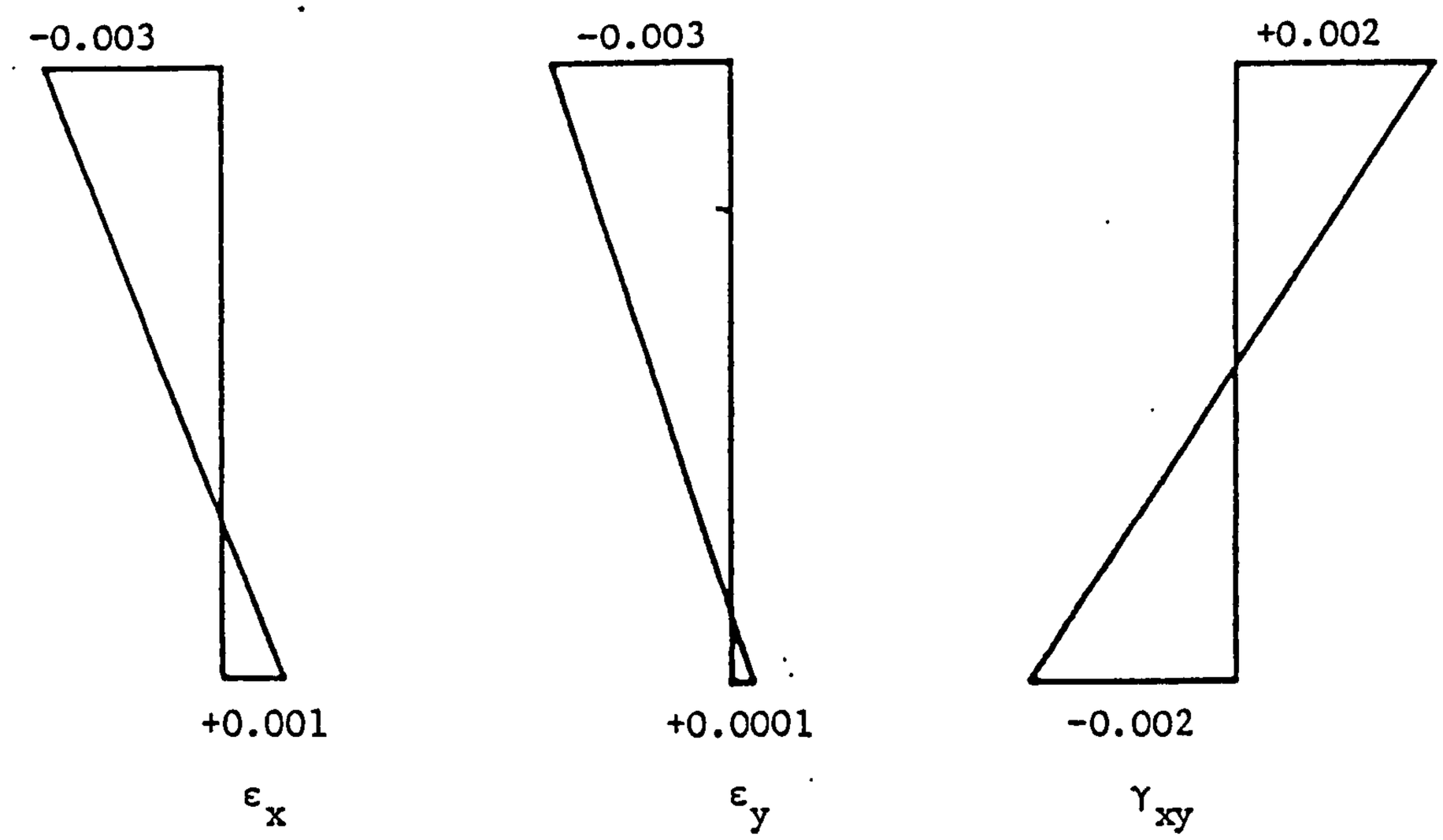

Figure 6.24. Assumed strain distributuon for a cracked and crushed concrete section under biaxial loading

+0.22 in the in-plane forces and moments respectively. For a cracked and crushed section Lobbato rule with 9 points gave the most accurate stress resultants with average percentage errors of -4.17 and -2.33 in the in-plane forces and moments respectively.

Lobbato rule with 9 points emerged as the best rule compared with the other rules, when the accuracy of the stress resultants for the cracked section and cracked and crushed section are both considered.

The average percentage errors for a cracked section and a cracked and crushed section with concrete assumed to have a linear tension stiffening with β =15.0 are given in Tables 6.15 and 6.16. The accuracy of the different integration rules were similar to those obtained for the different sections with concrete assumed to have a linear tension stiffening with β=6.0. Lobbato with 9 points again gave the best overall accuracy when the cracked section and cracked and crushed section are both considered.

Table 6.1. Percentage errors in in-plane force and moment for a cracked concrete section with the concrete assumed to carry no tensile stresses.

number of integration points	Simpsons		Lobbato		Newton-Cote		Gauss	
	F	M	F	M	F	M	F	M
5	+12.81	-3.59	+19.46	+16.76	+17.01	-1.80	+13.84	+6.58
7	+2.63	+3.57	+6.28	+0.97	+14.14	+13.38	-0.53	-1.93
9	-0.58	+1.10	-4.89	-3.12	-17.22	-6.37	-6.35	-2.87

Table 6.2. Percentage errors in in-plane force and moment for a cracked concrete section with the concrete assumed to have brittle failure in tension.

number of integration points	Simpsons		Lobbato		Newton-Cote		Gauss	
	F	M	F	M	F	M	F	M
5	+13.18	-3.45	+19.86	+16.92	+17.40	-1.66	+14.22	+6.74
7	+2.97	+3.73	+6.64	+1.12	+14.52	+13.55	-0.19	-1.79
9	-0.24	+1.25	-4.58	-2.98	-16.95	-6.23	-8.59	-3.89

Table 6.3. Percentage errors in in-plane force and moment for a cracked concrete section with the concrete assumed to have linear tension stiffening with β =6.0

number of integration points	Simpsons		Lobbato		Newton-Cotes		Gauss	
	F	M	F	M	F	M	F	M
5	+15.11	-2.85	+21.91	+17.65	+20.91	-1.05	+16.17	+7.40
7	+4.73	+4.36	+8.46	+1.74	+16.47	+14.25	+1.51	-1.18
9	-3.44	+0.18	-2.95	-2.39	-26.42	-9.42	-7.04	-3.30

Table 6.4. Percentage errors in in-plane force and moment for a cracked concrete section with the concrete assumed to have linear tension stiffening with β =15.0

number of integration points	Simpson		Lobbato		Newton-Cotes		Gauss	
	F	M	F	M	F	M	F	M
5	+17.06	-2.30	+22.15	+18.32	+21.83	-0.49	+16.96	+8.01
7	+5.79	+4.96	+9.41	+2.32	+16.87	+14.90	+2.59	-0.62
9	-3.52	-0.02	-1.77	-1.83	-27.54	-10.62	-5.80	-2.76

Table 6.5. Comparison between Lobbato and modified Lobbato [86] rules for a cracked concrete section with the concrete assumed to carry no tensile stresses.

number of integration points	Lobbato		modified Lobbato	
	F	M	F	M
5	+19.46	+16.36	+23.73	+20.67
7	+6.28	+0.97	-3.68	-5.57
9	-4.89	-3.12	-8.80	-5.12

Table 6.6. Percentage errors in in-plane force and moment for a cracked and crushed concrete section with concrete assumed to carry no tensile stresses.

number of integration	Simpsons		Lobbato		Newton-Cotes		Gauss	
points	F	M	F	M	F	M	F	M
5	+35.54	+49.22	-5.36	+36.41	+44.50	+59.16	-5.10	+12.51
7	+16.72	+41.42	-11.31	-8.44	-0.30	+37.68	-22.71	-30.93
9	-20.04	-37.34	+13.24	+22.50	-10.97	-58.32	+3.94	+4.64

Table 6.7. Percentage errors in in-plane force and moment for a cracked and crushed concrete section with concrete assumed to have linear tension stiffening with β =6.0

number of integration points	Simpsons		Lobbato		Newton-Cotes		Gauss	
	F	M	F	M	F	M	F	M
5	+33.94	+49.41	-12.76	+36.58	+44.04	+59.37	-10.62	+12.66
7	+13.28	+41.61	-15.89	-8.32	-6.76	+37.87	-26.61	-30.84
9	-20.59	-37.25	+10.68	+22.67	-4.95	-58.26	+1.73	+4.79

Table 6.8. Percentage errors in in-plane force and moment for a cracked and crushed concrete section with the concrete assumed to have linear tension stiffening with β =15.0

number of integration points	Simpsons		Lobbato		Newton-Cotes		Gauss	
	F	M	F	M	F	M	F	M
5	+35.06	+48.08	-16.31	+35.37	+46.04	+57.95	-12.88	+11.65
7	+12.82	+40.34	-17.60	-9.14	-9.59	+36.63	-28.04	-31.46
9	-20.87	-37.19	+10.78	+21.57	-1.99	-57.24	+1.91	+3.84

Table 6.9. Percentage errors in in-plane force and moment for a cracked concrete section using the proposed rule with 5 integration points

case	Simpsons		Lobbato		Newton-Cotes		Gauss	
	F	M	F	M	F	M	F	M
a	+0.060	+0.019	-0.003	+0.017	-0.110	-0.220	-0.001	0.000
b	+0.045	-0.008	+0.012	+0.035	-0.180	-0.290	-0.003	0.000
c	+0.049	-0.008	+0.015	+0.036	-0.180	-0.290	-0.001	0.000

Table 6.10. Percentage errors in in-plane force and moment for a cracked concrete section using the proposed rule with 3 integration points

case	Newton-cotes Simpsons Lobbato		Gauss	
	F	M	F	M
a	+2.588	+3.572	+0.103	+0.223
b	+3.468	+4.245	+0.189	+0.309
c	+3.530	+4.272	+0.194	+0.313

case:

a concrete assumed to carry no tensile stresses

b concrete assumed to have brittle failure in tension

c concrete assumed to have linear tension stiffening with β=6.0

Table 6.11. Percentage errors in in-plane force and moment for a cracked and crushed concrete section using the proposed rule with 5 integration points.

case	Simpsons		Lobbato		Newton-Cotes		Gauss	
	F	M	F	M	F	M	F	M
a	+0.060	0.000	-0.003	+0.028	-0.110	-0.270	-0.001	+0.001
b	+0.046	-0.036	+0.012	+0.046	-0.190	-0.350	-0.004	+0.002

Table 6.12. Percentage errors in in-plane force and moment for a cracked and crushed concrete section using the proposed rule with 3 integration points.

case	Newton-Cotes Simpsons Lobbato		Gauss	
	F	M	F	M
a	+2.629	+2.912	+0.104	+0.280
b	+3.627	+4.637	+0.192	+0.370

case:

a concrete assumed to carry no tensile stresses

b concrete assumed to have linear tension stiffening with β=6.0

Table 6.13. Average percentage errors in in-plane forces and moments for a cracked concrete section with concrete assumed to have linear tension stiffening with β =6.0

number of integration points	Simpsons		Lobbato		Newton-Cotes		Gauss	
	F	M	F	M	F	M	F	M
5	-2.51	+0.22	-3.80	+0.26	-2.73	+0.27	-3.45	+0.26
7	-2.59	+0.36	-2.89	+0.35	-3.61	+0.26	-6.68	+0.26
9	-0.39	+0.22	-2.18	+0.25	+3.38	-0.08	-1.86	+0.26

Table 6.14. Average percentage errors in in-plane forces and moments for a cracked and crushed concrete section with concrete assumed to have linear tension stiffening with β =6.0

number of integration points	Simpsons		Lobbato		Newton-Cotes		Gauss	
	F	M	F	M	F	M	F	M
5	+25.89	+10.96	+6.64	+3.25	+32.01	+14.56	-4.72	-0.50
7	+8.42	+3.13	-14.93	-4.06	+6.42	+3.01	+8.59	+2.18
9	+14.81	+5.33	-4.17	-2.33	+10.49	+2.15	-16.07	-5.96

Table 6.15. Average percentage errors in in-plane forces and moments for a cracked concrete section with the concrete assumed to have a linear tension stiffening with β =15.0

number of integration pointsF	Simpsons		Lobbato		Newton-Cotes		Gauss	
	F	M	F	M	F	M	F	M
5	-1.85	+0.24	-3.67	+0.23	-1.68	+0.22	-2.94	+0.32
7	-2.08	+0.24	-2.39	+0.25	-3.13	+0.26	-1.97	+0.28
9	+0.18	+0.06	-1.62	+0.15	+3.84	-0.19	-1.22	+0.19

Table 6.16. Average percentage errors in in-plane forces and moments for a cracked and crushed concrete section with the concrete assumed to have linear tension stiffening with β =15.0

number of integration points	Simpsons		Lobbato		Newton-Cotes		Gauss	
	F	M	F	M	F	M	F	M
5	+21.09	+8.79	+7.52	+4.09	+27.37	+12.31	-4.72	-1.04
7	+8.40	+3.57	-14.57	-4.60	+7.23	+3.91	+7.78	+2.33
9	+13.74	+5.60	-3.46	-2.06	+10.43	+3.05	-14.43	-5.82

CHAPTER 7

NUMERICAL EXAMPLES

7.1 GENERAL REMARKS

A number of plates and slabs have been analysed using the analysis procedures developed. The numerical results obtained have been compared with the available analytical, numerical and experimental data in order to demonstrate the validity of the procedures adopted.

The examples analysed are divided into three groups. The first group are examples for which linear elastic material properties were assumed and will be discussed in Section 7.2. These examples serve to illustrate the accuracy and validity of the procedures adopted when large deflections are considered.

The second group of examples, presented in Section 7.3, deals with the analysis of steel plates in which material nonlinearity and in some cases also geometric nonlinearity were considered in order to demonstrate the effect of the membrane forces on the behaviour of such structures.

The third group of examples, which will be presented in Section 7.4, deals with the analysis of reinforced concrete slabs. These examples serve to illustrate the validity of the procedures developed to predict the full response of reinforced concrete slabs where extensive cracking of the concrete and yielding of the reinforcing steel occur as the slab undergo large deflections.

In all the plates and slabs analysed the analyses were carried out for only a quarter of the structure because of the symmetry in geometry and loadings.

7.2 GEOMETRIC NONLINEARITY

Two examples with linear elastic material properties were selected to illustrate the different types of geometric nonlinearities that can be handled using the procedures adopted in the analysis

In the first example a square plate with different boundary conditions was analysed. In the second example a circular plate is analysed for different loadings.

A displacement convergence tolerance of 0.005, equation (16), was used in the analysis of the geometric nonlinear examples.

7.2.1 SQUARE PLATES

A 300.0 in. square plate, 3.0 in. thick, subjected to a uniformly distributed load, with either clamped or simply supported edges was analysed. These examples have been analysed by many investigators, [12] and [29], to check the geometric nonlinear Mindlin plate formulations.

Levy [87] solved the Von Karman's differentional equations for the

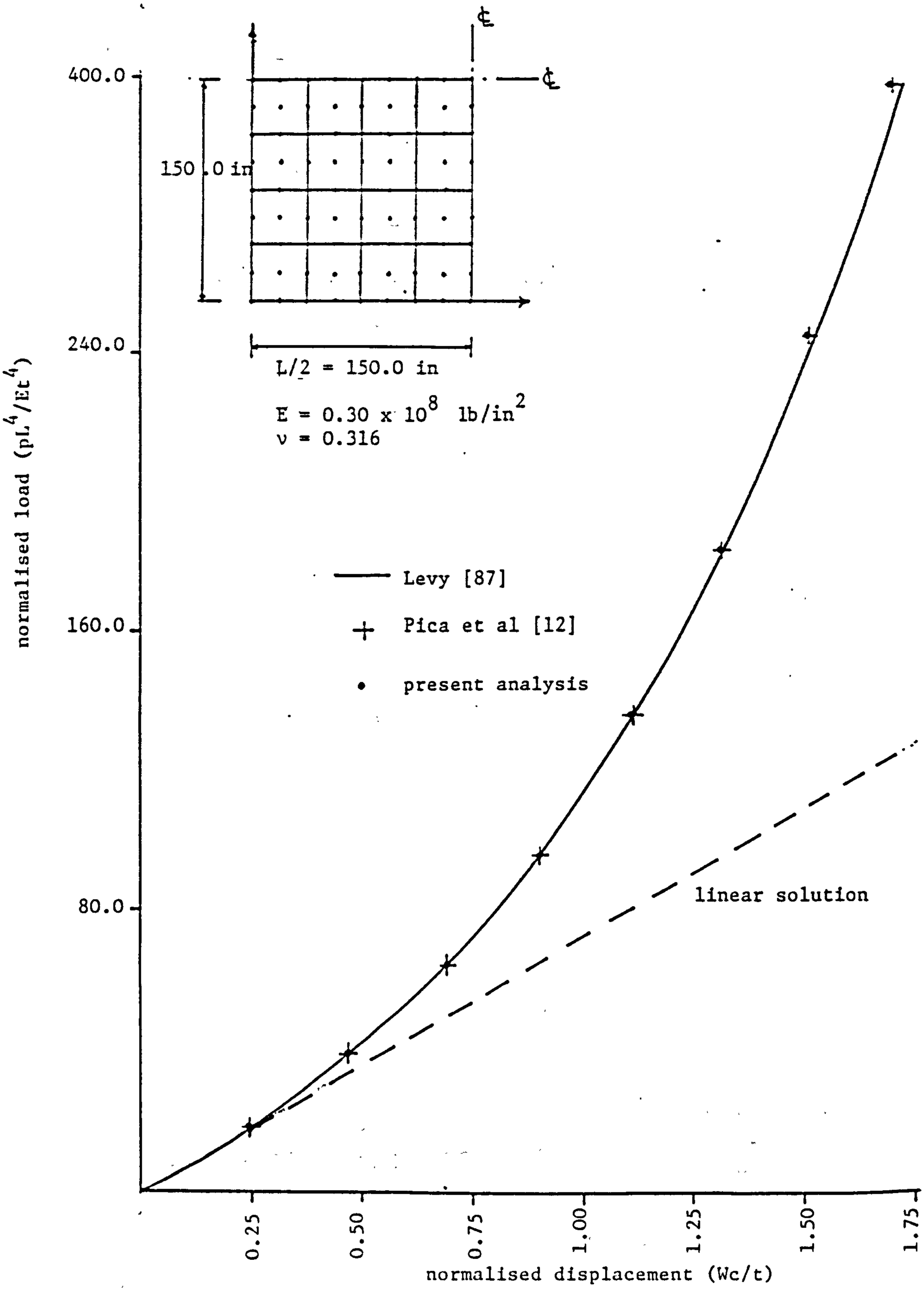

Figure 7.1. Load-deflection curves for clamped plate under uniformly distributed load.

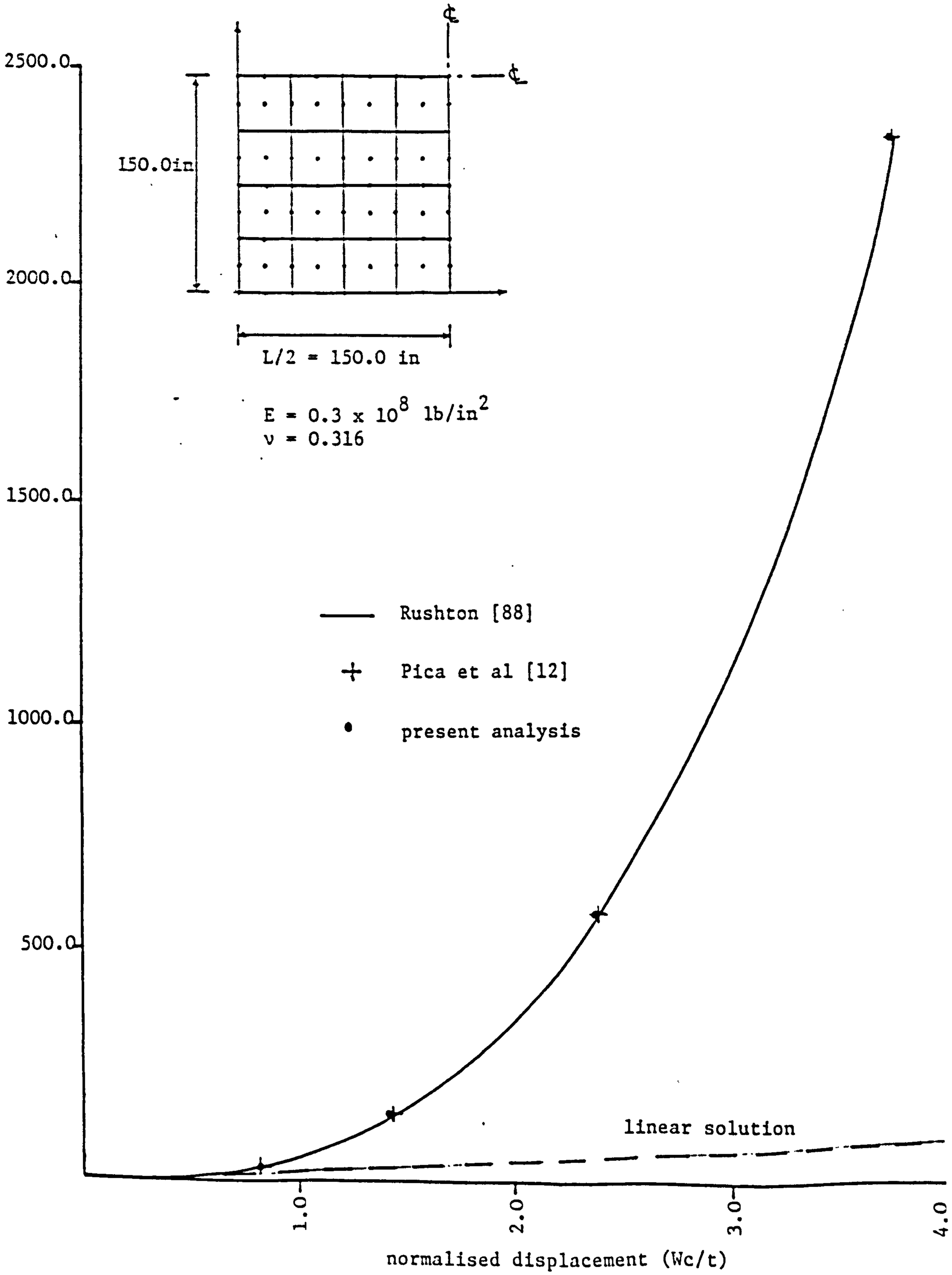

Figure 7.2. Load-deflection curves for simply supported plate under uniformly distributed load.

clamped square plate using a double Fourier series. The variation of the normalized load with the normalized central deflection obtained are shown in Fig.7.1, together with the analytical [87] and numerical results obtained by Pica et al [12] using a similar element. The results obtained gave good agreement with the analytical and numerical results.

The results of the simply supported plate were compared with the numerical results obtained by Rushton [88] using the finite difference method. The variation of the normalized load and deflections obtained are shown in Fig.7.2, together with those given in Refs.[12] and [88]. Again good agreement with the other results had been achieved. Yang et al [29] have also obtained similar results using a similar element.

7.2.2 CIRCULAR PLATES

A 100.0 in. radius clamped circular plate of 2.0 in. thickness was analysed for a uniformly distributed and a central point loads. The results obtained were compared with the analytical results obtained by Weil et al [89] and Schmit [90] for clamped circular plates under uniformly distributed and a central point loads respectively. The results obtained are shown in Figs.7.3 and 7.4. Good agreements between the analytical and numerical results have been obtained.

The plate under the uniformly distributed load had been also analysed using the displacement control method to check the validity of the formulation of the method. The lateral nodal displacement component

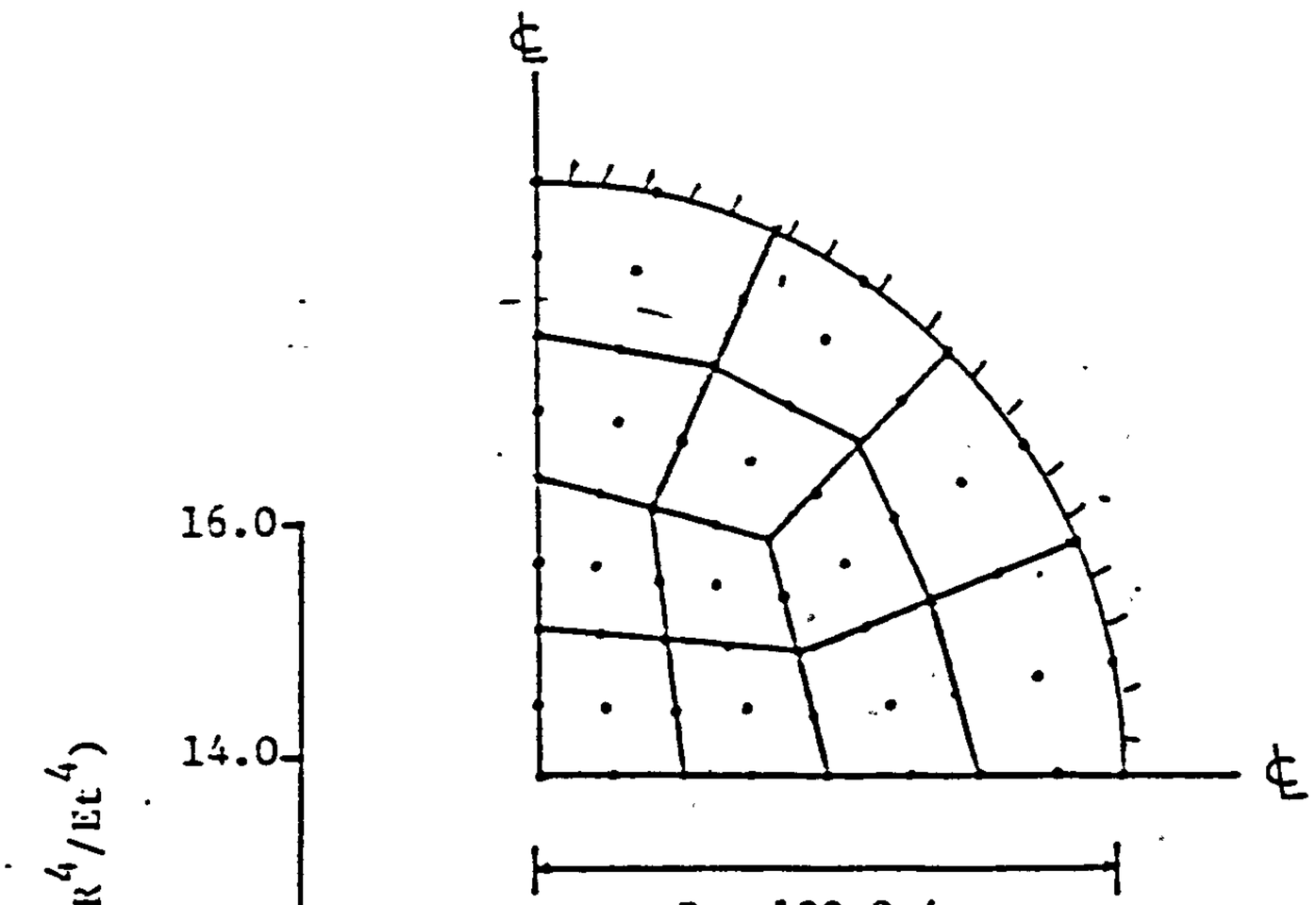

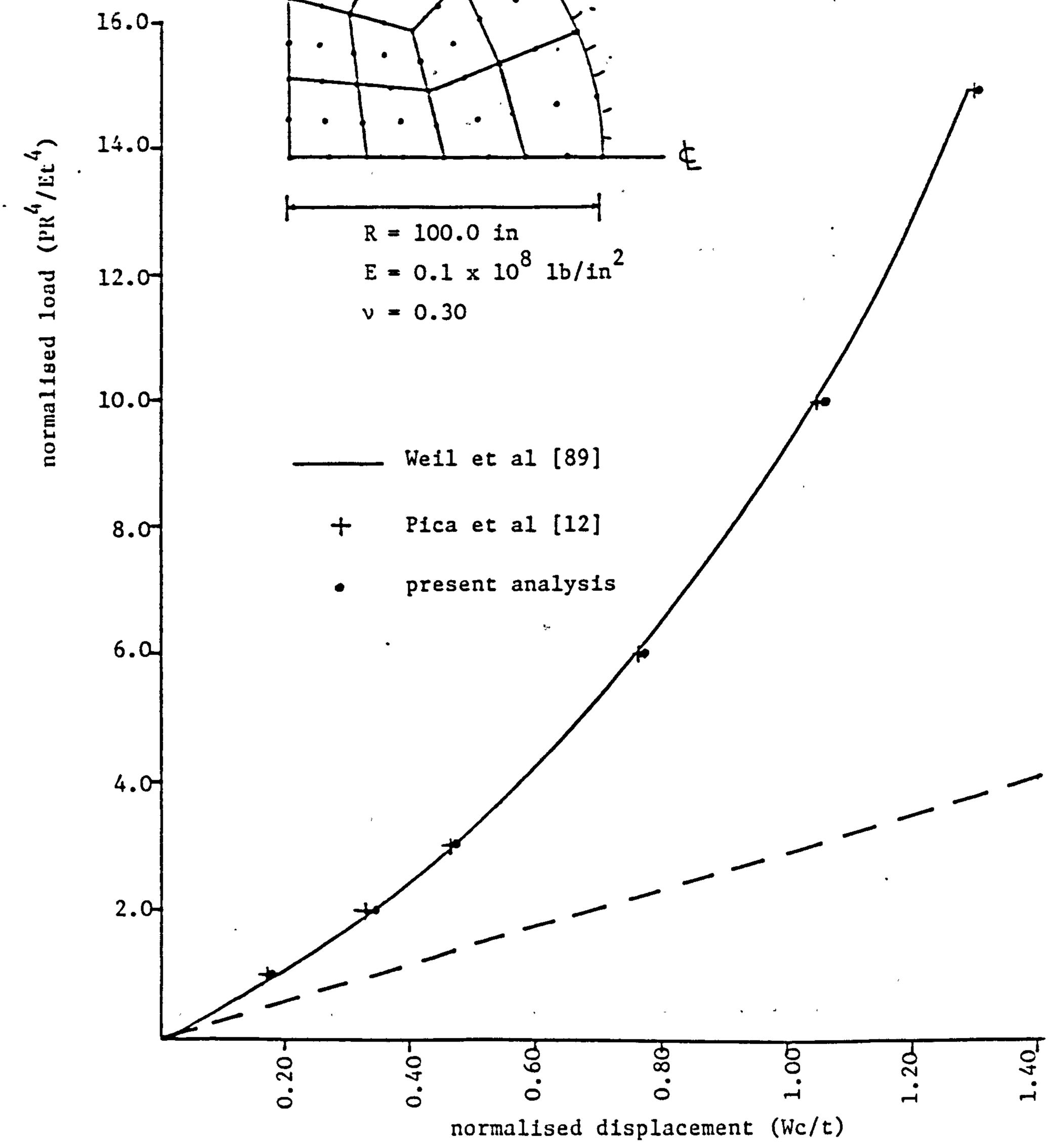

Figure 7.3. Load-deflection curve for clamped circular plate under uniformly distributed load

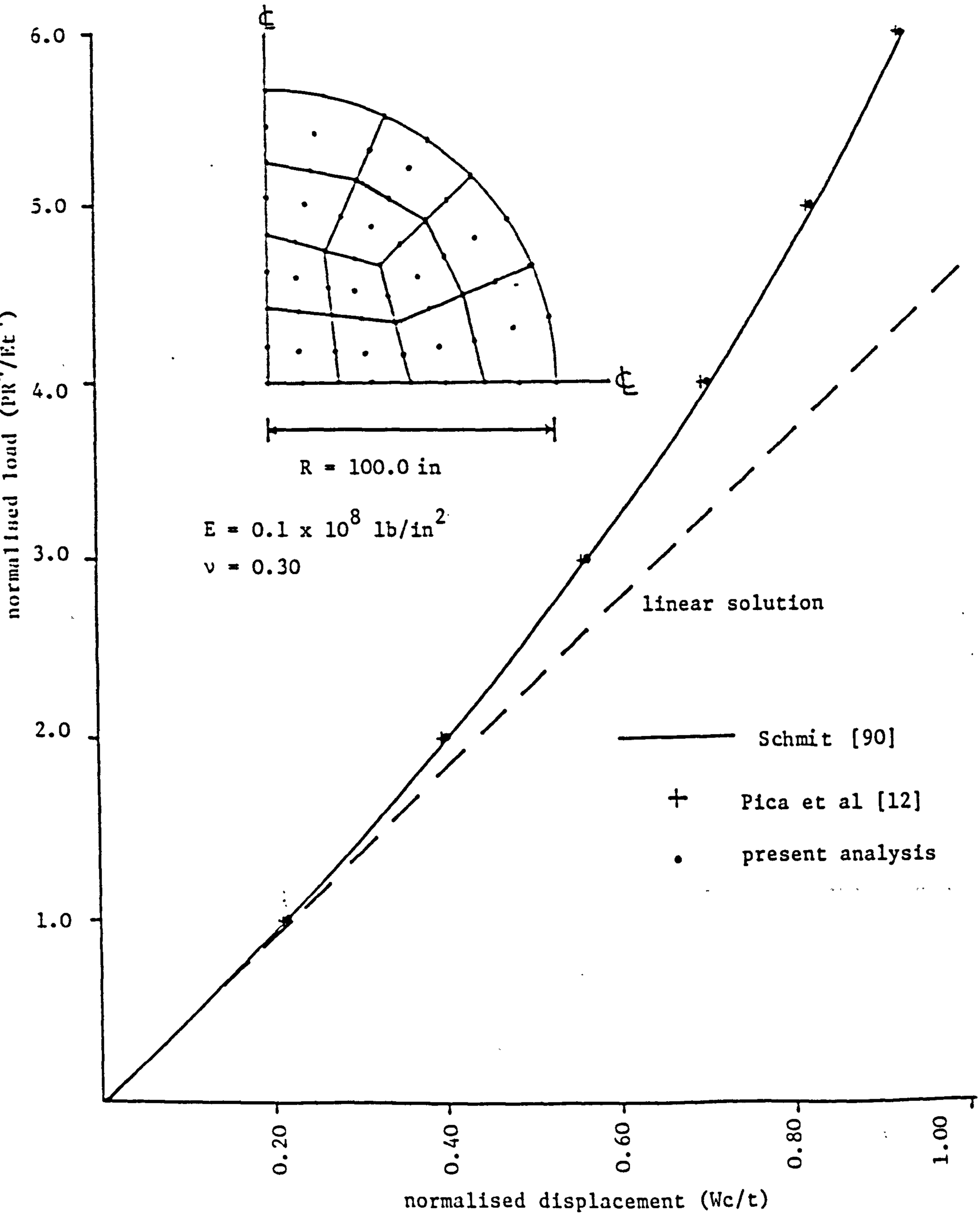

Figure 7.4. Load-deflection curves for clamped circular plate under central point load.

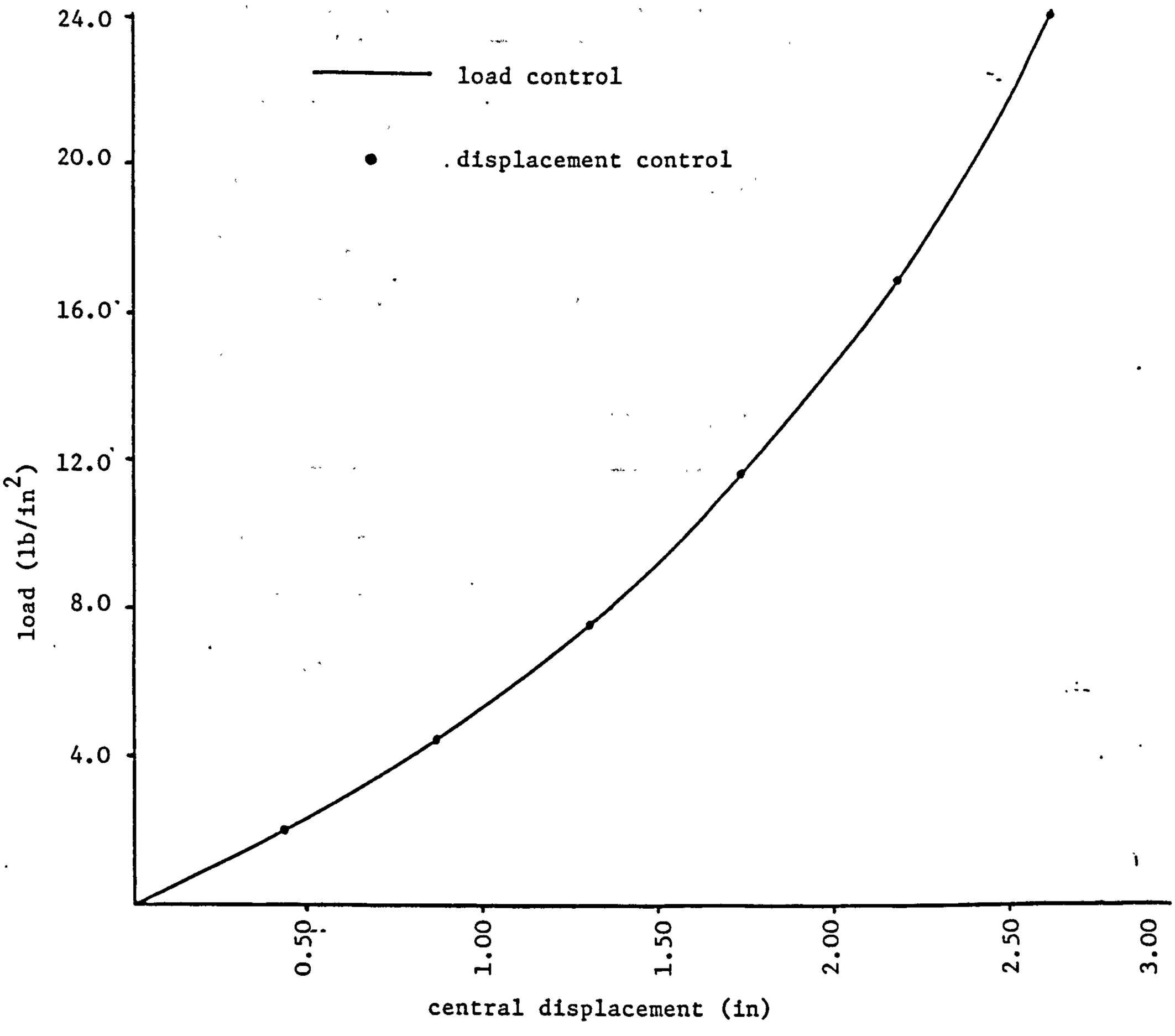

Figure 7.5. Load-deflection curves for circular plate using load control and displacement control methods.

Table 7.1. Comparison between the displacement control and the load control methods in the analysis of clamped circular plate subjected to uniformly distributed load.

displacement control		load control	
W_c(in)	λ (lb/in^2)	p(lb/in^2)	W_c(in)
0.434	2.0869	1.60	0.3361
0.868	4.4898	3.20	0.6460
1.302	7.5325	4.80	0.9180
1.736	11.5549	9.60	1.5400
2.170	16.9165	16.00	2.1040
2.604	23.9958	24.00	2.6040

W_c central displacement(in.)

p load intensity (lb/in^2)

λ load factor (lb/in^2)

of the central node of the plate was assigned a value of 0.434 inches at the beginning of each increment. The results obtained using the displacement control method are plotted in Fig.7.5 together with the results obtained using the load control method. As expected good correlation between the results has been obtained. The results are also given in Table 7.1.

7.3 STEEL PLATES

Three steel plates were selected for analysis. In the first example a simply supported steel plate was analysed in which only material nonlinearity was considered. In the second example the behaviour of a clamped steel plate was investigated when different combinations of material and geometric nonlinearities were considered and the performance of a number of integration rules, which were used to determine the stress resultants, was investigated. In the third example a simply supported circular steel plate, which undergoes large deflections and in which tensile and compressive membrane forces occurred, was analysed.

The nonlinear part of the stiffness matrix was updated at the end of the first iteration of each increment. The different analyses were carried out using a displacement convergence tolerance, equation (6.16), of 0.001.

7.3.1 SIMPLY SUPPORTED STEEL PLATE

A simply supported steel plate subjected to a uniformly distributed load which has been analysed by Owen et al [41] using a layered finite element approach, was selected for analysis. The steel was assumed to be an elasto-plastic material with no strain hardening. A 2x2 mesh was used to model a quarter of the plate. The stress resultants were determined using the modified trapezoidal rule with 5 sampling points throughout the plate thickness. The load was applied in 11 increments, as shown in Fig.7.6. Convergence was obtained in an average of 10 iterations per load increment. In Fig.7.6 it can be seen that the results obtained gave good agreement with those obtained by Owen et al [41].

7.3.2 CLAMPED STEEL PLATE

A 6.0 m. clamped square steel plate, 0.2 m. thick, under different loadings, was analysed by Owen et al [14], [91] using the finite element method. The plate was analysed using the small deflection theory. The analysis was carried out using a 3x3 mesh and the stress resultants were determined using the modified trapezoidal rule with 5 sampling points. The load-deflection curves obtained are shown in Fig.7.7 and 7.8, together with the numerical curves reported in Refs.[14] and [91]. The distributed load was applied in 6 steps, Fig.7.7, and convergence was obtained in an average of 9 iterations per load step, whilst the point load was applied in 10 steps, Fig.7.8, and convergence was obtained in 11 iterations per load step. The load-deflection curves obtained gave good agreement with those reported in Ref.[14] using a similar element with 8 layers assumed

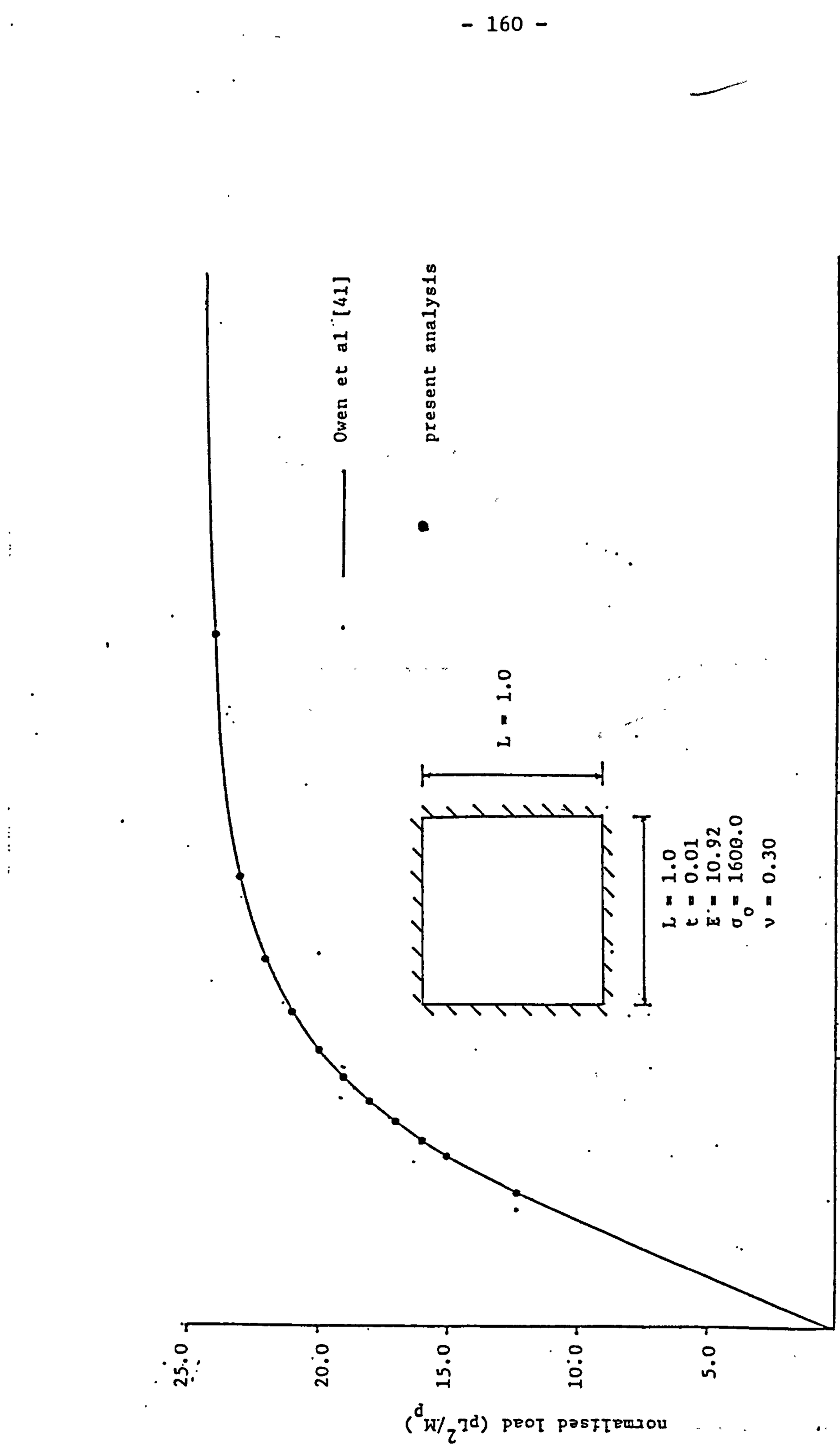

Figure 7.6. Load-deflection curves for simply supported plate under uniformly distributed load.

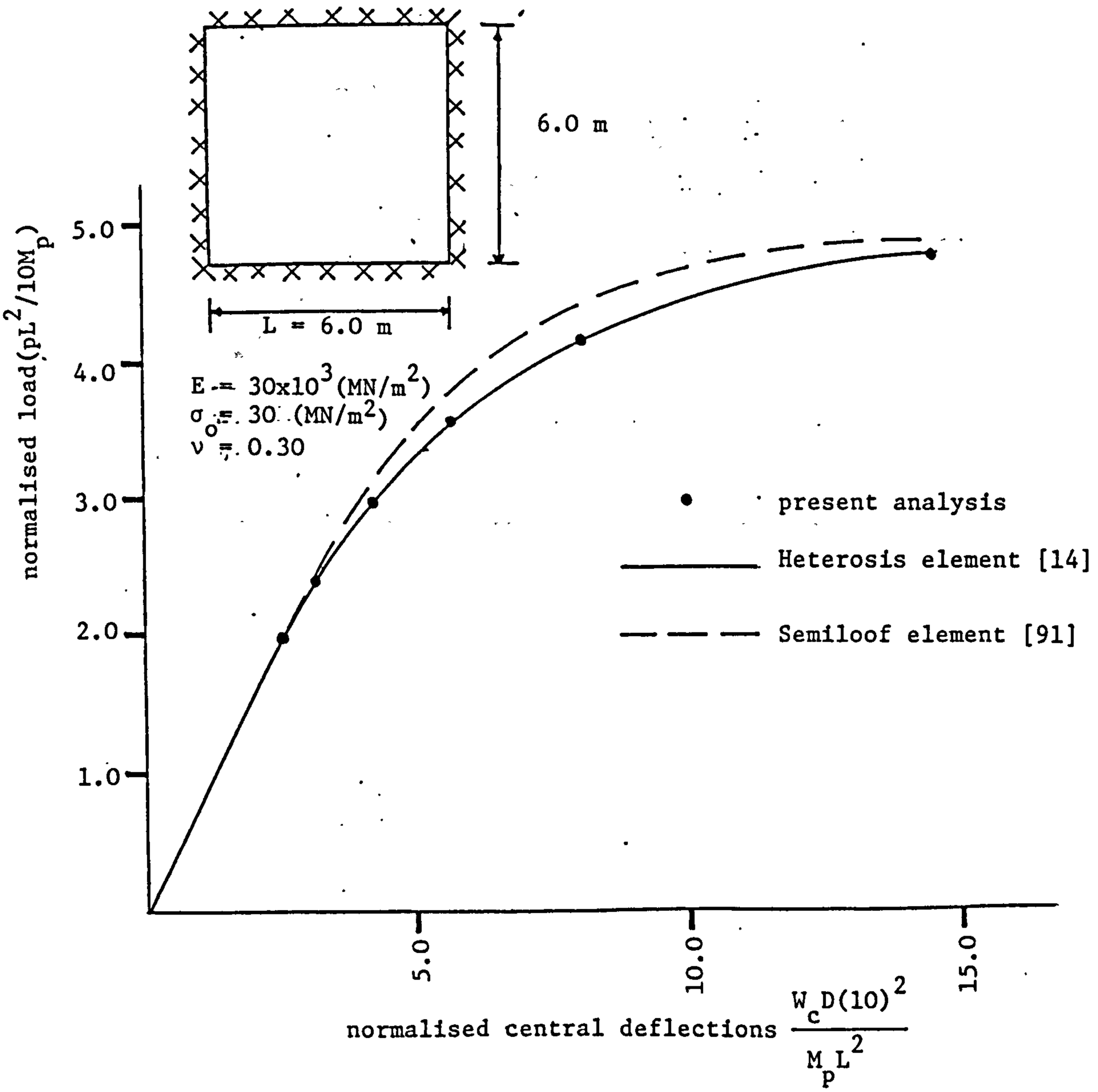

Figure 7.7. Load-deflection curves for clamped plate under uniformly distributed load.

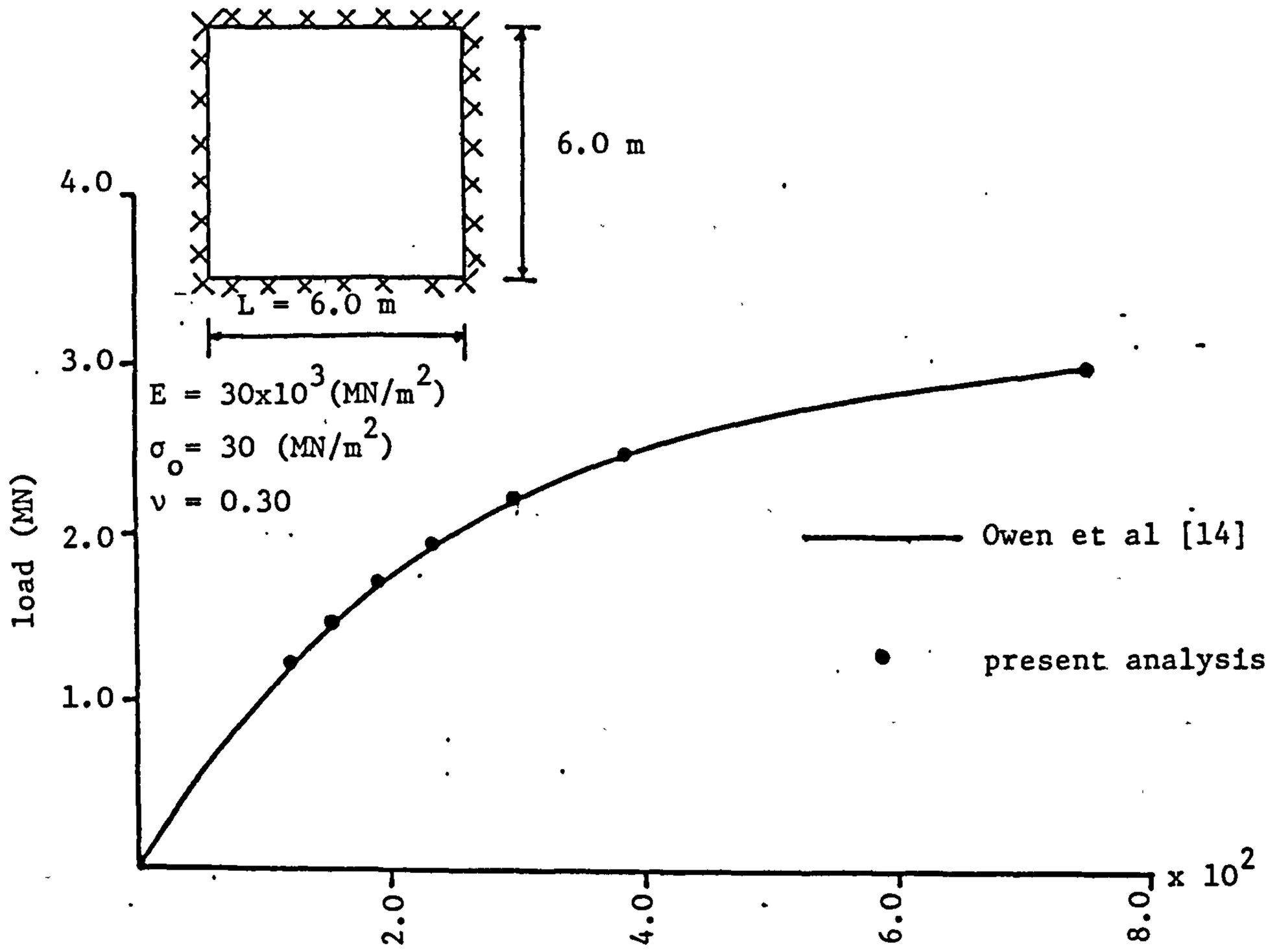

Figure 7.8. Load-deflection curves for clamped plate under central point load

throughout the plate thickness, while the results obtained using the Semiloof element [91] showed slightly stiffer structural response compared with those obtained using the Heterosis element.

The spread of the plastic zones at different load levels are shown in Figs.7.9 and 7.10, which shows that, as expected, the flow of plasticity is symmetric about the middle surface of the plate.

The steel plate under uniformly distributed load was reanalysed with both geometric and material nonlinearities considered to investigate the effect of the membrane forces on the plate behaviour. In Fig.7.11 the central deflection is plotted for the different load levels together with those obtained when only material nonlinearity was considered. The geometric and material nonlinear analysis predicted much higher loads than those predicted by the material nonlinear analysis. A comparison of the loads predicted by the different analyses is given in Table 7.2. The spread of the plastic zones obtained in the geometric and material nonlinear analysis are shown in Figs.7.12 and 7.13, which indicates that a tensile in-plane forces had developed throughout the plate.

To investigate the accuracy of the different integration rules that could be used to evaluate the stress resultants, the plate was analysed using a number of integration rules. The results obtained using the modified trapezoidal, Lobbato, Newton-Cotes and Simpson's rules with 5 integration points are given in Table 7.3 for the load-deflection relationships and the number of iterations required. Insignificant differences in the results obtained using the different

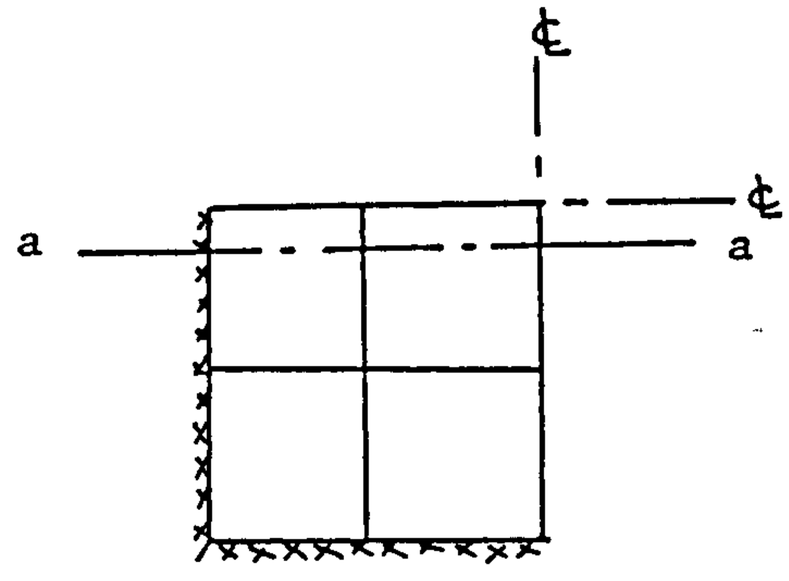

Figure 7.9. Spread of plastic zones through clamped plate under uniformly distributed load (section a-a)

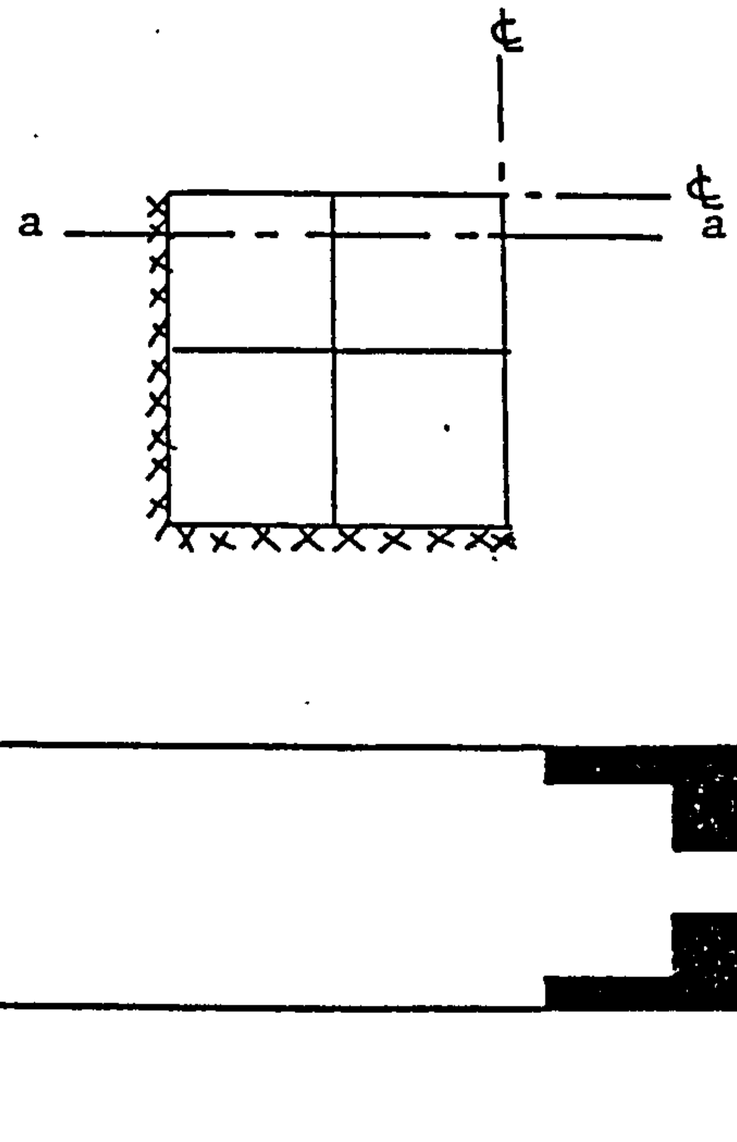

Figure 7.10. Spread of plastic zones through clamped plate under central point load (section a-a)

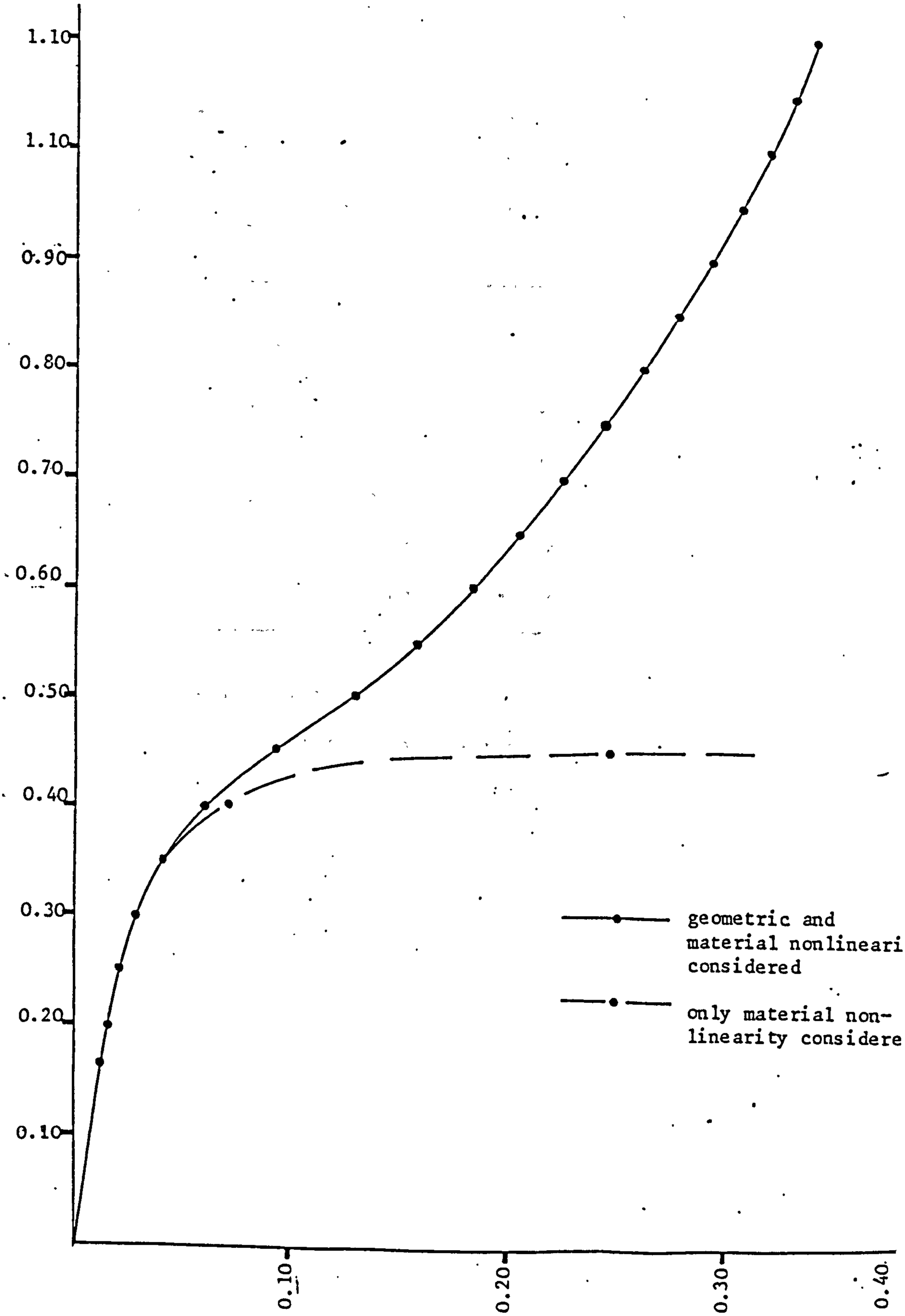

Figure 7.11. Load-deflection curves for clamped plate under uniformly distributed load with different

Table 7.2. Effect of the membrane forces on the behaviour of clamped square plate under uniformly distributed load.

ratio of central deflection to thickness	load intensity (MN/m^2)		% load increase
	A	B	
0.2500	0.38	0.38	0.0
0.6250	0.45	0.50	11.0
0.8750	0.45	0.58	29.0
1.0000	0.45	0.66	47.0
1.2500	0.45	0.78	73.0
1.5000	0.45	0.92	106.0
1.6875	0.45	1.07	139.0

A material nonlinear analysis

B geometric and material nonlinear analysis

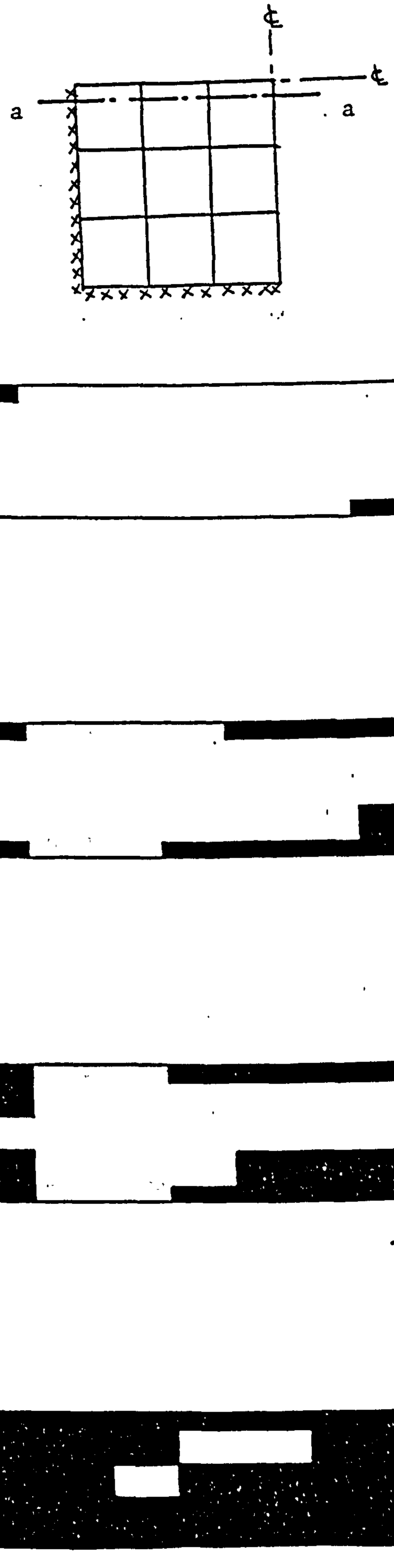

Figure 7.12. Spread of plastic zones through clamped plate under uniformly distributed load (Section a-a)

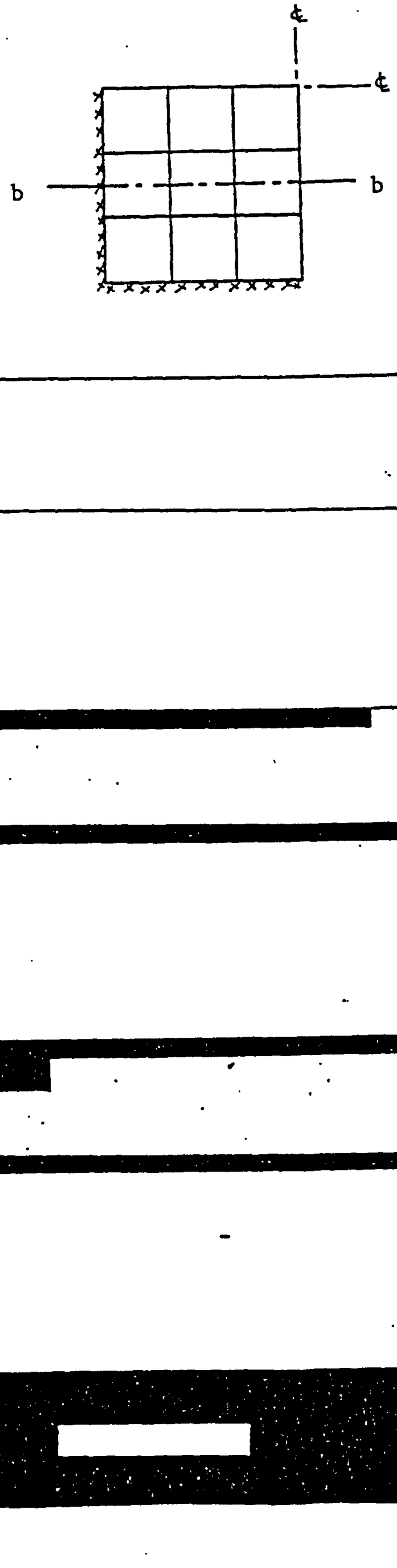

Fogure 7.13. Spread of plastic zones through clamped plate under uniformly distributed load (section b.b)

Table 7.3. Comparison between the different numerical integration rules in the analysis of clamped steel plate under uniformly distributed load.

Load	Trapezoidal		Lobbato		Newton-Cotes		Simpsons	
(MN/m^2)	W	N.I.	W	N.I.	W	N.I.	W	N.I.
0.20	0.0157	4	0.0154	3	0.0155	3	0.0155	4
0.25	0.0204	5	0.0199	6	0.0198	4	0.0199	4
0.30	0.0276	10	0.0259	8	0.0256	7	0.0259	8
0.35	0.0387	15	0.0347	13	0.0334	10	0.0341	20
0.40	0.0597	28	0.0539	26	0.0457	17	0.0478	19
0.45	0.0914	37	0.0851	31	0.0689	31	0.0729	32
0.50	0.1280	45	0.1141	36	0.1135	54	0.1157	52
0.55	0.1564	34	0.1458	44	0.1495	41	0.1496	39
0.60	0.1789	29	0.1739	38	0.1760	33	0.1749	31
0.65	0.1994	27	0.1943	27	0.1985	30	0.1970	29
0.70	0.2188	28	0.2128	26	0.2173	26	0.2155	25
0.75	0.2370	27	0.2293	23	0.2351	26	0.2340	27
0.80	0.2548	27	0.2455	24	0.2517	24	0.2505	24
0.90	0.2861	23	0.2765	23	0.2824	23	0.2818	23
0.95	0.2993	20	0.2910	22	0.2961	21	0.2959	22
1.00	0.3115	19	0.3041	20	0.3091	20	0.3089	20
1.05	0.3232	18	0.3170	20	0.3210	18	0.3208	19
1.10	0.3336	16	0.3286	18	0.3323	18	0.3324	18
T.N.I.	397		408		389		416	

W central deflection

N.I. number of iterations

T.N.I. total number of iterations

integration rules has been observed.

7.3.3 SIMPLY SUPPORTED CIRCULAR STEEL PLATE

A 3.1875 in. radius circular mild steel plate of 0.19 in. thickness was tested experimentally by Onat et al [92]. The plate was loaded by a 0.50 in. diameter circular punch at the centre of the plate. The plate has also been analysed by Stricklin et al [93] using a combined finite element-finite difference approach.

The analysis carried out included both geometric and material nonlinearities in order to compare the results obtained with the experimental results. The stress resultants were determined using the modified trapezoidal rule with 5 sampling points. The load-deflection curves are shown in Fig.7.14. The load-deflection curve obtained from the analysis gave good correlation with the experimental curve. The spread of the plastic zones at different load levels are shown in Fig.7.15. These zones had developed initially at the vicinity of the centre of the plate and then spread toward the boundaries at higher load levels. An investigation of the membrane forces throughout the plate indicated that tensile and compressive force rings had formed around the centre and the boundaries of the plate respectively. The principal in-plane forces developed in the plate at a load of 2100 lb are plotted in Fig.7.16, which indicates a tensile ring at the centre of the plate and a compressive ring at the boundaries.

To investigate the effect of the membrane forces on the plate

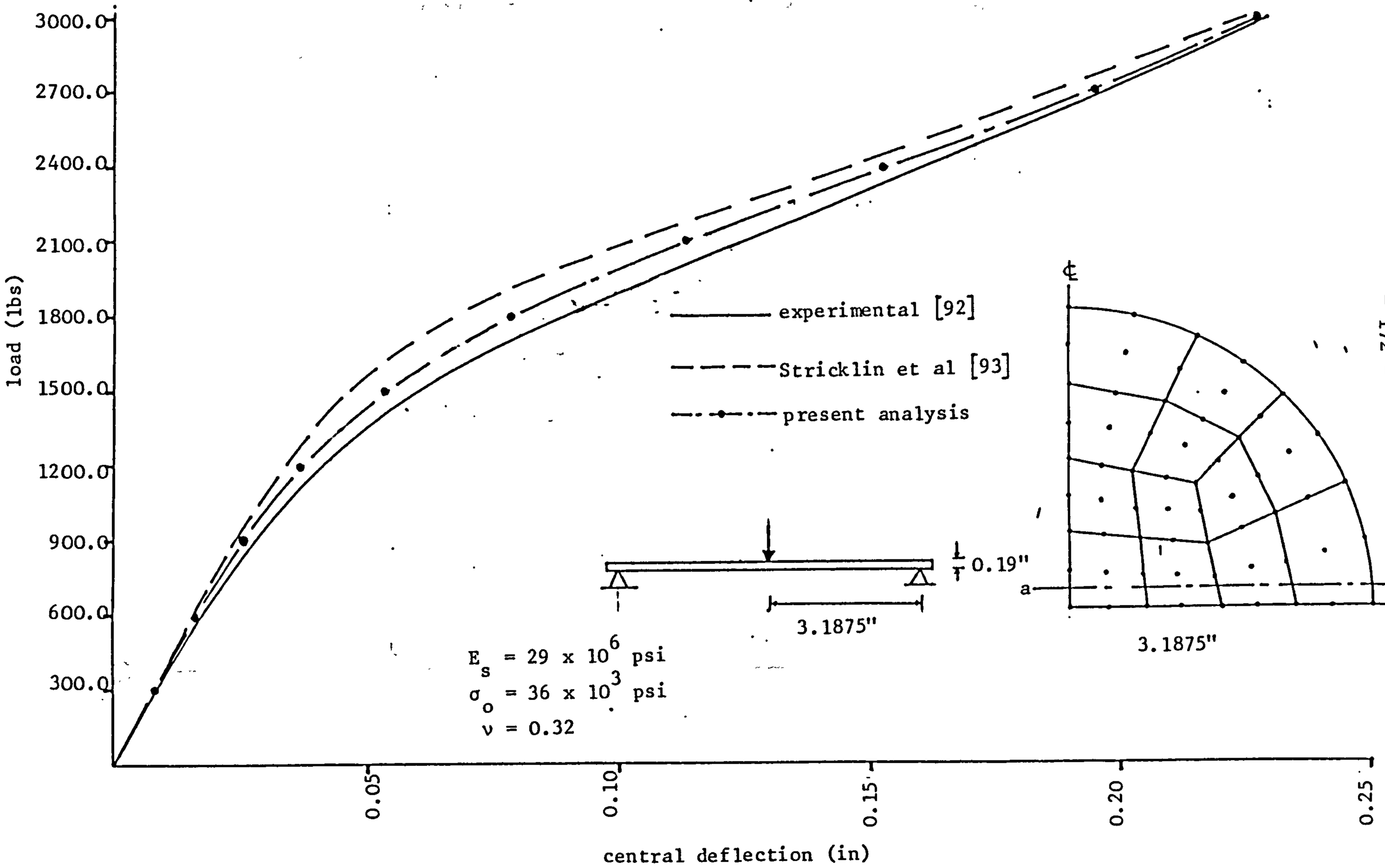

Figure 7.14 Load-deflection curves for simply supported plate under central point load

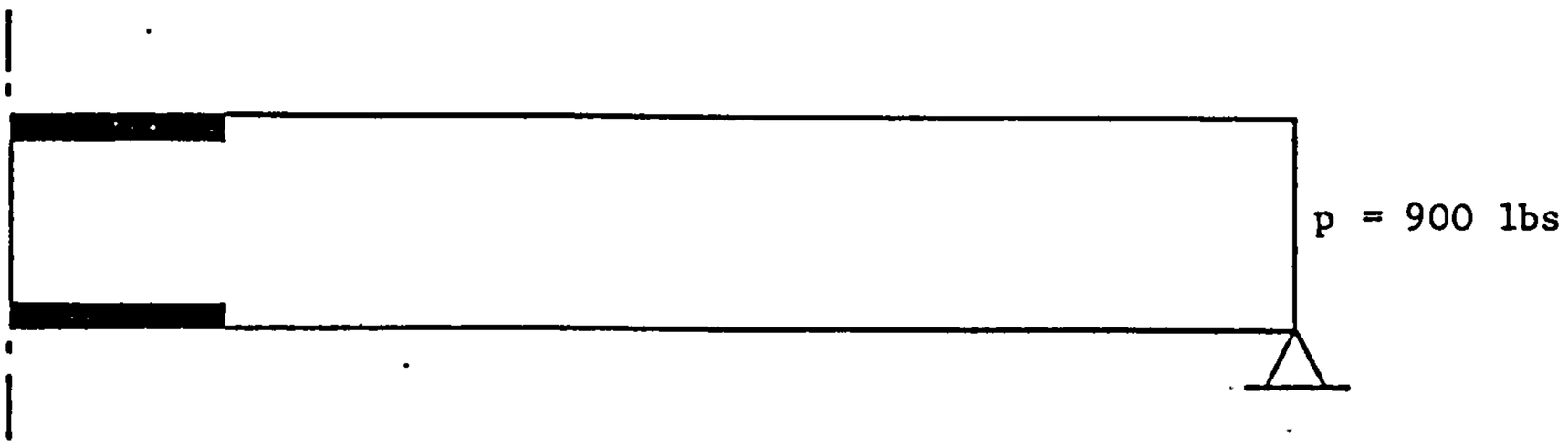

Figure 7.15. Spread of plastic zones through simply supported circular plate under central point load (section a-a)

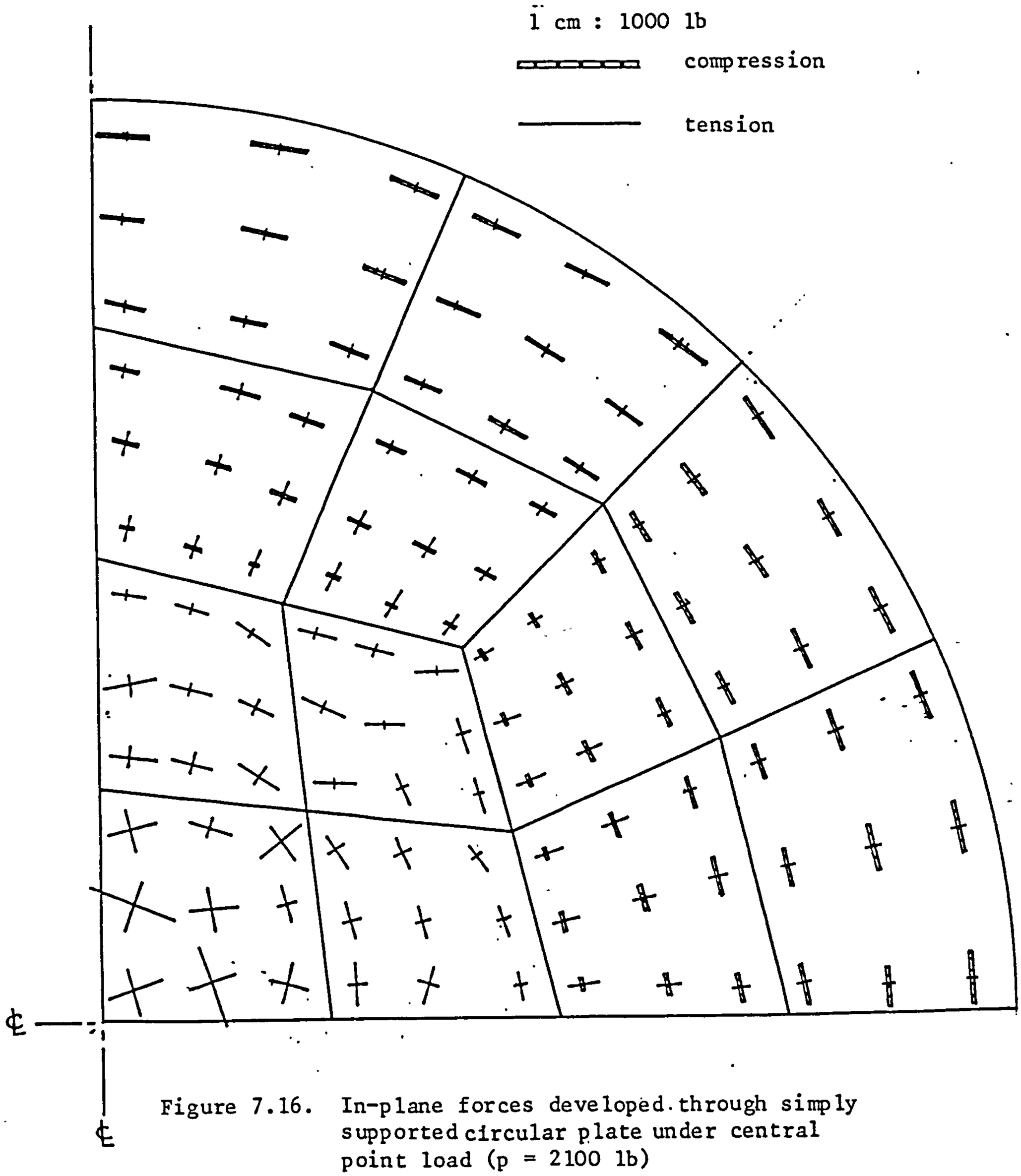

Figure 7.16. In-plane forces developed through simply supported circular plate under central point load (p = 2100 lb)

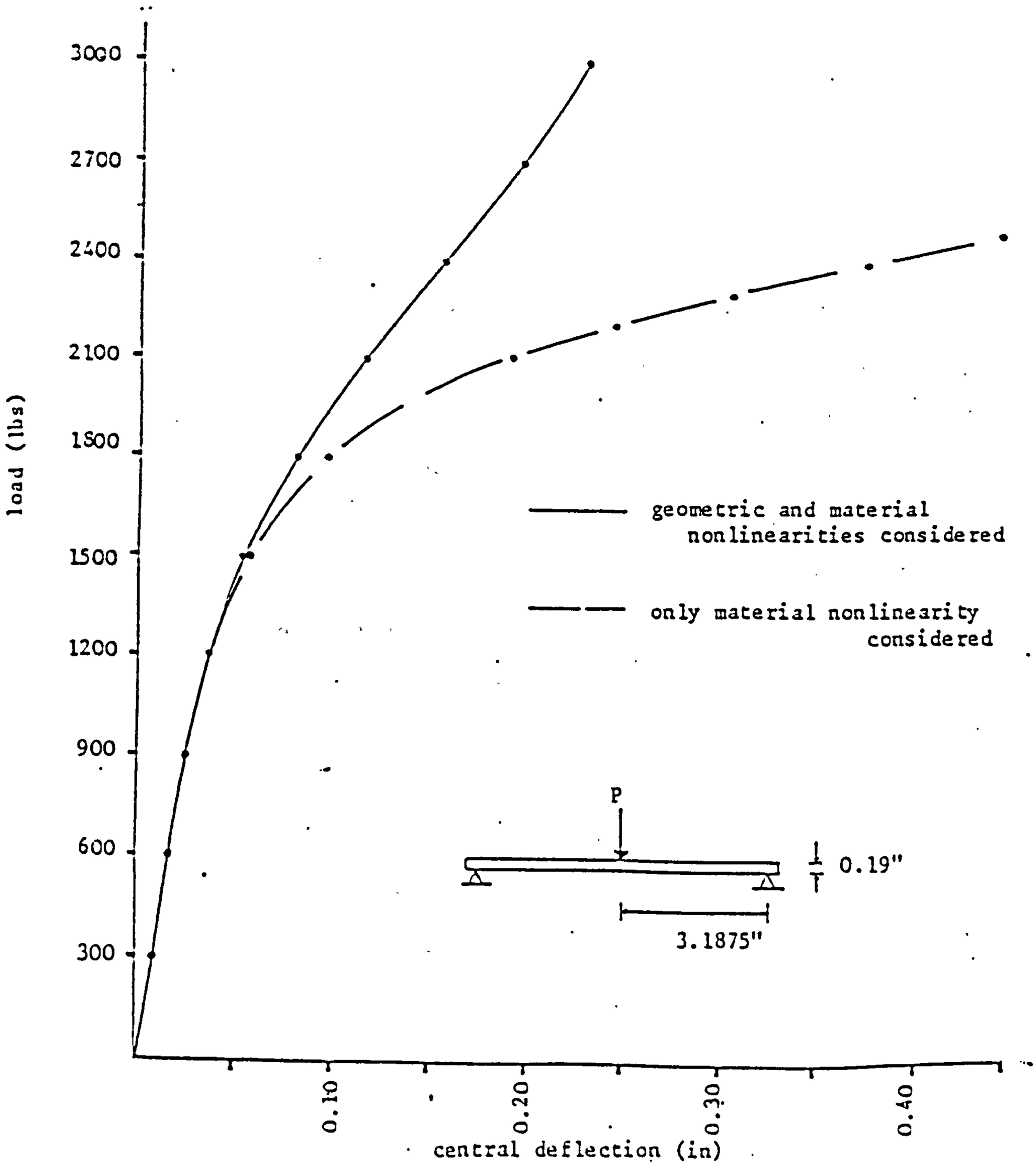

Figure 7.17. Load-deflection curves for simply supported plate under central point load with different nonlinearities considered

behaviour, the plate was reanalysed with only material nonlinearity considered. The load-deflection curve is shown in Fig.7.17, together with the curve obtained when both nonlinearities were considered in the analysis. These curves indicate that the load that the plate can sustain is likely to be underestimated when the membrane forces are ignored in the analysis.

7.4 REINFORCED CONCRETE SLABS

Several reinforced concrete slabs were analysed to demonstrate the validity of the procedures developed for the analysis of reinforced concrete slabs. In the first example the analysis was carried out for a simply supported slab in which both nonlinearities were considered. In the second example the behaviour of a simply supported slab was investigated when different combinations of the geometric and material nonlinearities were considered. In the next three examples the behaviour of clamped slabs which undergo large deflections was investigated.

In all the first five examples the behaviour of concrete was modelled using material model I with the multi-linear stress-strain curve for concrete in compression. The stress resultants were evaluated numerically using the modified trapezoidal rule with 5 sampling points. The final section is a study of the effect of the amount of reinforment on the behaviour of clamped slabs. The performance of the different material models and the effect of the inclusion of the line search on the analysis were also investigated.

The nonlinear part of the stiffness matrix was updated at the end of the first iteration and every ten iterations within each increment. The analyses were carried out using a displacement and an energy convergence tolerances, equations (6.16) and (6.17), of 0.005 and 0.02 respectively.

7.4.1 MCNIECE'S SLAB

A 914 mm. square reinforced concrete slab simply supported on the four edges was tested by McNiece et al [94]. This slab has been analysed by many researchers, [58] and [95], the majority of whom used a 6x6 element discretasition of a quarter of the slab. The slab is 44.5 mm. thick with 0.85% reinforcement both ways placed at 11.2 mm. from the slab bottom. The following material properties, which are given in Ref.[95], were used for the analysis:

concrete	steel
$E_c = 0.29 \times 10^5$ N/mm^2	$E_{st} = 2.0 \times 10^5$ N/mm^2
$f'_c = 32.4$ N/mm^2	$\sigma_o = 345.0$ N/mm^2
$f'_t = 3.20$ N/mm^2	$\sigma_{su} = 618.0$ N/mm^2
$\varepsilon_{cu} = -0.0035$ mm/mm	$\varepsilon_{su} = 0.10$ mm/mm
$\nu = 0.15$	

A 3x3 mesh was used to model a quarter of the slab. The central point load was applied in 11 load steps with an initial load of 4.0 KN and

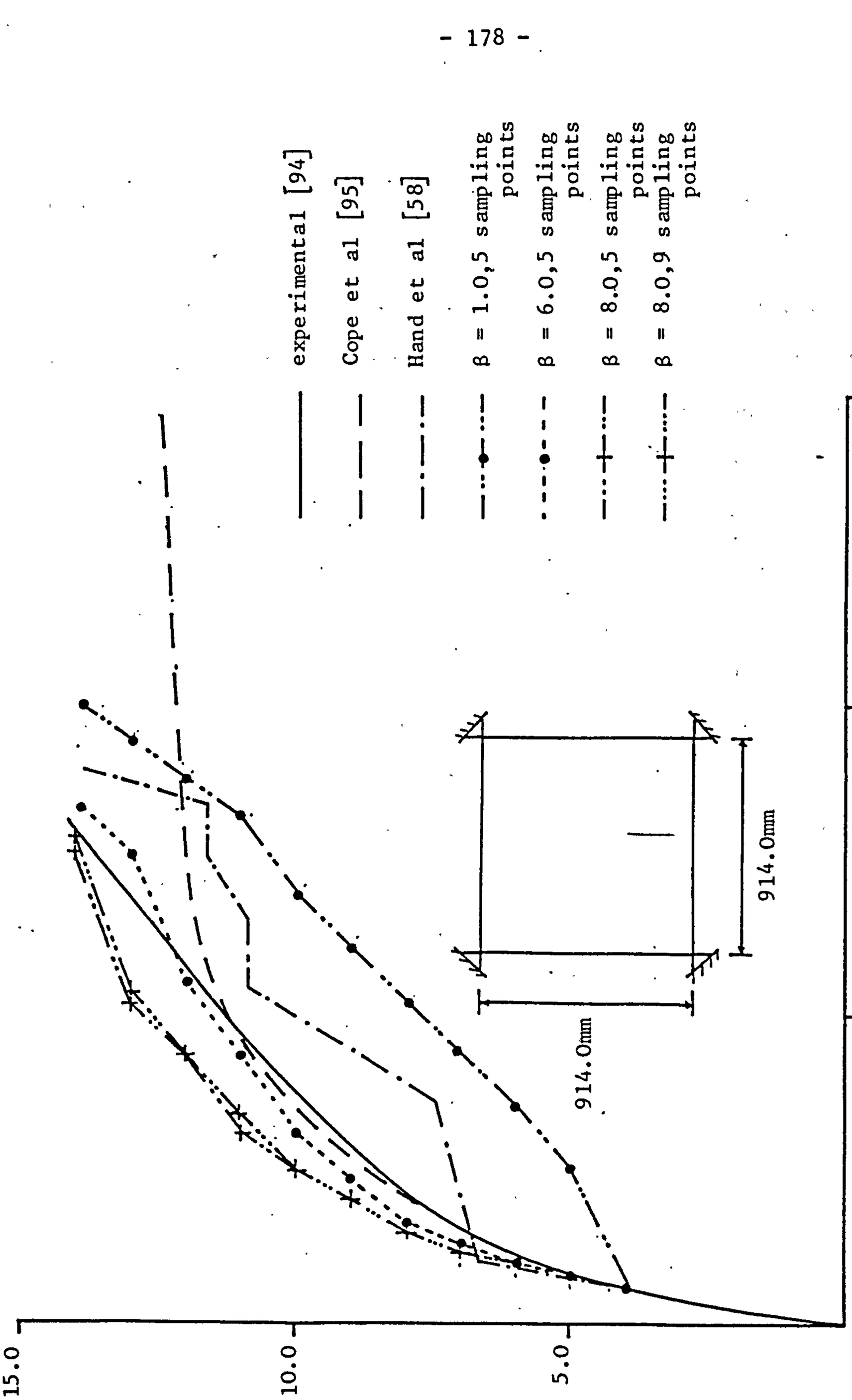

Figure 7.18. Load-deflection curves for McNiece's slab

subsequent increments of 1.0 KN. The effects of tension stiffening and the number of the sampling points throughout the slab thickness are illustrated by the load-deflection curves shown in Fig.7.18. The load-deflection curve obtained by Cope et al [95], using the initial stress method, gave good agreement over a portion of the experimental curve. The load-deflection curve obtained by Hand et al [58], using a variable stiffness approach, gave a step-like response which could be attributed to the change in the stiffness matrix. The assumption of brittle failure for the concrete, β =1.0, resulted in deflections being overestimated. Improvement in the correlation of the experimental and numerical results can be seen when allowance was made for tension. The results obtained with the tension stiffening parameter, β =6.0, and 5 sampling points gave an acceptable agreement with the experimental results with convergence obtained in an average of 11 iterations per load increment.

7.4.2 TAYLOR'S SLAB

A 72.0 in. square reinforced concrete slab simply supported on all edges was tested by Taylor et al [96]. The slab was 2.0 in. thick with a bottom reinforcement bar of 3/16 in. in diameter spaced every 2.5 in. in the x-direction and 3.0 in. in the y-direction. This slab has been analysed by Van Greunen [6] using a triangular finite element incorporating membrane and plate bending effects. The following material properties, which are given in Ref.[6], were used for the analysis:

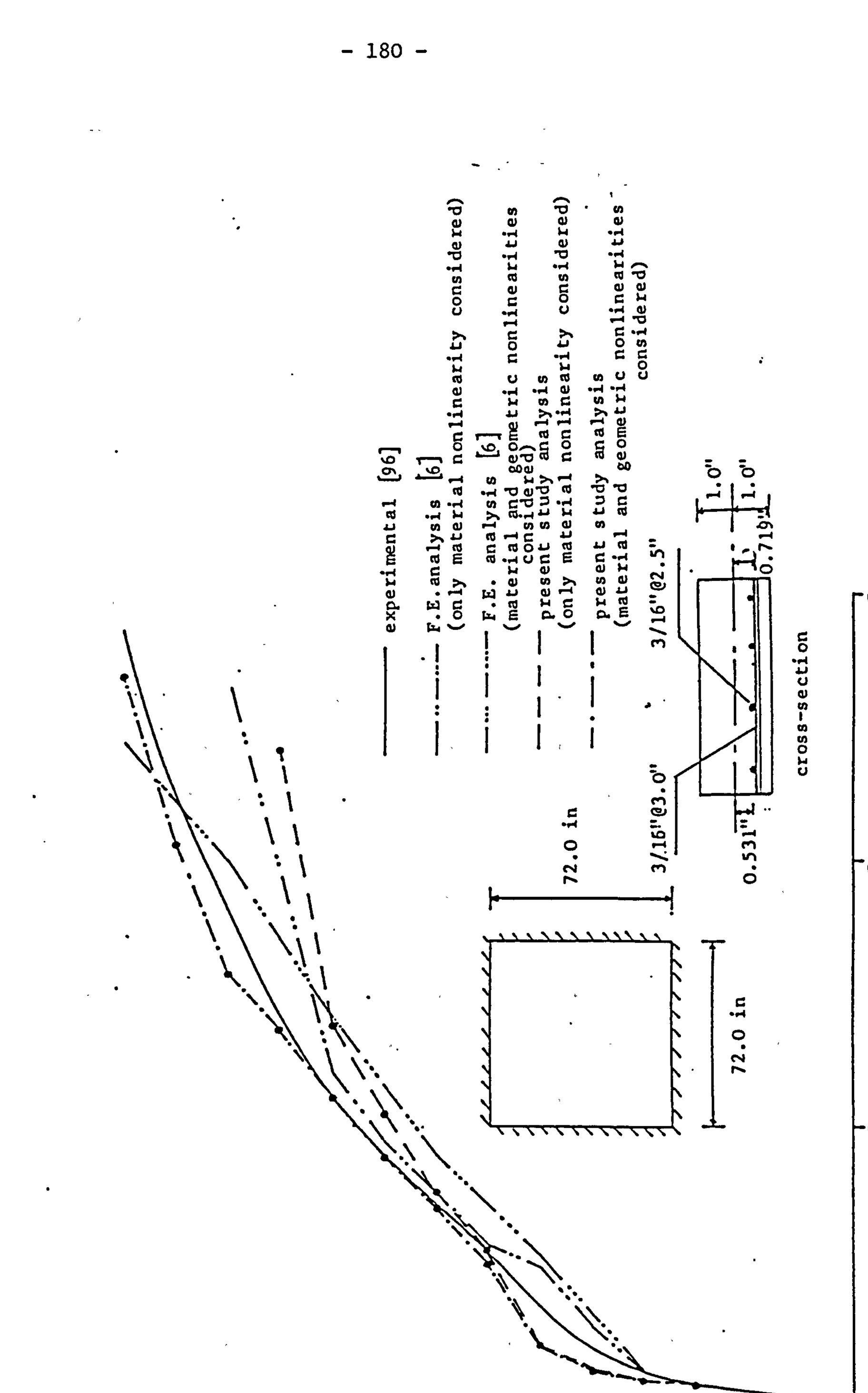

Figure 7.19. Load-deflection curves for Taylor's slab

concrete	steel
$E_c = 4.35 \times 10^6$ psi	$E_{st} = 30.0 \times 10^6$ psi
$f'_c = 5000.00$ psi	$\sigma_o = 54000.0$ psi
$f'_t = 522.0$ psi	$\sigma_{su} = 54000.0$ psi
$\varepsilon_{cu} = -0.0035$ in/in	$\varepsilon_{su} = 0.10$ in/in
$\nu = 0.18$	

A 2x2 mesh used to model a quarter of the slab. The concrete was assumed to have tension siffening with $\beta = 6.0$. Two analyses were carried out with different nonlinearities considered. In both analyses the stress resultants were determined using the modified trapezoidal rule with 5 sampling points. The slab was subjected to a uniformly distributed load applied in the steps shown in Fig.7.19. The load-deflection curve obtained in the analysis in which both nonlinearities were considered gave good agreement with the experimental curve. The importance of the nonlinear geometric effects can be clearly seen in that the predicted load is significantly higher than that predicted when they were neglected.

7.4.3 POWELL'S SLAB

A series of clamped rectangular reinforced concrete slabs subjected to uniformly distributed loads were tested by Powell [1]. The long span of the slabs was 36.0 in., the short span was 20.57 in. and their thickness was 1.286 in. One of the slabs with a reinforcement of 0.79% provided at the top and bottom of the slab in each direction was

selected for analysis. The following material properties were used for the analysis:

concrete	steel
$E_c = 3.5 \times 10^6$ psi	$E_{st} = 29 \times 10^6$ psi
$f'_c = 5800.0$ psi	$\sigma_o = 37000.0$ psi
$f'_t = 580.0$ psi	$\sigma_{su} = 66000.0$ psi
$\varepsilon_{cu} = 0.0035$ in/in	$\varepsilon_{su} = 0.09$ in/in
$\nu = 0.20$	

The analysis was carried out using the load control up to the ultimate compressive load and then the lateral nodal displacement component at the slab centre was assigned a value of 0.10 in. at the beginning of each increment. The load-deflection curves obtained using a 3x3 and a 2x2 meshes are shown in Fig.7.20. The ultimate compressive loads obtained were 51.7 lb/in^2 and 48.6 lb/in^2 using the 2x2 and 3x3 meshes respectively compared with the corresponding experimental value of 49.6 lb/in^2. The load then decreased dramatically with the increased deflections until it reached a value of approximately 23.0 lb/in^2 for both meshes. The load then increased substainally with the increased deflections. Convergence for the 2x2 and 3x3 meshes was obtained in an average of 14 and 16 iterations per increment respectively. The load-deflection curves obtained gave an acceptable agreement with the experimental curve, yet the 2x2 mesh required about 60% of the computation time compared with that required using the 3x3 mesh.

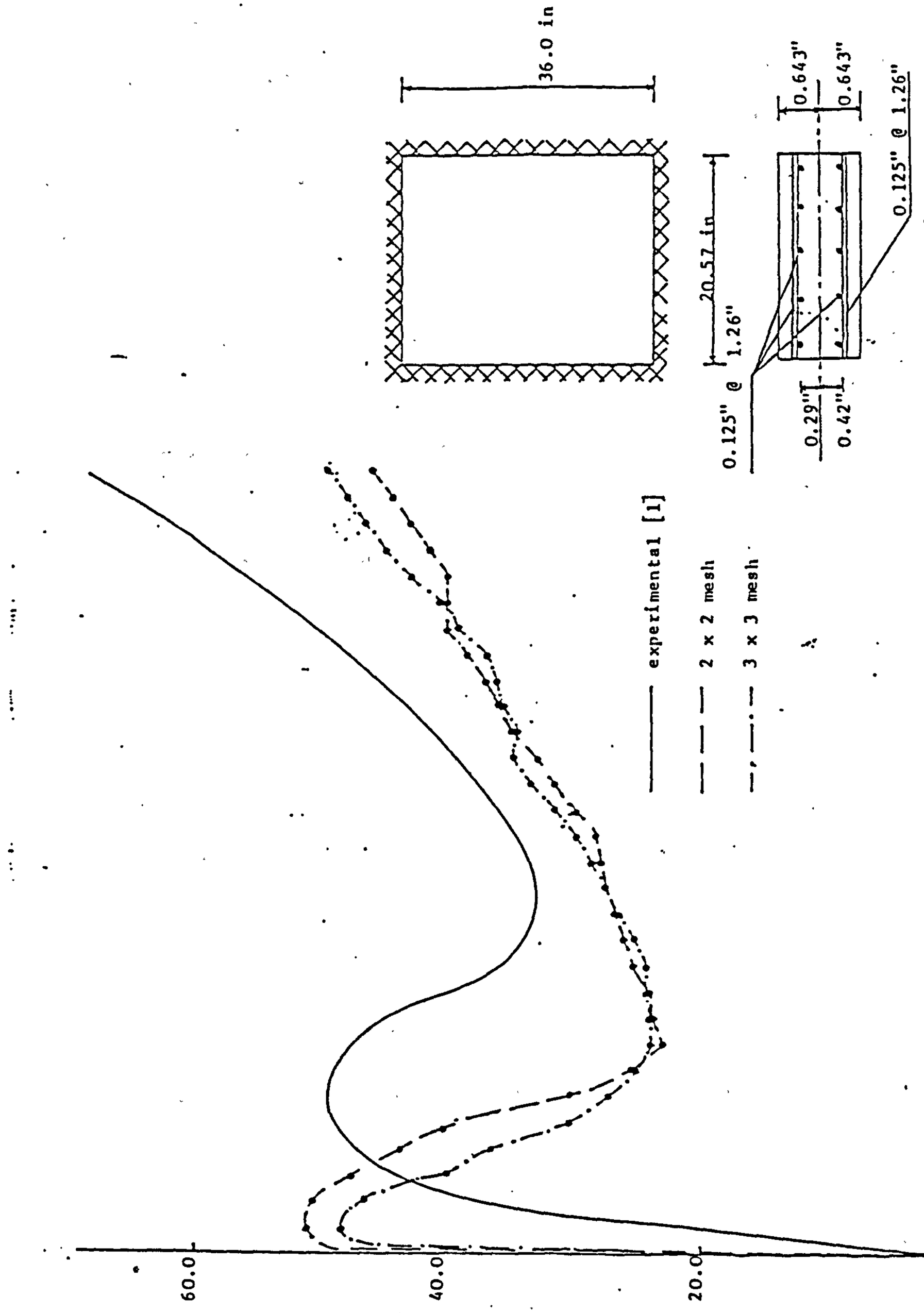

Figure 7.20 Load-deflection curves for Powell's slab

7.4.4 PARK'S SLAB

A number of clamped rectangular reinforced concrete slabs subjected to uniformly distributed loads were tested experimentally by Park [3]. The slabs were 60.0x40.0 in. and a thickness of 2.0 in. One of the slabs, with a reinforcement of 1.44% and 0.72% provided in the short direction placed at the top and bottom respectively, while the long span was provided with a reinforceement of 0.45% and 0.22% placed at the top and bottom respectively, was selected for analysis. The bottom steel was placed over the whole of the slab but the top steel extended from the edges a distance of 1/4 of the span. The following material properties were used for the analysis:

concrete	steel
$E_c = 3.5 \times 10^6$ psi	$E_{st} = 29 \times 10^6$ psi
$f'_c = 5000.00$ psi	$\sigma_o = 45000.0$ psi
$f'_t = 500.0$ psi	$\sigma_{su} = 45000.0$ psi
$\varepsilon = -0.0035$ in/in	$\varepsilon_{su} = 0.065$ in/in
$\nu = 0.20$	

A 2x2 mesh was used to model a quarter of the slab. The analysis was carried out using load control up to the ultimate compressive load and then a value of 0.125 in. was assigned to the lateral nodal displacement component at the centre of the slab and displacement control was used. The load-deflection curve obtained is plotted in Fig.7.21, together with the experimental curve. An ultimate compressive load of 41.6 lb/in^2 was obtained compared with the corresponding experimental value of 37.8 lb/in^2. Convergence was

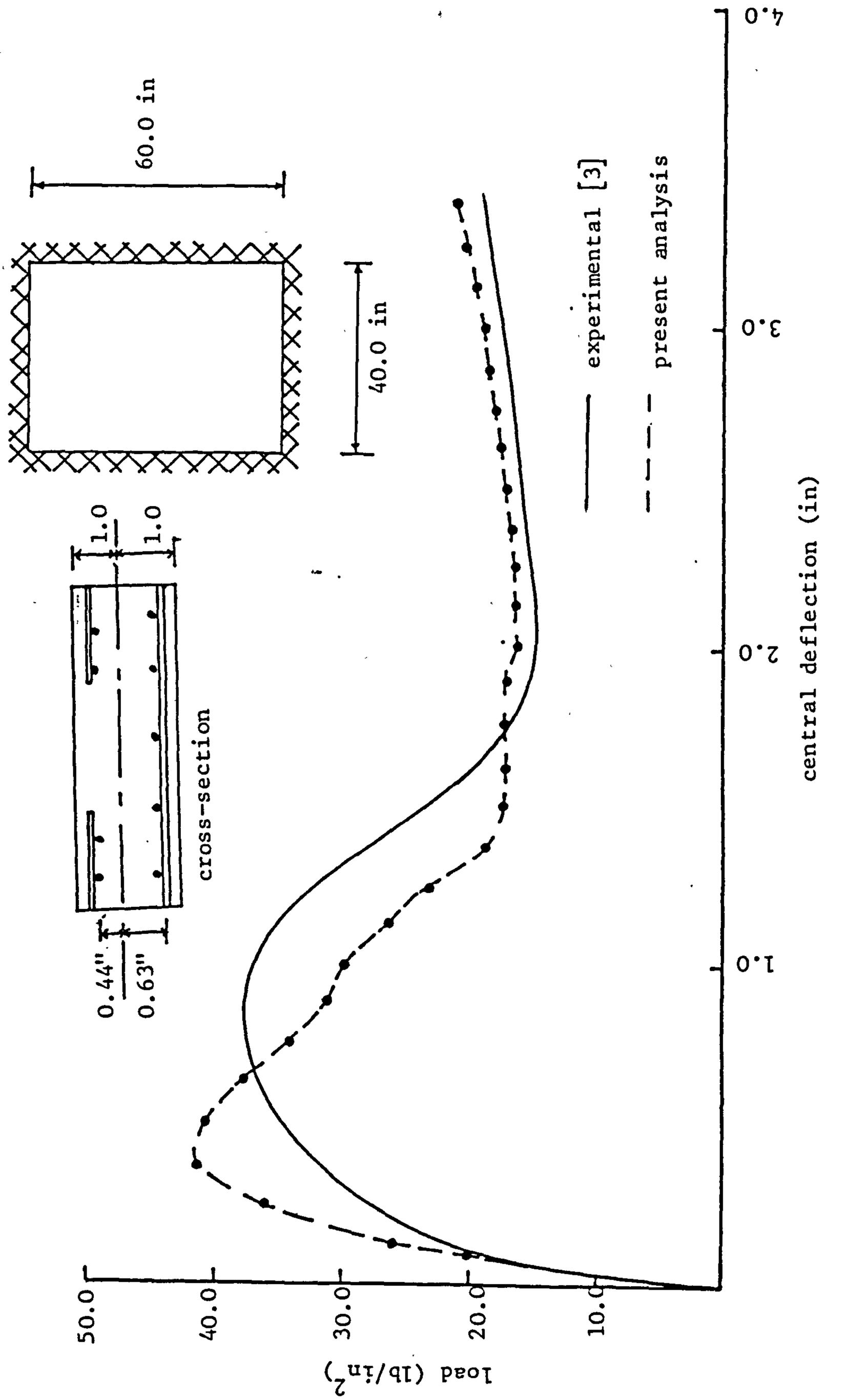

Figure 7.21. Load deflection curves for Park's slab

obtained in an average of 12 iterations per increment. Good agreement between the analytical and experimental curves was observed

7.4.5 BLACK'S SLAB

A number of clamped reinforced concrete slabs were tested by Black [5] to investigate the collapse of slabs with clamped edges. Both static and blast loads were considered. One of the slabs 29.0 in. square and 0.89 in thick and subjected to static pressure was selected for analysis. This slab has been also analysed by Van Greunen [6] using a triangular finite element incorporating membrane and plate bending effects. The slab was reinforced by a 0.08 in. diameter reinforcing bars. The reinforcement layout is shown in Fig.7.22. The following material properties, which are given in Ref.[6], were used for the analysis:

concrete	steel
$E_c = 3.5 \times 10^6$ psi	$E_{st} = 29 \times 10^6$ psi
$f'_c = 4000.0$ psi	$\sigma_o = 43600.0$ psi
$f'_t = 500.0$ psi	$\sigma_{su} = 73500.0$ psi
$\varepsilon_{su} = -0.0035$ in/in	$\varepsilon_{su} = 0.10$ in/in
$\nu = 0.15$	

A 2x2 mesh was used to model a quarter of the slab. Black [5] provided only the four points indicated on the load-deflection curve shown in Fig.7.22. The curve obtained in the analysis gave good

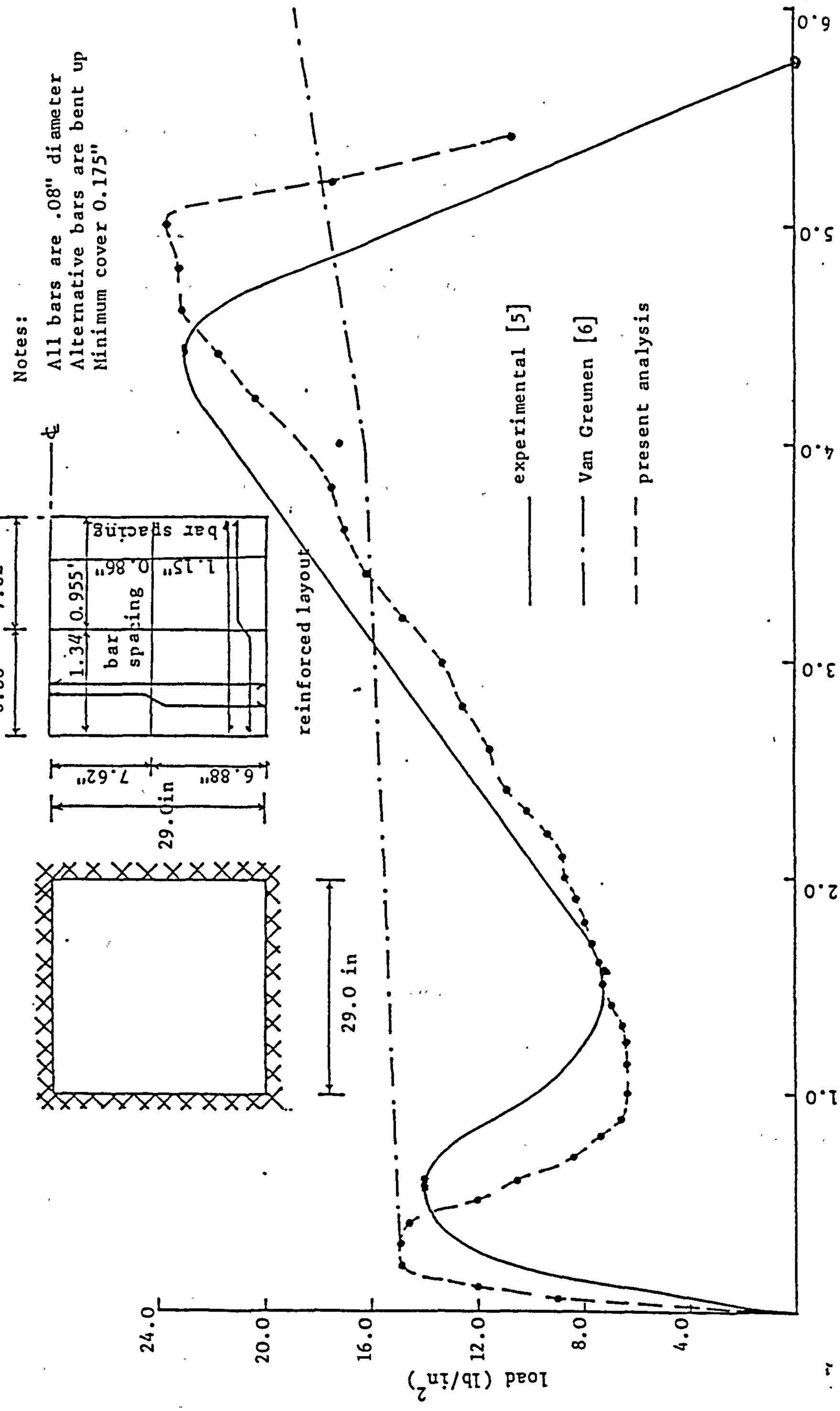

Figure 7.22. Load-deflection curves for Black's slab.

agreement with the experimental curve, whilst that obtained by Van Greunen [6], using a load control throughout the analysis, failed to pick up the snap-through response and gave a much lower ultimate tensile load compared to that recorded experimentally. The present analysis gave an ultimate compressive and tensile loads of 14.90 lb/in^2 and 23.70 lb/in^2 compared with the corresponding experimental vaules of 14.1 lb/in^2 and 23.2 lb/in^2 respectively. Convergence was obtained in an average of 11 iterations per increment.

7.4.6 EFFECT OF THE AMOUNT OF REINFORCEMENT

Two clamped square slabs subjected to uniformly distributed loads were analysed to investigate the effect of the amount of reinforcement on the behaviour of clamped slabs. The effect of the line search on the analysis and the performance of the different material models for concrete were also investigated. The slabs were 762.0 mm. square and 25.0 mm. thick. The slabs were assumed to be reinforced by a 2.0 mm. diameter reinforcing bars placed at equal spacings in both directions at the top and bottom of the slabs. A 25.0 mm. and 100.0 mm. spacings were assumed for slabs S1 and S2 respectively. The following material properties were used for the analysis:

concrete	steel
$E_c = 0.24 \times 10^5$ N/mm^2	$E_{st} = 2.0 \times 10^5$ N/mm^2
$f'_c = 27.6$ N/mm^2	$\sigma_o = 300.0$ N/mm^2
$f'_t = 3.40$ N/mm^2	$\sigma_{su} = 500.0$ N/mm^2
$\varepsilon_{cu} = -0.0035$ mm/mm	$\varepsilon_{su} = 0.10$ mm/mm
$\nu = 0.15$	

A 2x2 mesh was used to model a quarter of the slab. Fig.7.23 shows the load-deflection curves obtained using the analysis in which the concrete was modelled using model I with the multi-linear stress-strain relationship for concrete in compression. The amount of reinforcement had a mixed effect on the behaviour of the slabs at the different stages of the response. The ultimate compressive load obtained in the analysis of slab S1 was 27% higher than the corresponding vaule for slab S2. On the other hand the ultimate tensile load obtained in the analysis of slab S1 was approximately 405% higher than that obtained in the analysis of slab S2, which indicates that the ultimate tensile load is proportional to the amount of the reinforcement provided in the slab. The in-plane forces developed in the x-direction near the centre of slab S1 are shown in Fig.7.24. Compressive in-plane forces had developed initially at the centre of the slab and then began to change to tensile forces and grow outward toward the edges of the slab.

An investigation of the effect of the line search indicated that its inclusion in the analysis in order to speed up convergence resulted in reductions of approxiamtely 40% and 50% of the number of the iterations and the C.P.U. time respectively.

Slab S1 was reanalysed using the different material models to investigate their performance. The load-deflections curves obtained are shown in Fig.7.25. The different models predicted similar responses which is due to the fact that the nonlinear behaviour of reinforced concrete slabs undergo large deflections is mainly due to cracking of the concrete and yielding of the reinforcing steel.

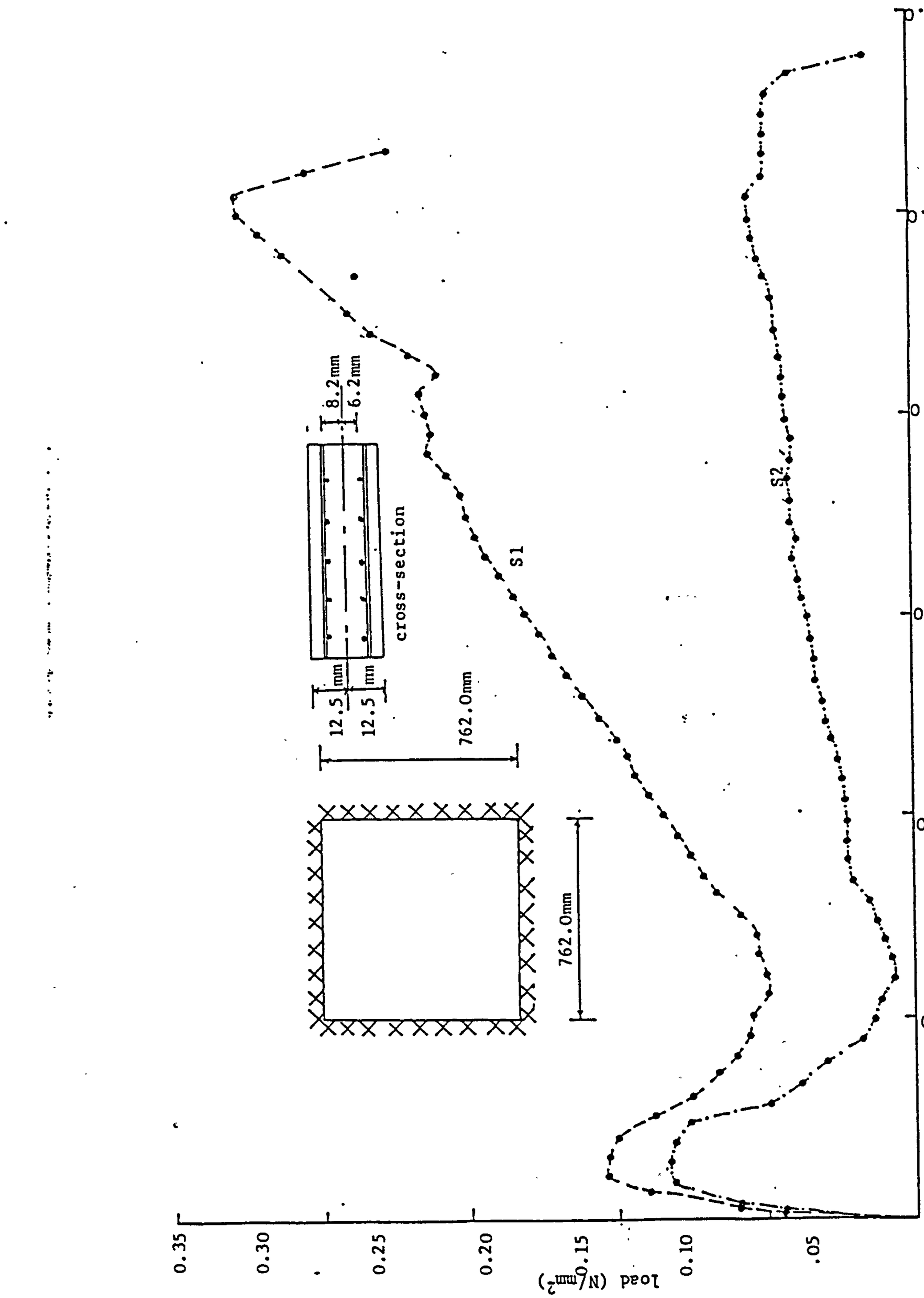

Figure 7.23. Load-deflection curves for clamped slabs S1 and S2

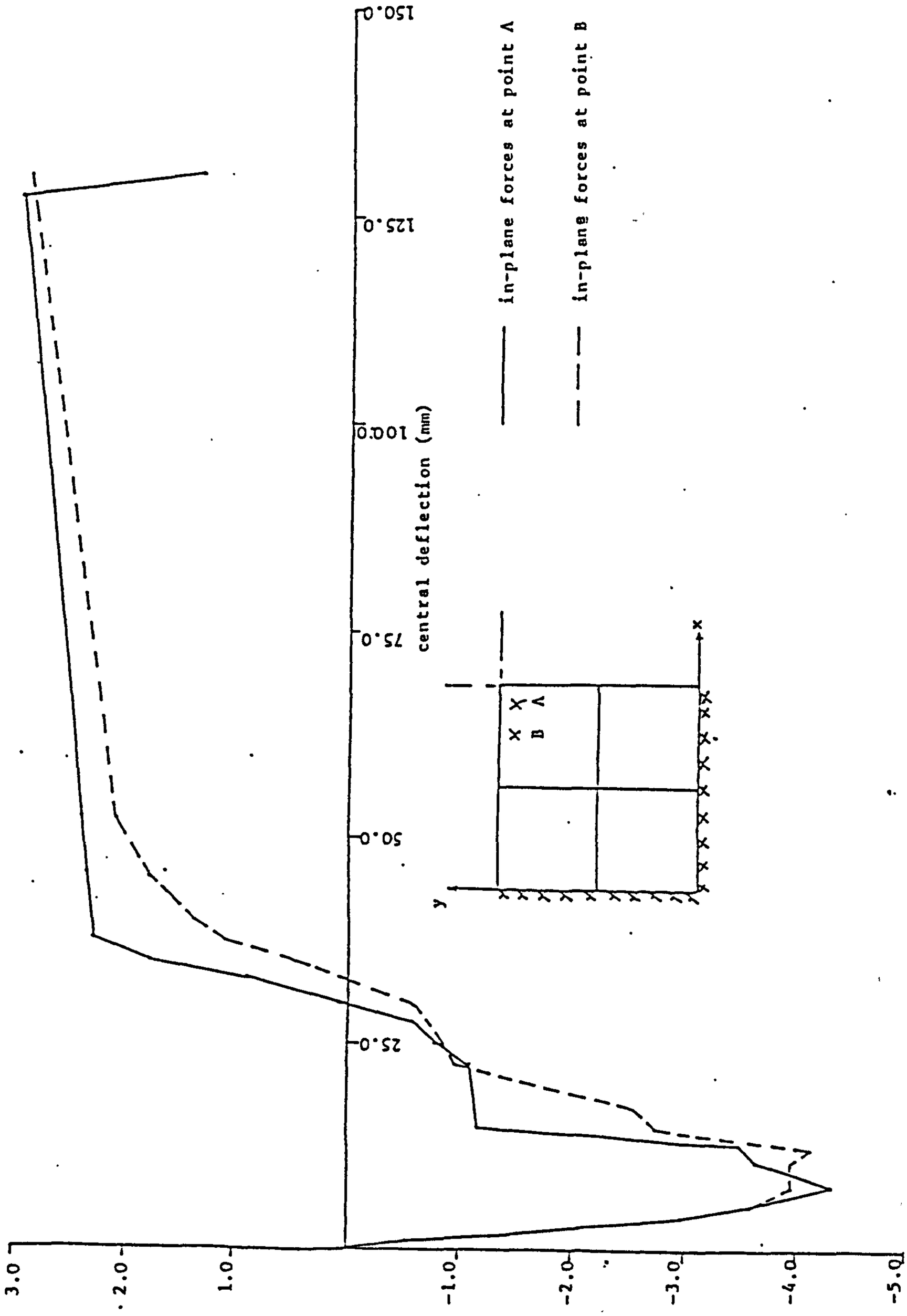

Figure 7.24. In-plane forces developed in slab S1

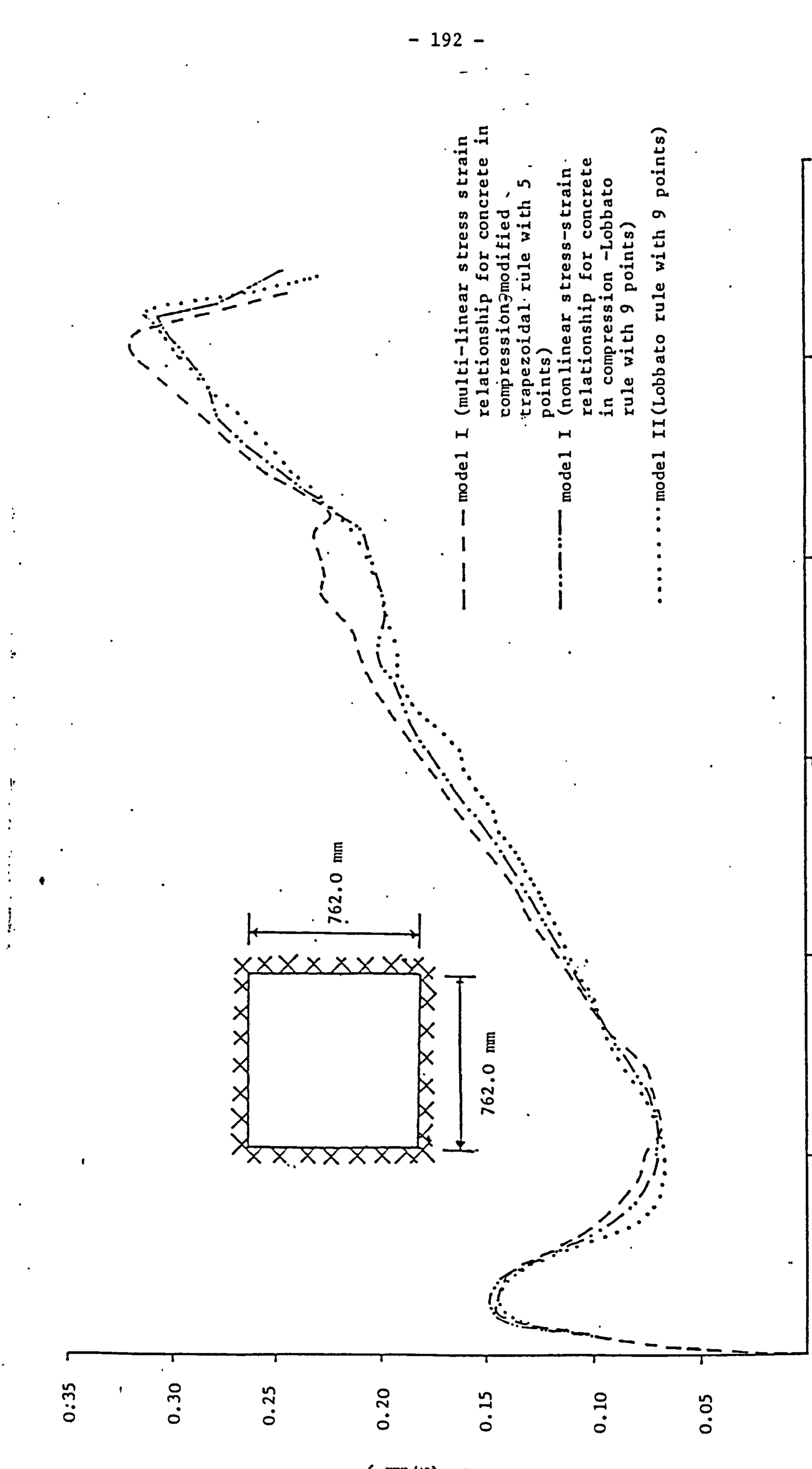

Figure 7.25. Load-deflection curves for slab S1

CHAPTER 8

SUMMARY AND CONCLUSIONS

8.1 SUMMARY

A numerical method of analysis using the finite element has been developed to investigate the behaviour of plates and slabs and which includes the effects of geometric and material nonlinearities. The structural behaviour such as in-plane, flexural and transverse shear effects have been incorporated in the analysis using Mindlin plate theory based on a total Lagrangian formulation.

The Heterosis plate bending element has been employed in the finite element formulation of plates and slabs which undergo either small or large deflections. The 8-node isoparametric membrane element has been employed to determine the in-plane stress distribution, due to in-plane edge loading, throughout a plate which is required for the elastic stability of plates.

The elastic buckling loads of plates with and without openings and under different edge loading conditions have been predicted. The collapse loads of steel plates and reinforced concrete slabs which include in-plane and flexural effects have been predicted. Failures due to plastic yielding in steel plates, cracking and crushing of concrete and yielding of reinforcing steel in reinforced concrete slabs have been considered.

The layered approach has been adopted in the analysis of plates and slabs. Steel plates have been modelled as series of layers.

Reinforced concrete has been modelled as a layered system of concrete and smeared steel layers with perfect bond assumed to exist at the interface of the two materials. The Mindlin assumption of normals to the middle surface remaining straight during deformations has been adopted to relate the displacements at the various levels through the plate thickness. This assumption reduces the problem to a two-dimensional one.

An incremental stress-strain formulation assuming that the material is isotropic has been adopted for the analysis of steel plates. For concrete a total stress-strain formulation assuming orthotropic behaviour under biaxial states of stress has been adopted for the analysis of reinforced concrete slabs. Nonlinear stress-strain relationships for concrete in compression have been incorporated in the analysis. Cracking of concrete has been modelled using a smeared crack model in which cracks allowed to rotate after their initial formation. Cracks can occur in two directions at right angles to each other and it is possible for cracks to close due to unloading. The tension stiffening effects have been included in the model using a linear unloading stress-strain relationship. The reinforcing steel has been represented using a bilinear stress-strain relationship in which strain hardening can also be included.

The modified Newton-Raphson method has been adopted in solving the nonlinear governing equations using both load control and displacement control methods in order to trace the entire structural response through elastic, inelastic loading ranges and up to collapse.

The stress resultants were determined by integrating the stresses at the various layers or sampling points throughout the plate thickness. The integration was carried out numerically using various numerical integration rules.

Finally several analyses to trace the response of steel plates and reinforced concrete slabs have been carried out using the computer program developed. The numerical results obtained have been compared to the availabe experimental, analytical and numerical results to demonstrate the validity and applicablity of the method of analysis presented in this study.

8.2 CONCLUSIONS

1- The finite element formulation adopted, using the Heterosis plate bending and the isoparametric membrane elements, to determine the elastic buckling loads for plates with and without openings and under different edge loading conditions has been demonstrated to be accurate and efficient when compared with other elastic stability finite element formulations.

2- The numerical procedures developed can be used to predict the entire response of steel plates and reinforced concrete slabs under monotonic loadings. The procedures could also be used, for example, to assess the performance of existing structures under unusual loadings.

3- The models adopted to represent the material behaviour are capable of simulating the different aspects of behaviour which affect most the response of steel plates and reinforced concrete slabs.

4- The membrane forces have considerable affect on the behaviour of plates and slabs which undergo large deflections. The inclusion of the membrane forces in the analysis of such structures is essential in order to predict a realistic response.

5- The load control method could be used to trace The structural response up to the ultimate load while the displacement control method could be used to trace the response beyond the ultimate load and up to failure.

6- The use of the line search technique in the analysis of reinforced concrete slabs improves the performance of the modified Newton-Rapshon method with a considerable reduction in the cost of the nonlinear analysis.

7- The accuracy of the stress resultants, for concrete sections sujected to uniaxial stresses and sections composed of isotropic materials subjected to biaxial stresses, can be improved considerably using the proposed integration rule when a total stress-strain formulation is used.

8.3 SUGGESTIONS FOR FUTURE WORK

1- A parametric study can be carried out to investigate the effect of the different parameters such as the aspect ratio and the material properties on the full range behaviour of plates and slabs.

2- The procedures developed could be used to obtain useful information which might help in the developement of more economic design methods for steel plates and reinforced concrete slabs.

3- More experimental data is needed on the full response of systems of plates and systems of slabs. Tests on such structures supported by beams and with openings could be useful to investigate the effects of the degree of edge restraints and the presence of the openings on the structural behaviour.

4- The present formulation could be extended to include a plate beam or a slab beam formulation by introducing a beam formulation such as Timoshinko beam which includes transverse shear deformations. The effects of the different degrees of edge restraints could be investigated by introducing springs to the nodal points located at the boundaries.

REFERENCES

[1] Powell,D.S.,'The ultimate strength of concrete panels subjected to uniformly distributed loads',M.sc. Thesis,Cambridge University,1956.

[2] Wood,R.H.,'Plastic and elastic design of slabs and plates,with particular reference to reinforced concrete slabs',Thames and Hudson,London,1961.

[3] Park,R.,'Ultimate strength of rectangular concrete slabs under short-term uniform loading with edges restrained against lateral movement',Proceedings of the Institution of Civil Engineers,Vol.28,1964,.125-150.

[4] Brotchie,J.F. and Holley,M.J.,'Membrane action in slabs',Special Publication SP-30,American Concrete Institute,Mich.,1971,pp.345-377.

[5] Black,M.S.,'Ultimate strength study of two-way concrete slabs',Journal of the Structural Division,ASCE,Vol.101,No.ST1,1975,pp.311-324.

[6] Van Greunen,J.,'Nonlinear geometric,material and time dependent analysis of reinforced and prestressed concrete slabs and panels',Ph.D. Thesis,University of California,Berkeley,1979.

[7] Crisfield,M.A.,'Local instabilities in the non-linear analysis of reinforced concrete beams and slabs',Proceedings of the Institution of Civil Engineers,Vol.73,1982,pp.135-145.

[8] Hinton,E.,Razzaque,A.,Zienkiewicz,O.C. and Davies,J.D.,´A simple finite element solution for plates of homogeneous,sandwich and cellular construction´,Proceedings of the Institution of Civil Engineers,Vol.59,1975,pp.43-65.

[9] Mindlin,R.D.,´Influence of rotatory inertia and shear on flexural motions of isotropic,elastic plates´,Journal of Applied Mechanics,ASME,Vol.18,1951,pp.31-38.

[10] Dupuis,G.A.,Hibbit,H.D.,McNamara,S.F. and Marcal,P.V.,´Nonlinear material and geometric behaviour of shell structures´,Computers and Structures,Vol.1,pp.223-239.

[11] Bathe,K.J.,Ramm,E. and Wilson,E.L.,´Finite element formulations for large deformation dynamic analysis´,International Journal for Numerical Methods in Engineering,Vol.9,1975,pp.353-386.

[12] Pica,A.,Wood,R.D. and Hinton,E.,´Finite element analysis of geometrically nonlinear plate behaviour using a Mindlin formulation´, Computers and Structures,Vol.11,1980,pp.203-215.

[13] Fung,Y.C.,´Foundations of solid mechanics´,Prentice-Hall,Englewood Cliffs,New Jersey,1965.

[14] Owen,D.R.J. and Figueiras,J.A.,´Anistropic elastic-plastic finite element analysis of thick and thin plates and shells´,International Journal for Numerical Methods in Engineering,Vol.19,pp.1983,pp.541-566.

[15] Timoshenko,S. and Goodier,J.N.,"Theory of elasticity",McGraw-Hill,London,1951.

[16] Zienkiewicz,O.C.,"The finite element method",McGraw-Hill,London,1977.

[17] Gallagher,R.H.,"Finite element analysis:Fundementals",Prentice-Hall, Englewood Cliffs,New Jersey,1975.

[18] Zienkiewicz,O.C. and Cheung,Y.K.,"The finite element method for analysis of elastic,isotropic and orthotropic slabs",Proceedings of the Institution of Civil Engineers,Vol.28,1964,pp471-488.

[19] Razzaque,A.,"Program for triangular bending element with derivative smoothing",International Journal for Numerical Methods in Engineering,Vol.6,1973,pp.333-343.

[20] Morely,S.,"The triangular equilibrium element in the solution of plate bending problems",Aero Quarterly,Vol.19,1968,pp.149-169.

[21] Bazeley,G.P.,Cheung,Y.K.,Irons,B.M. and Zienkiewicz,O.C.,"Triangular elements in Bending conforming and non-conforming solutions",Proceedings of the Conference on Matrix Methods in Structural Mechanics,Air Force Institue of Technology,Wright-Patterson A.F. Base,Ohio,1965.

[22] Pawsey,S.F . and Clough,R.W.,´Improved numerical integration of thick shell finite elemets´,International Journal for Numerical Methods in Engineering,Vol.3,1971,pp.575-586.

[23] Eughes,T.J.R.,Taylor,R.L. and Kanoknukulchai,W.,´A simple and efficient finite element for plate bending´,International Journal for Numerical Methods in Engineering,Vol.11,1977,pp.1529-1543.

[24] Zienkiewicz,O.C.,Taylor,R.L. and Too,J.M.,´Reduced integration technique in genereral analysis of plates and shells´,International Journal for Numerical Methods in Engineering,Vol.3,1971,pp.275-290.

[25] Baldwin,J.T.,Razzaque,A. and Irons,B.M.,´Shape function subroutine for an isoparametric thin plate element´,International Journal for Numerical Methods in Engineering,Vol.7,1973,pp.431-440.

[26] Hughes,T.J.R.,Cohen,M. and Haroun,M.,´Reduced and selective integration techniques in the finite element analysis of plates´,Nuclear Engineering Design,Vol.46,1978,pp.203-222.

[27] Pugh,E.D.L.,Hinton,E. and Zienkiewicz,O.C.,´A study of quadrilateral plate bending elements with reduced integration´,International Journal for Numerical Methods in Engineering,Vol.12,1978,pp.1059-1079.

[28] Hughes,T.J.R. and Cohen,M.,´The Heterosis finite element for plate bending´,Computers and Structures,Vol.9,1978,pp.445-450.

[29] Yang,R-J. and Bhatti,A.,´Nonlinear static and dynamic analysis of plates´,Journal of Engineering Division,ASCE,Vol.111,No.2,1985, pp.175-187.

[30] Hughes,T.J.R. and Tezduyar,´Finite elemet based upon Mindlin plate theory with particular reference to the four-node isoparametric elemet´,Journal of the Applied Mechanics,ASME,Vol.48,1981,pp.587-597.

[31] Timoshenko,S.P. and Woinowsky-Krieger,S.,´Theory of plates and shells´,McGraw-Hill,New York,1959.

[32] Hinton,E. and Bicanic,N.,´A comparison of Lagrangian and serendipity Midlin plate elements for free vibration analysis´,Computers and Structures,Vol.10.,1979,pp.483-493.

[33] Kapur,K.K. and Hartz,B.J.,´Stability of plates using finite element method´,Journal of the Mechanics Division,ASCE,Vol.92,No.EM2,1966,pp.177-195.

[34] Pifko,A.B. and Isakson,G.,´A finite element method for the plastic buckling analysis of plates´,Journal of the American Institute of Aeronautics and Astronautics,1969.

[35] Rockey,K.C.,Anderson,R.G. and Cheung,Y.K,´The behaviour of square shear webs having a circular hole´,Proceedings of the International Conference on Thin Walled Structures,Swansea,1967,pp.148-169.

[36] Shanmugam,N.E. and Narayanan,R.´,Elastic buckling of perforated square plates for various loading and edge Conditions´,International conference on Finite Element Method,Shanghai,1982.

[37] Sabir,A.B. and Chow,F.Y,´Elastic buckling of flat panels containing circural and square holes´,Proceedings of the Michael Horne Conference,Manchester,1983.

[38] NAG library documentation,Vol.4,Numerical Algorithms Group Ltd,United Kingdom.

[39] Winter,G. and Nilson,A.H.,´Desgin of concrete structures´,9th Ed., McGraw-Hill,New York,1979.

[40] Kupfer,H.,Hilsdorf,H.K. and Rush,H.,´Behaviour of concrete under biaxial stresses´,Journal of the American Concrete Institute,Vol.66, No.8,1969,pp.656-666.

[41] Owen,D.R.J. and Hinton,E.,´Finite Element in Plasticity:Theory and Practice´,Pineridge Press,Swansea,U.K.,1980.

[42] Nayak,G.C. and Zienkiewicz,O.C.,´Elasto-Plastic analysis.Generalization of various consitutive relations including strain softening´,International Journal for Numerical Methods in Engineering,Vol.5,1972,pp.113-135.

[43] State of the Art Report on´Finite element analysis of reinforced concrete´, American Society of Civil Engineering,1982.

[44] Ngo,D. and Scordelis,A.C.,'Finite element analysis of reinforced concrete beams',Journal of the American Concrete Institute,Vol.64,no.3,1967,pp.152-163.

[45] Kupfer,H.B. and Gerstle,K.H.,'Behaviour of concrete under biaxial stresses', Journal of the Engineering Mechanics Division,ASCE,Vol.99,No.EM4,1973, pp.852-866.

[46] Gerstle,K.H.,'Simple formulation of concrete behaviour',Journal of the American Concrete Institute,Vol.78,No.1,1981,pp.62-68.

[47] Liu,T.C.Y.,Nilson,A.H. and Slate,F.O.,'Biaxial stress-strain relations for concrete',Journal of the Structural Division,ASCE,Vol.98,No.ST5,1972, pp.1025-1034.

[48] Liu,T.C.Y.,Nilson,A.H. and Slate,F.O.,'Stress-strain response and fracture of concrete in uniaxial and biaxial compression',Journal of the American Concrete Institute,Vol.69,No.5,1972,pp.291-295.

[49] Darwin,D. and Pecknold,D.A.,'Analysis of RC shear panels under cyclic loading',Journal of the Structural Division,ASCE,Vol.102,No.ST2,1976, pp.355-369.

[50] Darwin,D. and Pecknold,D.A.,'Nonlinear biaxial stress-strain law for concret',Journal of the Engineering Mechanics Division,ASCE,Vol.103,No.EM2,1977, pp.229-241.

[51] Tasuji,M.E.,Nilson,A.H. and Slate,F.O.,´Biaxial stress-strain relationships for concrete´,Magazine of Concrete Research,Vol.31,No.109,1979,pp.217-224.

[52] Lin,C.S. and Scordelis,A.C.,´Nonlinear analysis of reinforced concrete shells of general form´,Journal of the Structural Division,ASCE,Vol.101,No.ST3,1975, pp.523-538.

[53] Chen,A.C.T. and Chen,W.F.,´Constitutive relations for concrete´,Journal of the Engineering Mechanics Division,ASCE,Vol.101,No.EM4,1975,pp.465-481.

[54] Buyukozturk,O.,´Nonlinear analysis of reinforced concrete structures´, Computers and Structures,Vol.7,1977,pp.149-156.

[55] Valanis,K.C.,´A theory of viscoplasticity without a yield surface´,Archiuum Mechaniki Stassowanej(Archives of Mechanis,Warsaw),Vol.23,1971,pp.517,551.

[56] Bazant,Z.P. and Bhat,P.,´Endochronic theory of inelasticity and failure of concrete´,Journal of the Engineering Mechanics Division,ASCE,Vol.102,1976, pp.701-722.

[57] Cope,R.J. and Rao,P.V.,´Nonlinear response of reinforced concrete,skewed, slab,bridges´,Research Report,Dept.Civil Engng.,University of Liverpool, Liverpool,1981.

[58] Hand,F.R.,Pecknold,D.A.,and Schnobrich,W.C.,'Nonlinear layered analysis of RC plates and shells',Journal of the Structural Division, ASCE,Vol.99,No.ST7,1973,pp.1491-1505.

[59] Saenz,L.P.,'Discussion of equations for the stress-strain curve of concrete by Desayi and Krishnan',Journal of the American Concrete Institute, Vol.61,No.9,1964,pp.1229-1235.

[60] Edwards,K.R.,'Nonlinear analysis of eccentrically stiffened reinforced concrete bridge decks',Ph.D.Thesis,University of Liverpool,Liverpool,1983.

[61] Tasuji,M.E.,'The behaviour of plain concrete subject to biaxial stress',Ithac, N.Y.,Cornell University,Dept. Structural Engng.,Research Report no.360,1976.

[62] Rots,J.G.,Nauto,P.,Kusters,G.M.A.,and Blaauwandraad,J.,'Smeared crack approach and fracture localization in concrete',HERON,Vol.30,No.1, 1985.

[63] Cope,R.J.,Rao,P.V.,Clark,L.A. and Norris,P.,'Modeling of reinforced concrete behaviour for finite element analysis of bridge slabs',Numerical Methods for Non-linear Problems,Prineridge Press,Swansea,1980,pp.457-470.

[64] Milford,R.V. and Schnobrich,W.C.,'Numerical model for cracked reinforced concrete',Proceedings of the International Conference on Computer Aided Analysis and Desgin of Concrete Structures,Pineridge Press,1984,pp.71-84.

[65] Cervera,M.,Abdel Rahman,H.H. and Hinton,E.,'Material and geometric nonlinear analysis of reinforced concrete plate and shell systems',Proceedings of the International Conference on Computer Aided Analysis and Desgin of Concrete Structures,Pineridge Press,1984,pp.547-563.

[66] Vecchio,F.,and Collins,M.P.,'The response of reinforced concrete to inplane shear and normal stresses',Publication No.82-03,University of Toronto, Canada,1982.

[67] Cardenas,A.,and Sozan,M.A.,'Strength and behaviour of isotropically and nonisotropically reinforced concrete slabs subjected to combinations of flexural and torsional moments',Civil Engineering Studies,SRS No.336, University of Illinios,Urbana,Illinios,1968.

[68] Duddeck,H.,Griebenow,G.,and Schaper,G.,'Material and time dependent nonlinear behaviour of cracked concrete slabs',in 'Nonlinear Behaviour of Reinforced Concrete Spatial Structures-Vol.1',Preliminary Report,IASS Symp.,Dusseldorf,1987,pp.101-133.

[69] Scanlon,A.,'Time dependent deflections of reinforced concrete slabs',Ph.D. Thesis,University of Alberta,Edmonton,Canada,1971.

[70] Gilbert,R.I. and Warner,R.F.,'Tension stiffening in reinforced concrete slabs',Journal of the Structural Division,ASCE,Vol.104,no.ST12,1978, pp.1885-1899.

[71] Zienkiewicz,O.C.,Valliappan,S. and King,I.P.,'Elasto-Plastic solutions of engineering problems.Initial Stress' finite element approach',International Journal for Numerical Methods in Enginerring, Vol.1,1969,pp.75-100.

[72] Riks,E.,'An incremental approach to the solution of snapping and buckling problems',International Journal of Solids and Structures, Vol.15,1979,pp.529-551.

[73] Haisler,W.E.,Stricklin,J.A. and Key,J.E.,'Displacement incrementation in nonlinear structural analysis by self-correcting methods',International Journal for Numerical Methods in Engineering,Vol.11,1977,pp.3-10.

[74] Abdel Rahman,H.H.,'Computational models for nonlinear analysis of reinforced concrete flexural systems',Ph.D. Thesis,University Collage of Swansea,Swansea,1982.

[75] Bathe,K.J. and Cimento,A.P.,'Some practical procedures for the solution of nonlinear finite element equations',Computational Methods in Apllied Mechanics and Engineering,Vol.22,1980,pp.59-85.

[76] Phillips,D.V. and Zienkiewicz,O.C.,´Finite element nonlinear analysis of concrete structures´,Proceedings of the Institution of Civil Engineers, Vol.61,1976,pp.59-88.

[77] Nayak,G.C. and Zienkiewicz,O.C.,´Note on the Alpha-Constant stiffness method for the analysis of nonlinear problems´,International Journal for Numerical Methods in Engineering,Vol.4,1972,pp.579-582.

[78] Cope,R.J.,Rao,P.V. and Edwards,K.,´Nonlinear finite element analysis techniques for concrete slabs´,Numerical Methods for Nonlinear Problems, Vol.1,Edited by Taylor,Hinton and Owen,Pineridge Press,Swansea,1980.

[79] Jennings,A.,´Accelerating the convergence of matrix iterative process´, Institution of Mathematical Applications,Vol.8,1971,pp.99-110.

[80] Hinton,E.,Abdel Rahman,H.H. and Zienkiewicz,O.C.,´Computational strategies for reinforced concrete slab systems´,in Advanced Mechanics of Reinforced Concrete Structures´,Final Report,IABSE Colloquium,Delft,1981,pp.303-313.

[81] Crisfield,M.A.,´Accelerated solution techniques and concrete cracking´, Computational Methods in Applied Mechanics and Engineering,Vol.30,1982.

[82] Crisfield,M.A.,'Variable step-lengths for nonlinear structural anslysis', Transport and Road Research Labaratory,Report 1049,Crowthorne,1982.

[83] Tellett,J.,'Pocket-Type reinforced brickwork retaining walls',Ph.D. Thesis, University of Warwick,Coventry,1984.

[84] Abramowitz,'Handbook of mathematical functions',Davies Publications, New York,1965.

[85] Aldstedt,E. and Bergan,P.G.,'Nonlinear,Time dependent concrete frame analysis',Jounral of the Structural Division,ASCE,Vol.104,1978, pp.1077-1097.

[86] Bergan,P.G.,'Some aspects of interpolation and integration in nonlinear finite element analysis of reinforced concrete structures',Proceedings of the Intenational Conference on Computer Aided Analysis and Design of Concrete Structures,Pineridge Press, pp.301-316,1984.

[87] Levy,S.,'Square plate with clamped edges under normal pressure producing large deflections',NACA Tech. Note 847,1942.

[88] Rushton,K.R.,'Large deflection of plates with initial curvature', International Journal of Mechanical Science,Vol.12,1970,pp.1037-1051.

[89] Weil,N.A. and Newmark,N.H.,'Large deflections of elliptical plates',Journal of Applied Mechanics,Vol.23,1956,pp.21-26.

[90] Schmit,R.,"Large deflection of a clamped circular plate",Journal of the Engineering Mechanics Divison,ASCE,Vol.94,1968,pp.1603-1606.

[91] Owen,D.R.J. and Figueiras,J.A.,"Elasto-Plastic analysis of anisotropic plates and shells by the Semiloof element", International Journal for Numerical Mehtods in Engineering,Vol.19,1983,pp.521-539.

[92] Onat,E.T. and Haythornthwait,R.M.,"Load carrying capacity of circular plates at large deflections", Journal of Applied Mechanics,Vol.23,1956, pp.49-55.

[93] Stricklin,J.A., Haisler,W.E. and Von Reisemann,W.A.,"Computation and solution procedures for non-linear anslysis by combined finite element-finite difference mehtods", Computers and Structures,Vol.2,1972,pp.955-974.

[94] McNeice,G.M. and Kemp,K.O.,"Comparison of finite element and unique limit analysis solution for certain reinforced concrete slabs", Proceedings of the Institution of Civil Engineers,Vol.43,1969,pp.629-640.

[95] Cope,R.J. and Rao,P.V.,"Nonlinear finite element analysis of concrete slab structures", Proceedings of the Institution of Civil Engineers,Vol.63,1977, pp.159-179.

[96] Taylor,R.,Maher,D.R.H. and Hayes,B.,'Effect of the arrangement of reinforcement on the behaviour of reinforced concrete slabs',Magazine of Concrete Research,Vol.98,1966,pp.85-94.

APPENDIX I

The eigenvalue problem.

The standard eigenvalue problem has been solved using the NAG library routines. The generalized eigenvalue problem can be transformed to the standard eigenvalue problem using matrix manipulation. The generalized eigenvalue problem is given by

$$\bar{\lambda} K \delta = \bar{K}_{\sigma} \delta \qquad \text{(i)}$$

where K is a symmetric positive definite banded matrix, which can be decomposed as

$$K = U\ L\ DD\ L^{T}\ U^{T} \qquad \text{(ii)}$$

where U is a unit upper triangular matrix, L is a unit lower triangular matrix and DD is a diagonal matrix. After the decompostion is performed K contains the elements of U, L and DD.

The generalized eigenvalue problem, equation (i), can be transformed to an equivalent standard eigenvalue problem such that

$$\bar{\lambda} y = c\ y \qquad \text{(iii)}$$

The eigenvalue of equation (iii) are then determined by the method of bisection.

APPENDIX II

Stiffness matrices for the displacement control method

In the finite element program the overall stiffness matrix [K] was assembled and stored in a banded form. The different matrices, rows and column vectors used in equations (6.13) and (6.14) are extracted as follows:

Consider the following banded stiffness matrix of n rows and m columns, where n represents the total degree of freedom of the system and m is the semi-bandwidth.

$$[K] = \begin{bmatrix} 0 & 0 & 0 \ldots . & 0 & 0 & K(1,1) \\ 0 & 0 & 0 \ldots . & 0 & K(2,1) & K(2,2) \\ 0 & 0 & 0 \ldots . & k(3,1) & K(3,2) & K(3,3) \\ \cdot & \cdot & \cdot \cdot \cdot & \cdot & \cdot & \cdot \\ \cdot & \cdot & \cdot \cdot \cdot & \cdot & \cdot & \cdot \\ & & A & & & K(i.m) \\ \cdot & \cdot & \cdot \cdot \cdot & \cdot & \cdot & \cdot \\ \cdot & \cdot & \cdot \cdot \cdot & \cdot & \cdot & \cdot \\ & & B & & & \\ \cdot & \cdot & \cdot \cdot \cdot & \cdot & K(n-1,m) & \\ \cdot & \cdot & \cdot \cdot \cdot & \cdot & K(n,m) & \end{bmatrix}$$

The row vector $\{K_{21}\}$ is formed by extracting the ith row of the matrix $[K_{11}]$ starting from the diagonal term K(i,m) and then moving horizontally m times, this process is indicated diagrammatically by path A. The remainder of the terms of the row vector $\{K_{21}\}$ are extracted by moving diagonally m-n times along path B. Matrix $[K_{11}]$ is formed by replacing the terms along paths A and B by zeros and

replacing the diagonal term k(i,m) by unity. This is equivalent t
multiplying the diagonal term by a large number.